Université de Montréal

Modélisations de maladies des motoneurones en utilisant le poisson zébré

par Alexandra Lissouba

Département de pathologie et biologie cellulaire
Faculté de médecine

Thèse présentée à la Faculté de médecine
en vue de l'obtention du grade de Philosophiae Doctor (Ph.D.)
en pathologie et biologie cellulaire
option Système nerveux

Août 2018

Résumé

Les paraplégies spastiques familiales (PSF) sont un groupe de maladie neurodégénératives hétérogènes affectant les neurones moteurs supérieurs et causant une faiblesse musculaire progressive des membres inférieurs entrainant des problèmes de marche. Plus de 60 gènes ont été lies à cette maladie, leur nombre augmentant régulièrement. La sclérose latérale amyotrophique (SLA) est une maladie neurodégénérative à déclenchement tardif qui affecte les neurones moteurs supérieurs et inférieurs, entrainant une atrophie musculaire accompagnée de spasticité. La mort, causée par une insuffisance respiratoire survient dans les 2 à 5 ans après le début de la maladie. Ces deux maladies de neurones moteurs, bien que différentes, ont des gènes et des mécanismes pathologiques en commun. Ainsi, accroitre notre connaissance de leurs similarités et de leurs différences pourra nous aider à mieux comprendre chacune individuellement.

Pour étudier ces deux maladies, nous avons utilisé des modèles de poisson zébré précédemment caractérisés et en avons développé de nouveaux pour approfondir nos connaissances sur les mécanismes physiopathologiques.

Dans la première partie de cette thèse, nous avons identifié le stress du réticulum endoplasmique (RE) comme un nouveau mécanisme pathologique induit par la perte de fonction de spastin, un gène impliqué dans la PSF, et avons montré que des modulateurs du stress du RE sont capables de renverser le phénotype locomoteur. Nous avons aussi identifié un nouveau gène causatif de la PSF, *CAPN1* (SPG76), et avons validé *in vivo* la pathogénicité de sa perte de fonction en identifiant une désorganisation des réseaux de microtubules comme phénotype principal.

Dans la deuxième partie de cette thèse, nous avons généré plusieurs nouveaux modèles de poisson zébré de la SLA. Deux lignées transgéniques exprimant la protéine humaine de type sauvage ou mutante sous le contrôle d'un promoteur inductible nous ont permis de reproduire des résultats obtenus précédemment par l'injection d'ARNm et d'identifier des changements transcriptomiques similaires à ceux obtenus récemment avec des modèles de souris. Nous

avons aussi généré deux nouvelles lignées en introduisant des mutations ponctuelles liées à la SLA dans les gènes *tardbp* et *fus* du poisson zébré en utilisant la technologie CRISPR/Cas9.

Ces résultats soulignent la valeur du poisson zébré comme modèle pour étudier les maladies des neurones moteurs et leurs mécanismes physiopathologiques, et suggèrent de nouvelles approches thérapeutiques.

Mots-clés : Sclérose latérale amyotrophique, paraplégie spastique familiale, poisson zébré, stress RE, TDP-43, FUS, spastin, calpain 1, CRISPR/Cas9

Abstract

Hereditary spastic paraplegias (HSP) are a group of heterogeneous neurodegenerative diseases affecting upper motor neurons, causing progressive gait dysfunction and more than 60 genes have been linked to this disease. On the other hand, amyotrophic lateral sclerosis (ALS) is a late-onset progressive neurodegenerative disorder that affects both upper and lower motor neurons, leading to muscle atrophy with spasticity and death in two to five years due to respiratory failure. These two motor neuron disorders, while separate, share common genes and pathological mechanisms and as such, increasing our knowledge about their similarities and differences can help us have a better understanding of each of them individually.

In order to study these two diseases, we used previously characterized zebrafish models and developed new ones to deepen our understanding of the pathophysiological mechanisms of HSP and ALS.

In the first part of this thesis, we identified ER stress as a new pathological mechanism at play in HSP due to spastin loss-of-function and showed that ER stress modulators are able to rescue the locomotor phenotype. We also identified a new gene causative of HSP, *CAPN1* (SPG76), provided *in vivo* validation of its loss-of-function pathogenicity and identified microtubule networks disorganization as one of the main defects.

In the second part of this thesis, we generated several new zebrafish models to study ALS. Two transgenic lines expressing either a wild-type or a mutant TDP-43 protein under the control of an inducible promoter allowed us to recapitulate previous findings obtained with mRNA injections and identify transcriptomic changes due to the mutant protein that are in line with recent transcriptomic data obtained in mouse models. We also generated two new lines with knock-in of ALS-causative point mutations in the *tardbp* and *fus* zebrafish endogenous genes using the CRISPR/Cas9 technology.

These results underscore the value of the zebrafish model to study motor neuron disorders and their pathophysiological mechanisms as well as open new therapeutic avenues.

Keywords : Amyotrophic lateral sclerosis, hereditary spastic paraplegia, zebrafish, ER stress, TDP-43, FUS, spastin, calpain 1, CRISPR/Cas9

Table des matières

Liste des tableaux

Annexe 7:

Liste des figures

Liste des sigles et abréviations

AD: autosomal dominant

ALS: amyotrophic lateral sclerosis

AR: autosomal recessive

CaP: caudal primary motor neuron

CAPN1: Calpain 1

CRISPR/Cas9: clustered regulatory-interspaced short palindromic

DNA: deoxyribonucleic acid

DSB: double-strand break

ER: endoplasmic reticulum

fALS: familial ALS

FTD: fronto-temporal dementia

FUS: Fused in Sarcoma

HSP: hereditary spastic paraplegia

LMN: lower motor neuron

MiP: middle primary motor neuron

MND: motor neuron disorders

NES: nuclear export signal

NHEJ: non-homologous end joining

NLS: nuclear localization signal

NMJ: neuromuscular junction

PBP: progressive bulbar palsy

PLS: primary lateral sclerosis

PMA: progressive muscular atrophy

repeats/CRISPR associated protein 9

RNA: ribonucleic acid

RoP: rostral primary motor neuron

ROS: reactive oxygen species

sALS: sporadic ALS

SPG: spastic paraplegia

TALEN: Transcription activator-like effector nucleases

TARDBP: Transactive Response DNA Binding Protein

Tardbpl: Transactive Response DNA Binding Protein - like

TILLING: Targeting Induced Local Lesions IN Genomes

UMN: upper motor neuron

UPR: unfolded protein response

XL: X-linked

ZFN: zinc-finger nuclease

Dédicace

À mon grand-père qui a ouvert la voie

Remerciements

Voilà, c'est la fin. Après toutes ces années, difficile de trouver les mots pour remercier tous ceux qui m'ont accompagnée, soutenue et encouragée pendant mon doctorat. Je vais m'y essayer malgré tout, car vous le méritez.

Et d'abord, merci à Pierre de m'avoir donné ma chance il y a un certain nombre d'années (que l'on ne nommera pas). Merci pour ton soutien, tes encouragements et toutes les opportunités que tu m'as offertes, scientifiques et personnelles. Ton enseignement a été formateur et ta vision positive de la science est marquante. Anything is possible indeed! J'en ai des histoires à raconter grâce à toi, que ce soit dans les Highlands, en Australie, ou sur la côte Californienne!

Merci également à tous les membres du labo, passés et actuels. La recherche ne peut pas se faire seul, et votre regard critique, vos questions et votre aide m'ont poussée à devenir une meilleure chercheuse, surtout lorsque ces discussions étaient prises avec des bières, sur le canapé du labo (RIP). Merci à Guy et Marina pour toute l'aide à l'animalerie, et un énorme merci à Meijiang. You know that the lab wouldn't run without you and I personally can't thank you enough. You always believed in me, thank you. Merci donc à Édor, Sébastien, Valérie, Nathalie, Edna, Claudia, Zhipeng, Laura, Hamid, Sarah, Aurélie, Raphaelle, Stefka, Gary, Kessen, Éric, Amrutha, Poulomee, Hamid and Alexandre. Et à tous nos stagiaires d'été, en particulier Marc et Alexis, ainsi qu'à Chloé pour les poissons. Vous avez égayé mes étés, ça n'aurait pas été pareil sans vous.

Merci aussi à tous mes collaborateurs et d'abord aux Drs Alex Parker et Patrick Dion, qui m'ont accompagné en tant que parrains pendant mon doctorat. J'ai eu la chance d'avoir non seulement vos conseils, mais aussi de collaborer avec vous sur deux projets inclus dans cette thèse. Merci également aux laboratoires des Drs Rouleau et Bolduc ainsi qu'au Dre Bencheikh pour notre travail collectif sur ces articles. And of course thank you so much Gary for all your help, your advice and our co-authorship.

Et rien ne serait arrivé sans tout le support administratif présent et passé au CRCHUM et en patho. Manon, Carline, Benoit, Katherine, mais aussi Christine, Marielle, Lucie,

Matenda, Mikelsie et bien d'autres. Et en parlant de patho, Diane, tu as été un soutien essentiel et ta gentillesse m'a énormément marquée.

Merci aussi à Alexandre A. et à Agnès A.-P. sans votre support, cette thèse n'aurait jamais été écrite.

Rien ne serait arrivé également sans financement et je me dois de remercier les organismes qui ont mis leur confiance en mes capacités. Merci donc à ALS Canada qui m'a donné la possibilité d'avoir la bourse IRSC priorité sur l'ALS, et avant eux merci au FRQS ainsi qu'au GRSNC. Merci également à la Rare Disease Fundation pour leur microgrant.

Ah, le GRSNC! Parlons-en de tout ça. Parce que mon doctorat a aussi été l'opportunité de m'impliquer : GRSNC, Cerveau en Tête, l'asso de patho… Ces moments étaient aussi des bouffées d'air frais lorsque le labo était plus difficile. J'en retiens des instants très forts et surtout des gens supers. Et puis les cocktails des conf Eli Lilly, ça ne s'oublie pas! Léa, Stefanny, Emilie, Chris, Guillaume, Alexandre, Dom, Elsa, Cathou,… la liste est longue. Sans oublier Camille, membre honoraire de toutes nos activités de neuro!

Et on continue avec les amis, rencontrés par le labo ou pas, qui sont encore là ou pas, mais qui m'ont aidé à passer à travers toutes les mauvaises passes, et à célébrer tous les succès. Louis et Fanny, toujours là, quoi qu'il arrive, Vi, Yousra, Sabrina, Fred, Swantje, Sasha, Camille, Kianoush, Chuck, Loic, Maxime, Tiphaine, Constantin, Sandra, Alexandra la brune, Anaïs, Marc-André, Arnaud, Gary, toute l'équipe de rugby de Westmount et puis bien évidemment les cool peeps, Marc, Stefka, Raphaelle et surtout Éric et Kessen qui m'ont accompagnée jusqu'aux tout derniers moments avec cette thèse. Merci à tous les deux, votre aide et votre implication a été inestimable.

Et puis qu'aurais-je fait sans ma famille? Maman, merci pour tout ton soutien, ta patience, tes encouragements. Je n'aurais pas pu aller jusqu'au bout sans toi, merci merci merci. Merci à mes 3 frères, Lionel, Vladimir et Vassily, toujours là pour me changer les idées avec leurs photos lorsqu'ils sont dans des endroits lointains comme la Thaïlande, la Nouvelle-Zélande, ou l'Île des Sœurs. Merci à Atessa pour tes encouragements et ta présence et pour Dalia aussi, petit rayon de bonheur dans nos vies. Tatibi, Shane, Lanéa, Julie, Brigide, merci à toutes pour vos encouragements continus. Merci à Pascale pour ce repas de midi il y a un an,

qui m’a fait chaud au cœur. Et merci à toi Nenette, ma grand-mère adorée qui a toujours, toujours été là pour moi.

J’en oublie probablement, difficile de résumer tant d’années, tant de support, tant de moments importants en quelques lignes. Sachez que même si vous n’avez pas été nommé, vous étiez dans mes pensées.

Et puis pour finir, merci à toi Laetitia. C’est probablement pour toi que j’arrive le moins à trouver les mots, il ne me reste donc que les actes. Bonne lecture.

Chapter 1: Introduction

Motor neuron disorders

Historical generalities

In the 19th century, neurologists started combining clinical observation with pathological examination, in order to have a better classification of diseases. One of the challenges they faced was to understand how to separate disorders due to a deficiency of the muscular system, from those due to a deficiency of the motor nervous system. Being able to do thorough post-mortem examinations of well-defined clinical cases allowed them to start answering this question, and in the second part of the 19th century, many different diseases were defined following this process. In 1836, Charles Bell presented the case of a middle-aged woman with progressive paralysis of limbs and tongue but without sensory defects, and whose autopsy showed degeneration of the anterior portion of the spinal cord, indicating a link between spinal cord degeneration and motor disorders [1]. In 1850, Aran, with previous observations from Duchenne [2], first described progressive muscular atrophy (PMA), which he first thought was a disease of the muscles [3]. In 1853, Cruveilhier showed that patients with PMA had an atrophy of the anterior horn of the spinal cord [4]. The first description of idiopathic progressive bulbar palsy (PBP) was done by Robinson in a letter to Charles Bell in 1825 [5] but Duchenne was the first to publish a description in 1860, under the term primary labio-glosso-pharyngeal paralysis [6]. In 1865, Charcot first described the disease [7] that he will later name amyotrophic lateral sclerosis (ALS), during two lectures where he described the clinical and pathological features of the disease, based on the history and examination of 20 cases, 5 of them with post-mortem analysis [8]. In 1875, Erb first proposed primary lateral sclerosis (PLS) as a distinct disorder [9]. In 1879, Kahler and Pick showed atrophy of the motor cortex in ALS [10, 11]. In 1880, Strümpell first clinically identified hereditary spastic paraplegia (HSP) as a distinct disorder [12] and in 1898 Lorrain provided a more thorough description of this disorder [13]. In 1891 and 1892 Werdnig and Hoffman respectively provided the first descriptions for spinal muscular atrophy (SMA) [14, 15]. And in 1933, Brain grouped for the first time PMA, ALS and PBP under the term motor neuron disease in his

textbook, underscoring that motor neurons are pathologically affected in all of these three diseases [16].

Definition of motor neuron disorders

Nowadays, one may define motor neuron disorders (MND) as a group of clinically and pathologically heterogeneous disorders characterized by progressive degeneration of motor neurons and their axons, leading to weakness, atrophy, spasticity and/or paralysis of the muscles. MNDs include both developmental disorders, as well as neurodegenerative ones. As evidence of the difficulty of properly classifying MNDs, not every list of MNDs contains the same disorders. Moreover, there are some controversies as to whether some of these diseases are independent entities, or are part of a larger spectrum with ALS.

Under the tenth International Classifications of Diseases and Related Health Problems (ICD-10, http://apps.who.int/classifications/icd10), only ALS (G12.21, includes PMA), PBP (G12.22), pseudobulbar palsy (G12.29) and PLS (G12.23) are identified under the general G12.2 motor neuron disease category. However, HSP (G11.4) is often also considered a motor neuron disorder and grouped under the denomination MNDs. In the case of this thesis, MNDs refer to all the previously named disorders.

Classification of MNDs

While progress is being made in identifying the molecular basis of these disorders, an often used classification is made depending on which category of motor neurons are affected in the disease: either the upper motor neurons (UMN), the lower motor neurons (LMN) or both.

The UMN originate in the primary motor cortex and in the brainstem. Their axons form the corticospinal and corticobulbar tract and relay motor information either directly to the LMN or to interneurons, which then contact the LMN. The LMN originate in the cranial motor nuclei in the brainstem as well as in the spinal cord. They relay motor impulses to skeletal muscles at the level of the neuromuscular junction (NMJ) [17, 18].

The signs of affected UMN generally include weakness, spasticity, overactive tendon reflexes, Hoffman and Babinski signs, clonus, as well as speech problems and emotional lability. The signs of affected LMN are characterized by weakness, attenuated reflexes, muscle wasting, cramps and twitching [19, 20]. However, there is often a clinical as well as a pathophysiological overlay between UMN and LMN signs, making it difficult to establish a precise diagnostic, especially as some of these symptoms evolve with time and may appear later. Additionally, UMN signs are difficult to discern and may be masked by LMN signs [20, 21]. As a result, diagnosis of most MNDs is a lengthy process and is usually made by exclusion with confirmation coming only from post-mortem examination [22].

Over the course of this thesis, I studied two of these MNDs, HSP and ALS in order to better udnderstand their pathophysiological mechanisms. I will first present HSP and ALS in details, including the genes and proteins I have studied over the course of this thesis.

Hereditary spastic paraplegia

Definition and epidemiology

HSP is a general term used for a group of clinically and genetically heterogeneous neurodegenerative inherited disorders characterized by a slowly progressing spasticity and weakness in the lower limbs due to axonopathy of the UMN [23]. The symptoms usually start with small gait impairments and will progress over the years with the development of a spastic gait and lower extremities hyperreflexia due to a distal axonopathy of the lateral corticospinal tract and of the posterior columns [18, 24, 25]. While HSPs do not affect the life expectancy of the patients, the disease can be debilitating and the patients may completely lose the ability to walk independently, requiring walking aids including wheelchairs. The symptoms may start asymmetrically, but overtime will usually affect both legs similarly. The first symptom is usually spasticity, followed by weakness. It is accompanied by increased lower limbs muscle tone, hyperreflexia and extensor plantar response. A reduced sensation of vibration in the lower extremities can also be present, as well as neurogenic bladder disturbances, leading to increased urinary urgency [25-28].

The worldwide median prevalence of HSPs is of 1.8:100,000, but with geographical variability ranging from 0.1:100,000 in Japan to 9.6:100,000 in Spain [29, 30]. No incidence data is available.

Classification

A clinical classification initiated by Harding [23] gives rise to two broad categories of HSP: when patients present with muscle weakness and spasticity in the lower limbs with primary sensory modalities preserved and no extrapyramidal signs are considered as having pure or uncomplicated HSP. Decreased vibration sensing at the ankles, pes calvus and bladder dysfunction are also possible. When, in addition to the symptoms of pure HSP, the patients experiencing additional neurological impairments and for which no other causes can be identified are considered as having complicated or complex HSP. These additional symptoms include, but are not limited to dementia, cognitive impairments, ataxia, cerebellar atrophy, basal ganglia symptoms, extrapyramidal symptoms, seizures, and thin corpus callosum [23, 29, 31].

Clinical features

There is a high variability in HSP, including an intrafamilial variability (despite sharing the same mutations), with a variable age of onset, variable disease progression, variable penetrance and variable presence of additional neurologic features [23, 25-28, 32]. The age of onset ranges from birth to the seventh decade and follows a bimodal distribution, with a first peak before 10 years old, and a second between 30 and 60 years old [32, 33]. While often debilitating, HSPs are not lethal. The median disease duration until the loss of independent walking is 22 years [32]. Complicated HSP is usually associated with a more severe disease course than pure HSP, especially if dysarthria, dysphagia, extrapyramidal signs or cognitive impairments are present. The onset of the symptoms can be subtle and hard to precisely identify and the disease progression is usually over months or years, with many patients reaching a plateau in term of worsening, after several years [26-29, 32]. The severity of the disease can be assessed using the spastic paraplegia rating scale (SPRS) [34].

A recent Canadian study conducted in 6 different recruitment centers across the country identified a mean age of onset at 18.9 years (range 0-67), reflecting the high number of paediatric patients in this study [35].

Diagnosis

A clinical history of slowly progressive spastic paraplegia with a hard to pinpoint onset, with or without complicated symptoms and with or without a familial history is a first step to a potential diagnosis of HSP. The diagnosis can then be established by the identification of mutations in known HSP-causing locus/genes. If this cannot be achieved, the diagnosis will be made by excluding other diseases that are potential mimics of HSPs, such as multiple sclerosis, spastic ataxias, PLS, ALS or spinocerebellar ataxias [26-28, 31].

Treatment

There is currently no treatment to either prevent or reverse the disease course, but medication to alleviate some of the symptoms is available. For example, baclofen can be used to reduce spasticity or anticholinergic drugs to alleviate the bladder dysfunctions. Additionally, regular physical exercise often improves walking ability and lessens the pain [25-27, 31].

Neuropathology

Post-mortem studies show degeneration of the longest myelinated fibres of the descending lateral corticospinal tracts, starting at the distal ends and that is maximal in the thoracic spinal cord. To a lesser extent, degeneration of the fasciculus gracilis fibres is also present, and is maximal in the cervicomedullary region [36-38].

The axonopathy is a progressive “dying back” process that starts at the distal end of the axons, leading to dysregulation of the synapses between the UMN and the LMN. A reduction in the area and axonal density in both the corticospinal tract and the ascending dorsal column can be seen [36].

While there may be some loss of anterior horn cells and a decrease in the number of Betz cells seen in some autopsies, it is not a generalized feature. As a result, the motor neuron involvement is subclinical and not evident on electromyography and nerve conducting testing [37]. In the majority of cases, only the UMN are affected, but sometimes the LMN are also targeted and a phenotype closer to ALS can be seen [33]. Additionally, even in pure HSP, the presence of subclinical cognitive disturbance and dementia signs are possible [39, 40].

Aetiology

Genetic classification of HSP

The majority of HSP cases are inherited, in an autosomal dominant manner (AD-HSP) in around 48% of cases, autosome recessive (AR-HSP) in around 12% of cases, or X-linked (XL-HSP) and maternally inherited through mitochondrial DNA in some rare cases. However, up to 40% of HSP cases are apparently sporadic cases, either due to an incomplete family history, incomplete penetrance of the disease-causing mutations, or de novo mutations [32, 41, 42]. AD-HSP is usually associated with pure HSP, while AR-HSP with complicated HSP [27, 32]. The first genes linked to HSP were identified using linkage analysis [43-45], but the use of next generation sequencing allowed for the identification of an increasingly higher number of genes and loci linked to the disease [46-48].

By convention, the designation SPG, for spastic paraplegia is used for each different genetic type of HSPs, numbered by their order of discovery. For example, SPG1 designate HSP due to mutations in the gene *L1CAM*, an axonal glycoprotein important for neuronal migration and differentiation. It was the first causative gene linked to HSP and is inherited in an X-linked manner, with complicated features including mental retardation, hydrocephalus, aphasia and adducted thumbs [44]. At the time of writing, a total of 79 SPG loci involved in HSP have been identified [31, 46, 48, 49]. However, additional genes that have been linked to HSP but have not yet received the SPG denomination increase this number, as for example HSPs due to mutations in mitochondrial genes do not receive the SPG designation.

Amongst the identified 79 SPG loci, the genes and causative mutations have been identified for 64 of them. To this day, 22 loci are responsible for AD-HSP, with 15 identified

genes; and 53 loci are responsible for AR-HSP with 48 identified genes [27, 28, 31]. Five loci have been identified for XL-HSP: SPG1, SPG2, SPG22, SPG16 and SPG34, but the genes have been identified only for SPG1 (*L1CAM*), SPG2 (*PLP1*) and SPG22 (*SLC16A2*) [27, 28, 44, 50-52]. Interestingly, some of the causative genes are responsible for both AR- and AD-HSP, such as SPG3 (*ATL1*), SPG58 (*KIF1C*) and SPG72 (*REEP2*) [53-55]. Despite the high number of genetic loci identified, around 36% to 38% of AD-HSP and 40% to 53% of AR-HSP still have unidentified genetic causes [28, 32]. HSP inherited through mutated mitochondrial DNA are usually heterogeneous multisystem disorders, for which spastic paraplegia is only one of the symptoms. As such, the consensus as to whether the genes identified are specifically causative for HSP is not as strong, and different literature reviews include one to four of these genes as causative of HSP [25-28, 31].

Main genes involved in HSP

While more than 80 loci and genes have been linked to HSP cases, most of them have only been identified in less than 10 families. In these cases, the number of patients studied with the identified variants can be extremely small and they are thus not well characterized [25]. For example, SPG24 (gene unknown), causing AR-HSP, has only been identified in 5 individuals from one family [56]. On the other hand, SPG4 (*SPAST*), SPG3A (*ATL1*), SPG31 (*REEP1*) and SPG10 (*KIF5A*) are responsible for around half of AD-HSP cases, whereas SPG11 (*KIAA1840*), SPG5A (*CYP7B1*), SPG7 (*PGN*) and SPG15 (*ZFYVE26*) are responsible for around 30% of AR-HSP [27, 28]. Amongst these, SPG4 is the most common type of AD-HSP and accounts for 40% of all AD-HSP, and 10% to 20% of sporadic HSP cases [27, 41, 45], and is responsible for 48% of all HSPs in Canada [35]. I will briefly discuss the other main genes involved in HSP and SPG4 will be discussed in more details in a later section:

SPG3A/*ATL1*

Mutations in the gene *ATL1*, coding for the protein Atlastin 1, represent 5% to 20% of AD-HSP globally and is the second most common cause of AD-HSP, as well as the most frequent cause of early-onset HSP, with a mean age of onset of 5 years old [57-60].

Atlastin 1 is a dynamin related GTPase which is mainly involved in ER and Golgi morphogenesis as well as neurite outgrowth and intracellular membrane trafficking [61-64].

SPG31/*REEP1*

2% to 8% of AD-HSP are due to mutations in *REEP1*, leading to SPG31, a typically pure HSP with an age of onset varying from the first two decades to an adult onset [65-68].

REEP1 encodes the protein receptor expression-enhancing protein 1 (REEP1), a chaperon-like protein located at the mitochondria and at the ER [68-71].

SPG10/*KIF5A*

Mutations in *KIF5A* lead to SPG10, an HSP that can be either pure or complex. It is responsible for 2% to 10% of AD-HSP, with a usually adult age of onset, although infantile-onset has been described [72-76].

KIF5A encodes the protein kinesin heavy chain 5A (KIF5A), a microtubule based motor protein involved in the transport of organelles and most mutations in SPG10 are localized in the highly conserved motor domain [77].

SPG11/*KIAA1840*

Mutations in *KIAA1840*, encoding the protein Spatacsin, lead to SPG11, the most common form of AR-HSP, representing around 20% of AR-HSP cases and with an age of onset ranging in the first three decades of life. SPG11 is associated with complicated HSP, the main features being a thin corpus callosum, cognitive impairment and intellectual disability, white matter lesions and cerebellar symptoms [32, 78-84]. The progression of SPG11 is considered severe compared to pure HSP, with patients being wheelchair bound on average 16 years after the disease onset [82].

Spatacsin is widely expressed in the central nervous system, including in the cerebellum, in the UMN and in the LMN [85]. Although its exact role is still unclear, Spatacsin is thought to be involved in autophagy and lysosome turnover, as well as in membrane trafficking through interactions with proteins encoded by SPG genes, Spastizin (SPG15/*ZFYVE26*) and KIAA0415 (SPG48/*AP5Z1*), the latest one being part of the fifth adaptor protein complex (AP-5) [86-89].

SPG5A/*CYP7B1*

Mutations in *CYP7B1* represent up to 8% of AR-HSP [90-92]. They are responsible for SPG5A, leading to either a pure or complicated HSP, with a variable age of onset ranging from early infantile onset to the fifth decade of life, with a high intrafamilial variability. The disease course is usually a slowly progressive pure HSP, but complicated cases have also been described, with white matter lesions and cerebellar involvement leading to ataxia, as well as optical atrophy [90, 91, 93, 94].

CYP7B1 encodes the cytochrome P450 oxysterol 7-alpha-hydroxylase protein, which is part of the cytochrome P450 family and is involved in the metabolism of brain cholesterol, in particular in the neurosteroid biosynthetic pathway, as well as in the bile acid pathway [90, 95]. In SPG5A, an accumulation of 27-hydroxy-cholesterol is seen in the blood and in the cerebrospinal fluid of patients due to the loss of function of this enzyme, although the mechanism and role of this accumulation is not yet fully understood [95].

SPG7/*PGN*

SPG7 is due to mutations in the gene *PGN*, coding for the protein Paraplegin and representing up to 8-10% of AR-HSP [96-98]. SPG7 has a wide-ranging age of onset, going from the first decade to the 7th decade of life. The disease usually starts as pure HSP and progresses slowly, with complex pathological signs appearing during the course of the disease, such as cerebellum atrophy, and bilateral optic disc pallor [96, 99-101].

Paraplegin is a mitochondrial AAA metalloproteinase located in the mitochondria membrane and is involved in removal of misfolded proteins, the activation of essential mitochondrial proteins and in ribosome maturation [102, 103].

SPG15/*ZFYVE26*

Mutations in *ZFYVE26*, encoding Spastizin, cause SPG15, a type of AR-HSP that is extremely similar to SPG11, and is responsible for around 4% of AR-HSP globally [80, 104-106]. The phenotype observed is a complex HSP, often associated with thin corpus callosum, white matter lesions, cerebellar atrophy, hearing loss and Kjellin syndrome, a pigmentary maculopathy [106-109]. The onset is usually during childhood, and the course of the disease is similar to SPG11, making it hard to distinguish both types of HSP [80, 106, 109, 110].

As previously mentioned, Spastizin interacts with Spatacsin and KIAA0415 and colocalizes with microtubules, mitochondria and the nucleus [85, 87-89, 111]. Mutations of Spastizin lead to loss-of-function of the protein and defective autophagy [112].

More information about all the different SPG and identified HSP-causative genes can be found in the different reviews cited previously [25-28, 46]. The next section will discuss in more details SPG4, the main cause of HSP.

SPG4/*SPAST*

Structure and localisation

Spastin is a multifunctional protein belonging to the AAA (ATPases associated with a variety of cellular activities) protein family encoded by the gene *SPAST*. The gene, which contains 17 exons, is located on chromosome 2p22.3 and spans around 90 kb [45].

Four main spastin isoforms are found in human, due to the presence of two initiation codons in the first exon and the alternative splicing of the fourth exon. A first initiation codon at position 1 of the main open reading frame (ORF) is responsible for a first isoform of 616 amino acid residues and a molecular weight of 68 kDa, called M1. The initiation codon is surrounded by a weak Kozak sequence, leading to a leaky scanning of this first ATG [113]. A second initiation codon at position 259 of the main ORF is surrounded by a better Kozak sequence and leads to a second shorter isoform of 530 amino acid residues of 60 kDa called M87 and the presence of a cryptic promoter in the first exon leads to the specific expression of this promoter in a tissue specific manner [113, 114]. Two additional isoforms are obtained from the M1 and M87 spastin by alternative splicing of the 4th exon, of respectively 64 kDa and 55 kDa [113, 115]. Normal splice variants of exons 8 and 15 have also been observed, but at very low level [115].

The most abundant spastin isoform is the M87 one, which is ubiquitously expressed and is found in both the cerebellar cortex and the spinal cord, whereas the M1 isoform is expressed significantly only in the spinal cord [116]. The M87 isoform is found in both the cytoplasm and nucleus, while the M1 isoform is only located in the cytoplasm.

The spastin protein contains 4 identifiable domains (**Figure 1**):

- An N-terminal domain, with a hydrophobic region spanning the amino acid residues 49 to 80, which can form into a hairpin and insert into the endoplasmic reticulum (ER) membrane, where it interacts with the Atlastin 1 and REEP1 proteins, also involved in HSP. This domain is the only one present only in the M1 isoform and not in the M87 isoform [69, 117, 118].

- The microtubule interacting and trafficking domain (MIT), located at the 116 to 194 amino acid residues and present in both M1 and M87 isoforms. The MIT domain is required for interactions with different proteins, including some proteins associated with the ESCRT-III complex (endosomal sorting complexes required for transport, involved in endosomal sorting) and with the Reticulon 1 protein (involved in vesicular trafficking) [119-121].

- The microtubule binding domain (MTBD), located at amino acid residues 270 to 328, is sufficient for spastin to bind to microtubules through an RKKK-motif and associate with negatively charged tubulin. This domain is also necessary for the microtubule-severing function of spastin [122, 123].

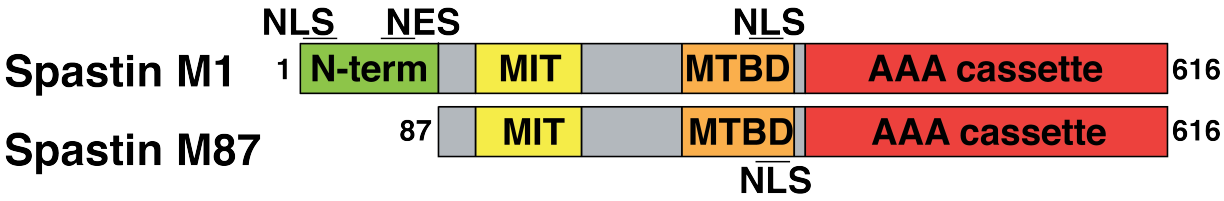

Figure 1. **Structure of spastin isoforms M1 and M87**

A first initiation codon at position 1 is responsible for the M1 isoform whereas a second initiation codon at position 87 is responsible for the M87 isoform. M87 lacks the N-terminal region with a hydrophobic domain. NLS, nuclear localisation signal; NES, nuclear export sequence; N-term, N-terminal domain; MIT, microtubule interacting domain; MTBD, microtubule binding domain.

- The ATPase AAA cassette, located at the amino acid residues 342 to 599. This cassette contains three conserved ATPase domains, the Walker motif A; the Walker motif B; and the AAA minimal consensus sequence, at amino acid residues 480 to 498. The two Walker motifs are important for the catalytic ATPase activity [45]. This cassette is necessary for spastin microtubule-severing function [122].

Two nuclear localization signals (NLS) are present at the amino acid residues 4 to 10 and 309 to 312, and two overlapping nuclear export signals (NES) have been found between residues 60 to 76. Since these two NES are only present in the M1 isoform, they presumably lead to its absence from the nucleus, in contrast to the M87 isoform [113, 124].

Functions

Microtubule severing

One of the main functions of spastin is to break microtubules into shorter fragments by removing tubulin dimers from the middle of the microtubule filaments, creating new dynamic plus-ends. This function requires the MTBD domain in order for spastin to bind to the microtubules and the AAA+ cassette to severe the microtubules [122, 123, 125].

Spastin monomers appear to first bind to the microtubules through electrostatic interactions. This weak bond allows them to migrate along the microtubules until they encounter additional subunits with which they can first dimerize before rapidly forming a homo-hexameric ring with additional subunits [123, 125, 126]. The pore at the center of this hexameric ring binds to the negatively-charged carboxy-terminal tail of tubulin and pull it out from the microtubule filament, leading to the severing of the microtubule in an ATP hydrolysis-dependent manner [122, 125, 127]. The severing of microtubules allows for the regulation of the microtubule dynamics, as it controls the number of microtubules and the amount of dynamic plus-ends available [128-130].

As the severing activity of spastin depends on the negatively-charged β-tubulin tails, microtubule modifications that increase these negative charges lead to a higher activity of spastin. This is the case for example with polyglutamylation, which usually happens in the more stable regions of microtubule filaments (compared to the more dynamic ends) and thus

stimulates spastin severing of the microtubules in these stable regions, rather than at the ends of the filaments [131]. However, after a threshold of glutamylation has been reached, it inhibits spastin activity by lowering its mechanochemical coupling, and spastin stays bound to the microtubules without severing them, thus adding to their stabilization [132].

The microtubule-severing functions of spastin appear to be necessary for different cellular processes, including at the centrosome and midbody [133, 134] and for abscission at the end stage of cytokinesis [135-137]. Spastin is also involved in axonal outgrowth and branching, presumably through its microtubule-severing activities: depletion of the spastin ortholog in zebrafish embryos led to impaired outgrowth of the spinal and branchiomotor neurons [138-141]; in *Drosophila*, lack of the spastin ortholog led to decreased NMJ synaptic area and an increased number of synaptic buttons, accompanied by an accumulation of acetylated-tubulin at the NMJ presynaptic terminal, while the total amount of tubulin was reduced [142-144];cultured rat hippocampal neurons lacking spastin showed shorter, less branched and less numerous branched primary neurites [145], and a similar result was found in SPG4 patient-derived neurons, with an increased number of acetylated-tubulin [146]. As acetylated-microtubules are more stable, these results indicate a reduce severing of stable microtubules due to a lack of spastin [147].

These last studies show that microtubule severing is important for proper axonal outgrowth and for the formation of new branches. Severing microtubules leads to a greater number of plus-ends, and these more dynamic microtubules plus-ends are necessary for efficient microtubule transport, in order to have rapid movement of cargos in a concerted manner, for interactions with microtubule-binding proteins and the cellular cortical structures, in addition to being essential for the generation and maintenance of the microtubule arrays [148-150].

Other functions

While it appears that the main function of spastin is its microtubule-severing activity, spastin is also involved in other cellular processes:

One of the main other function of spastin is mediated by the N-terminal hydrophobic region present only in the M1 isoform. This hydrophobic region forms a hairpin that can insert

in tubular ER membrane and interacts with the hairpin regions from atlastin 1 and REEP1, other proteins that are mutated in HSP (SPG3A and SPG31 respectively) [69, 117, 118]. It is thought that these three proteins cooperate to help shape the curvature of the ER tubules, and spastin may mediate the ER-microtubule interactions necessary to build the ER network [18, 69, 151, 152].

Through its MIT domain, spastin interacts with CHMP1B and IST1, two proteins involved in the ESCRT-III complex, which is implicated in cytokinesis and endosomal sorting [18, 119, 135, 136, 151]. It is through this interaction that spastin is brought to the site of abscission at the end stage of cytokinesis. But the ESCRT-III complex also promotes the fission from the recycling tubules of the endosome and helps control the balance between receptor degradation and recycling [141, 151]. Spastin is also important to regulate BMP signalling, through its inhibition by a yet unknown mechanism [153].

SPAST mutations in HSP (SPG4)

More than 200 mutations in *SPAST* have been identified in SPG4 patients from more than 130 families and novel pathological variants are regularly found [45, 49, 154, 155]. While the vast majority of the missense mutations are clustered around the AAA cassette, other nonsense, splice site and insertion/deletion mutations are found all over the gene, with the exception of the fourth exon, which is alternative spliced [115, 155]. Additionally, around 18% to 20% of patients have large deletions [41, 156, 157]. This large panel of different type of mutations point to a general loss-of-function due to haploinsufficiency as the main pathological mechanism, especially of the microtubule-severing functions, as most mutations are located around the AAA domain and lead to truncated proteins. However, no correlation between specific mutations and the severity of the phenotype has been established [154, 155, 158, 159].

Mutations of spastin are responsible for 40% of AD-HSP, but this number can be as high as 60% in some populations [32, 49]. Similar to other types of HSP, the clinical presentation (pure or complicated HSP), the severity of the disease (walking but not running; walking with aid; wheelchair bound), the age of onset (mean age of onset at 29 years old but ranging from 1 year of age to around 80 years old) is variable, and this variability can be seen

in a family sharing the same mutation [160]. The penetrance of the mutations is usually high but age dependent, with an estimated 50% penetrance at 27 years old, and 80% at 50 years old, while 6% of cases that will remain asymptomatic [161]. SPG4 usually presents with a pure HSP, but patients with complicated HSP have been identified, with cognitive impairments, cerebellar signs or epilepsy for example [39, 162, 163].

Most SPG4 mutations are nonsense, insertions and deletions and splice site mutations may lead to the truncation of the spastin protein due to the presence of premature stop codons [120, 155]. This phenomenon could induce non-sense mediated RNA decay and while truncated mRNA are detectable in some mouse models [164, 165], no truncated spastin protein has been detected in mouse brain [164-166], lymphoblastoid cell lines derived from human SPG4 patients [167] or neuronal cells derived from fibroblasts of SPG4 patients [146, 168], underlining the idea that truncated mutant spastin are either not expressed, less stable than the full-length proteins, or expressed at levels too low to be responsible for the axonal degeneration through a toxic gain-of-function mechanism. Thus, as SPG4 are autosomal dominant HSP cases, haploinsufficiency is the favoured pathophysiological mechanism.

Additionally, 25% of spastin mutations are missense mutations and the majority of these are also located in the AAA domain [154, 155]. The general view is that these missense mutations lead to a full-length but dysfunctional protein preventing the optimal severing of microtubules [115, 130]. As spastin must assemble as a hexamere in order to sever microtubules, a dominant negative mechanism is possible in the case where a dysfunctional spastin protein is produced due to missense mutations in the AAA domain, preventing the proper function of the spastin hexamere [129, 130].

Zebrafish has been previously used to study Spastin loss-of-function, and these results will be presented in a later section.

Amyotrophic lateral sclerosis

Definition and epidemiology

Amyotrophic lateral sclerosis, also known as Lou Gehrig's disease in North America, maladie de Charcot in France and more generally as motor neuron disease (MND) in the UK and Australia, is a late-onset progressive neurodegenerative disorder that affects both upper and lower motor neurons, leading to muscle atrophy with spasticity and is the most common MND [169, 170]. The disease onset is around 60 years of age overall [170], with a median survival period of 2-4 years post disease onset [171, 172] and death is usually caused by respiratory failure, due to diaphragm denervation [173]. While in some patients cognitive dysfunction can be seen, there are no sensory or autonomous abnormalities [169, 174]..

The global worldwide incidence of ALS is around 1.6-2.1 person per 100,000 per years [170]. Most epidemiological studies come from Europe, where the global incidence is of 2.16:100,000 [171]. The incidence also varies according to gender, as males are more prone to develop ALS, with a male to female ratio of 1.3:1 [170, 175] and by age, as the incidence increases with age until 75 years old and then decreases [176]. The prevalence is estimated to be around 5.40:100,000 in Europe [170], but both the prevalence and the incidence vary geographically [169]. The lifetime prevalence of developing ALS is estimated to be around 1:350 for men and 1:400 for women [177]. In Canada, the most recent study found an incidence of 3.29:100,000 in British Colombia [178], while the Canadian prevalence is estimated to be around 10:100,000 by the Canadian Community Health Survey, although they do advise caution as the coefficient of variation is between 16.6% and 33.3% [179].

Diagnosis

The difficulties in distinguishing between the different MNDs translate into difficulties in making a clear diagnosis of ALS [180]. In 1994, the El Escorial diagnosis criteria for ALS were established by the World Federation of Neurology and have been regularly updated to incorporate recent genetic and neurophysiological advances [19, 181, 182]. However, the diagnosis remains in most cases by exclusion, taking 9 to 15 months on average to be

established and can only be confirmed by post-mortem examination of the brain and spinal cord [22, 170].

Clinical features

ALS is a heterogeneous disorder, with a variable age of onset and disease progression. The mean age of onset of typical ALS is around 54-67 years old, with a median time of survival of 2 to 3 years, following respiratory failure [183]. However, 10% of patients survive for more than 8 years [184]. ALS can be classified depending on the localisation of the first symptoms at onset (**Figure 2**): spinal ALS occurs in 65% of the cases, when distal members are the first to be affected; in 30% of cases, the first manifestations of the disease are in the bulbar area and consist of dysarthria and dysphalgia, the muscles of the tongue being the first affected; the remaining 5% have respiratory problems as the first symptoms, leading to dyspnea [171, 185, 186]. The spinal form of ALS has a better prognosis, followed by the bulbar form and then the respiratory one [185]. Disease progression depends on the site of onset of the first symptoms, as motor neurons are affected in a sequential manner [187]. The symptoms are usually asymmetrical and underscore the loss of LMN, with cramps, weakness, muscular atrophy, denervation and sometimes fasciculation, as well as the loss of UMN with spasticity, hypertonia and hyperreflexia [188]. The progression of the disease is ineluctable, causing a general paralysis. The patient's condition becomes critical following denervation of the respiratory muscles, leading to respiratory failure. Cerebral functions were first thought to be fully preserved in all ALS cases, but it is now well known that around 13% of ALS patients also suffer from fronto-temporal dementia (FTD) and up to 50% have cognitive or behavioural impairments [174, 189]. ALS is now considered to be part of a clinical continuum with (FTD), as there are overlapping genes and clinical features between the two diseases, with some patients presenting with pure ALS, some with pure FTD, and some with symptoms of both diseases (**Figure 6**) [190].

Treatments

More than 30 years after the discovery of the first gene implicated in ALS [191] and after dozens of phase II and III clinical trials [192], riluzole is the only drug approved

worldwide to treat ALS [193, 194]. Riluzole stabilises sodium channels and is thought to reduce excitotoxicity. It has but a modest effect on the life expectancy of patients, prolonging life by 2 to 4 months on average by extending the time spent in the last stage of the disease [195-197]. Similar to HSP, most treatments are used to alleviate the symptoms of ALS, as well as monitoring closely the patient in term of nutritional and respiratory care [186] Recently, a new drug, edaravone was allowed to bypass regular FDA, Japanese and Canadian processes to be allowed as an ALS treatment, but not European ones [198]. Edaravone reduces oxidative stress and seems to be efficient for patients with mild symptoms and a short disease duration however its administration is difficult and the treatment is 2.2 to 12 times more expensive than riluzole [199].

Neuropathology

Atrophy of skeletal muscles, as well as sclerosis of the corticospinal and corticobulbar tracts are amongst the major pathological hallmarks of ALS. Additionally, thinning of the hypoglossal nerves and of the ventral roots of the spinal cord are also present. These symptoms are accompanied by a loss of around 50% of LMN and a more variable loss of UMN. Signs of denervation of re-innervation of skeletal muscles are also present, as are astrogliosis, spongiosis and microglial activation [200-202]. However, the major histopathological hallmark is the presence of aggregated and accumulated ubiquitin-positive inclusions in the cytoplasm of motor neurons. In ALS cases due to mutations of *SOD1*, SOD1 is the main protein found inside these aggregates [203]. On the other hand, in cases due to mutations of *FUS*, FUS is the main protein found in these aggregates [204, 205]. However, in the remaining ~97% cases of ALS, whether they are due to mutations of *TARDBP* or not, TDP-43, the protein encoded by this gene, is the main protein found in these aggregates [206, 207]. Whether these aggregates are pathological or are a protection mechanism of the cell to prevent the toxicity of insoluble high-molecular weight toxic complexes is still highly debated.

Aetiology

The causes of ALS are numerous and in still mostly unknown, a set of genetic and environmental factors combining to increase the risk to develop the disease [208]. Several

epidemiological studies have been done to try to understand the influence of different environmental and societal factors (Recently reviewed in [209]. A consensus has been reached for the increased risk of ageing and being male while smoking has been established as a possible risk, the latter in particular for women. However, there is still much debate about other potential risk factors such as physical activity, pesticide and heavy metal exposition and military service. Unfortunately, many epidemiological studies suffer from a sampling size that is too small, an inadequate methodology and a lack of reproducibility, making it harder to interpret the results [209, 210]. The genetic causes of ALS are not fully deciphered but we are starting to understand them better.

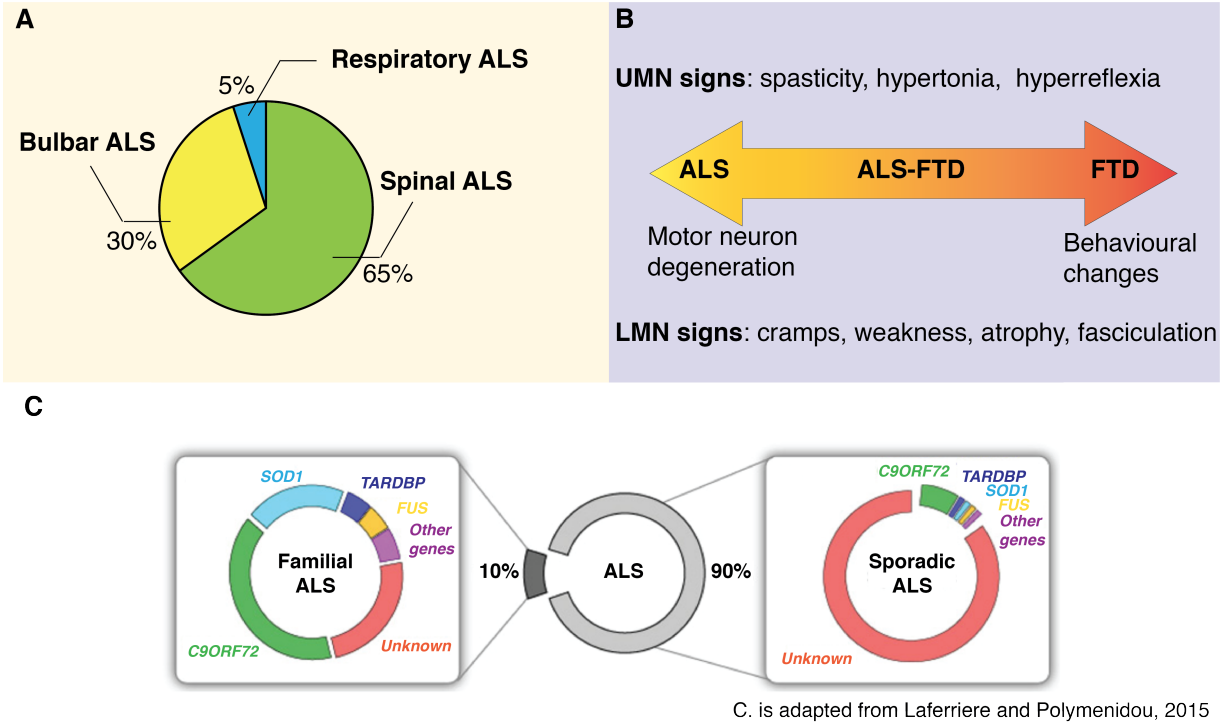

C. is adapted from Laferriere and Polymenidou, 2015

Figure 2. **Classifications of ALS**

ALS can be classified in different ways. (A) Classification of ALS by site of onset. (B) Classification of ALS on the spectrum with FTD. (C) Genetic classification of ALS based on the presence (familial) or absence (sporadic) of familial history of the disease (panel (C), is adapted from Laferriere and Polymenidou, Swiss Med Wkly, 2015 [211]).

Around 90% of ALS cases appear to be sporadic in nature (sALS, sporadic ALS), while the remaining 10% are heritable, with a familial history of the disease (fALS, familial ALS or hALS, heritable ALS) (**Figure 2**) [212]. There is however no difference in the presentation of the symptoms or in the natural history of the disease between the two forms of ALS [172]. Additionally, riluzole has a beneficial effect on both forms of the disease [197]. The percentage of fALS varies in different populations, but this number can be estimated to be as low as 5% and as high as 20% in individuals with European descent [213-216]. More than 25 mendelian-inherited genes have now been linked to ALS [217], and several of them have also been implicated in sALS [218]. A twin study estimated that the heritability of sALS to be around 60% [219]. The main causal genes of ALS that have been identified to date are *SOD1* (15%-20% of fALS and 1% of sALS [191]), *TARDBP* (4% of fALS and <1% of sALS [220, 221]), *FUS* (4% of fALS and <1% of sALS [222, 223]) and *C9ORF72* (30-40% of fALS and 7% of sALS, [224, 225]) and together they are responsible for up to 70% of all fALS cases and up to 10% of sALS (**Figure 2**) [212, 226].

TARDBP and *FUS*

The discovery of TDP-43, the protein encoded by *TARDBP,* in cytoplasmic inclusions found in neurons of ALS and FTD patients allowed for the first time to link *TARDBP* to ALS [206, 207]. Since then, more than 40 mutations have been found and account for 4%-6% of fALS cases and 1%-2% of sALS cases [212, 221, 227]. This discovery led to the identification of *FUS* [222, 223], encoding the protein FUS as a causative gene in ALS. TDP-43 and FUS are two structurally and functionally similar proteins implicated in RNA metabolism and the response to stress. However, the effect of these mutations on their functions and their role in the pathophysiology of ALS are still not fully understood.

Protein structure of TDP-43 and FUS

TDP-43

TDP-43 is encoded by *TARDBP*, a gene localized at the locus 1p36.22 and containing 6 exons [228]. TDP-43 is a 414 amino acids long protein of 43 kDa molecular weight. The protein is expressed ubiquitously as a homodimer [229]. Structurally, TDP-43 is similar to

other heterogeneous ribonuclear proteins (hnRNP) [230, 231]. Four domains can be identified (**Figure 3**):

- An N-terminal domain (amino acid residues 1-102), which can adopt a ubiquitin-like or a DIX-domain-like fold in solution [232, 233].

- It has two RNA recognition motifs (RMM), RRM1 (amino acid residues 106-177) and RRM2 (amino acid residues 192-259). The RRM1 is required not only to bind RNA but also DNA [230, 234, 235], whereas the RRM2 seems to be mainly implicated in the remodelling of chromatin and TDP-43 dimerization [235, 236].

- An intrinsically disordered carboxy-terminal domain at amino acid residues 274 to 414. This domain is separated in four additional regions, a glycine-rich motif, a hydrophobic segment, a glutamine/asparagine-rich region and a glycine/serine-rich region. This domain is involved in several aspects of splicing and the C-terminal region in general is responsible for protein-protein interactions, including interactions with other hnRNPs [234, 237-240]. Five phosphorylation sites are present in the C-terminus region, Ser 379, Ser 403/404 and Ser409/410 [241]. Two caspase-3 cleavage sites are localized at the amino acid residues 86-89 and 216-219, resulting in 35 kDa and 25 kDa fragments, although they can also be obtained by alternative splicing of *TARDBP* [242-244].

TDP-43 is a mainly nuclear protein, but up to 30% is found in the cytoplasm in physiological conditions [236, 245]. A bipartite NLS is found in the N-terminal region and a leucine-rich NES is located in the RRM2, allowing the protein to travel between the nucleus and the cytoplasm [230, 246-248].

FUS

The protein FUS is encoded by the *FUS* gene, located on chromosome 16p11.2 and containing 15 exons. Fus is a 526 amino-acid long protein and like TDP-43 it is a member of the hnRNP family [249, 250], as well as a member of the FET/TET family [251]. Several domains have been identified in the protein (**Figure 3**):

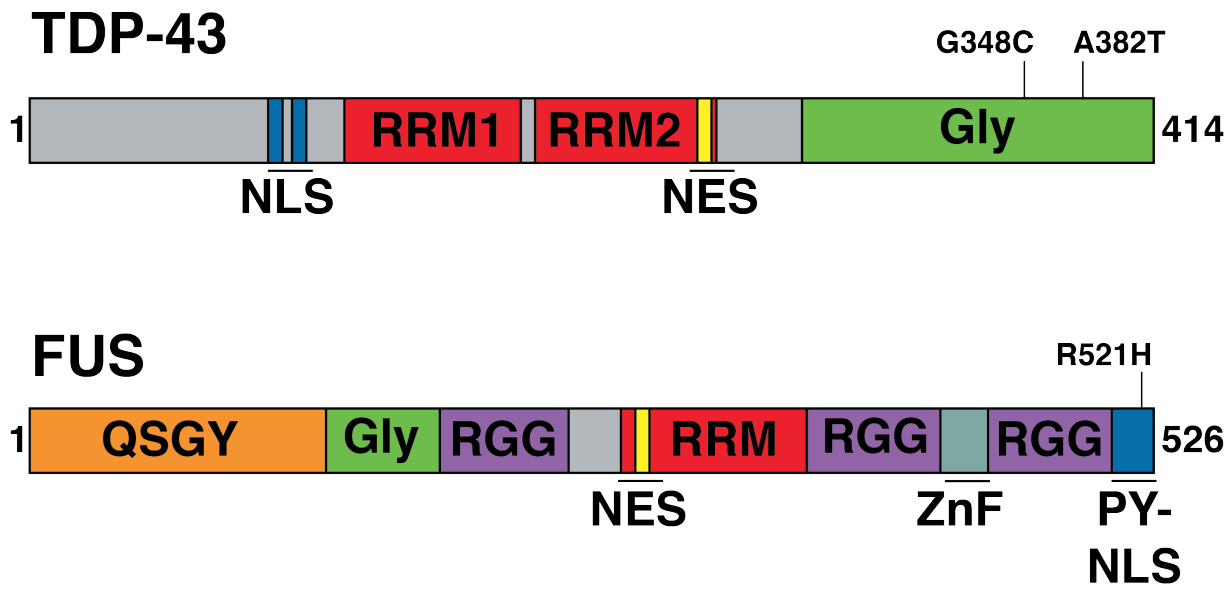

Figure 3. **Structures of the TDP-43 and FUS proteins**

TDP-43 and FUS are two structurally similar proteins. The two TDP-43 mutations and the one FUS mutation that have been studied as part of this thesis are indicated. RRM, RNA recognition motif; Gly, glycine-rich region; RGG, arginine/glycine/glycine-rich domain; QSGY, glutamine/glycine/serine/tyrosine-rich domain; ZnF, Zinc-finger domain; NLS, nuclear localisation signal; NES, nuclear export signal; PY-NLS, non-classical NLS.

- an N-terminal domain enriched in glutamine, glycine, serine and tyrosine residues (QSGY-rich domain, amino acid residues 1 to 162) , which is involved in transcriptional activation,

- a glycine-rich region, which is a prion-like domain (amino acid residues 163 to 213),

- an RRM (amino acid residues 279 to 360),

- several arginine and glycine rich regions which contains multiple arginine, glycine, glycine (RGG) repeats are found along the proteins, at amino acid residues 214-267, 361-412 and 447-497,

- a C2/C2 zinc finger motif (ZnF) found in the C-terminal region, at amino acid residues 413-446

These domains are all required to mediate the protein-RNA and protein-protein interactions. Similar to TDP-43, FUS is a predominantly nuclear protein in neurons and glial cells with a low amount in the cytoplasm in physiological condition [252]. This shuttling between the nucleus and the cytoplasm is accompanied through a NES located in the RRM, and a non-classical NLS, with a conserved proline and tyrosine residues (PY-NLS) is found at the C-terminus end of the protein, at amino acid residues 498-526.

Physiological functions of TDP-43 and FUS

TDP-43 and FUS, as RNA binding proteins, have a plethora of physiological functions pertaining to all steps of RNA metabolism, such as transcription, RNA splicing, RNA transport and stability and miRNA biogenesis. Their functions are highly similar, although their exact targets seem to differ and some differences exist. They both carry functions in the nucleus and in the cytoplasm, which will be briefly summarized here (**Figure 4**).

Nuclear roles of TDP-43 and FUS: transcription, DNA repair, RNA splicing and miRNA

Transcriptional regulation

TDP-43 was first discovered in 1995 as a transcription factor [231]. Ou and colleagues showed that the protein binds to a pyrimidine-rich sequence of the Transactive response element via its RRM domains, repressing the expression of long terminal repeats of the human immunodeficiency virus-1. It is from this first role that derives its name, Transactive response (TAR DNA-binding protein – *TARDBP* and TDP). TDP-43 also repress the expression of SP-10, coding for the acrosomic sperm protein in somatic tissues and this regulation requires not only RRM1 but also the C-terminus of TDP-43 [253]. Similar to TDP-43, FUS was first identified as a transcription factor for external transcribed spacer-related gene ERG in acute myeloid leukemia, through binding of chromatine by its QGSY-rich region [254-257]. Since then FUS was shown to be involved in the transcription activation of several genes, including RNA pol III [258]. FUS is also a co-activator of several transcription factors including NF-kappaB [259].

DNA repair

Contrary to TDP-43, FUS also has a role in DNA repair, as it promotes homologous recombination during DNA double-strand break repair [260]. Additionally, FUS interacts with the Poly(ADP-ribose) polymerase 1 (PARP1) and HDAC1 protein at the site of DNA damage [261-263].

Pre-mRNA splicing

In addition to their role as a transcription factors, FUS and TDP-43 regulate the splicing of several RNAs. TDP-43 regulates the splicing of several genes such as the cystic fibrosis transmembrane conductance regulator (CFTR) [264], the apolipoprotein A-II [265], cyclic dependent kinase 6 [236] and survival motor neuron 2 (SMN2) [266]. FUS also participates directly and indirectly in RNA splicing, as it binds to both SMN, to U1 small nuclear ribonucleoprotein (snRNP) and to Sm-snRNP complex, which are all necessary for proper assembly of the spliceosome [267, 268]. TDP-43 can also regulate splicing in combination with other proteins. For example, TDP-43 interacts directly with the SMN protein, implicated in the assembling of the spliceosome [266]. TDP-43 is also a member of an hnRNP complex which functions include the inhibitions of exons splicing [240]. TDP-43 and FUS also interact via TDP-43 C-terminus and together they co-regulate the mRNA of histone deacetylase 6 [269].

Several studies have been done to identify the RNA targets of both FUS and TDP-43 through either regular cloning or high-throughput methods [270-274]. More than 6000 RNA targets have been identified for TDP-43, and it was shown that TDP-43 preferentially binds RNA presenting UG-rich motifs mainly in intronic regions, and at the 3'-UTR [274]. Most of the targets are involved in synaptic formation and function, regulation of neurotransmitter processes, splicing, RNA processing and maturation, and include several genes involved in neurodegeneration such as *Fus*, *Grn*, *Mapt*, *Atxn1*, *Atxn2* and *Tardbp* itself [275]. Indeed, TDP-43 binds to its own transcript and autoregulates its own levels by binding to its 3'UTR inducing differential regulation of polyadenylation sites by splicing [276]. This process leads to very well-regulated TDP-43 levels in the cells. FUS also binds to more than 5,500 RNAs,

many of them having long introns [270, 277]. While several studies have tried to identify FUS targets [270, 277-283] there is little overlap between these different data sets [284]. Similarly to TDP-43, FUS can bind to its own pre-mRNA to regulate its expression level, this time by causing non-sense mediated decay [285]. TDP-43 is also important to control the splicing of non-conserved cryptic exons, as it represses their splicing, preventing them from being expressed, which would introduce frameshifts leading to premature stop codons and nonsense mediated decay [286-288]. This control of cryptic exons seems to be cell specific [289].

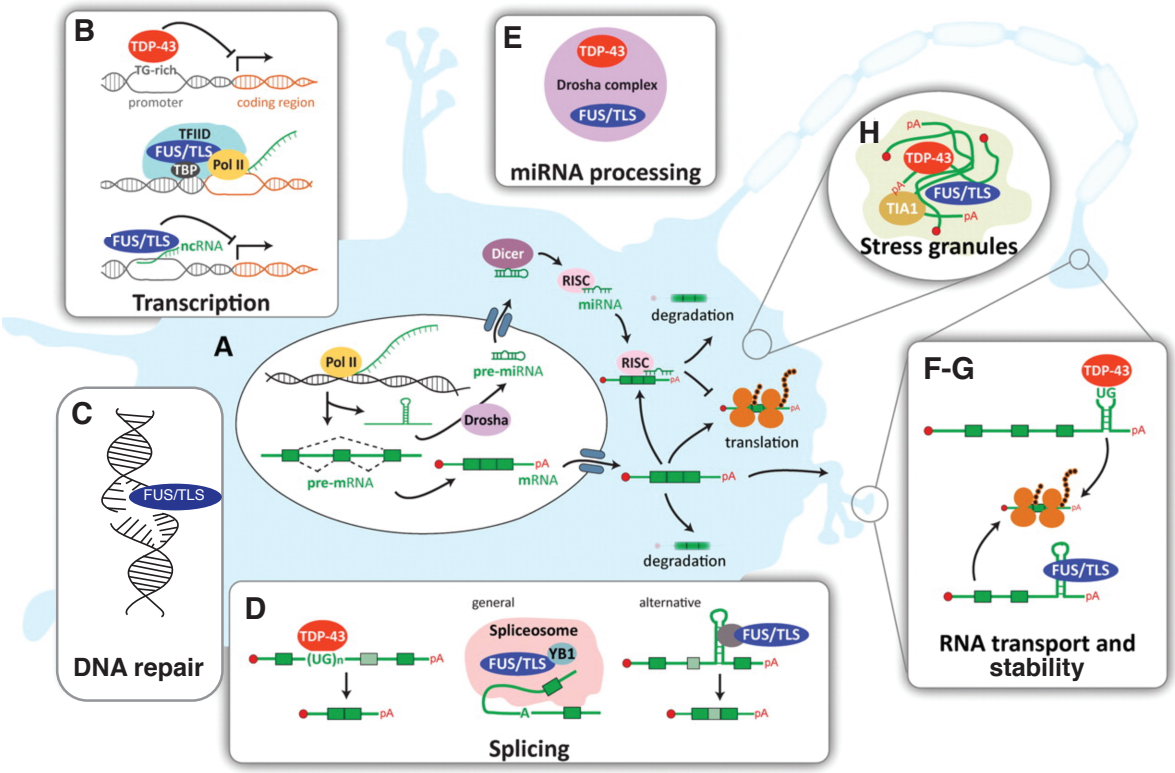

Adapted from Lagier-Tourenne et al., 2010

Figure 4. **Functions of TDP-43 and FUS**

TDP-43 and FUS have similar functions and are mainly involved in RNA metabolism. (A) is a general view of their functions and (B) to (H) display specific functions.

Figure adapted from Lagier-Tourenne et al., Hum Mol Genet, 2010 [290].

MicroRNA biogenesis

TDP-43 is implicated in the biogenesis of microRNA (miRNA) [291, 292]. Depletion of TDP-43 from the nucleus leads to the specific down-regulation of let-7b, a family of miRNA important for cellular differentiation [291]. Additionally, TDP-43 is associated with the Drosha complex, which is implicated in the biogenesis of primary miRNA [292]. However, TDP-43 has been shown to control the stability of the Drosha protein, thus having in theory a general responsibility in the biogenesis of all miRNA [293]. FUS colocalizes with TDP-43 at the Drosha complex [292] and it is in part responsible to recruit Drosha at the chromatin of active transcription sites to promote pre-miRNA processing [294]. FUS expression is also in part regulated through a negative forward loop by miR141 and miR200a, two miRNAs that are increased by FUS, and that bind to FUS own 3'UTR, leading to the down-regulation of FUS expression [295]. TDP-43 and FUS act in the regulation of splicing of several important genes and have a direct and indirect role on the biogenesis of miRNA. However, the role of TDP-43 and FUS in the RNA metabolism is not limited to the nucleus and continues in the cytoplasm.

Cytosolic functions of TDP-43 and FUS: RNA stability and transport, stress granules

mRNA stability

TDP-43 also participates to mRNA stabilisation. For example, TDP-43 interacts with the mRNA of *NFL* and this interaction stabilizes and prevents its degradation [238, 296]. FUS binds to the 3'UTR sequence of some of its mRNA targets and may be implicated in their transport to the cytoplasm and their stability. Indeed, FUS is part of a complex regulating mRNA 3'-end processing and polyadenylation, and is at least necessary for the stability of GluA1 mRNA [297].

mRNA transport

In addition to stabilizing NFL mRNA, TDP-43 also regulates its translocation to the cytoplasm and its translation [248]. In the cytoplasm, TDP-43 is found in cytoplasmic RNA

granules such as mRNA transport granules, which are responsible for stocking inactive mRNA transporting them to their translation sites, in particular to synaptic sites [298-301]. This transport depends on microtubules and involves different motor proteins [302]. TDP-43 has been shown to be enriched in dendrites, presumably to regulate local translation [301]. Like TDP-43, FUS is part of RNA granules transporting mRNAs to their site of translation in the dendrites [303, 304]. FUS is transported to dendrites not only by microtubules, but also through association with actin filaments and by a mechanism involving ER tubules and the neurofilament cytoskeleton [304-306].

Interestingly, TDP-43 is also found to be present in mitochondria and to repress expression of mitochondrial RNAs and seems to specifically be implicated in the impairment of the oxidative phosphorylation complex I [307, 308].

Stress granules

In stress situation, TDP-43 associates with stress granules, which are responsible for triage of stalled mRNA under stress conditions and to selectively promote mRNAs necessary for the response to the stress [309, 310]. Stress granules are formed in response to different stresses and TDP-43 is important for stress granules formation and maintenance [311-313]. These changes occur concomitantly with a redistribution of the protein from the nucleus to the cytoplasm, and with an increase in the expression level of TDP-43 [314-316]. FUS has also been shown to colocalize with some stress granule markers, although its exact role is still unclear [252, 317-321].

These data indicate the complex roles that TDP-43 and FUS play in all the steps of RNA metabolism. It is thus not surprising that mutations in *FUS* or *TARDBP* lead to human disorders. However how these mutations lead to specific motor neuron phenotype in ALS is still a subject of debate.

TDP-43 and FUS in ALS

TDP-43-related ALS

The link between ALS and TDP-43 was established in 2006, when TDP-43 was identified as being one of the main components of the ubiquitin-positive inclusions found in the neurons of ALS and FTD patients [206, 207]. These inclusions are present not only in the spinal cord, but also in the temporal and frontal neocortex, in the central grey nucleus and in the limbic structures [206, 207, 322-326]. They are found mainly in the cytoplasm and in the dysmorphic neurites of neurons and glial cells, along with a loss of nuclear TDP-43 occuring early in the pathology [206, 207, 323-325, 327-330]. In these inclusions, TDP-43 is hyperphosphorylated and ubiquitinated and the 25 kDa and 35 kDa TDP-43 fragments are also present in these inclusions [206, 207, 331]. However, these C-terminus fragments are mainly found in the cortex and are rarely found in the spinal cord [328, 332]. These inclusions do not contain fibrils, are not amyloid and are referred to as being ubiquitin-positive, tau-negative and α-synuclein-negative [333]. This TDP-43 "pathology", as it is often called is found in almost all ALS cases, except the ones due to mutations of SOD1 or FUS [222, 223, 329, 334, 335]. It should be noted that TDP-43 pathology is not specific to ALS. It is also found in 80% to 94% of FTD cases, almost identical except for the absence of inclusions in the spinal cord [206, 207, 336]. Similar markings are found in other diseases, in 40% of Alzheimer's disease patients, mainly in the limbic system [337-339], in other type of dementia [338-340], in around 20% of Parkinson's disease patients [338, 340] and in some cases of Huntington's disease [341]. However, this pathology is also found in the brain of 29% of healthy patient 65 years old or older, mainly in the limbic system [342]. It is still debated whether this abnormal immunostaining of TDP-43 is a cause or a consequence of the neurodegenerative process, or whether it is part of a cell protection process that we still have to elucidate. Despite the presence of this pathology in a great number of neurodegenerative disorders, mutations of TDP-43 are mainly causative of ALS and rarely of FTD [343].

Following the first identification of these positive inclusions for TDP-43, several mutational analysis of *TARDBP* were done, leading to the discovery of the first causative

mutations of this gene in ALS patients [221, 227, 325, 326, 344]. Patients with *TARDBP* mutations have generally a classical presentation of ALS, sometimes with FTD and the so-called TDP-43 pathology [345, 346]. To this date, More than 50 mutations have been identified, but with variable penetrance [347, 348]. These mutations are mainly localised in the C-terminus of the protein encoded by exon 6 and are all missense mutations except for one, Y374X [349, 350]. It is possible that the different mutations lead to toxicity through different ways: for example, the P112H [351], N529S [352] and D169G mutation [221], are not found in the C-terminus, but in the RRMs and they could interfere with the binding of RNA and DNA or promote caspase-3 cleavage [244, 353, 354]. Several mutations can increase the propensity of TDP-43 to be phosphorylated, in particular the ones introducing threonine or serine residues, such as A315T or N267S. The mutation that interested us the most for this thesis, G348C, may increase TDP-43 tendency to aggregate, due to the introduction of a cysteine residue promoting intermolecular bridges [221].

Several animal models have been generated, including zebrafish, to study the mechanism of some of these mutations and study the pathogenicity of wild-type TDP-43. These results will be presented in a later section.

FUS-related ALS

Following the discovery of mutations in *TARDBP*, attention turned to other RNA binding proteins possible implication in ALS, leading to the discovery of mutations in FUS in some fALS cases and in sporadic FTD cases [222, 223]. Similar to TDP-43, FUS, a mainly nuclear protein, was found to be depleted from the nucleus and to accumulate in the cytoplasm, with a strong association to stress granules [355-358]. In ALS cases due to mutations in *FUS*, FUS is the main protein found in ubiquitin-positive inclusions in affected neuronal cells and not TDP-43 [222, 359]. Similarly to TDP-43, this FUS pathology (depletion from nucleus and cytoplasmic inclusions) can also be found in other disorders, such as in some FTD cases, in some polyglutamine diseases and in intranuclear inclusion body disease [358, 360, 361].

Mutations in *FUS* account for around 4% of fALS and 1% of sALS [362]. Postmortem histopathological studies of patients with FUS mutations showed a severe LMN loss, a less

severe UMN loss in the brainstem and a milder loss of UMN in the motor cortex [222, 223]. FUS pathological inclusions were found in neurons and glial cells and their number positively correlated with disease duration [363]. One important feature of FUS-causative ALS is a generally younger age of onset, as mutations of FUS are responsible for around 35% of ALS cases with an onset prior to 40 years old, the average of onset for ALS patients with FUS mutations is around 44 years old and juvenile ALS cases with patients as young as their late teens have been reported [205, 362, 364-366].

More than 50 FUS mutations have been identified in ALS cases, most of them missense mutations, with some mutations located in the 3'UTR [362, 367, 368]. The mutations cluster in two regions, with a first cluster of two-thirds of the mutations at the C-terminus of the protein, from the RGG2 to the PY-NLS, and a second cluster at the N-terminus, from the QGSY-domain to the RGG1 region, where the remaining one-third of the mutations are located. Interestingly, mutations in the C-terminus are more prevalent in fALS than in sALS, whereas the mutations clustered around the N-terminus are mainly found in sALS and may have poor penetrance [362]. The pathogenicity of all FUS mutations has not yet been confirmed, but zebrafish has been a model of choice to study ALS-related FUS mutations.

Zebrafish, a model system

In all four articles presented in this thesis, we have used zebrafish to study HSP and ALS, either by using previously published models or by generating additional models using new technology such as CRISPR/Cas9. In this section, I will briefly introduce the zebrafish and how it has been used for biomedical research.

Generalities

The zebrafish (*Danio rerio*) is a small teleost fish from South-East Asia that was first described in 1822 by Francis Buchanan-Hamilton in his book ''*An account of the fishes found*

in the river Ganges and its branches'' [369]. These fish are native of the Ganges River, and are found in most type of fresh water, from slow streams to stagnant ponds [370]. They are thus tolerant to a wide range of water parameters and became one of the most popular aquarium fish for this reason.

Zebrafish present many advantages for research, thanks to an ever evolving genetic toolbox, allowing for both forward [371] and reverse genetic screens [372]. Additionally, adult zebrafish, which are on average 3 cm in length, can be kept in high number in a small tank at a low price. They become sexually mature in 3 months and an adult female zebrafish can lay hundred of eggs in one day and reproduce weekly, giving rise to a high number of embryos with synchronized development. The eggs are externally fertilized and develop rapidly. The embryos are transparent, allowing for a direct observation of internal organs. Genetic manipulations are easy and are usually done by injecting a construct into newly fertilized eggs by using a needle connected to a micromanipulator. These advantages are similar to those of some popular invertebrates models such as *Caenorhabditis elegans* and *Drosophila melanogaster [373, 374]*, but are complemented by the fact that the structures and organs of the zebrafish are similar to those of mammals, although somewhat simplified. Additionally, the biological processes as well as the genetic pathways are similar to those found in mammals [375]. However, contrary to mammals, the embryos expressing lethal mutations can be studied without fear of a faulty uterine implantation, or post-hatching lethality, and this for several days.

Modeling diseases

Zebrafish have been used in research since the 1960s-1970s, in topics such as cancer [376], developmental biology and cognition [377] or toxicology [378], and were used by soviet cosmonauts during early space missions [379-381]. However, the development of numerous genetic and molecular tools in the 1980s placed the zebrafish in an ideal place as a reliable and pertinent research tool. The development of cloning [382], mutagenesis [383], transgenesis [384] and genetic cartography techniques [385] began the era of the zebrafish as an avant-garde genetic model. Its use was popularised in several fields of biomedical research such as cancer research [386], heart developmental and cardiac disorders [387], immunity and

infectious diseases [388], visual system and associated disorders [389], developmental biology [390], psychiatric disorders [391] and finally neurobiology and neurodegenerative disorders [392].

One of the advantages of zebrafish in MNDs is the fact that the zebrafish neuromuscular system is similar to those of mammals, albeit simplified [393-395]. Zebrafish embryos develop a motor circuit early in development, and the behaviour of this motor system has been extensively studied and is known to be extremely stereotyped [396].

The next sections will first detail the development of the zebrafish with emphasis on some key stage, followed by a more detailed description of its neuromuscular system, before detailing the different genetic tools that are available for zebrafish scientists.

Development and behaviour

Specific morphological features have been used to define the different stages and the transitions from embryo, larval, juvenile and adult fish. Most of the research done on zebrafish is during the first few stages of development, with embryonic and larval zebrafish.

Embryogenesis

The zebrafish stages of embryogenesis are well documented and have been described in details by Kimmel [395]. Embryogenesis of the zebrafish is defined to be from the time of fertilization until hatching of the embryo, which occurs around the 3rd day post fertilization (dpf), at the protruding mouth stage. It is divided into different stages based in parts on the hours or days elapsed fertilization (hpf, hours post fertilization).

The first stage is the zygote period (0 hpf – 0.75 hpf), during which the newly fertilized egg has its first cell division. Right after fecundation, cell division starts with the cleavage period (0.75 hpf – 2.25 hpf) and the fertilized egg goes from 2 cells to 128 cells in six rapid and synchronous cleavages. The blastula period (2.25 hpf – 5.25 hpf) sees the start of epiboly, which continues until the gastrula period (5.25 hpf – 10.33 hpf). During that stage, gastrulation starts, producing the primary germ layers in a few hours by a process of involution and convergence movements. Over the segmentation period (10.33 hpf – 24 hpf) and the

pahryngula period (24 hpf – 48 hpf), primary somatogenesis and organogenesis begin. The hatching period (48 hpf – 72 hpf) is a more variable period, as embryos from the same clutch may hatch anytime between 48 hpf – 72 hpf, and sometimes even earlier or later. By the end of this period, all of the organs have been at least rudimentarily developed.

From larvae to adulthood

Starting at the protruding-mouth stage (3 dpf), zebrafish are now considered larvae, until approximately the 30th day of development [397]. The larval stage marks the transformation of the embryonic features toward the juvenile stage of the development, where the fish acquire adult-like morphology [397, 398]. By 5 dpf, exogenous feeding begins and is crucial for the health of the fish by the end of the first week [399]. In order to feed themselves, a rapid development of the sensory-motor systems ensues, and several complex visuo-motor behaviours emerge by the end of the first week of development [400]. By the time they reach adulthood, at around 90 dpf, the fish are sexually mature. However, most studies on larval zebrafish have been done at the early-larval stage, as experimental accessibility decreases with age.

All of these behaviours necessitate a functional neuromuscular system, which development is first established during embryogenesis.

Neuromuscular system

The trunk and the spinal cord of the zebrafish embryo are divided into thirty or so segments called somites, which will give rise to the muscles, bones and skin [395, 401]. Each somite contains a similar set of neurons, including interneurons, sensory neurons and motor neurons [402, 403]. The spinal motor neurons appear in 2 phases, giving rise first to the primary motor neurons and then to the secondary motor neurons.

Primary motor neurons

Each somitic hemisegment is innervated by three primary motor neurons, which appear during gastrulation at around 9-10 hpf [404, 405]. They are located in the medial motor column and are easily recognizable by their large cell body. Each of these three neurons is

positioned in the rostro-caudal axis in a very stereotypical and this positioning is used for nomenclature: the most rostral MN is named rostral primary motor neuron (RoP); the most caudal one is named caudal primary motor neuron (CaP); and the one in between these two is named middle primary motor neuron (MiP) (**Figure 5**) [404]. The CaP is the first of the primary motor neurons to extend its axon outside the spinal cord, through an exit point called the ventral root exit point. CaPs axons then go on to innervate muscle fibres from the ventral myotome. MiPs are the second primary motor neurons to extend their axons. Since the MiP soma is more rostral, its axonal growth cone must first extend caudally to reach the ventral root exit point. They then fasciculate with the CaPs axon until the horizontal myoseptum and then extend dorsally to innervate the muscle fibres of the dorsal myotome. The RoPs axons are the latest to extend, and will extend caudally and fasciculate with the axons of the MiPs, and then of the CaPs after reaching the ventral root exit point. They will then innervate the muscle fibres in the region of the horizontal myoseptum (**Figure 5**) [404, 406]. The primary motor neurons start their differentiation at around 15 hpf and their axons start innervating their targets at around 17 hpf [406]. They persist through adulthood and are involved in the startle response and fast swimming [315, 407, 408]. Another kind of primary MN called variable primary motor neuron (VaP) are also present and innervate the muscles fibres located between the ones innervated by the RoP and the MiP. However, they undergo apoptosis at around 36 hpf [409-411].

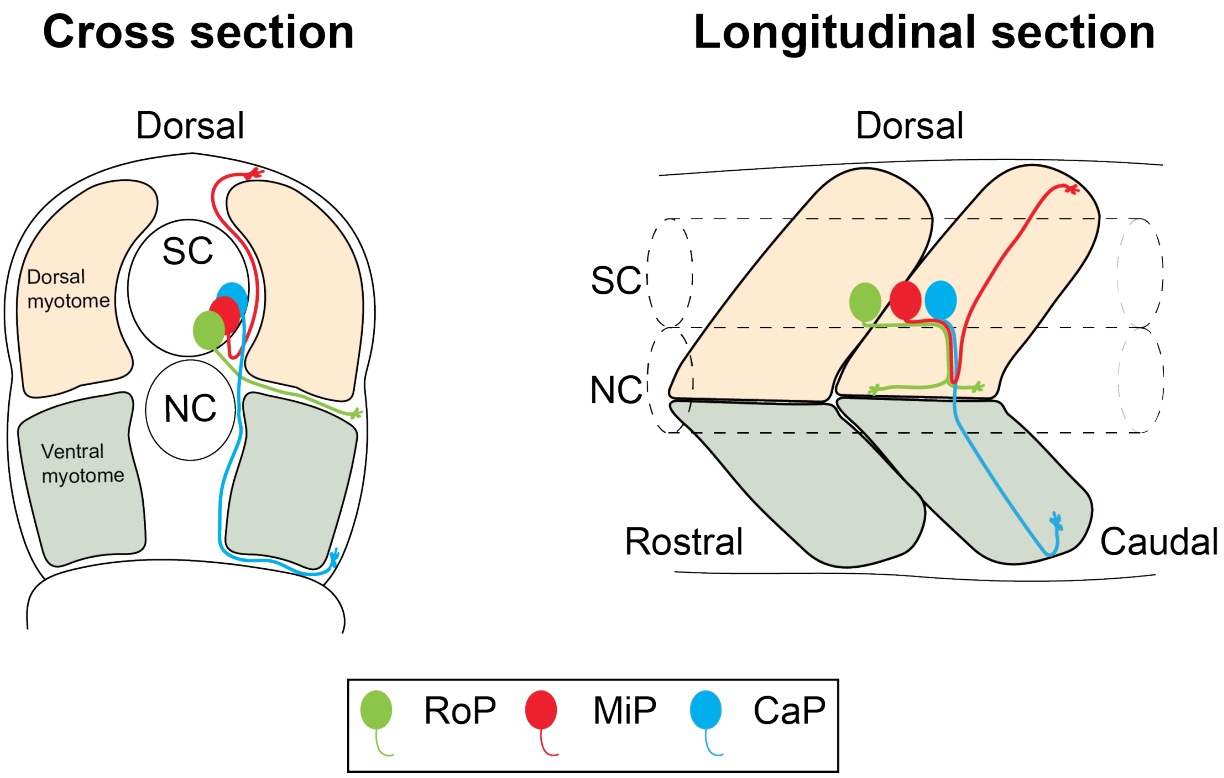

Figure 5. **Schematic representation of primary motor neurons in the zebrafish embryo**

Primary motor neurons have a stereotyped positioning along the rostro-caudal axis and axonal pathfinding. RoP, rostral primary motor neuron; MiP, middle primary motor neuron; CaP, caudal primaru motor neuron; SC, spinal cord; NC, notochord.

Secondary motor neurons

The secondary motor neurons start to appear around 14-15 hpf and start extending their axons by 26 hpf [405, 406, 412]. Approximately 30 secondary motor neurons are present in each hemisegment. Their cell bodies are smaller, their axons are finer and their axonal arborisations are less dense than those of primary motor neurons. The axons of both primary and secondary motor neurons fasciculate to create the ventral motor nerve [406, 412]. Their somata are located in the medial motor column and innervate both fast and slow myotomal

muscles [413, 414]. They are mainly involved in slow swimming, but are also recruited during fast swimming and the startle response [407, 408, 413-415].

Muscle fibres

Similarly to the segmentation of the early spinal cord in distinct somites, the early zebrafish musculature consists in a series of myomeres arranged in a rostro-caudal pattern [416]. Two different types of muscle fibres are found in this myomeric musculature. The slow fibres are mononucleated and fatigue-resistant and form the superficial monolayers found directly under the skin [417-419]. The fast fibres result from the fusion of myoblasts and thus are multinucleated. They are fatigable, found deeper in the myotome and form the majority of the musculature [420, 421]. In the zebrafish embryos, the first motor behaviours, such as spontaneous coiling and the response to touch are mediated by these slow fibres [422-424]. But burst swimming is mediated by fast fibres [425]. In the adult fish, there is a polyneural and multiterminal innervation of the muscle fibres, and one primary MN and up to four secondary motor neurons innervate each fast fibre, whereas each slow fibre is innervated by several secondary motor neurons [426]. This differential control of the two types of fibres allow for different uses and functions depending on the type of movements required. Slow fibres are active during sustained swimming, whereas fast fibres get activated during rapid swimming movements such as the escape response [416].

Establishment of the first motor behaviours

Between 15 and 17 hpf, the axons of the primary motor neurons start exiting the spinal cord and first migrate near the center of the body segment. They form “en passant” synapses along the way with muscle cells [427, 428] and the first motor behaviours are observed as soon as 17 hpf, when the axons of the primary motor neurons reach their targets and start forming the neuromuscular junctions [428, 429]. These are cholinergic synapses, and are thus using acetylcholine as a neurotransmitter [430].

The first motor behaviour consists of a spontaneous contractile activity starting at 17 hpf and is mediated by contractions of the trunk and tail which are propagated in a rostro-caudal orientation, alternating between both sides of the embryo. The maximum frequency of these

spontaneous single coils is of 1 Hz at 19 hpf, before going down to 0.1 Hz at 24 hpf, leading to the hatching of the embryo at around 52 hpf [424]. The response to touch develops around 21 hpf, and at that time consists of 1 to 3 contractions, the first being always contralateral to the tactile stimulus and the next ones alternating between the ipsilateral and contralateral sides [424]. The superficial slow-twitch muscles mediate these two first motor behaviours [424, 431, 432]. Starting at 24 hpf, the spontaneous motor behaviour starts to get more complex with the appearance of double coiling, consisting in two contralateral contractions of the trunk within 1 second. By 27 hpf, these double coils represent the majority of the spontaneous events [433]. Finally, at around 27-28 hpf, swimming episodes start to appear, characterized by high frequency and low amplitude contractions, resulting in a forward displacement of a few centimeters of the hatched embryo [424]. The swim frequency is approximately 8 Hz at 28 hpf and increases to reach 30 Hz to 70 Hz in embryos of 52-55 hpf [415]. These events of burst swimming are mediated by fast-twitch muscles [425]. The use of high-resolution videography to study the motor behaviour of 48-55 hpf embryos allow for a global and fast analysis of the motor activity. Since this activity is extremely stereotyped, any change is in theory easily observable and quantifiable and can be used to study mutations linked to MNDs [392].

One of the main drives towards the use of zebrafish in research in the 1980s-1990s was to understand developmental processes including motor behaviours. The zebrafish was first used for forward genetic studies and with the development of new genetic tools, it also revealed itself as an ideal model for reverse genetic studies. In the last 10 years, different genome editing techniques have been developed in the zebrafish community, including two during the course of this thesis (TALENs and CRISPR/Cas9), adding new genetic tools to the well-diversified ones already present. The strength of the zebrafish as an animal model to study human diseases and in particular MNDs depends in part on how strong and precise the genetic tools available are. While not all the techniques described in the following section have been used for this thesis, most have been used by other zebrafish researchers studying MNDs.

The zebrafish genetic toolbox

The zebrafish genome

One of the strength of the zebrafish as a model organism is its well-characterized genome. Long efforts started in the 1990s by the creation of the genetic map [434, 435], followed by the creation of the Zebrafish Genome Sequencing Project by the Sanger project in 2011 (http://www.sanger.ac.uk/science/data/zebrafish-genome-project), eventually led to the complete sequencing of the zebrafish genome [436], with regular updates in the assembly leading to better annotation, the latest being the GRCz11, released in may 2017 (https://www.ncbi.nlm.nih.gov/grc/zebrafish).

For relevance to the use of zebrafish to study human diseases, 71,4% of human genes have at least one zebrafish ortholog, and amongst these, 47% have a one-to-one relationship with their zebrafish ortholog. Inversely, 69% of zebrafish genes have at least one human ortholog. Howe and colleagues also compared the 3,176 human genes listed in the Online Mendelian Inheritance in Man (OMIM) database to the zebrafish genes and found that 82% have at least one zebrafish ortholog, highlighting the potential use of zebrafish to study human disorders [436].

One of the striking features of the zebrafish genome compared to the human one, is the fact that like other teleost, it underwent a third round of whole genome duplication in addition to the two rounds that occurred in early vertebrates [437-439]. This teleost-specific whole genome duplication occurred at the base of the teleost fish lineage, 350 to 320 million years ago [437, 439]. As a result, zebrafish, with an estimated number of 26,842 genes [440], have more genes than the current estimate of 22,333 for human [441, 442]. Additionally, many zebrafish genes have one or more paralogs, and amongst the estimated 26,842 zebrafish genes, 3,991 duplicated gene sets have been identified. The function of these duplicated genes may be similar, divergent or completely lost compared to the original paralog [440].

This fully sequenced genome now facilitates research for zebrafish scientists. However, many different genetic tools were developed before this achievement and shaped the use of zebrafish in research. In the following sections, an overview of some of the most important techniques is

given, in a generally chronological order, from mutagenesis, transgenesis and transient techniques, to the more recent precise genome editing possibilities.

Mutagenesis

TILLING

TILLING, or targeting induced local lesions in genome, is a technique that allows identification of induced lesions in loci of interest following mutagenesis by the the alkylating agent N-ethyl-N-nitrosourea (ENU). TILLING was first implemented in the Henikoff laboratory to identify desired mutant alleles in the genome of Arabidopsis following mutagenesis [443, 444] and was quickly adapted in the zebrafish [445, 446]. The protocol starts with a classic ENU-mutagenesis and individual genomic DNA from these fish is obtained to create a library of potential mutants and regions of interest are sequenced to identify the presence of induced-lesions in specific loci or genes. The individual fish with the desired mutations is then outcrossed to generate the new mutant line [446]. This method allowed for the generation of many zebrafish mutant lines, including several of used for MNDs, such as the creation of a knockout *tardbp* line to model TDP-43 [447].

Transgenesis

Tol2 transposon system

Most zebrafish transgenic lines are done using the Tol2 transposon system first identified in Medaka [448-450]. This minimal Tol2 sequence is only around 200 bp long and can be easily cloned to the flanking side of the transgene of interest [451]. A series of Tol2 vectors have been made freely available for zebrafish scientists through the Tol2kit multisite Gateway system, democratizing the process of generating transgenic fish [452, 453] (http://tol2kit.genetics.utah.edu).

Conditional transgenesis

With efficient transgenesis techniques came the possibility of generating conditional transgenic lines, allowing for the toxic overexpression of wild-type, mutant, dominant-negative or dominant-active versions of a gene, that may prevent the proper development of

the zebrafish and thus the transmission of the transgene to the next generations. They also allow for spatial and temporal control of the expression of the transgene depending on the chosen promoter. Tissue specific promoters can be used for spatial expression of the transgene, such as the *cmlc2* promoter for cardiac expression [454] or the *elavl3* promoter (formerly known as *HuC*) for an early marker of post-mitotic neurons [455]. The use of an inducible promoter allows for a temporal control of the transgene expression. One such promoter is the *hsp70l* promoter, which allows for expression of the transgene following a heat shock above the normal rearing temperature of the fish [456].

Transient modifications

Knockdown techniques

Morpholino

Morpholinos are designed as artificially synthesized oligonucleotide, where the ribose backbone of nucleic acids have been replaced by morpholine rings, making these antisense oligonucleotides resistant to nuclease digestion, and with an enhanced binding ability to the complementary RNA sequence [457, 458]. These single-stranded antisense oligonucleotides target the RNA of the gene of interest, either at the translation start site, targeting the 5'-UTR of the mature mRNA and preventing translation and blocking the mRNA in the cytoplasm by hindering ribosomes assembly [372, 459]; or at regions spanning splicing donor or splicing acceptor sites, preventing the normal splicing the pre-mRNA by inhibiting binding of spliceosome components and blocking it in the nucleus [459, 460]. Their popularity grew during a time where efficient stable reverse genetic techniques were not yet available in the zebrafish community, as a way to efficiently and rapidly analyse gene functions through a loss-of-function paradigm, in the context of zebrafish development.

Morpholinos are injected early after the eggs fertilization, during the 1- to 8-cell stages. Since they are resistant to degradation, they remain in the cells, but the quantity of morpholinos present in each cells decreases with each division, and this diluting effect renders the morpholinos effective only during the first few days of development, up until 3 to 5 dpf. As such, they are useful for *in vivo* analysis of gene function only as a transient, functional

knockdown. Additionally, off-target effects due to non-specific up-regulation of the p-53 apoptosis pathway occurs with the use of 15% to 20% of morpholinos and can confound the observed phenotypes [459, 461, 462]. One important caveat in the use of morpholinos are studies that showed that when morphants and mutants phenotype were compared for equivalence, around 70 % did not have a similar phenotype [463, 464].

Despite these caveats, and while the use of other reverse genetic methods have now been developed and allowed for the generation of germline transmissible mutant lines, morpholinos are still widely used in the zebrafish community, as they allow for a rapid analysis of the loss-of-function of potential gene of interests before the generation of mutant lines.

Thus, despite a variable degree of knockdown and an effect limited in time, morpholinos are still one of the most widely used technique in the zebrafish community, and especially to study MNDs [139, 465, 466].

Overexpression techniques

DNA and mRNA injections

Similar to transient knockdown, transient expression of mRNA or DNA is a widely used technique in the zebrafish field, as it allows to express specific gene products at early stages of development, without having to wait several months to generate a stable transgenic line. It allows for a rapid assessment of the effects of an overexpression or misexpression of a specific zebrafish gene, or of an ectopic gene in the zebrafish embryo, as well as the expression of specific mutant alleles found in human diseases. In order to control for the expression of the transiently expressed protein, fluorescent or epitope tags can be fused to the construct.

While these techniques are still widely used, precise genome editing tools allowing for precise, specific, targeted and transmissible modifications of the zebrafish genome are now available for zebrafish scientists.

Precise genome editing

In the last 10 years, three different techniques have been developed and adapted for use in zebrafish, allowing for the introduction of targeted lesions in the genome, leading to precise genome editing: Zinc-finger nucleases, TALENs and the CRISPR/Cas9 system. In all three strategies, the aim is first to create double-strand breaks (DSB) in specific loci of the genome targeting a region (gene or otherwise) of interest (**Figure 6**). The DSB can then be repaired by either the error-prone non-homologous end joining (NHEJ) process, creating insertions and/or deletions (indels) in the gene of interest and often resulting to a non functional protein usually due to a frameshift in the coding sequence, leading to the presence of premature stop codons; or by homology directed recombination, using a donor template displaying homologous sequence to the region flanking the cleavage site, co-injected with the constructs used to generate the DSB [467]. This facilitates specific alteration to the sequence of the target gene, to introduce specific point mutations for example.

Zinc-finger nucleases

The first genome editing strategy applied to zebrafish were zinc-finger nucleases (ZFN), a chimeric construct formed by a Cys_2His_2 Zinc Finger Array (ZFA) and the cleavage domain of the FokI endonuclease [468]. The ZFA provide sequence specificity, as each zinc-finger recognizes and binds to a specific DNA nucleotide triplet. The FokI endonuclease needs to dimerize to be fully functional so ZFNs are designed and used in pair, with each ZFN targeting one DNA strand with a spacer where the dimerized FokI can induce DSB (**Figure 6**) [469, 470].

Many mutations have been successfully obtained by ZFNs in zebrafish, including loss-of-function lines of the *tardbp* and *tardbp-like* gene, the zebrafish orthologs of human *TARDBP*, the gene coding for the TDP-43 protein implicated in ALS [471].

TALENs

Transcriptor activator-like effector nucleases (TALENs) work in a similar manner to ZFNs, as they are engineered constructs working in pairs, consisting on the fusion of a DNA binding region to the FokI endonuclease. For TALENs, the DNA binding region is derived

from the plant pathogen Xanthomonas TALE proteins [472]. Similar to ZFNs, the FokI endonuclease has to dimerize to be functional and so TALENs must be used in pairs (**Figure 6**).

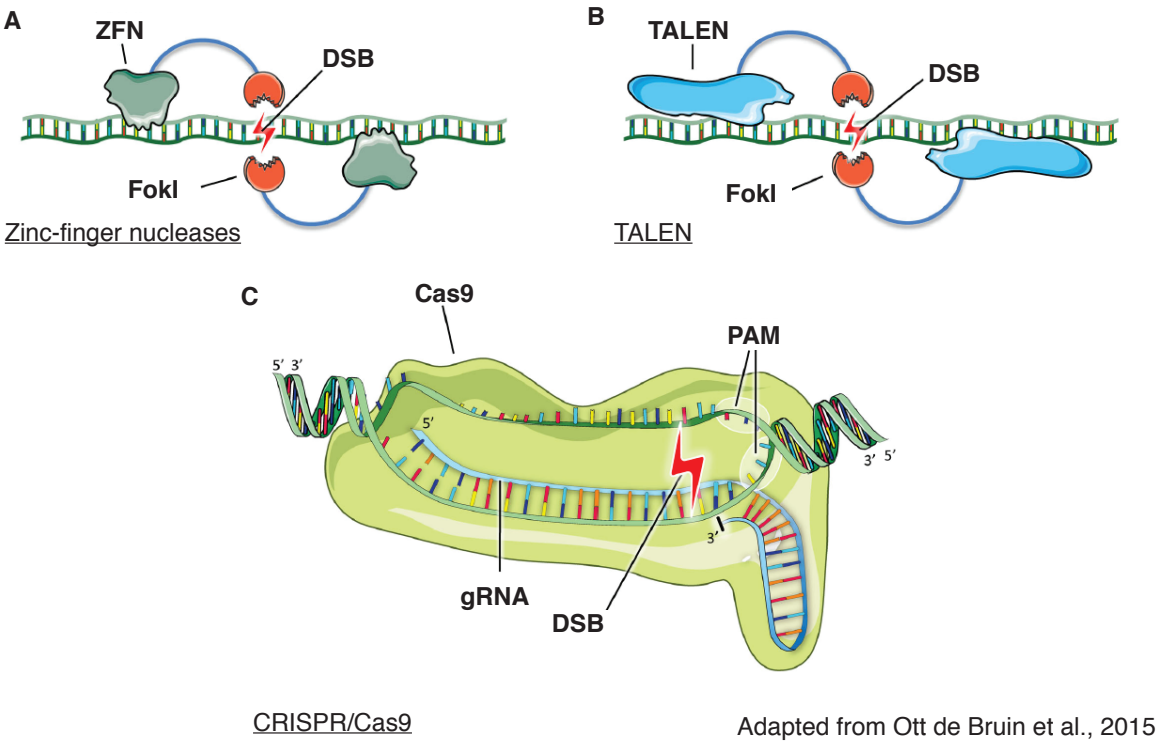

Figure 6. **Genome editing techniques**

(A) Zinc-finger nucleases (ZFN) combine DNA binding-protein with the FokI endonuclease to induce double-strand breaks (DSB) and TALEN (B) use a similar system. (C) The CRISPR/Cas9 system consists of a guide RNA (gRNA) coupled with the Cas9 protein to induce DSB. PAM, protospacer-adjacent motif. Figure adapted from Ott de Bruin et al., *Front immunol 2015* [473].

CRISPR/Cas9

The Clustered, Regularly Interspaced, Short Palindromic Repeat (CRISPR)/CRISPR-associated 9 (Cas9) system is the latest tool added to the zebrafish genetic toolbox. The CRISPR/Cas9 system is originally a tri-partite system, with a CRISPR RNA (crRNA), a trans-activating crRNA (tracrRNA) and the Cas9 protein. The crRNA array is made of short foreign

DNA fragments of around 20 nt called the protospacers and retained from previous encountered with viruses and/or phages, spaced by short palindromic repeats. The tracrRNA mediates the maturation of the crRNA into short fragments, including the spacer, or target sequence and interacts with the crRNA, resulting in the formation of an RNA duplex. The Cas9 protein is guided and bound to the RNA duplex by the tracrRNA and mediates the cleavage of the DNA when sufficient base pair complementarity is found between the spacer and the target DNA. To activate the Cas9 protein, it is necessary to have the presence of a three-nucleotide protospacer-adjacent motif (PAM), NGG, adjacent to the target DNA. The Cas9 protein will cleave the target DNA between the third and fourth base pair upstream of the PAM site [474, 475]. One crucial step for the development of a CRISPR/Cas9 system that can be routinely used for genome editing was the generation of a chimeric single-guide RNA (sgRNA) sequence made of the crRNA and tracrRNA (**Figure 6**) [474].

CRISPR/Cas9 has already been used to generate several lines useful for the study of ALS in zebrafish [476-478].

Zebrafish models of HSP and ALS

As previously mentioned in this introduction, the zebrafish has already been extensively used to study both HSP and ALS. In the next section, I will present the zebrafish models that have been previously published, specifically to gain a better understanding of the pathogenicity of SPG4 for HSP, and of TDP-43 and FUS mutations for ALS.

Zebrafish models of SPG4

Prior to the work presented in **Chapter 2**, four papers modelled SPG4 in zebrafish [138-141].

The zebrafish has only one ortholog of *SPAST*, the *spast* gene located on chromosome 1. It encodes the spastin protein that has a 60% identity with the human spastin and the MIT and AAA domains are well conserved between the human and zebrafish proteins [139], as shown by the protein sequence alignement (**Annexe 1**). While only one long isoform has been identified in the zebrafish to date, it has the potential to also have a longer (equivalent to the M1 isoform) and shorter one (equivalent to the M87 isoform), as the zebrafish *spast* first ATG

is surrounded by a weak Kozak sequence (tgaATGa), whereas the second ATG is surrounded by a stronger Kozak sequence (gccATGg), coding for the methionine at position 61. Woods and colleagues also showed by in situ hybridization that the *spast* transcript is maternally expressed and ubiquitously expressed at low level until at least 24 hpf [139].

In their article, Wood and colleagues used an ATG-blocking morpholino and splice-blocking morpholino targeting the junction between the intron 7-8 splice donor site to induce a knockdown of *spastin*. This knockdown induced abnormal axonal projection of the branchiomotor neurons, with shorter and less numerous axonal branches and abnormal positioning of their cell bodies. Additionally, the axonal projections of the spinal motor neurons were drastically shortened and a reduced staining of the axonal projections in the spinal cord was also identified. Apoptosis was detected specifically in the CNS, with a reduction of 20% of the Islet-1 positive spinal motor neurons. Acetylated-tubulin staining showed an absence of the longitudinal fascicles in the spinal cord, with thickened microtubules [139].

Butler and colleagues [140] used the same ATG- and splice-blocking morpholinos against *spastin* than Wood and used fluorescently labeled End-binding protein 3 (EB3) as a marker to follow microtubule growth. EB proteins are microtubules plus-end tracking proteins and permit to follow the growth of microtubules [479]. The discreet comet-like punctate that were observed in wild-type embryos were almost completely absent following *spastin* knockdown, although a slight drift of the remaining fluorescent punctate was observed, indicating the reduced availability of microtubules plus-ends in the context of spastin reduction. Knockdown of *spastin* also reduced the number of outgrowth events at the growth cone of spinal motor neurons [140].

Zhang and colleagues [138] used the same splice-blocking morpholino than the previous two studies and showed general developmental and morphological defects of the morphants, with hydrocephaly and impaired yolk-sac extension, as well as a similar defect in the axonal outgrowth of spinal motor neurons [138].

Finally, Allison and colleagues [141] used the same ATG-blocking morpholino from Wood study [139] and observed identical aberrant branching and truncation of the axonal

projections of spinal motor neurons. This axonal phenotype was correlated with significantly enhanced tubulation of SNX1, a protein that drives endosomal tubules formation, and an increased number of complex tubular SNX1 structures in the axon and growth cones of cultured spinal motor neurons. This showed an inefficient fission of endosomal tubules and defective endosomal sorting due to *spastin* knockdown [141].

These results indicate that zebrafish is an adequate model to further study the pathophysiological effects of the loss of spastin. Since one of the spastin isoforms appears to be involved in the modulation and maintenance of the ER, we postulated that the loss-of-function due to spastin haploinsufficiency would not only affect its microtubule-severing functions, but also its functions at the ER. This loss-of-function, by impairing the ER homeostasis could lead to ER stress, which in turn may worsen the general phenotype including the microtubule disorganization. Our group previously investigated the potential of ER stress modulators to rescue the phenotype of ALS [480], a disease with common pathological mechanism with HSP ([392] found in **Annexe 8**). We thus investigated whether ER stress was also a pathological mechanism in play in SPG4 in zebrafish, fly and worms models in which the spastin orthologs were knocked-down or knocked-out.

Zebrafish models of TDP-43 and FUS related ALS

Zebrafish models of TDP-43 related ALS

Several groups have used the zebrafish to study how mutations in the *TARDBP* gene could impact the physiological functions of TDP-43. Interstingly, zebrafish tdp-43 and human TDP-43 have a 74% similarity (see protein sequence alignement in **Annexe 3**) alignement [466] All of these studies were performed using morpholino and mRNA overexpression except one. In the first article published by our group, the effects of overexpression of human $TARDBP^{WT}$ and of three different mutant *TARDBP* mRNAs (A315T, G348C and A382T) were investigated [466]. While overexpression of $TARDBP^{WT}$ had a mild phenotype, overexpression of any of the three mutants induced a robust locomotor phenotype in 2 dpf embryos, with $TARDBP^{A315T}$ having the milder phenotype, whereas $TARDBP^{G348C}$ having the stronger phenotype. The different mutant mRNAs also induced similar but slightly different axonal motor neuron phenotypes, with only $TARDBP^{G348C}$ and $TARDBP^{A382T}$ leading to

reduced axonal length, while *TARDBP*^{G348C} also induced aberrant axonal branching [466]. Interestingly, knocking down zebrafish *tardbp* by morpholino induced a similar phenotype, which was rescued by co-injection with *TARDBP*^{WT} mRNA, but not by any of the three mutant *TARDBP* mRNAs. These results indicate that human TDP-43 seems to be functional in the zebrafish, with similar functions, as human WT TDP-43 can rescue the loss of zebrafish tdp-43 [466]. These results were replicated by another group [481]. However, they observed a dose-dependent toxicity of *TARDBP*^{WT}, which was not observed in the study done by Kabashi [466]. The concentration of the mRNA used in this experiment was more than 20 times greater compared than the ones used by Kabashi; unfortunately, since Kabashi and colleagues did not specify the quantity of mRNA injected, it is not possible to compare the doses [466, 481]. Laird and colleague also observed that overexpression of human WT Progranulin (*PGRN*) could partially rescue the phenotype caused by overexpressing *TARDBP*^{A315T} [481]. This result was replicated with overexpression of *TARDBP*^{G348C}, but also with *tardbp* knockdown by the Bennett group [482]. However, *TARDBP*^{WT} was not able to rescue *pgrn-a* knockdown, the zebrafish ortholog of *PGRN*. These results indicate that PGRN and TDP-43 may be part of a common genetic network, with PGRN being downstream of TDP-43 [482]. Van Hoecke and colleagues identified *EPHA4* as an ALS disease-modifier and showed that knockdown of the zebrafish ortholog *rtk1* rescued the axonal phenotype induced by mutant TDP-43 mRNA overexpression [483].

Embryos overexpressing *TARDBP*^{G348C} show electrophysiological abnormalities at the NMJ that can be rescued by treatment with L-type calcium channel agonists, indicating that calcium homeostasis is perturbed by mutant TDP-43 [484]. Using this same system, our group with collaborators working on *C. elegans* models of ALS, showed that overexpression of mutant *TARDBP* induced oxidative and ER stress, which could be rescued by Methylene blue and by ER stress modulators, not only in zebrafish, but also in a *C. elegans* model expressing mutant human TDP-43 [480, 485]. This same two-animal model system was then used for a medium throughput screen of FDA approved compounds to identify molecules that can rescue the phenotypes of our animal models in an unbiased way [486]. Pimozide, a T-type calcium channel antagonist currently used as a neuroleptic was the most potent molecule identified and

was shown to stabilise motility in a short clinical trial of sporadic ALS patients, thus validating the use of zebrafish to study ALS [392].

Of interest, *tardbp* has a paralog in zebrafish, *tardbp-like* (*tardbpl*), which lacks the glycine-rich domain. However, two groups identified that the knockdown or knock out of *tardbp* led to the up-regulation of a spliced version of *tardbpl*, functionally compensating for the loss of *tardbp* [447, 471]. When knocking down *tardbp* in a *tardbp* knockout line, NMJ defects were observed, with an increase in the frequency of quantal acetylcholine release at the NMJ, thus confirming the importance of TDP-43 for synaptic function preservation [487].

Thus, zebrafish models of TDP-43-related ALS have helped us gain a better understanding of the pathophysiology of mutant TDP-43, identify and validate downstream effectors and identify new therapeutic avenues for ALS.

Zebrafish models of FUS-related ALS

The zebrafish fus has a 66% identity with the human FUS (see protein sequence alignement in **Annexe 4**). Dormann and colleagues first used the zebrafish to validate that the C-terminus of FUS is necessary and sufficient to promote nuclear import and that the presence of the P525L mutations prevented this import [319]. However, Bosco and colleagues showed that not all missense mutations in the NLS lead to nuclear depletion, as the FUS^{G515X} and FUS^{R521G} mutant proteins were seen in the nucleus of neurons following their overexpression in zebrafish embryo, whereas FUS protein with NLS truncations (R495X and G515X) have a cytoplasmic localisation [317]. Furthermore, they showed that FUS^{R521G}, FUS^{R495X} and FUS^{G515X} but not FUS^{WT} co-localize with TIAR, a stress granule marker, while the FUS^{H517Q} would only rarely be seen in stress granules [317], indicating that mutations impacted the functions of FUS differently. These results were further confirmed in a zebrafish transgenic line expressing either FUS^{WT} or FUS^{R521C}, as cell culture from this transgenic line showed FUS^{R521C} cytoplasmic mislocalisation and recruitment to stress granules [488]. Our group investigated the effects of *fus* loss-of-function and observed a severe locomotor phenotype as well as abnormal motor neurons axons, which can be rescued by overexpression of FUS^{WT} or of $FUS^{S57\Delta}$, only partially by FUS^{R521C} and not at all by FUS^{R521H} [489]. Furthermore, only overexpression of FUS^{R521H} induced locomotor defects and axonal abnormalities, and not any

of the other mRNA overexpression. Motor neurons from embryos overexpressing this mutant *FUS* mRNA were more excitable and displayed electrophysiological abnormalities at the NMJ [490]. We studied the genetic interactions between FUS, TDP-43 and SOD1 and found that while $TARDBP^{WT}$ is unable to rescue the phenotype seen by *fus* knockdown, overexpression of FUS^{WT} was able to rescue the phenotype seen by *tardbp* knockdown to the same level as $TARDBP^{WT}$, indicating that both TDP-43 and FUS are in a common pathway, with FUS being downstream of TDP-43. Interestingly, $SOD1^{WT}$ was not able to rescue either knockdown of *tardbp* or *fus* indicating that SOD1 toxicity is induced by a different pathogenic mechanism than TDP-43 and FUS [489]. Moreover, Chitramuthu also demonstrated that overexpression of $PGRN^{WT}$ was able to rescue both the loss of *fus* and the overexpression of FUS^{R521H} (while overexpression of FUS^{WT} was not able to rescue *pgrn-a* knockdown) indicating that PGRN is downstream of both TDP-43 and FUS [482]. Finally, we also showed that the phenotype induced by mutant FUS could be rescued by Methylene blue and Pimozide, in the two studies previously commented in the previous section [485, 486].

Overall, these results underscore the use of zebrafish models of ALS as they can be used to gain a better understanding of the pathophysiology of both mutant TDP-43 and FUS, study genetic interactions between several genes involved in ALS and to investigate compounds that could be used as potential treatment. However, as these models only transiently express the proteins and necessitate daily mRNA injections with experimenter-variability, the need for stable zebrafish models of ALS is crucial. Additionally, the current zebrafish models indicate variability in the pathophysiology of different ALS-causing mutations, underscoring the need to generate multiple models with specific mutations. Furthermore, while transient techniques are useful for a first foray into modeling ALS in zebrafish, in order to further study the pathophysiology of FUS and TDP-43, better models are needed with a stable expression of human mutant protein, or by mutating the zebrafish genes themselves by introducing disease-causing mutations similar to the ones found in ALS patients.

Thesis overview

The zebrafish, like *C. elegans* or *Drosophila*, is a genetic model, rather than strictly a disease model. The objectives most of the time are not to reproduce every single aspect of a disease, but to study the different factors that may have a role in its pathophysiology. The introduction of a mutated human gene in the genome of the zebrafish through transient, transgenic or genome editing techniques, can allow us to study how specific mutations in specific genes can lead to the toxicity observed in human and whether it is possible to block or even reverse the pathology.

In this thesis, I have used the zebrafish and many of the genetic tools developed for this system to model and study two motor neuron disorders, HSP and ALS:

HSP

1. Loss-of-function mutations of the *SPAST* gene, encoding the Spastin protein, are the most prevalent cause of autosomal-dominant HSP and no treatment is yet available for this disease. We explored whether ER-stress modulator compounds could rescue the phenotype of a *spastin* loss-of-function in zebrafish generated through morpholino-mediated knockdown of the zebrafish *spastin*, as well as in *C. elegans* and *Drosophila* models (**Chapter 2** and [491]).
2. In order to establish the causative mutations of three families with autosomal-recessive HSP, we performed whole-genome sequencing on nine individuals with autosomal-recessive HSP and found loss-of-function mutations in the *CAPN1* gene coding for the Calpain 1 protein. We used morpholino-based knockdown of the zebrafish *calpain 1a* to validate *in vivo* the pathogenicity of loss-of-function of Calpain 1 (**Chapter 3** and [492]).

ALS

1. More than 50 mutations in the gene *TARDBP*, encoding the protein TDP-43 have been linked to ALS. TDP-43 is an RNA binding protein with glycine-rich domains that binds to more than 6,000 RNAs in the human brain. However, ALS-related mutations

do not appear to affect the function of these genes, indicating that a toxic gain-of-function may occur. We generated transgenic zebrafish lines expressing either the wild-type or an ALS-causative mutant TDP-43 and used them for RNA-sequencing, to identify transcripts that are differentially modulated by the mutant TDP-43 (**Chapter 4**, Lissouba et al., 2018, accepted for publication in *Frontiers in Molecular Neuroscience*).

2. Transgenic expression of a human gene in the zebrafish may lead to non-specific toxic effects. For this reason we have also generated CRISPR/Cas9 knockin lines where we introduced specific point mutations similar to ones that are ALS-causative in human in *tardbp* and in *fus*, another gene linked to ALS (**Chapter 5** and [478]).

Chapter 2: Conserved pharmacological rescue of hereditary spastic paraplegia-related phenotypes across model organisms

Carl Julien†, **Alexandra Lissouba**†, Surya Madabattula†, Yasmin Fardghassemi, Cory Rosenfelt, Alaura Androschuk, Joel Strautman, Clement Wong, Andrew Bysice, Julia O'Sullivan, Guy A. Rouleau, Pierre Drapeau, J. Alex Parker and François V. Bolduc

Human Molecular Genetics, 2016, Vol. 25, No. 6 1088–1099

Doi: 10.1093/hmg/ddv632

Authors contribution

†The first three authors are co-first authors

I am a co-first author

For this manuscript, each co-first author was responsible for one animal model. As such, I designed all the zebrafish experiments with PD, realized all the zebrafish experiments, analyzed all the zebrafish results, produced the zebrafish figure (Figure 9) and wrote the part of the manuscript specific for zebrafish.

Manuscript

Conserved pharmacological rescue of hereditary spastic paraplegia-related phenotypes across model organisms

Carl Julien[1†], Alexandra Lissouba[1†], Surya Madabattula[2,3†], Yasmin Fardghassemi[4], Cory Rosenfelt[3], Alaura Androschuk[3], Joel Strautman[2,3,] Clement Wong[3], Andrew Bysice[3], Julia O'Sullivan[3], Guy A. Rouleau[5], Pierre Drapeau[1], J. Alex Parker [1] and François V. Bolduc[2,3*]

[1] CRCHUM and Department of Neuroscience, Université de Montréal, Montréal, Québec, Canada

[2] Institute for Neuroscience and Mental Health, University of Alberta, Canada

[3] Department of Pediatrics, University of Alberta, Edmonton, Alberta, Canada

[4] CRCHUM and Department of Biochemistry, Université de Montréal, Montréal, Québec, Canada

[5] Montreal Neurological Institute and Hospital, McGill University, Montreal, Quebec, Canada

*Corresponding authors at:

University of Alberta, 3020 Katz Group Centre, 11315 87th Avenue

Edmonton, Alberta, Canada T6G 2E1 Tel.: +1 780-492-9616. Fax: +1 780-492-0723 Email: fbolduc@ualberta.ca

†The first three authors are co-first authors

Abstract

Hereditary spastic paraplegias (HSPs) are a group of neurodegenerative diseases causing progressive gait dysfunction. Over 50 genes have now been associated with HSP. Despite the recent explosion in genetic knowledge, HSP remains without pharmacological treatment. Loss-of-function mutation of the SPAST gene, also known as SPG4, is the most common cause of HSP in patients. SPAST is conserved across animal species and regulates microtubule dynamics. Recent studies have shown that it also modulates endoplasmic reticulum (ER) stress. Here, utilizing null SPAST homologues in *C. elegans*, Drosophila, and zebrafish, we tested FDA approved compounds known to modulate ER stress in order to ameliorate locomotor phenotypes associated with HSP. We found that locomotor defects found in all of our spastin models could be partially rescued by phenazine, methylene blue, N-acetyl-cysteine, guanabenz and salubrinal. In addition, we show that established biomarkers of ER stress levels correlated with improved locomotor activity upon treatment across model organisms. Our results provide insights into biomarkers and novel therapeutic avenues for HSP.

Introduction

Hereditary spastic paraplegia (HSP) represents a group of neurodegenerative disorders leading to progressive deterioration in gait first described by Strumpel in 1880 (1). Neuropathological changes are most commonly observed in the longest ascending and descending axons of the cortico-spinal tract and ascending axons of the dorsal column neurons (2). HSP can manifest clinically with various patterns. In some patients, motor symptoms and signs are the only manifestations of the disease (known as pure form), whereas other patients present associated signs of cognitive defects, seizures or sensory symptoms (known as complicated form) (3). Over 50 genes are now associated with HSP (4). Nonetheless, many patients remain without a genetic diagnosis, suggesting that even more genes or unknown causes are involved with HSP. Several cellular pathways are disrupted in HSP. Changes in microtubule dynamics, axonal transport, and mitochondrial function are thought to explain the distal end neurodegeneration seen in HSP and could be a common pathological mechanism for several causative genes (5, 6).

Mutations in the gene *SPASTIN* represent the most common cause of autosomal dominant (AD) HSP (40 % of pure AD-HSP). Most mutations described to date (missense, truncating (5) or splice site mutations (7, 8)) lead to loss-of-function *via* defects in the ATPase Associated with the diverse cellular Activities (AAA) domain (9). So far, most cellular studies have focused on the role of SPAST in microtubule stability and severing from the AAA domain (10,11) Moreover, microtubule modifying drugs such as taxol, vinblastine, epothilone D and noscapine were identified as rescuing peroxisome trafficking deficit in HSPs patient-derived stem cells (12). Previous research of the SPAST homologue in *C. elegans* has identified a microtubule binding region with ATPase microtubule severing activity (13-15). However, little is know about the consequences of mutations in SPAST homologue on locomotion, as much of the previous research has focused on imaging. Loss-of-function in the *Drosophila* spastin homologue results in microtubule network abnormalities, increased levels of the stabilized acetylated form of microtubules leads to abnormal axonal arborisation and axonal regeneration in spastin mutant flies, locomotor defects, and early mortality (16-18). Work in zebrafish also revealed that depletion of its SPAST homologue alters microtubules

(19), axon outgrowth (20, 21), and provokes abnormal endosomal tubulation (22).

Here we investigated a novel mechanism that could lead to neurodegeneration in HSP, the ER stress response. In addition to its role in microtubule regulation, spastin has also been linked to the endoplasmic reticulum (ER) network (23-26). We have previously shown that methylene blue, salubrinal, guanabenz, and phenazine target the ER stress response and protect against proteotoxicity in simple models of another neurodegenerative disorder, amyotrophic lateral sclerosis (27, 28). Here, we utilized multiple animal models for spastin including worm, fly, and zebrafish in order to investigate if these drugs are able to rescue locomotor and cellular defects observed in SPAST mutant animals. We show that our models of *spastin* loss-of-function present defects in locomotion that can be partially rescued using these compounds. Moreover, improved locomotion correlated with return to wild-type level for biomarkers of ER stress.

Results

MODEL 1: *C. elegans*

spas-1 mutants develop an HSP-related motor phenotype in *C. elegans*

In *C. elegans*, we first examined for HSP-related phenotypes in mutants for the homologous genes SPG1 (L1CAM/*lad-2*), SPG4 (SPAST/*spas-1*) and SPG3A (ATL1/*atln-1*) (**Table 1**). Interestingly, using paralysis assays, we observed that the *spas-1*(*ok1608*) ($P < 0.0001$, N=83-371) and the *spas-1*(*tm683*) mutants displayed progressive motor defects compared to wild-type N2 worms ($P = 0.0002$, N=51-371) (**Figure 1A**). RT-PCR revealed that *spas-1*(*ok1608*) mutants display a loss of *spas-1* expression (**Figure 1B**). We also observed that the *lad-2*(*hd-31*) ($P < 0.0001$, N=359-371) and the *lad-2*(*tm3056*) ($P < 0.0001$, N=234-371), but not the *atln-1-related* mutant *Y54G2A.2*(*ok1144*) ($P = 0.4665$, N=80-371)

nematodes exhibit a progressive paralysis phenotype compared to wild-type N2 worms (**Supplemental Figure 1**). This is the first time a locomotor defect is shown in *C. elegans spastin* mutants.

Guanabenz, salubrinal, phenazine, and methylene blue rescue the motor phenotype in *C. elegans* models of HSPs

We previously identified that methylene blue, salubrinal, guanabenz, and phenazine target the ER stress response and have beneficial effects against human mutant TDP-43 neuronal toxicity *in vivo* (27, 28). In this study, we first tested these compounds at doses previously found to be efficient (27, 28) in our HSP models in *C. elegans* and found that all these drugs rescued the paralysis phenotype of *spas-1*(*ok1608*) ($P < 0.0001$-0.0032, N=50-85) (**Figure 2**) and *lad- 2*(*hd31*) mutants ($P < 0.0001$, N=64-83) (**Supplemental Figure 2**).

Guanabenz, salubrinal and methylene blue but not phenazine prolong the lifespan in *spas-1* mutants in *C. elegans*.

We next asked whether drugs that beneficially affect the motor phenotype in *spas-1* and *lad-2* mutants could also ameliorate another key marker of these HSP models, their lifespan. We observed that guanabenz, salubrinal and methylene blue, but not phenazine, prolonged the lifespan of *spas-1*(*ok1608*) ($P < 0.0001$, N=65-84) (**Figure 3**) and *lad-2*(*hd31*) worms ($P < 0.0001$-0.0281, N=46-84) (**Supplemental Figure 3**).

Methylene blue, guanabenz, salubrinal and phenazine prevent oxidative stress induced by a *spas*-1 mutation in *C. elegans*

In order to identify mechanisms of our compounds on HSP-related motor phenotypes, we first investigated their antioxidant properties, since guanabenz was shown to inactivate nitric oxide synthase (NOS) (29), salubrinal is known to be a specific inhibitor of the eIF2α phosphatase enzymes (30) and methylene blue is a monoamine oxidase A inhibitor (31). In addition, phenazine has a structure similar to that of methylene blue. We observed that 10 mM

N-Acetyl- L-cysteine, a strong antioxidant, reduced the paralysis phenotype in the *spas-1*(*ok1608*) (**Figure 4A)** (P = 0.0275, N=189-199) and in the *lad-2*(*hd31*) (**Supplemental Figure 4**) (P < 0.0001, N=90) nematodes. In addition, following 2′,7′-dichlorofluorescein diacetate (DCF-DA) exposure, fluorescence measurements at 488 nm revealed that the *spas-1*(*ok1608*) worms display increased levels of ROS (**Figure 4B,C**) (P = 0.0067, N=17-26). The esterified substrate is cleaved by an esterase activated by ER stress, releasing fluorescein as a marker.

We next wanted to examine if methylene blue, guanabenz, salubrinal and phenazine could have an effect on the oxidative stress detected in the *spas-1* mutants and we observed that all the four compounds reduced the levels of ROS using DCF-DA in the *spas-1*(*ok1608*) nematodes (**Figure 4B,C**) (P = < 0.0001-0.0172, N=17-26). Thus, these results suggest that the beneficial effects of the compounds could be due, at least in part, to their antioxidant properties.

Methylene blue, guanabenz, salubrinal, and phenazine rescue the ER stress response caused by *spas-1* knockdown in *C. elegans*

We previously showed that methylene blue, guanabenz, salubrinal and phenazine increase expression of *hsp-4*, the *C. elegans* ortholog of the protective Hsp70/BiP, which is induced by ER stress (32), using the *zcIs4*[*hsp-4*::GFP] reporter strain (28). Here, we also observed that methylene blue and phenazine induced the expression of *hsp-4*/BiP in the *hsp-4*::GFP reporter strain (**Figure 4D,E**) (P < 0.0003-0.0134, N=23-25). However, we did not observe an increase in *hsp-4*/BiP expression following treatment with guanabenz or salubrinal (**Figure 4D,E**). These discrepancies could be due by the treatment parameters. Here, the nematodes were exposed to the compounds from birth to adult day 1, compared to L4 to adult day 1 in the previous study. Also, in this study, the control worms were in a RNAi experiment paradigm with exposition to an empty vehicle control for RNAi with 1 mM isopropyl-β-D-thiogalactopyranoside (IPTG) compared to only OP50 in the previous study. However, more interestingly here, treatment with the four compounds tested, methylene blue, guanabenz, salubrinal and phenazine, restored the control *hsp-4*/BiP levels in *spas-1*

knockdown using RNAi in *hsp-4*::GFP worms (**Figure 4D,E**) ($P < 0.0001$-0.0002, N=23-25).

MODEL 2: *Drosophila*

Methylene blue, phenazine, and *N*-Acetyl-L-cysteine rescue the negative geotaxis defects caused by *spastin* loss-of-function in *Drosophila*

Considering the beneficial effect of treatments targeting ER stress in worms, we tested if the compounds could also rescue the locomotor defects previously shown in *Drosophila* with *spastin* loss-of function (13, 16, 33). First, considering potential variability between animal models, developmental stages, and drug delivery and absorption, we established a dose response curve for each drugs in our model (**Supplementary Figure 5**). We started by using pan neuronal (Elav-GAL4) expression of transgenic RNA interference (RNAi) against *spastin*. We observed a significant defect in locomotion compared to wild-type controls ($P \leq 0.001$, N=10), which was rescued using methylene blue ($P \leq 0.01$, N=6) (**Figure 5A,B**), phenazine ($P \leq 0.01$, N=10) (**Figure 6A,B**), or N-acetyl-cysteine ($P \leq 0.05$, N=6) (**Figure 7A,B**). We obtained similar results when using the previously extensively characterized *spastin* deletion mutants (spastin$^{5-75}$/spastin$^{17-7}$). They presented severe climbing defects ($P \leq 0.001$, N=10) that were significantly improved after acute treatment of adult flies using methylene blue ($P \leq 0.001$, N=7) (**Figure 5 C,D**), phenazine ($P \leq 0.01$, N=10) (**Figure 6C,D**), and *N*-Acetyl-L-cysteine ($P \leq 0.01$, N=8) (**Figure 7C,D**). None of the drugs had effect on wild-type control flies (N=10).

We performed immunohistochemistry of the Drosophila brain and identified increased level of BiP levels in brain of flies with pan-neuronal expression of the SpasRNAi used in the behavioral experiments (N=5, P=0.0037) (**Figure 8A,B,D**). Treatment with methylene blue restored BiP levels to the level of wild-type flies (N=5, P=0.2787) (**Figure 8B,C,D**).

MODEL 3: Zebrafish

All four compounds partially rescue the morphological phenotype and reduce microtubule defects of the *spastin* morphant in zebrafish

Next, we validated the *C. elegans* and *Drosophila* findings in a vertebrate model. We knocked down *spastin* in zebrafish embryos by injecting an antisense morpholino (MO) against the first translation initiation site of *spastin* (13, 16, 17). Morphants injected with *spastin* MO but not with an irrelevant control MO (CoMO) had abnormal morphological features, including hydrocephalia, perturbed yolk sac extension and an arched-back phenotype, similar to what has been previously reported with the same morpholino (19, 20, 22), or a splice-blocking morpholino against exon 7 of *spastin* (19, 21). Following a 12-hour treatment with either methylene blue, guanabenz, salubrinal or phenazine from 18 hours post fertilization (hpf), these phenotypes were partially rescued, mainly by methylene blue and salubrinal (**Figure 9A-B**).

Immunofluorescent staining against acetylated-tubulin showed that *spastin* morphants exhibited disorganized microtubule networks in the spinal cord and thinner microtubules in the spinal motor neuron axons. Similarly, these defects could be partially rescued by a 12-hour incubation with either methylene blue, guanabenz, salubrinal, or phenazine (**Figure 9C**).

We assessed the levels of oxidative stress in the fish using DCF-DA. Similar to what was obtained in the other two models, a strong fluorescent signal was observed upon the knockdown of *spastin*, compared to the use of a control morpholino. This fluorescent signal was reduced by treatment with any of the 4 ER-modulating drugs (**Figure 9D,E**). Collectively, these data suggest that methylene blue, guanabenz, salubrinal, and phenazine are able to reduce the level of oxidative stress generated by the loss-of-function of *spastin*.

Taken together, these results show that methylene blue, salubrinal, and to a lesser extent guanabenz and phenazine can partially rescue the morphological phenotype and microtubule defects in a vertebrate genetic model of HSP.

Discussion

HSP represents a group of neurodegenerative disorders causing progressive gait impairment. HSPs are caused by over 50 genes and remain without pharmacological treatment. Here we targeted the most common HSP gene, *SPASTIN*, in three model organisms, *C. elegans*, *Drosophila*, and the vertebrate zebrafish.

Recent evidence linking HSP to ER stress prompted us to investigate the oxidative stress inhibitors as a potential means to alleviate the phenotypic manifestations of HSP. Previous success of oxidative stress inhibitors with another neurodegenerative disease, ALS, led us to consider the role of the same compounds-phenazine, guanabenz, salubrinal, methylene blue, and N-acetyl cysteine as potential therapeutic agents in our HSP models of disease. All selected therapeutic agents, with the exception of phenazine, are FDA approved and could rapidly be translated into clinical trials. We show for the first time that inhibition of ER stress may be key at preventing microtubule disorganization, which is a common feature of many genes involved in HSP. Our data suggests that *spastin* knockdown induces the ER stress response, and that treatments with the compounds examined in this study rescue this exacerbated response. We also found that both lifespan and locomotion were rescued in our three model organisms with *spastin* mutations.

Future work will be required to extend our findings to other mammalian models but using FDA- approved compounds is likely to accelerate the application to clinical trials for HSP patients.

Material and Methods

MODEL 1: C. elegans experiments

Strains and genetics

Standard methods of culturing and handling worms were used. Worms were maintained on standard nematode growth media (NGM) plates streaked with OP50 *E. coli*. All strains were scored at 20°C. Mutations used in this study were: *lad-2*(*hd-31*), *lad-2*(*tm3056*), *spas-1*(*ok1608*), *spas-1*(*tm683*), *Y54G2A.2*(*ok1144*). Mutant strains were obtained from the *C. elegans* Genetics Center (University of Minnesota, Minneapolis). Deletion mutant were verified by PCR and each had been outcrossed a minimum of three times to wild-type N2 worms prior to use.

Paralysis assay

Mutant *lad-2*, *spas-1*, *Y54G2A.2* were scored for paralysis from adult day one to adult day twelve as described previously (34-36). Briefly, 30 L4 animals were transferred to NGM-FUDR and, the subsequent days, were counted as positive if they failed to move after being prodded with a worm pick. Worms scored as dead if they failed to move their head after prodding on the nose.

Lifespan assay

For lifespan assay, thirty L4 *lad-2*, *spas-1*, *Y54G2A.2* mutants were transferred on NGM-FUDR plates and tested daily from adult day one until death. Worms were scored as dead if they failed to respond to tactile stimulus

Drug exposure

The nematodes were exposed from birth to 60 µM methylene blue, 50 µM salubrinal, 50 µM guanabenz, 25 µM phenazine or 10 mM *N*-acetyl-L-cysteine incorporated into NGM solid medium or NGM solid medium only as control. All the medium plates were streaked with OP50 *E. coli*. Compounds were purchased from Sigma-Aldrich (St. Louis, MO) and Tocris Bioscience (Ellisville, MO). Briefly, ~5-7 adult hermaphrodites were placed on solid media with or without the drugs for 3-4 days and kept at 20°C. Then, ~30 L4 worms were picked were plated on corresponding NGM-FUDR medium and behavioral tests, lifespan assays and fluorescence microscopy were performed.

RT-PCR assays

RNA samples were obtained from 15 confluent plates of worms, following Trizol (Invitrogen)/chloroform extraction and quantified with a Nano-Photometer (Implen). 1 µg of RNA were reverse transcribed preceded by gDNA wipeout. 1 µl of cDNA was used for *spas-1* amplification using the following primers: forward, 5'-TGAGAGCCGCGATTGAAATGG-3'; C24B5.2 reverse, 5'-TCTGATTTCACTTCTCCGGGTTT-3'.

Reactive oxygen species measurements

The *in vivo* detection of reactive oxygen (ROS) species in *C. elegans* is previously described (27, 28). Briefly, worms were incubated on a slide with 5 µM 2′,7′-dichlorofluorescein diacetate (DCF-DA, Sigma-Aldrich) for 30 min at room temperature and washed three times for 5 min with PBS 1X. N2 wild type and *spas-1*(*ok1608*) mutants worms 2 days aged were visualized by fluorescence microscopy under a 488 nm wavelength excitation. The ROS was expressed as percentage of *spas-1*(*ok1608*) mutants.

RNAi experiments

RNA interference (RNAi)-treated *hsp-4*::GFP worms were fed *E. coli* (HT115) containing an

empty vector or *E. coli* expressing dsRNA against *spas-1*(C24B5.2). The RNAi clone was from the ORFeome RNAi library (Open Biosystems). RNAi experiments were performed at 20 °C. Worms were grown on Nematode Growth Media enriched with 1 mM isopropyl-β-D-thiogalactopyranoside. Synchronized L1 worms were grown on plates with RNAi bacteria until adult day 1, when they were assayed for fluorescence microscopy.

Fluorescence microscopy

For visualization of *hsp-4*::GFP and DCF-DA-exposed animals, M9 buffer with 60% glycerol was used for immobilization. Animals were mounted on slides with 2% agarose pads and examined for fluorescence. Fluorescent expression for quantification was visualized with a Zeiss Axio Imager M2 microscope. Fluorescent expression was visualized with a DIC microscope Carl Zeiss AxioObserver A1. The software used was AxioVs40 4.8.2.0. Twenty-seven to thirty-three worms were visualized. Image processing and quantification were done with Adobe Photoshop. To compare fluorescence, we calculated the changes in the ratio (size/intensity of fluorescence).

Statistics

Paralysis and lifespan curves were generated and compared using the Log-rank (Mantel-Cox) test. All experiments were repeated at least three times. For fluorescence, parametric Student's *t*-tests were realized. Prism 6 (GraphPad Software) was used for all statistical analyses.

MODEL 2: *Drosophila* experiments

Fly stocks

Drosophila were raised at 22^{o}C with 40% humidity. Drosophila spastin$^{5\text{-}75/Tb}$ and spastin$^{17\text{-}7}$ / TAGS were a generous gift of Dr. Nina Sherwood (Duke University). Drosophila spastin RNAi transgenic were obtained from the Vienna Drosophila RNAi center. The transgenic line

used for this study is # U108739. Flies were raised in incubator with a 12:12 light:dark cycle.

Negative geotaxis (Climbing) assay

Climbing testing was performed as described previously (33). Briefly, 20 flies (1 day old) are collected the day before the experiments in food vials containing either the vehicle or the drug being studied. Flies are transferred into a 250 mL glass cylinder and displaced to the bottom of the cylinder by tapping against soft rubber padding. The number of flies above the target distance of 17.5 cm is recorded over a total time of 2 minutes. The percentage of flies above the target line versus the total number of flies is represented at every 10-second intervals.

Statistical analysis comparing the performance of flies in the vehicle group (fed fly media plus vehicle) versus the drug group (containing both fly media and drug) is performed with a t-test (GraphPad Prism). All graphs depict mean ± S.E.M.

Pharmacological treatment

Drosophila were raised on standard food media and transferred to vials containing drug dissolved in food. Flies were collected and placed on the drug or regular food around noon the day before testing. Testing occurred the following day from 9-12h. Drugs used for these experiments include phenazine (Sigma P13207), methylene blue (Sigma M9140), and N-Acetylcysteine (Sigma A7250). For phenazine, doses tested ranged from 75-150uM. For methylene blue, doses tested ranged from 50-300 uM. For N-Acetylcysteine dose tested ranged from 100-750 uM. Methylene blue and NAC were dissolved in water to make concentrated stock solutions. Phenazine was solubilized in pure DMSO to form a concentrated stock solution. The required amount of stock solution was dissolved in standard food. Drug was added to food when cooled at 60^{o}C.

Immunohistochemistry

1-3 days old female flies were dissected and processed as previously described (37). Flies were selected if the food colorant used in the drug treatment was seen in the abdomen to control for

drug intake. Flies were dissected in 1X PBS and the brains were transferred to 4% PFA to fix for 10 minutes at room temperature. Following the 10-minute fixation period, the brains were placed in a vacuum for 1.5 hours in a solution of 0.25% Triton 4% PFA. The brains were then incubated in a penetration/blocking buffer (2%PBST, 10% NGS, 0.02% Sodium Azide) on rocker for 2 hours at 4^{o}C and following completion transferred to primary antibody solution (1:50 α- GRP78/HSPA5 ThermoFisher Scientific PA5-22967) and 1% PBST with 0.25% NGS) and incubated overnight at 4^{o}C. Following overnight incubation, brains were washed 3 times in 1% PBST for 20 minutes. Brains were subsequently incubated with secondary antibody solution (1:200 Cy3 α-Rabbit Jackson ImmunoResearch 111-165-003) overnight at 4^{o}C. Following incubation with secondary antibody, brains were washed 3 times with 1% PBST and mounted. Imaging was completed using Zeiss LSM 700 confocal microscope and images were quantified using ImageJ.

MODEL 3: Zebrafish experiments

Maintenance

Zebrafish (*Danio rerio*) embryos were collected and staged using standard methods (27). The local animal care committee at the CRCHUM, having received the protocol relevant to this project relating to animal care and treatment, certified that the care and treatment of animals was in accordance with the guidelines and principles of the Canadian Council on Animal Care. Further, all matters arising from this proposal that related to animal care and treatment, and all experimental procedures proposed for use with animals were reviewed and approved by the committee before they were initiated or undertaken. This review process was ongoing on a regular basis during the entire period that the research was being undertaken. Zebrafish embryos (no adults were used) are insentient to pain. Fish embryos were incubated for 12 hours in each compound, examined and then disposed. Zebrafish embryos were used over a two-day period then terminated.

Morpholino injections

Morpholino (Spast MO: 5'-ATTCATTCACCCTTCTCGGGCTCTC-3') against *spastin* translation initiation site was obtained from Gene Tools and described earlier (19). As a control, an irrelevant morpholino was used (CoMO: 5'-CCTCTTTACCTCAGTTACAATTTATA-3'). The morpholinos were diluted in deionized water with 0.05% Fast Green vital dye (Sigma-Aldrich) and 10 ng per embryo was pulse-injected into 1-2 cell stage embryos using a Picospritzer III pressure ejector.

Drug treatments

18 hpf embryos injected with Spast Mo or CoMO were placed in individual wells in a 24 well plate and were treated for 12 hours with methylene blue (60 μM), salubrinal (20 μM), guanabenz (20 μM) or phenazine (20 μM) diluted in Evans solution (in mM): 134 NaCl, 2.9 KCl, 2.1 $CaCl_2$, 1.2 $MgCl_2$, 10 HEPES, 10 glucose, pH 7.8, 290 mOsm, with 0.1% DMSO. The embryos were then morphologically assessed and fixed for immunohistochemistry.

Immunostaining

Monoclonal antibodies anti-acetylated tubulin were used to assess the microtubule integrity in the spinal cord and motor neuron axons at 30 hpf. Embryos were fixed with Dent's fixative (80% methanol, 20% DMSO), in order to preserve microtubules, at 4°C overnight. After the fixation, embryos were progressively rehydrated in 75%, 50% and 25% methanol in PBS and wash several times in PBST before block. The embryos were incubated overnight at 4°C in primary monoclonal antibody anti-acetylated tubulin (Sigma-Aldrich, 1:500), washed in PBST for a day, then incubated in the secondary antibody conjugated with Alexa Fluor 488 (Molecular Probes, Carlsbad, CA, 1:1000) for 4–6 h at room temperature. Embryos were washed several times in PBS, cleared in 70% glycerol and mounted. Fluorescent images of fixed embryos were taken using a Quorum Technologies spinning-disk confocal microscope mounted on an upright Olympus BX61W1 fluorescence microscope equipped with an Hamamatsu ORCA-ER camera. Image acquisition was performed with Volocity software (PerkinElmer) and images were processed using ImageJ (NIH).

Reactive Oxygen Species measurements

The *in vivo* detection of reactive oxygen species was done as before (27, 28). Briefly, live 30 hours post-fertilization (30 hpf) were incubated in 5 μM 2′,7′-dichlorofluorescein diacetate (DCF-DA) (Sigma-Aldrich) for 20 minutes at 28.5°C and washed three times for 5 min with embryo media. Fluorescence was observed under a 488 nm wavelength excitation. The ROS was expressed as percentage of control.

Statistical analysis

Significance was determined using two-way ANOVA and Holm-Sidak method of comparison was used for non-normal distributions.

Acknowledgments

Some worm strains were provided by the CGC, which is funded by NIH Office of Research Infrastructure Programs (P40 OD010440). This research was funded by the Canadian Institute of Health Research-CIHR (GAR, PD, AP and FB). C.J. is supported by CIHR and Huntington's Society of Canada fellowships. A.L. is supported by a CIHR and ALS Canada scholarship. P.D. and G.A.R. hold Canada Research Chairs. J.A.P. holds a career development award from the Fonds de recherche du Québec - Santé. We would like to thank Dr. N Sherwood for the Drosophila *spastin* mutant flies. We thank VDRC for Drosophila RNAi stocks. F.B. holds a career development award from the Canadian Child Health Clinician Scientist Program (CCHCSP).

Conflict of Interest Statement

Disclosure statement: The authors declare no actual potential conflict of interest.

References

1. McDermott, C., White, K., Bushby, K. and Shaw, P. (2000) Hereditary spastic paraparesis: a review of new developments. *J. Neurol. Neurosurg. Psychiatry*, **69**, 150–160.

2. Behan, W.M. and Maia, M. (1974) Strümpell's familial spastic paraplegia: genetics and neuropathology. *J. Neurol. Neurosurg. Psychiatry*, **37**, 8–20.
3. Schule, R. and Schols, L. (2011) Genetics of hereditary spastic paraplegias. *Semin. Neurol.*,**31**, 484–493.

4. Fink, J.K. (2013) Hereditary spastic paraplegia: clinico-pathologic features and emerging molecular mechanisms. *Acta Neuropathol.*, **126**, 307–328.

5. Salinas, S., Proukakis, C., Crosby, A. and Warner, T.T. (2008) Hereditary spastic paraplegia: clinical features and pathogenetic mechanisms. *Lancet Neurol.*, **7**, 1127–1138.

6. Hedera, P., DiMauro, S., Bonilla, E., Wald, J.J. and Fink, J.K. (2000) Mitochondrial analysis in autosomal dominant hereditary spastic paraplegia. *Neurology*, **55**, 1591–1592.

7. Svenson, I.K., Ashley-Koch, A.E., Pericak-Vance, M.A. and Marchuk, D.A. (2001) A second leaky splice-site mutation in the spastin gene. *Am. J. Hum. Genet.*, **69**, 1407–1409.

8. Svenson, I.K., Ashley-Koch, A.E., Gaskell, P.C., Riney, T.J., Cumming, W.J., Kingston, H.M., Hogan, E.L., Boustany, R.M., Vance, J.M., Nance, M.A., et al. (2001) Identification and expression analysis of spastin gene mutations in hereditary spastic paraplegia. *Am. J. Hum. Genet.*, **68**, 1077–1085.

9. Salinas, S., Carazo-Salas, R.E., Proukakis, C., Schiavo, G. and Warner, T.T. (2007) Spastin and microtubules: Functions in health and disease. *J. Neurosci. Res.*, **85**, 2778–2782.

10. Errico, A., Claudiani, P., D'Addio, M. and Rugarli, E.I. (2004) Spastin interacts with the centrosomal protein NA14, and is enriched in the spindle pole, the midbody and the distal axon. *Hum. Mol. Genet.*, **13**, 2121–2132.

11. Evans, K.J., Gomes, E.R., Reisenweber, S.M., Gundersen, G.G. and Lauring, B.P. (2005) Linking axonal degeneration to microtubule remodeling by Spastin-mediated microtubule severing. *J. Cell. Biol.*, **168**, 599–606.

12. Fan, Y., Wali, G., Sutharsan, R., Bellette, B., Crane, D.I., Sue, C.M. and Mackay-Sim, A. (2014) Low dose tubulin-binding drugs rescue peroxisome trafficking deficit in patient-derived stem cells in Hereditary Spastic Paraplegia. *Biol. Open*, **3**, 494–502.

13. Matsushita-Ishiodori, Y., Yamanaka, K., Hashimoto, H., Esaki, M. and Ogura, T. (2009) Conserved aromatic and basic amino acid residues in the pore region of Caenorhabditis

elegans spastin play critical roles in microtubule severing. *Genes Cells*, **14**, 925–940.

14. Matsushita-Ishiodori, Y., Yamanaka, K. and Ogura, T. (2007) The C. elegans homologue of the spastic paraplegia protein, spastin, disassembles microtubules. *Biochem. Biophys. Res. Commun.*, **359**, 157–162.

15. Yu, W., Qiang, L., Solowska, J.M., Karabay, A., Korulu, S. and Baas, P.W. (2008) The microtubule-severing proteins spastin and katanin participate differently in the formation of axonal branches. *Mol. Biol. Cell.*, **19**, 1485–1498.

16. Sherwood, N.T., Sun, Q., Xue, M., Zhang, B. and Zinn, K. (2004) Drosophila Spastin Regulates Synaptic Microtubule Networks and Is Required for Normal Motor Function. *PLoS Biol.*, **2**, e429.

17. Trotta, N., Orso, G., Rossetto, M.G., Daga, A. and Broadie, K. (2004) The hereditary spastic paraplegia gene, spastin, regulates microtubule stability to modulate synaptic structure and function. *Curr. Biol.*, **14**, 1135–1147.

18. Stone, M.C., Rao, K., Gheres, K.W., Kim, S., Tao, J., La Rochelle, C., Folker, C.T., Sherwood, N.T. and Rolls, M.M. (2012) Normal spastin gene dosage is specifically required for axon regeneration. *Cell Rep.*, **2**, 1340–1350.

19. Wood, J.D., Landers, J.A., Bingley, M., McDermott, C.J., Thomas-McArthur, V., Gleadall, L.J., Shaw, P.J. and Cunliffe, V.T. (2006) The microtubule-severing protein Spastin is essential for axon outgrowth in the zebrafish embryo. *Hum. Mol. Genet.*, **15**, 2763–2771.

20. Butler, R., Wood, J.D., Landers, J.A. and Cunliffe, V.T. (2010) Genetic and chemical modulation of spastin-dependent axon outgrowth in zebrafish embryos indicates a role for impaired microtubule dynamics in hereditary spastic paraplegia. *Dis. Model. Mech.*, **3**, 743–751.

21. Zhang, C., Li, D., Ma, Y., Yan, J., Yang, B., Li, P., Yu, A., Lu, C. and Ma, X. (2012) Role of spastin and protrudin in neurite outgrowth. *J. Cell. Biochem.*, **113**, 2296–2307.

22. Allison, R., Lumb, J.H., Fassier, C., Connell, J.W., Martin, Ten, D., Seaman, M.N.J., Hazan,
J. and Reid, E. (2013) An ESCRT-spastin interaction promotes fission of recycling tubules from the endosome. *J. Cell. Biol.*, **202**, 527–543.

23. Mannan, A.U., Boehm, J., Sauter, S.M., Rauber, A., Byrne, P.C., Neesen, J. and Engel, W. (2006) Spastin, the most commonly mutated protein in hereditary spastic paraplegia interacts with Reticulon 1 an endoplasmic reticulum protein. *Neurogenetics*, **7**, 93–103.

24. Rismanchi, N., Soderblom, C., Stadler, J., Zhu, P.-P. and Blackstone, C. (2008) Atlastin GTPases are required for Golgi apparatus and ER morphogenesis. *Hum. Mol. Genet.*, **17**, 1591–1604.

25. Hu, J., Shibata, Y., Zhu, P.-P., Voss, C., Rismanchi, N., Prinz, W.A., Rapoport, T.A. and

Blackstone, C. (2009) A class of dynamin-like GTPases involved in the generation of the tubular ER network. *Cell*, **138**, 549–561.

26. Orso, G., Pendin, D., Liu, S., Tosetto, J., Moss, T.J., Faust, J.E., Micaroni, M., Egorova, A., Martinuzzi, A., McNew, J.A., et al. (2009) Homotypic fusion of ER membranes requires the dynamin-like GTPase atlastin. *Nature*, **460**, 978–983.

27. Vaccaro, A., Patten, S.A., Ciura, S., Maios, C., Therrien, M., Drapeau, P., Kabashi, E. and Parker, J.A. (2012) Methylene Blue Protects against TDP-43 and FUS Neuronal Toxicity in C. elegans and D. rerio. *PLoS ONE*, **7**, e42117.

28. Vaccaro, A., Patten, S.A., Aggad, D., Julien, C., Maios, C., Kabashi, E., Drapeau, P. and Parker, J.A. (2013) Pharmacological reduction of ER stress protects against TDP-43 neuronal toxicity in vivo. *Neurobiol. Dis.*, **55**, 64–75.

29. Nakatsuka, M., Nakatsuka, K. and Osawa, Y. (1998) Metabolism-based inactivation of penile nitric oxide synthase activity by guanabenz. *Drug Metab. Dispos.*, **26**, 497–501.

30. Boyce, M., Bryant, K.F., Jousse, C., Long, K., Harding, H.P., Scheuner, D., Kaufman, R.J., Ma, D., Coen, D.M., Ron, D., et al. (2005) A selective inhibitor of eIF2alpha dephosphorylation protects cells from ER stress. *Science*, **307**, 935–939.
31. Ramsay, R.R., Dunford, C. and Gillman, P.K. (2007) Methylene blue and serotonin toxicity: inhibition of monoamine oxidase A (MAO A) confirms a theoretical prediction. *Br. J. Pharmacol.*, **152**, 946–951.

32. Urano, F., Calfon, M., Yoneda, T., Yun, C., Kiraly, M., Clark, S.G. and Ron, D. (2002) A survival pathway for Caenorhabditis elegans with a blocked unfolded protein response. *J. Cell Biol.*, **158**, 639–646.
33. Madabattula, S.T., Strautman, J.C., Bysice, A.M., O'Sullivan, J.A., Androschuk, A., Rosenfelt, C., Doucet, K., Rouleau, G. and Bolduc, F. (2015) Quantitative Analysis of Climbing Defects in a Drosophila Model of Neurodegenerative Disorders. *J. Vis. Exp.*, 10.3791/52741.

34. Therrien, M., Rouleau, G.A., Dion, P.A. and Parker, J.A. (2013) Deletion of C9ORF72 results in motor neuron degeneration and stress sensitivity in C. elegans. *PLoS ONE*, **8**, e83450.

35. Tauffenberger, A., Julien, C. and Parker, J.A. (2013) Evaluation of longevity enhancing compounds against transactive response DNA-binding protein-43 neuronal toxicity. *Neurobiol. Aging*, **34**, 2175–2182.
36. Tauffenberger, A. and Parker, J.A. (2014) Heritable transmission of stress resistance by high dietary glucose in Caenorhabditis elegans. *PLoS Genet.*, **10**, e1004346.

37. Bolduc, F.V., Bell, K., Cox, H., Broadie, K.S. and Tully, T. (2008) Excess protein synthesis in Drosophila fragile X mutants impairs long-term memory. *Nat. Neurosci.*, **11**, 1143–1145.

Tables

Table 1. Human and orthologous genes associated with hereditary spastic paraplegias used in this study.

Human gene (protein)	***C. elegans* orthologous gene**	**Strain in *C. elegans* used in this study**	**Drosophila orthologous gene**	**Zebrafish orthologous gene**
SPG1 - L1CAM (L1 cell adhesion molecule)	*lad-2*	*lad-2 (hd31)* and *lad-2 (tm3056)*	*nra*	*nadl1.1*
SPG4 - SPAST (Spastin)	*spas-1*	*spas-1 (tm683)* and *spas-1 (ok1608)*	*spas*	*spast*
SPG3A - ATL1 (Atlastin-1)	*atln-1*	*Y54G2A.2 (ok1144)*	*atl*	*atl1*

Abbreviations

HSP: Hereditary spastic paraplegia

ALS: Amyotrophic lateral sclerosis

Figures

Figure 1

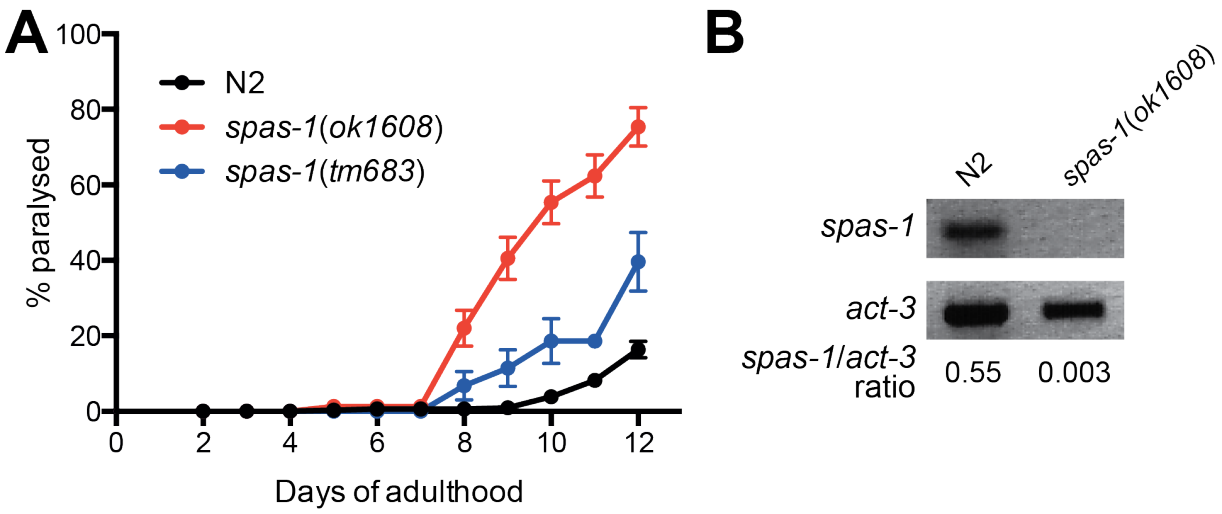

Figure 1. *spas-1* mutation caused age-dependent HSP-related motor phenotype in *C. elegans*. Wild-type N2 nematodes showed no clear paralysis phenotype until the age of day 12 of adulthood. *spas-1*(*ok1608*) and *spas-1*(*tm683*) strains displayed a progressive paralysis phenotype. (**B**) RT-PCR analysis revealed a loss of expression of the *spas-1* gene in the *spas-1*(*ok1608)* nematodes.

Figure 2

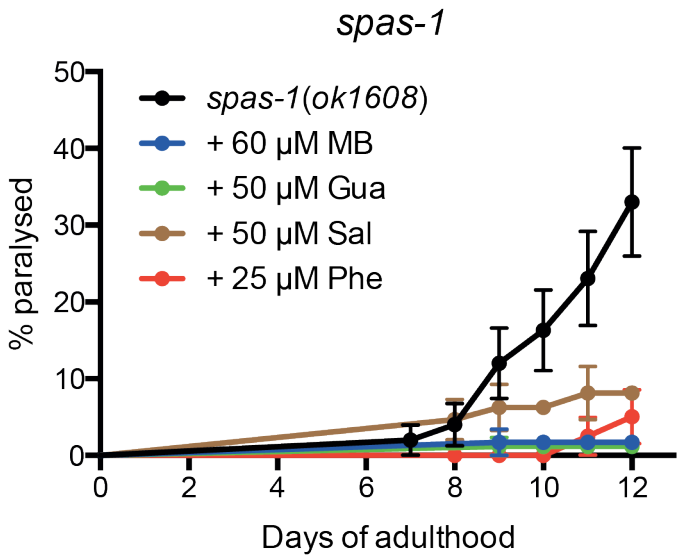

Figure 2. Methylene blue, guanabenz, salubrinal and phenazine prevented the HSP-related motor phenotype in *spas-1* mutation in *C. elegans*. 60 µM methylene blue (MB), 50 µM guanabenz (Gua), 50 salubrinal (Sal) and 25 µM phenazine (Phe) reduced the % of paralysis in *spas-1*(*ok1608*) worms.

Figure 3

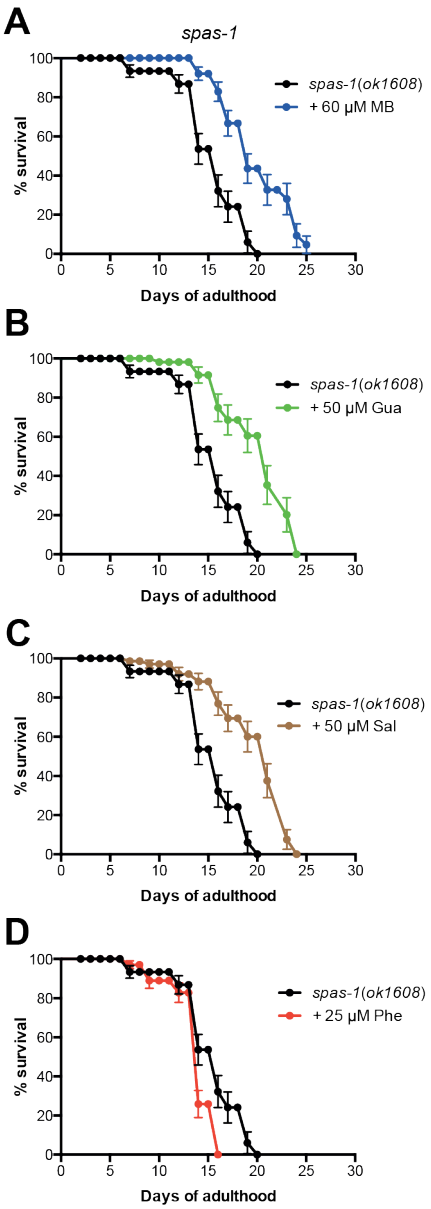

Figure 3. Methylene blue, guanabenz, salubrinal and phenazine extended the lifespan of *spas-1* mutant in *C. elegans*. (**A**) Methylene blue (MB), (**B**) guanabenz (Gua) and (**C**) salubrinal (Sal), (**D**) but not phenazine (Phe), prolonged the lifespan in *spas-1*(*ok1608*) mutants in *C. elegans*.

Figure 4

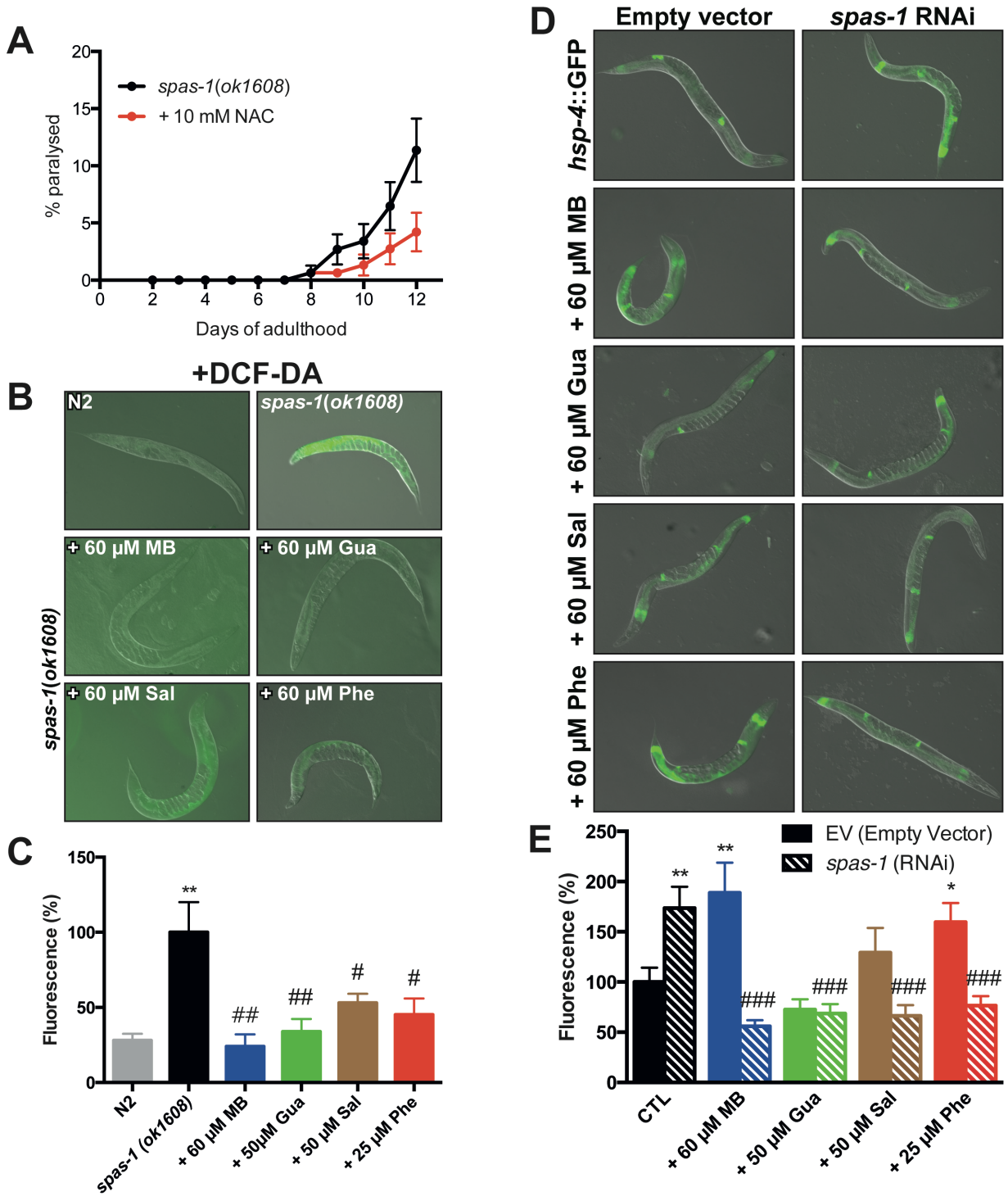

Figure 4. Oxidative stress is associated with the paralysis observed in the *spas-1* mutants, and methylene blue, guanabenz, salubrinal and phenazine prevent this oxidative stress in *spas-1*

mutant nematodes. (**A**) 10 mM *N*-Acetyl-L-cysteine (NAC), a strong antioxidant, reduced the % of paralysis in the *spas-1*(*ok1608*) nematodes. (**B**) 2′,7′-dichlorofluorescein diacetate (DCF-DA) fluorescent photos (**C**) and quantification of *spas-1*(*ok1608*) worms after treatment with methylene blue (MB), guanabenz (Gua), salubrinal (Sal) and phenazine (Phe). $^{**}P < 0.01$ versus N2 controls; $\#P < 0.05$, $\#\#P < 0.01$ versus *spas-1*(*ok1608*) nematodes (Student's *t*-tests). Silencing *spas-1* induces the ER-related *hsp-4*/BiP expression, and methylene blue, guanabenz, salubrinal and phenazine prevent the *hsp-4* increase in *C. elegans*. (**D**) Representation and (**E**) quantification of *spas-1* RNAi which induces the *hsp-4*/BiP expression in the *zcIs4*[*hsp-4*::GFP] worms, but exposure to methylene blue (MB), guanabenz (Gua), salubrinal (Sal) and phenazine (Phe) prevent this *hsp-4*::GFP increase. $^{*}P < 0.05$, $^{**}P < 0.01$ versus untreated empty vector (EV) controls, ### $P < 0.001$ versus untreated *spas-1* RNAi (Student's *t*-tests).

Figure 5

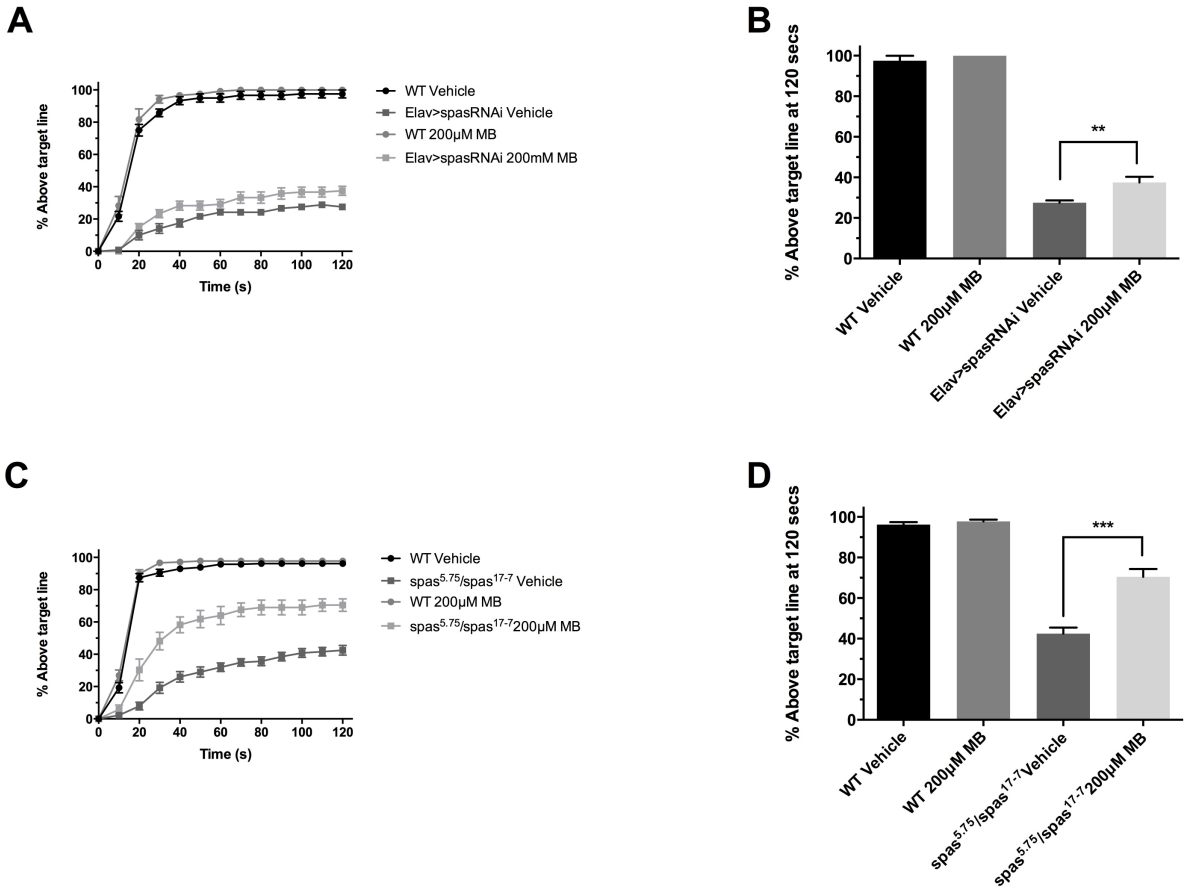

Figure 5. Methylene blue rescues the locomotor defects caused by *spastin* loss-of-function in *Drosophila*. (**A**) Flies expressing pan-neuronal RNAi against *spastin* display poor climbing performance (N=6) which is rescued with overnight Methylene blue treatment. (**B**) Significantly increased climbing performance is observed at 2 minutes with spastin RNAi transgenic flies treated with Methylene blue ($P \leq 0.01$, t-test). (**C**) Transheterozygous spastin mutants ($spastin^{5-75}/spastin^{17-7}$) display poor climbing performance (N=7) which is rescued with overnight Methylene blue treatment. (**D**) Significantly increased climbing performance is observed at 2 minutes with transheterozygous flies treated with Methylene blue ($P \leq 0.001$, t-test).

Figure 6

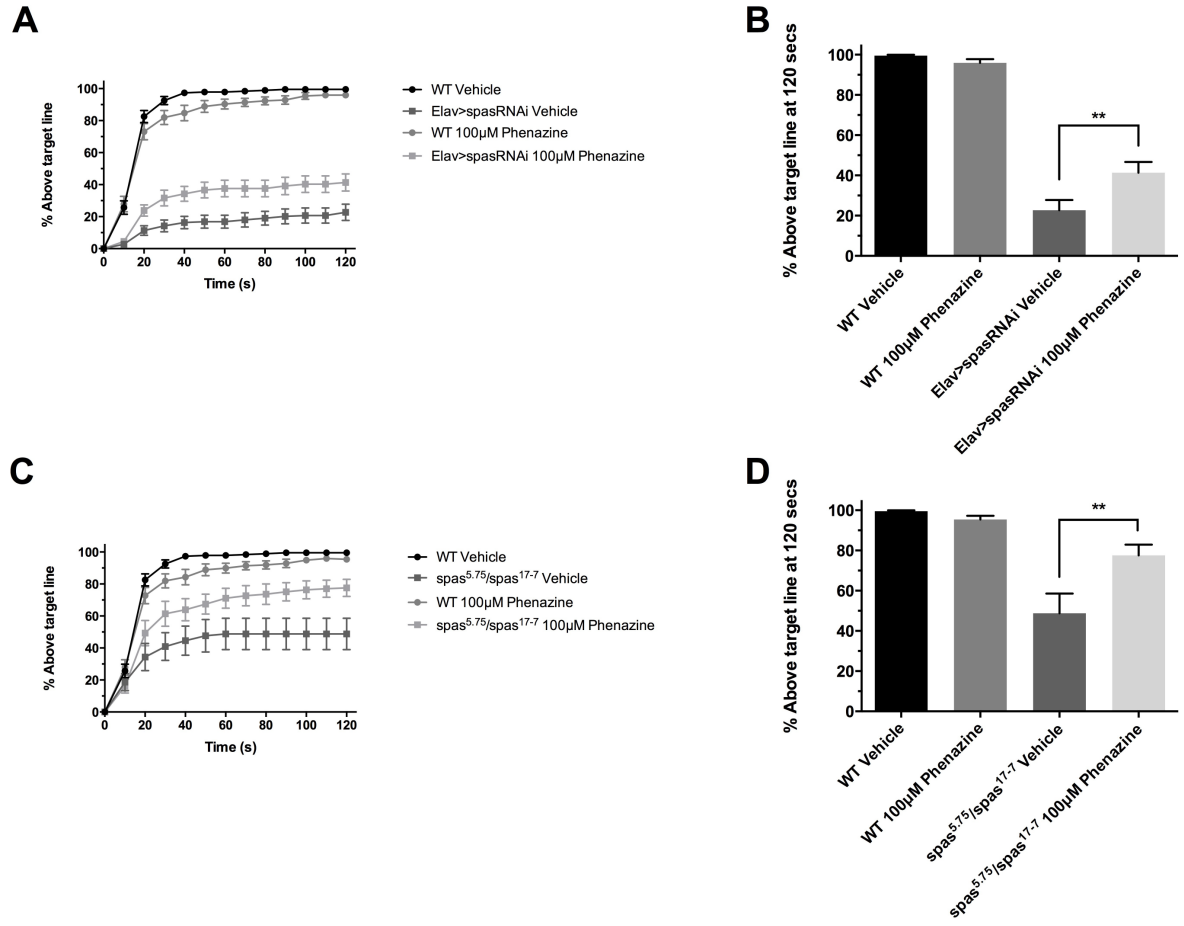

Figure 6. Phenazine rescues the locomotor defects caused by *spastin* loss-of-function in *Drosophila*. (**A**) Flies expressing pan-neuronal RNAi against *spastin* display poor climbing performance (N=10) which is rescued with overnight phenazine treatment. (**B**) Significantly increased climbing performance is observed at 2 minutes with spastin RNAi transgenic flies treated with phenazine ($P \leq 0.01$, t-test). (**C**) Transheterozygous spastin loss-of-function mutants (*spastin*$^{5\text{-}75}$/*spastin*$^{17\text{-}7}$) display poor climbing performance (N=10) which is rescued with overnight phenazine treatment. (**D**) Significantly increased climbing performance is observed at 2 minutes with transheterozygous flies treated with methylene blue ($P \leq 0.01$, t-test).

Figure 7

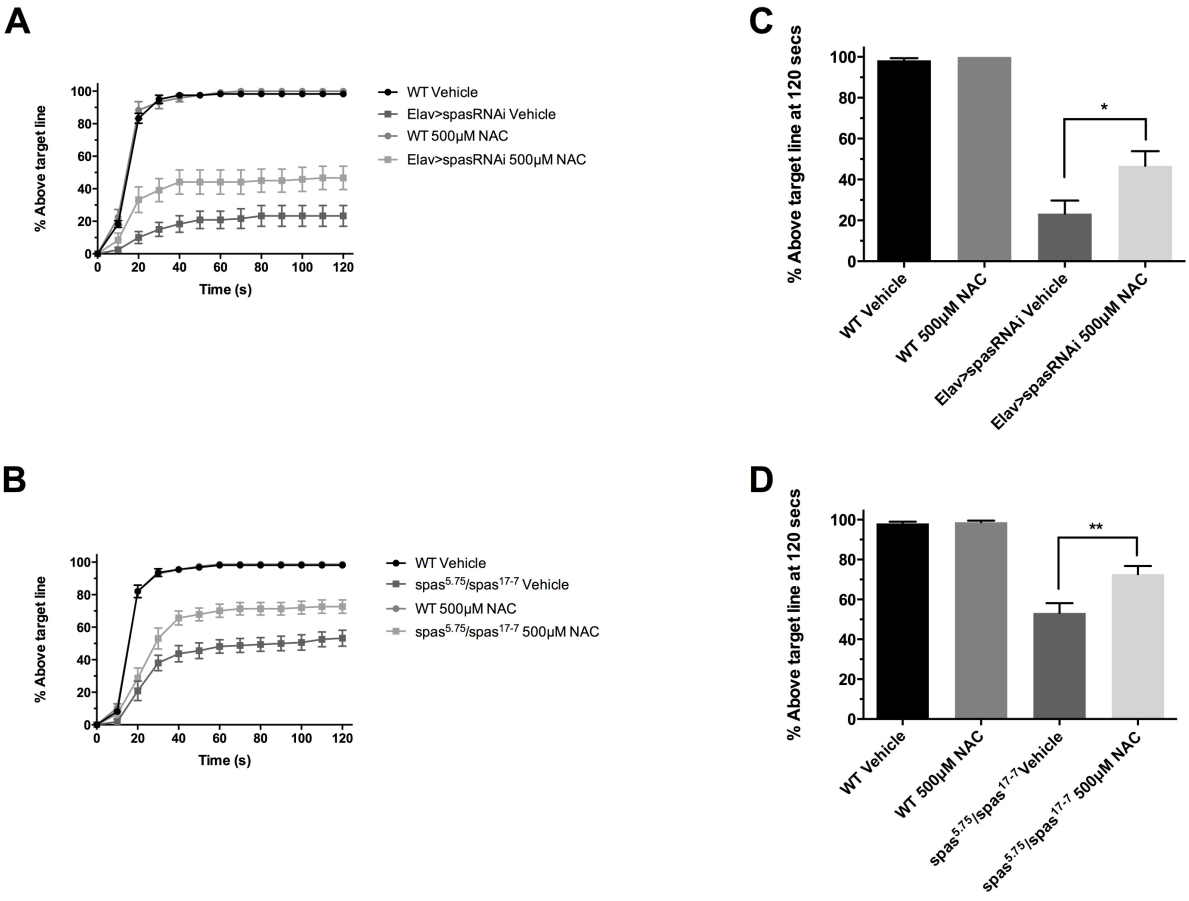

Figure 7. *N*-Acetyl-L-cysteine rescues the locomotor defects caused by *spastin* loss-of-function in *Drosophila*. (**A**) Flies expressing pan-neuronal RNAi against *spastin* display poor climbing performance (N=6) which is rescued with overnight *N*-Acetyl-L-cysteine treatment. (**B**) Significantly increased climbing performance is observed at 2 minutes with spastin RNAi transgenic flies treated with *N*-Acetyl-L-cysteine ($P \leq 0.05$, t-test). (**C**) Transheterozygous spastin mutants ($spastin^{5-75}/spastin^{17-7}$) display poor climbing performance (N=8) which is rescued with overnight *N*-Acetyl-L-cysteine treatment. (**D**) Significantly increased climbing performance is observed at 2 minutes with transheterozygous flies treated with *N*-Acetyl-L-cysteine ($P \leq 0.01$, t-test).

Figure 8

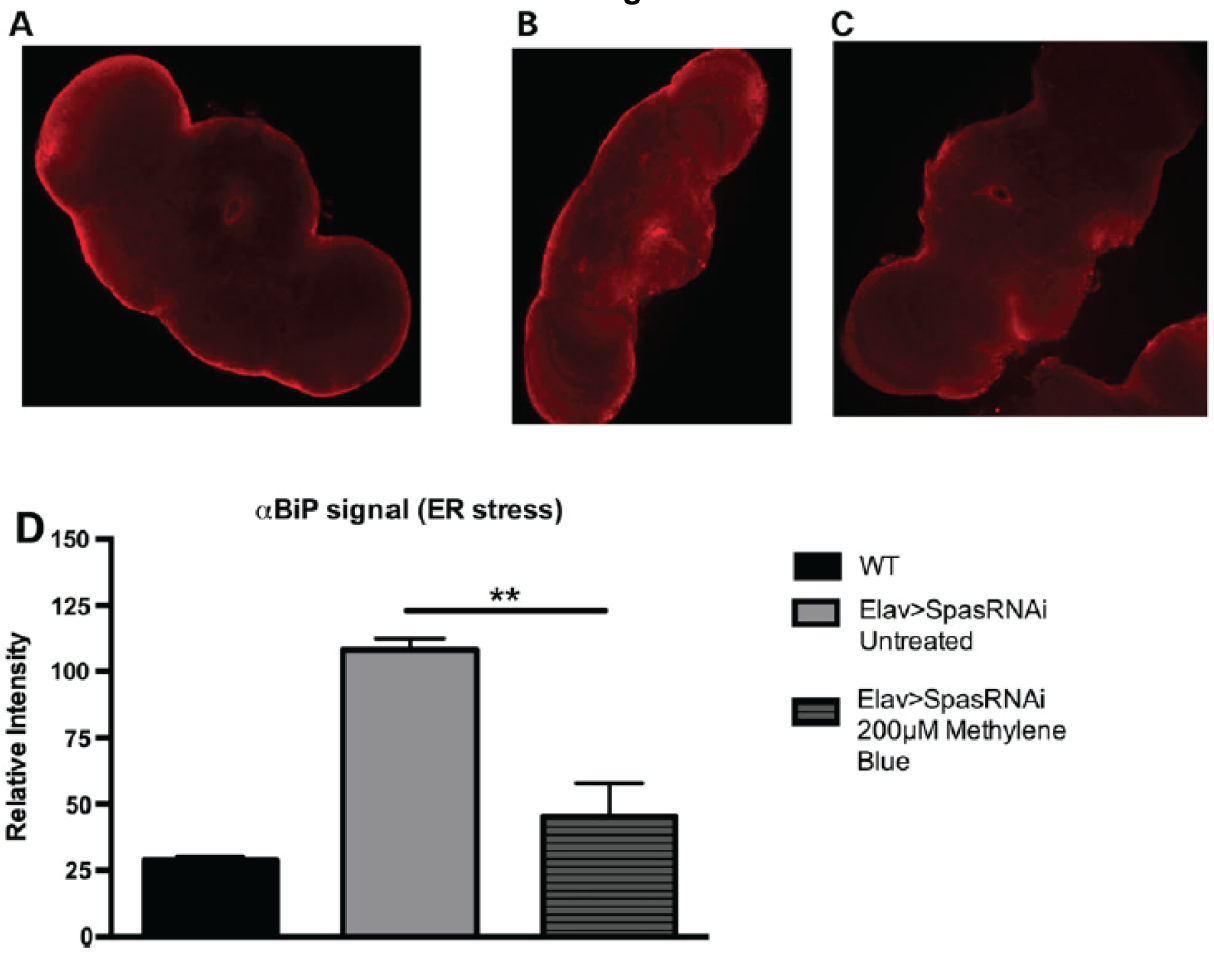

Figure 8. Methylene blue rescues exaggerated oxidative stress caused by *spastin* loss-of-function in *Drosophila*. Representative confocal images of BiP immunostraining in A) wild-type, B) *spastin* RNAi expressing flies treated with vehicle and C) *spastin* RNAi flies treated with methylene blue. D) Flies expressing pan-neuronal RNAi against spastin display elevated BiP level compared to wild type flies. This level is rescued to normal level by the administration of methylene blue provided in the negative geotaxis experiments (N=5, $P<0.01$, t-test).

Figure 9

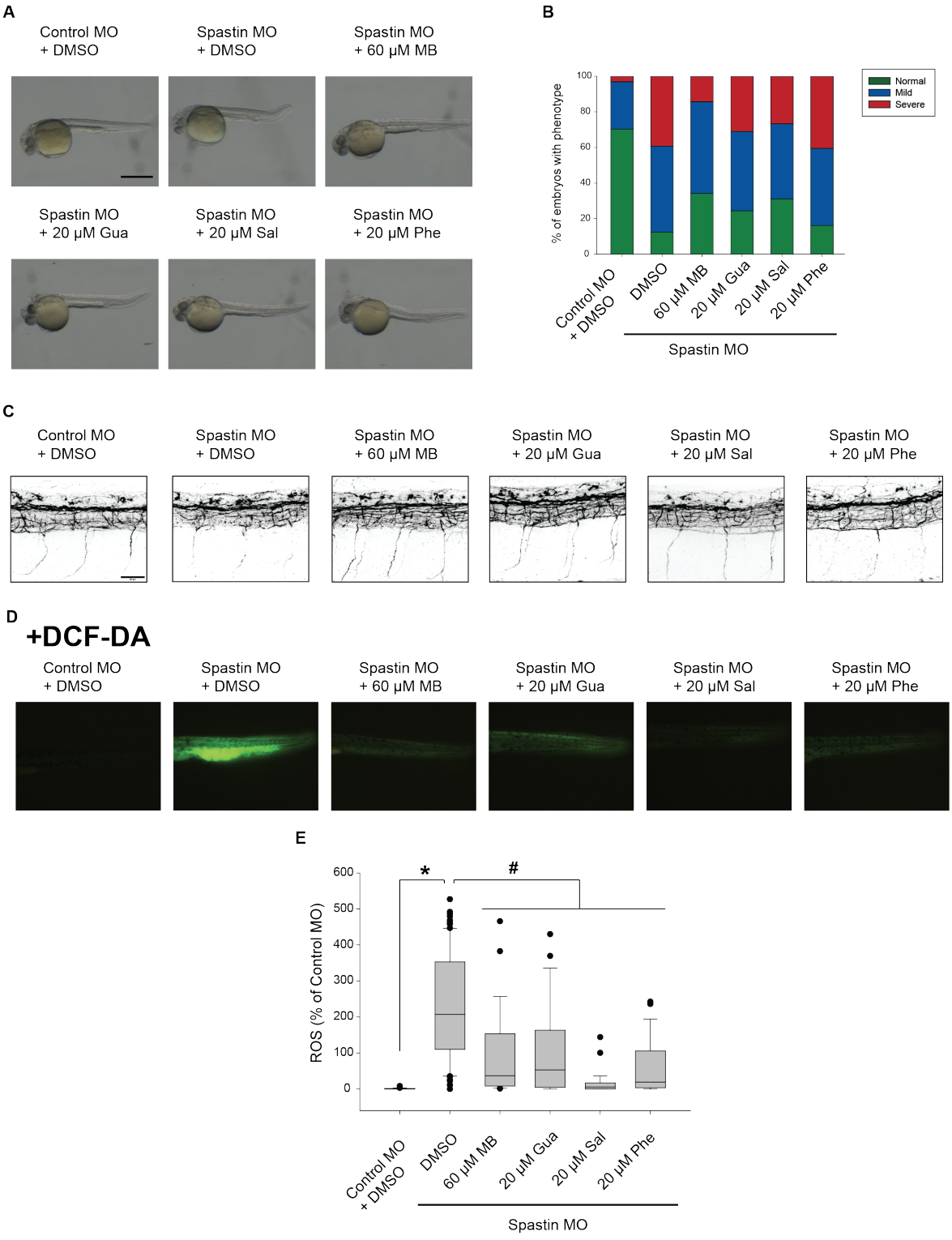
A
Control MO + DMSO
Spastin MO + DMSO
Spastin MO + 60 µM MB
Spastin MO + 20 µM Gua
Spastin MO + 20 µM Sal
Spastin MO + 20 µM Phe
B
% of embryos with phenotype
Normal
Mild
Severe
Control MO + DMSO
DMSO
60 µM MB
20 µM Gua
20 µM Sal
20 µM Phe
Spastin MO
C
Control MO + DMSO
Spastin MO + DMSO
Spastin MO + 60 µM MB
Spastin MO + 20 µM Gua
Spastin MO + 20 µM Sal
Spastin MO + 20 µM Phe
D
+DCF-DA
Control MO + DMSO
Spastin MO + DMSO
Spastin MO + 60 µM MB
Spastin MO + 20 µM Gua
Spastin MO + 20 µM Sal
Spastin MO + 20 µM Phe
E
ROS (% of Control MO)
*
#
Control MO + DMSO
DMSO
60 µM MB
20 µM Gua
20 µM Sal
20 µM Phe
Spastin MO

Figure 9. Methylene blue, guanabenz, salubrinal and phenazine partially rescue the morphological phenotype and reduce microtubule defects of the zebrafish *spastin* morphant. (**A**) Zebrafish embryos at 30 hours post fertilization (hpf). *spastin* morphant embryos show abnormal morphological features compared to embryo injected with control morpholino. Arrows show defects in the head, yolk sac extension and tail. These defects are partially rescued by 60 μM methylene blue (MB), 20 μM guanabenz (Gua), 20 μM salubrinal (Sal) and 20 μM phenazine (Phe). Scale bar is 500 μm. (**B**) Quantification of morphological defects shown in (A). (**C**) Whole-mount immunohistochemistry of 30 hpf zebrafish embryos labeled with a microtubule marker. A lateral view of the trunk is shown, with the rostral side of the embryo to the left. *spastin* morphants show a disorganized spinal cord, with thin microtubules at the level of the motor neuron axons. These defects are partially rescued by 60 μM methylene blue (MB), 20 μM guanabenz (Gua), 20 μM salubrinal (Sal) and 20 μM phenazine (Phe). Scale bar is 30 μm, MO: morpholino. (**D**) Zebrafish embryos injected with a control morpholino show very low level of fluorescence when treated with 2′,7′-dichlorofluorescein diacetate (DCF-DA) (a biomarker for oxidative stress) compared to embryos injected with a morpholino against spastin. Methylene blue, guanabenz, salubrinal and phenazine reduced the fluorescence. (**E**) Quantification of fluorescence in DCF-DA-treated embryos show a significant reduction of fluorescence upon treatment with the 4 drugs (**P* < 0.001 versus control morphant embryos; #*P* < 0.01 versus *spastin* morphant embryos).

Supplemental figures

Supplemental Figure 1

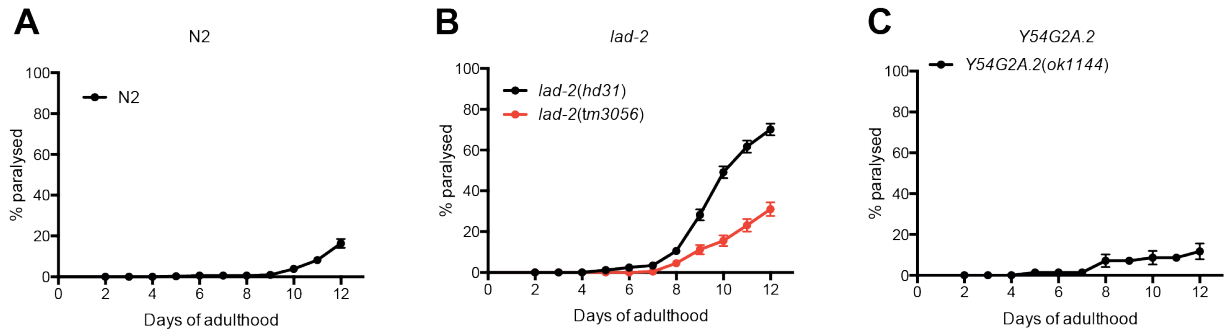

Supplemental Figure 1. *lad-2* mutation caused age-dependent HSP-related motor phenotype in *C. elegans*. Wild-type N2 nematodes showed no clear paralysis phenotype until the age of day 12 of adulthood. (**B**) *lad-2*(*hd31*), *lad-2*(*tm3056*) strains displayed a paralysis phenotype (**C**) but not the *atln-1-related* mutant *Y54G2A.2*(*ok1144*).

Supplemental Figure 2

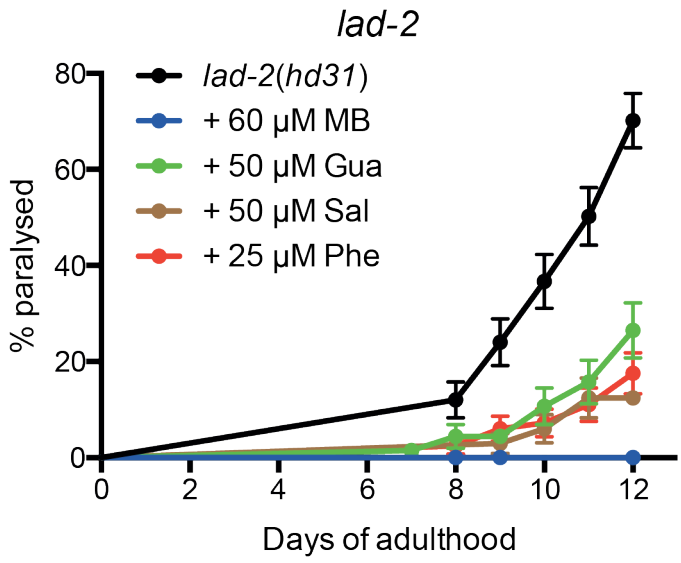

Supplemental Figure 2. Methylene blue, guanabenz, salubrinal and phenazine prevented the HSP-related motor phenotype in *lad-2* mutation in *C. elegans*. 60 µM methylene blue (MB), 50 µM guanabenz (Gua), 50 salubrinal (Sal) and 25 µM phenazine (Phe) reduced the % of paralysis in *lad-2*(*hd31*) worms.

Supplemental Figure 3

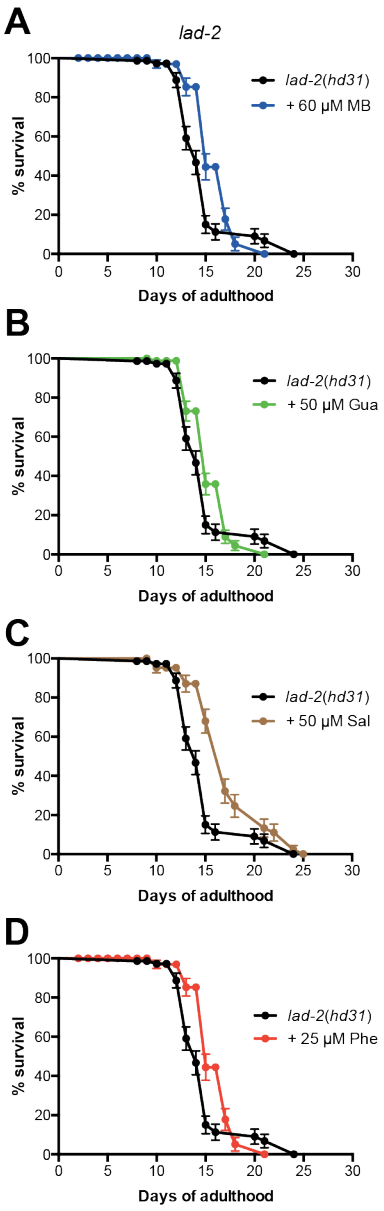

Supplemental Figure 3. The compounds extended the lifespan of *lad-2* mutant in *C. elegans*. (**A**) Methylene blue (MB), (**B**) guanabenz (Gua), and (**C**) salubrinal (Sal), (**D**) but not phenazine (Phe), prolonged the lifespan in *lad-2*(*hd31*) mutants in *C. elegans*.

Supplemental Figure 4

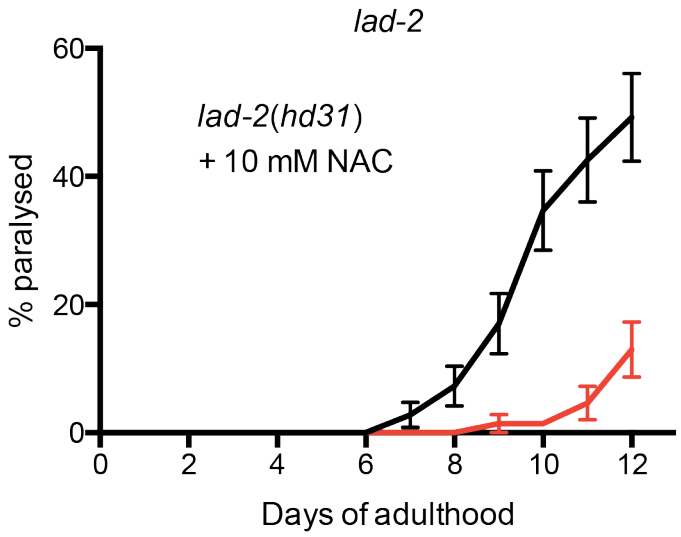

Supplemental Figure 4. Antioxidant effect on the paralysis phenotype in *lad-2* mutant in *C. elegans*. 10 mM *N*-Acetyl-L-cysteine (NAC), a strong antioxidant, reduced the % of paralysis in the *lad-2*(*hd31*) nematodes.

Supplemental Figure 5

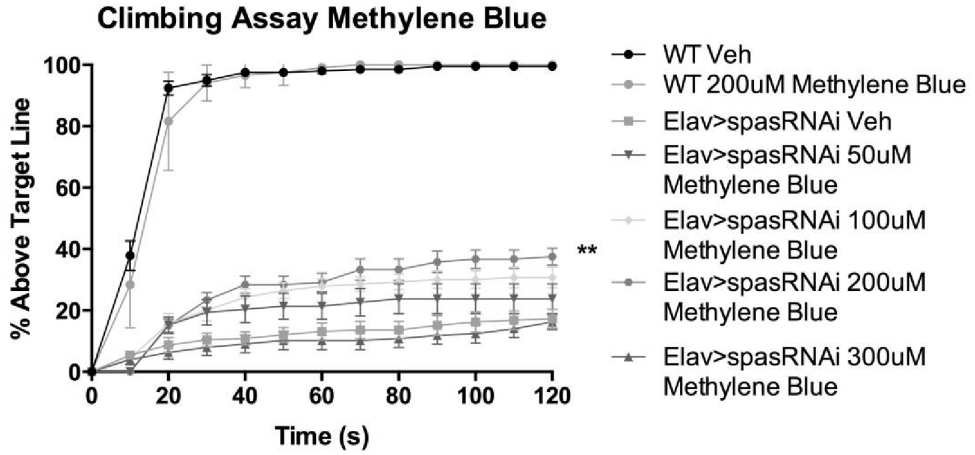

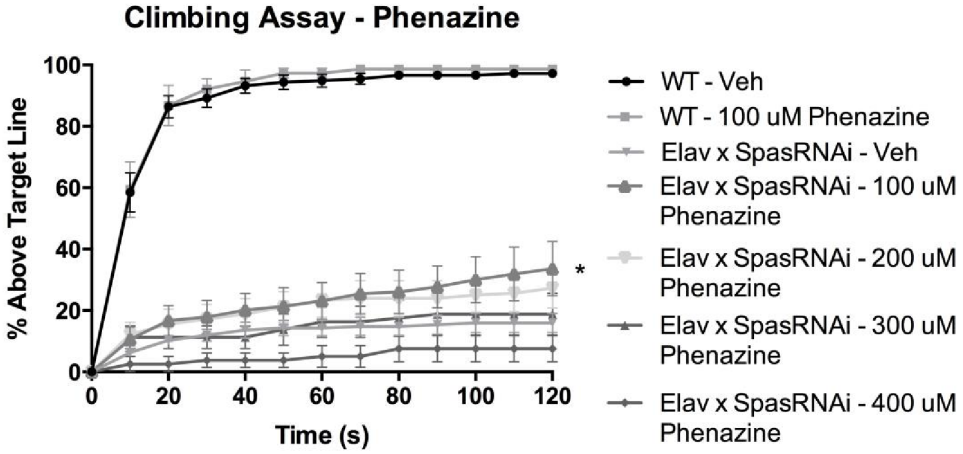

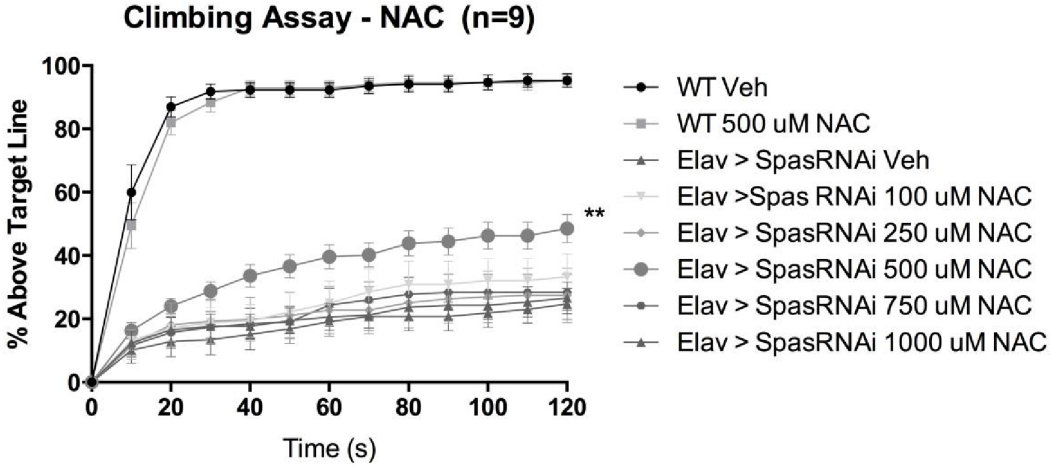

Supplemental Figure 5. Dose response curve in transgenic flies with pan-neuronal expression of spastin-RNAi. A) Dose response curve with methylene blue identified a inverted U shape response. Optimal dose is seen at 200uM. (N=10, P= 0.0013) B) Dose response curve with phenazine also identified an inverted U shape response with optimal dose at 100uM. (N=9, P=0.0035). C) Dose response curve with N-Acetyl-cysteine (NAC) identified an inverted U shape response with optimal dose at 500uM. (N=9, P=0.0019).

Chapter 3: Mutations in *CAPN1* Cause Autosomal-Recessive Hereditary Spastic Paraplegia

Ziv Gan-Or,* Naima Bouslam,* Nazha Birouk,* **Alexandra Lissouba**,* Daniel B. Chambers, Julie Vérièpe, Alaura Androschuck, Sandra B. Laurent, Daniel Rochefort, Dan Spiegelman, Alexandre Dionne-Laporte, Anna Szuto, Meijiang Liao, Denise A. Figlewicz, Ahmed Bouhouche, Ali Benomar, Mohamed Yahyaoui, Reda Ouazzani, Grace Yoon, Nicolas Dupré, Oksana Suchowersky, Francois Bolduc, J Alex Parker, Patrick A. Dion, Pierre Drapeau, Guy A. Rouleau, Bouchra Ouled Amar Bencheikh

The American Journal of Human Genetics 98, 1038–1046, 2016

Doi: 10.1016/j.ajhg.2016.04.002

Authors contribution

*The first four authors are co-first authors

I am a co-first author on this manuscript

For this manuscript, I was responsible for all the zebrafish experiments. As such I designed the zebrafish experiments with PD, realized all the zebrafish experiments, analyzed all the zebrafish experiments, produced all the zebrafish figures (Figure 3, Figure 4, Supplemental Figure 4, Supplemental Figure 5, Supplemental Figure 6) and wrote the parts of the manuscript specific for zebrafish.

Manuscript

Mutations in *CAPN1* Cause Autosomal Recessive Hereditary Spastic Paraplegia

Ziv Gan-Or,[1,2,3,*] Naima Bouslam,[4,*] Nazha Birouk,[5,*] Alexandra Lissouba,[6,7,*] Daniel B. Chambers,[8] Julie Vérièpe,[6,9] Alaura Androschuck,[8] Sandra B. Laurent,[1,3,] Daniel Rochefort,[1,3] Dan Spiegelman,[1,3] Alexandre Dionne-Laporte,[1,3] Anna Szuto,[1] Meijiang Liao,[6,7] Denise A. Figlewicz,[10] Ahmed Bouhouche,[4] Ali Benomar,[4] Mohamed Yahyaoui,[4,] Reda Ouazzani,[5] Grace Yoon,[11,12] Nicolas Dupré,[13] Oksana Suchowersky,[14] Francois Bolduc,[8] J Alex Parker,[6,7] Patrick A. Dion,[1,3] Pierre Drapeau,[6,7] Guy A. Rouleau,[1,2,3]* Bouchra Ouled Amar Bencheikh.[1,6]

Affiliations:

[1] Montreal Neurological Institute and Hospital, McGill University, Montréal, Québec, H3A 2B4, Canada

[2] Department of Human Genetics, McGill University, Montréal, Québec, H3A 0G4, Canada

[3] Department of Neurology and Neurosurgery, McGill University, Montréal, Québec, H3A 0G4, Canada

[4] Service de Neurologie et de Neurogénétique, Hôpital des spécialités, Centre Hospitalier Ibn Sina, Université Mohammed V Souissi, Rabat, BP 6527 Maroc

[5] Service de Neurophysiologie Clinique, Hôpital des spécialités, Centre Hospitalier Ibn Sina, Université Mohammed V Souissi, Rabat, BP 6527 Maroc

[6] Centre de Recherche du Centre Hospitalier de l'Université de Montréal (CRCHUM), Montréal, Québec, H2X 0A9, Canada

[7] Département de pathologie et biologie cellulaire, Université de Montréal, Montréal, Québec, H3C 3J7, Canada

[8] Department of Pediatrics, Neuroscience and Mental Health Institute, University of Alberta,

Edmonton, Alberta, T6G 2R3, Canada

[9] Département de neurosciences, Université de Montréal, Montréal, Québec, H3C 3J7, Canada

[10] Schulich School of Medicine and Dentistry, Western University, London, Ontario, N6A 5C1, Canada

[11] Division of Neurology, Department of Pediatrics, University of Toronto, The Hospital for Sick Children, Toronto, M5G 1X8 Canada

[12] Division of Clinical and Metabolic Genetics, Department of Pediatrics, University of Toronto, The Hospital for Sick Children, Toronto, M5G 1X8 Canada

[13] Division of Neurology, CHU de Québec, and Faculty of Medicine, Laval University, Quebec City, Quebec, G1V 0A6 Canada

[14] Division of Neurology, University of Alberta, Edmonton, Alberta, T6G 2R3 Canada

[*] These authors contributed equally to the work

*Corresponding author:

Guy A. Rouleau,
Director, Montréal Neurological Institute and hospital
Address: 3801, University Street, Office 636
Montréal, Québec H3A 2B4
Tel: +1-514-398-2690, Fax. +1-514 398-8248
Email: guy.rouleau@mcgill.ca

Abstract

Hereditary Spastic Paraplegia (HSP) is a genetically and clinically heterogeneous disease characterized by spasticity and weakness of the lower limbs, with or without additional neurological symptoms. Although more than 70 genes and genetic loci have been implicated in HSP, many families remain genetically undiagnosed, suggesting that other genetic causes of HSP are still to be identified. HSP can be inherited in an autosomal-dominant or -recessive, or X-linked manner. In the current study, we analyzed three families with autosomal-recessive HSP, with a total of 9 affected individuals who were tested with whole exome sequencing. Rare homozygous and compound heterozygous nonsense, missense, frame-shift and splice-site mutations in *CAPN1* were identified in all affected individuals, and sequencing in additional family members confirmed the segregation of these mutations with the disease. *CAPN1* encodes calpain 1, a protease that is widely expressed in the central nervous system. Calpain 1 is involved in synaptic plasticity, synaptic restructuring and axon maturation and maintenance. Three models of calpain 1 deficiency were further studied. In *C. elegans*, loss of calpain 1 function resulted in neuronal and axonal dysfunction and degeneration. Similarly, loss-of-function for the *Drosophila melanogaster* orthologue calpain B caused locomotor defects and axonal anomalies. Knockdown of calpain 1a, a *CAPN1* orthologue in *Danio rerio*, resulted in abnormal branchiomotor neurons migration and disorganized acetylated tubulin axonal networks in the brain. The identification of mutations in *CAPN1* in HSP expands our understanding of the disease causes and potential mechanisms.

Main text

Hereditary Spastic Paraplegias (HSP) are a rare group of neurological disorders with an estimated prevalence of 2-10/100,000 in different populations.[1-3] HSP can be classified as pure or complicated, based on the clinical presentation. Pure HSP is characterized by progressive spasticity and weakness, limited to the lower limbs, often presenting with deep tendon hyperreflexia and extensor plantar response. Additional features of the pure form that are often reported are hypertonic bladder and lower limb sensory disturbances. Complicated HSP is accompanied by other neurological symptoms, including seizures, ataxia, intellectual disability, dementia, extrapyramidal symptoms, peripheral neuropathy (if other causes of peripheral neuropathy were ruled out), amyotrophy, optic atrophy and others.[3; 4] While HSP can be debilitating, individuals with HSP often have normal life span, therefore post-mortem studies are not common and neuropathological data are limited. However, the available information indicates that HSP is typically characterized by axonal degeneration of descending corticospinal tract and ascending sensory fibers.[5] HSP is a genetically heterogeneous disease; currently, there are more than 70 known or suspected genes or genetic loci in which mutations have been suggested to cause HSP.[6; 7] Some of the genes are exclusively associated with pure or complicated HSP, however, other genes are associated with both forms of HSP, indicating that other genetic or environmental factors can modify the disease course. HSP can be inherited in autosomal dominant (AD-HSP), autosomal recessive (AR-HSP) or X-linked (XL-HSP) manner. Mutations in *SPAST* (MIM: 604277) account for about 40% of autosomal dominant HSP (MIM: 182601),[8] and homozygous or compound heterozygous mutations in *SPG11* (MIM 610844) are the most common cause for AR-HSP (MIM: 604360).[4] Both genes are thought to be involved in endosomal trafficking, and other HSP related genes are involved in different pathways such as mitochondrial regulation, lipid metabolism and endoplasmic reticulum regulation, as was previously reviewed.[3; 6] In the current. study, we used whole exome sequencing (WES) to analyse three families with AR-HSP and identified homozygous or compound heterozygous mutations in *CAPN1* (MIM: 114220) as the cause for HSP in these families. We further studied the effects of *CAPN1* orthologues loss-of- function in *Caenorhabditis elegans*, *Drosophila*

melanogaster and *Danio rerio* models.

The three families (Figure 1) included two consanguineous Moroccan families (families A and B) and one family from Idaho and Utah, US (family C). Of note, the pedigree of Family B is a pseudo- dominant pedigree, due to multiple intra-familial marriages within this family. They live in a small village in the north-west of Morocco, in which many of the residents are related due to common ancestors. The clinical data on the affected individuals from these three families are detailed in Table 1. Families A and B were diagnosed and followed up by a neurologist at the Clinical Neurophysiology department, Specialities Hospital, Chis Ibn Sina, Rabat-Sale, Morocco, and members from family C were diagnosed and followed up by neurologists from Idaho and Utah, US. All individuals signed an informed consent form before entering the study, and the study design and protocols were approved by the Institutional Review Boards. Table 1 details the clinical characteristics of eight individuals from the three families with available clinical data. The average age at onset was 28.5 years (±8.05, range 19-39), and the affected individuals presented with symptoms of complicated HSP. In addition to lower extremity spasticity and hyperreflexia, seven of the eight individuals had upper extremity hyperreflexia, six had dysarthria, and ataxia was reported in three. Six individuals had foot deformities, five with the typical pes cavus and one with pes valgus. Abnormal bladder function was reported in two individuals. No seizures were reported. Overall, the motor impairment was mild to moderate, and two of the individuals (Family B, IV-2 and Family C, IV-13) had started using a cane to aid walking. No vision abnormalities were reported or identified in the neurological examinations. Blood Samples for DNA analysis were available from nine affected individuals from the three families (Family A – V-1, V-2, V-4, Family B – IV-1, IV-2, IV-5 and IV-9 and Family C – IV-7, IV-13, Figure 1) and all nine samples went through whole exome sequencing (WES). Additional samples from unaffected individuals were available from four individuals of Family A (IV-2, IV-3, V-3 and V-6), three individuals from Family B (III-2, III-3 and IV-11), and four individuals of Family C (III-1, III-2, IV-9, IV-15). These additional samples were used for validation and segregation analysis of the mutations. DNA was extracted using a standard salting out protocol, and was captured for whole exome sequencing (WES) using the Agilent SureSelect Human All Exon V4 Kit according to the manufacturer instructions (Agilent Technologies,

Santa Clara, CA). The captured DNA was sequenced using the Illumina HiSeq2000 (2×100 bp, three samples per lane) at the Innovation Genome Center, McGill University and Genome Quebec. Sequence processing, alignment and variant calling were done using Burrows-Wheeler Aligner,[9; 10] (BWA) the Broad Institute Genome Analysis Toolkit[11] (GATK v.4) and ANNOVAR.[12] Following the annotation, data on the detected variants were extracted from publicly available databases - the 1000 Genomes Project,[13] Exome Variant Server (EVS) - NHLBI GO Exome Sequencing Project (ESP), Seattle, WA, the Exome Aggregation Consortium (ExAC) and dbSNP132. In addition, the frequencies of these variants were calculated in our in-house dataset of over 1,600 samples that underwent WES. To estimate the potential effects of the mutation, we used the online prediction and conservation tools SIFT,[14] PolyPhen 2,[15] MutationTaster,[16] PhyloP[17] and GERP++.[18] Details on the filtering process can be found in the supplementary data. In order to validate and examine the segregation of the candidate mutations with the disease, DNA from all affected and unaffected family members with available samples was amplified using specific primers and sequenced by Sanger sequencing (Applied Biosystem's 3730xl DNA Analyzer technology, primers detailed in Table S1).

The average coverage of the nine samples that were sequenced using WES was 129X, 99% of the bases had a coverage >10X and 97% had a coverage > 20X. In order to identify potential causative mutations, all variants with allele frequency > 0.005 in either the 1000 genome project, EVS, dbSNP132 or variants that were already found in our in-house dataset were excluded. Synonymous, 5' UTR, 3' UTR and intronic variants that are not within the 6 nucleotides at splice- sites were subsequently excluded, to include only nonsynonymous, frame-shift, stop and splice- site mutations. Further filtering was done based on prediction of deleterious effects and conservation. In families A and B homozygous mutations were considered, and in family C both homozygous and compound heterozygous variants were considered (Table S2). No mutations in exons covered by the exome sequencing in known or suspected HSP genes segregated with the disease in any of the families. In the three families, mutations in only one gene, *CAPN1*, segregated with the disease after the filtering (Figure 1). In family A, the three affected individuals were homozygous for a missense mutation in exon 8 of *CAPN1*, c.884G>C, leading to a p.Arg295Pro substitution (NM_005186), which is

predicted to be deleterious (SIFT score 0, PolyPhen2 score 1) and highly conserved (GERP++ score >2, Figure 2C). This substitution is located next to an active site in position 296, the amino acid Asparagine which is a critical Ca^{2+} binding site,[19; 20] at the end of a β-strand (Figure 2D). In family B, the four affected individuals were homozygous for a nonsense mutation in exon 14, c.1579C>T, resulting in a p.Gln527* (NM_005186) early termination of the protein. Homozygosity mapping of the 7 individuals from these two families confirmed that a region on chromosome 11, spanning 3.5 Mb and containing *CAPN1*, is the only shared homozygous region. In family C, the two affected individuals were compound heterozygous for a frame-shift mutation on exon 4, c.406delC (p.Pro136Argfs*40, Figure 2G) and a splicing mutation c.1605+5G>A (Figure 2E-G). None of these variants from the three families were identified in the 1000 genome project, ESP, or our in-house > 1600 exome-sequencing samples. The coding variants were also not detected in the ExAC database and the c.1605+5G>A splice-site mutation had a frequency of 0.0001. All mutations were validated using Sanger sequencing, and all the available DNA samples from family members were also sequenced. In Family A, the two parents (IV-2 and IV-3, Figure 1) and two siblings (V-3 and V-6) of the affected individuals were all heterozygous for the *CAPN1* p.Arg295Pro substitution. In Family B, the two parents (III-2 and III-3) and one sibling (IV-11) of the four individuals that were sequenced using WES, were all heterozygous carriers of the *CAPN1* p.Gln527* early terminated protein. In Family C, both parents (III-1 and III-2) and two siblings (IV-9 and IV-15) were sequenced. The father, III-1, was a heterozygous carrier of the c.1605+5G>A mutation, and the mother, III-2, was a heterozygous carrier of the c.406delC mutation, confirming phasing. The sibling IV-9 was a non- carrier of both variants, and IV-15 was a heterozygous carrier of the c.1605+5G>A mutation. To examine the predicted effect of the splice-site c.1605+5G>A mutation, RNA was produced from immortalized lymphoblasts from individual IV-7 (Family C) and from healthy family members, and cDNA was produced using the Invitrogen SuperScript® III Reverse Transcriptase kit (InVitrogen Corp.). Specific primers were designed to amplify the cDNA around the c.1605+5G>A mutation, forward 5'- ACTATTGGCTTCGCGGTCTA and reverse 5'- ATTGTCCGCAACTCCTTCAC, with a cDNA amplicon length of 389 bp (DNA amplicon length 3405 bp). Individual IV-7 had 2 copies of cDNA around the c.1605+5G>A splice-site mutation with different lengths (Figure 2E). Sequencing of the cDNA after

separation on gel demonstrated that this splice variant resulted in exon 14 skipping and early stop codon (Figure 2E-G). RNAi knock down of the *C. elegans* orthologue of *CAPN1, clp-1,* led to neurodegeneration of GABAergic motor neurons and age-dependent paralysis phenotype (see Figure S1 for details on the experiments and results). Similarly, loss-of-function of *CAPN1* orthologue in Drosophila led to locomotor defects and axonal abnormalities (see figures S2 and S3 for details on the experiments and results). RNAi against the Drosophila orthologue, *calpain B*, led to age-dependent negative geotaxis (Figure S2). Defects in axons were observed in transgenic flies expressing *calpain B* with the pan-neuronal driver Elav. Axons appeared to have larger diameter and increased level of acetylated tubulin (Figure S3).

Zebrafish (*Danio rerio*) embryos were collected and staged using standard methods.[21] The local animal care committee at the Centre de Recherche du Centre Hospitalier de l'Université de Montréal (CRCHUM), having received the protocol relevant to this project relating to animal care and treatment, certified that the care and treatment of animals was in accordance with the guidelines and principles of the Canadian Council on Animal Care. Zebrafish embryos (no adults were used) are insentient to pain. Similarly to the findings in Drosophila, Figure S4 demonstrates clusters of acetylated tubulin in capn1a morphants zebrafish. Increased acetylated tubulin is associated with hyperstabilization of microtubules and has been associated with *SPAST* mutations previously. The zebrafish *calpain 1a* (*capn1a*) and *calpain 1b* (*capn1b*) both encode proteins that are orthologues of the human *CAPN1*.[22] Morpholino oligonucleotides against both genes were used to model the loss-of-function of *CAPN1*. Only the *capn1a* morpholino (*capn1a* Mo) led to a phenotype, but not the *capn1b* morpholino (data not shown). Details on the knockdown of the zebrafish calpains, morphology measurements and imaging are in the legend for Figure S5. *capn1a* Mo resulted in several developmental defects visible at 2 dpf, and moderate to severe phenotype was exhibited by 78% of injected embryos at 5 dpf, indicating that these defects are long lasting (Figure S5). Knockdown with *capn1a* Mo was confirmed in western blots at 48 hpf (Figure S6). However, co-injecting the human wild-type CALPAIN 1 mRNA (up to 500 pg of RNA) in wild-type and morpholino-injected eggs failed to show a toxic effect of the RNA on its own, or a rescue of the morpholino-induced phenotype. By western blotting (Figure S6), the

zebrafish and human Calpain 1 proteins showed exclusive patterns that explain the failure of rescue. Specifically, the human protein was detected at 24 hpf but no longer at 48 hpf, whereas the zebrafish protein was detected only later at 48 hpf. Thus the early expression of human mRNA may well have failed to rescue the later knockdown phenotype. Due to the lack of rescue, the role of the *CAPN1* p.Arg295Pro substitution could not be established in this model, and other models will be necessary to examine the effect of this substitution. As *capn1a* is mainly expressed in the brain starting at 24 hours post fertilization,[22] we injected *capn1a* Mo in the Islet1::GFP transgenic fish expressing GFP in the motor neurons, including the branchiomotor neurons. We observed a disorganisation of these motor neurons compared to control, as well as migration defects of the nV trigeminal nuclei in rhombomeres 2 and 3 (r2 and r3) and of the VII facial branchiomotor neuronal cell bodies, which have not fully migrated from r4 to r6. Furthermore, the vagal motor neurons had an aberrant positioning and spacing, probably due to a defect in cell motility (Figure 3).

Growing axons in the brain and spinal cord were then observed using an antibody against acetylated tubulin. The microtubule network in the brain of *capn1a* morpholino injected embryos (Figure 4B, 4D) appeared to be following a different pattern than in the mismatch-injected morphants (Figure 4A, 4C). Reduced acetylated-tubulin staining could be observed at the level of the optic tectum and cerebellum, while a stronger staining is found in the telencephalon. Strikingly, clusters of acetylated tubulin could be observed in some cells in the dorsal-most part of the brain (Figure 4B, 4D). Furthermore, acetylated tubulin staining in the spinal cord demonstrated that microtubules in the motor neuron axons are thinner and more disorganized, although this effect was not as strong as in the brain (Figure 4E, 4F). While the exact pattern varied from embryo to embryo, the vast majority of embryos injected with the *capn1a* morpholino (29/30) exhibited a similar staining, while none of the controls did, either non-injected embryos (0/30, data not shown) or mismatch injected embryos (0/30).

The current study demonstrates that rare homozygous or compound heterozygous mutations in *CAPN1* cause a complicated form of HSP. Most of the affected individuals from the three families suffer from additional neurological symptoms in addition to the typical spasticity of the lower limbs, such as upper extremity hyperreflexia, dysarthria and gait ataxia (Table 1).

These are features that are seen in other autosomal recessive forms of HSP. For example, individuals with AR-HSP caused by *SPG7* mutations (MIM: 607259) often present with very similar phenotypes to those described the current study, including symptoms such as dysarthria, ataxia, upper extremity hyperreflexia, amyotrophy, *pes cavus* and sensory neuropathy.[23-25] Similar phenotypes were also observed in individuals with *KIF1A* mutations (MIM: 610357)[26; 27] and other forms of AR-HSP.[28] In our dataset that includes 405 individuals with HSP from 252 families, *CAPN1* mutations account for 2.2% of the affected individuals and 1.2% of the families. However this is an overestimation, since our dataset does not include families in which the genetic cause was established prior to our study. Therefore these values should be considered as maximal. *CAPN1*, located on chromosome 11q13, encodes calpain 1, also known as the large subunit of μ-calpain, a calcium-activated cysteine protease which is widely expressed in the central nervous system (CNS).[29] Calpain 1 is probably important for several functions in the CNS, but its exact role in humans is still not clear. Calpain 1 is involved in synaptic plasticity[30-33], and several mechanism for its function were suggested in animal models. For example, it was shown that calpain interacts with Cdk5 and NR2B to control NMDA receptor degradation and synaptic plasticity.[34] Another study suggested that calpain 1 can affect synaptic plasticity through degradation of its substrate, glutamate receptor-interacting protein, thus affecting AMPA receptors.[35] However, there are contradicting results regarding the roles of calpains in neuroprotection and neurodegeneration, as several studies suggest that calpain inhibition may be neuroprotective.[36; 37] A recent study may offer a solution for this contradiction, by demonstrating that selective knockout of *calpain 1* (μ- calpain) may lead to increased neurotoxicity, and that its activity is in fact neuroprotective, while knockout of m-calpain is neuroprotective.[38] Our animal models support the neuroprotective role of *calpain 1*, as its knockdown led to neurodegeneration or disorganization of neurons. Therefore it is likely that different forms of calpains have different or even opposing effects on neurodegeneration, and that calpains may have different effects in different disorders and different species.

This can be further exemplified by mice deficient of calpain 1, which have normal gross brain development and architecture, yet have reduced spine density and ramifications of basal and apical dendrites in hippocampal CA1 pyramidal neurons, emphasizing the importance of

calpain 1 in regulation and organization of dendritic trees in hippocampal CA1 neurons.[39] Moreover, a knockout mouse model of another HSP related gene, *CYP7B1* (MIM: 270800), also resulted in lack of obvious CNS phenotype. [40] These observations are comparable to human HSP, since in humans too, brain imaging and development often seem to be normal, while the affected individuals in fact suffer from axonal degeneration of the descending corticospinal tract and ascending sensory fibers.[5] Interestingly, loss-of-function mutations in *CAPN1* were suggested to cause spinocerebellar ataxia in dogs,[41] a neurological disorder that shares features with HSP. Of note, all but one of the individuals in our studies have cerebellar signs such as dysarthria and ataxia.

In zebrafish embryos, the knockdown of *calpain 1a* resulted in disruption of brain development, in particular of branchiomotor neuron migration and positioning. The microtubule network in the brain was disorganized, with some regions showing an abnormal accumulation of axonal acetylated tubulin while others were depleted. This disruption of the microtubule network was more prominent in the brain, but motor neuron axons in the spinal cord were also moderately affected. The presence of large clusters of acetylated tubulin in some cells of the brain is specific to the knockdown of calpain 1a, since it was not observed in other embryos exhibiting hydrocephalus and branchiomotor neuron migration defects.[42; 43] Similarly, the neuromuscular junction of *Drosophila* with *calpain B* knockdown showed abnormal levels of acetylated tubulin. Interestingly, similar observations were reported for spastin, encoded by *SPAST*, in which mutations are the most common genetic cause of HSP.[44; 45] This may suggest that the two genes might be involved in a similar mechanism, however, whether *CAPN1*- and *SPG4*-associated HSP share the same mechanisms is still to be determined.

In order to fully understand the roles of the different calpains in general, and calpain 1 specifically, more studies are necessary, especially in human tissues. Such studies should focus on isolating the effects of specific calpains on neurodegeneration and neuroprotection. In addition, efforts should be made to identify more individuals with *CAPN1*-associated HSP to expand our knowledge of its phenotype.

Supplemental Data

Supplemental data includes case-reports, Figures S1-S6, Tables S1-S3

Acknowledgements

We thank the families for their participation.

This study was funded by CIHR Emerging Team Grant, in collaboration with the Canadian Organization for Rare Disorders (CORD), grant number RN127580 – 260005. This work was done as a part of a Canadian collaboration to study HSP (CanHSP). ZGO is supported by a postdoctoral fellowship from the Canadian Institutes for Health Research (CIHR). PD holds a Canada Research Chair in Neuroscience and AL has a CIHR ALS Canada doctoral award. GAR holds a Canada Research Chair in Genetics of the Nervous System and the Wilder Penfield Chair in Neurosciences. We thank Helene Catoire, Pascale Hince, Cynthia Bourassa and Cathy Mirarchi for their assistance.

All authors report no conflict of interests.

Web resources

OMIM,://www.omim.org/

NHLBI GO Exome Sequencing Project (ESP), http://evs.gs.washington.edu/EVS/ dbSNP132, http://www.ncbi.nlm.nih.gov/projects/SNP/snp_summary.cgi?build_id=132 ExAC, http://exac.broadinstitute.org/

References

1. McDermott, C., White, K., Bushby, K., and Shaw, P. (2000). Hereditary spastic paraparesis: a review of new developments. J Neurol Neurosurg Psychiatry 69, 150-160.
2. Salinas, S., Proukakis, C., Crosby, A., and Warner, T.T. (2008). Hereditary spastic paraplegia: clinical features and pathogenetic mechanisms. Lancet Neurol 7, 1127-1138.
3. Blackstone, C. (2012). Cellular pathways of hereditary spastic paraplegia. Annu Rev Neurosci 35, 25-47.
4. Lo Giudice, T., Lombardi, F., Santorelli, F.M., Kawarai, T., and Orlacchio, A. (2014). Hereditary spastic paraplegia: clinical-genetic characteristics and evolving molecular mechanisms. Exp Neurol 261, 518-539.
5. Deluca, G.C., Ebers, G.C., and Esiri, M.M. (2004). The extent of axonal loss in the long tracts in hereditary spastic paraplegia. Neuropathol Appl Neurobiol 30, 576-584.
6. Noreau, A., Dion, P.A., and Rouleau, G.A. (2014). Molecular aspects of hereditary spastic paraplegia. Exp Cell Res 325, 18-26.
7. Novarino, G., Fenstermaker, A.G., Zaki, M.S., Hofree, M., Silhavy, J.L., Heiberg, A.D., Abdellateef, M., Rosti, B., Scott, E., Mansour, L., et al. (2014). Exome sequencing links corticospinal motor neuron disease to common neurodegenerative disorders. Science 343, 506-511.
8. Hazan, J., Fonknechten, N., Mavel, D., Paternotte, C., Samson, D., Artiguenave, F., Davoine, C.S., Cruaud, C., Durr, A., Wincker, P., et al. (1999). Spastin, a new AAA protein, is altered in the most frequent form of autosomal dominant spastic paraplegia. Nat Genet 23, 296-303.
9. Li, H., and Durbin, R. (2009). Fast and accurate short read alignment with Burrows-Wheeler transform. Bioinformatics 25, 1754-1760.
10. Sidransky, E., Nalls, M.A., Aasly, J.O., Aharon-Peretz, J., Annesi, G., Barbosa, E.R., Bar-Shira, A., Berg, D., Bras, J., Brice, A., et al. (2009). Multicenter analysis of glucocerebrosidase mutations in Parkinson's disease. N Engl J Med 361, 1651-1661.
11. McKenna, A., Hanna, M., Banks, E., Sivachenko, A., Cibulskis, K., Kernytsky, A., Garimella, K., Altshuler, D., Gabriel, S., Daly, M., et al. (2010). The Genome Analysis Toolkit: a MapReduce framework for analyzing next-generation DNA sequencing data. Genome Res 20, 1297-1303.
12. Wang, K., Li, M., and Hakonarson, H. (2010). ANNOVAR: functional annotation of genetic variants from high-throughput sequencing data. Nucleic Acids Res 38, e164.
13. Genomes Project, C., Abecasis, G.R., Auton, A., Brooks, L.D., DePristo, M.A., Durbin, R.M., Handsaker, R.E., Kang, H.M., Marth, G.T., and McVean, G.A. (2012). An integrated map of genetic variation from 1,092 human genomes. Nature 491, 56-65.
14. Kumar, P., Henikoff, S., and Ng, P.C. (2009). Predicting the effects of coding non-synonymous variants on protein function using the SIFT algorithm. Nat Protoc 4, 1073-1081.
15. Adzhubei, I.A., Schmidt, S., Peshkin, L., Ramensky, V.E., Gerasimova, A., Bork, P.,

Kondrashov, A.S., and Sunyaev, S.R. (2010). A method and server for predicting damaging missense mutations. Nat Methods 7, 248-249.
16. Schwarz, J.M., Cooper, D.N., Schuelke, M., and Seelow, D. (2014). MutationTaster2: mutation prediction for the deep-sequencing age. Nat Methods 11, 361-362.
17. Pollard, K.S., Hubisz, M.J., Rosenbloom, K.R., and Siepel, A. (2010). Detection of nonneutral substitution rates on mammalian phylogenies. Genome Res 20, 110-121.
18. Davydov, E.V., Goode, D.L., Sirota, M., Cooper, G.M., Sidow, A., and Batzoglou, S. (2010). Identifying a high fraction of the human genome to be under selective constraint using GERP++. PLoS Comput Biol 6, e1001025.
19. Khorchid, A., and Ikura, M. (2002). How calpain is activated by calcium. Nat Struct Biol 9, 239-241.
20. Moldoveanu, T., Hosfield, C.M., Lim, D., Elce, J.S., Jia, Z., and Davies, P.L. (2002). A Ca(2+) switch aligns the active site of calpain. Cell 108, 649-660.
21. Kimmel, C.B., Ballard, W.W., Kimmel, S.R., Ullmann, B., and Schilling, T.F. (1995). Stages of embryonic development of the zebrafish. Dev Dyn 203, 253-310.
22. Lepage, S.E., and Bruce, A.E. (2008). Characterization and comparative expression of zebrafish calpain system genes during early development. Dev Dyn 237, 819-829.
23. Casari, G., and Marconi, R. (1993). Spastic Paraplegia 7. In GeneReviews(R), R.A. Pagon, M.P. Adam, H.H. Ardinger, S.E. Wallace, A. Amemiya, L.J.H. Bean, T.D. Bird, C.R. Dolan, C.T. Fong, R.J.H. Smith, et al., eds. (Seattle (WA).
24. Wilkinson, P.A., Crosby, A.H., Turner, C., Bradley, L.J., Ginsberg, L., Wood, N.W., Schapira, A.H., and Warner, T.T. (2004). A clinical, genetic and biochemical study of SPG7 mutations in hereditary spastic paraplegia. Brain 127, 973-980.
25. Brugman, F., Scheffer, H., Wokke, J.H., Nillesen, W.M., de Visser, M., Aronica, E., Veldink, J.H., and van den Berg, L.H. (2008). Paraplegin mutations in sporadic adult-onset upper motor neuron syndromes. Neurology 71, 1500-1505.
26. Klebe, S., Azzedine, H., Durr, A., Bastien, P., Bouslam, N., Elleuch, N., Forlani, S., Charon, C., Koenig, M., Melki, J., et al. (2006). Autosomal recessive spastic paraplegia (SPG30) with mild ataxia and sensory neuropathy maps to chromosome 2q37.3. Brain 129, 1456-1462.
27. Klebe, S., Lossos, A., Azzedine, H., Mundwiller, E., Sheffer, R., Gaussen, M., Marelli, C., Nawara, M., Carpentier, W., Meyer, V., et al. (2012). KIF1A missense mutations in SPG30, an autosomal recessive spastic paraplegia: distinct phenotypes according to the nature of the mutations. Eur J Hum Genet 20, 645-649.
28. Coutinho, P., Barros, J., Zemmouri, R., Guimaraes, J., Alves, C., Chorao, R., Lourenco, E., Ribeiro, P., Loureiro, J.L., Santos, J.V., et al. (1999). Clinical heterogeneity of autosomal recessive spastic paraplegias: analysis of 106 patients in 46 families. Arch Neurol 56, 943-949.
29. Goll, D.E., Thompson, V.F., Li, H., Wei, W., and Cong, J. (2003). The calpain system. Physiol Rev 83, 731- 801.
30. Lynch, G., and Baudry, M. (1984). The biochemistry of memory: a new and specific hypothesis. Science 224, 1057-1063.
31. Denny, J.B., Polan-Curtain, J., Ghuman, A., Wayner, M.J., and Armstrong, D.L. (1990). Calpain inhibitors block long-term potentiation. Brain Res 534, 317-320.
32. Vanderklish, P., Bednarski, E., and Lynch, G. (1996). Translational suppression of

calpain blocks long- term potentiation. Learn Mem 3, 209-217.
33. Zadran, S., Jourdi, H., Rostamiani, K., Qin, Q., Bi, X., and Baudry, M. (2010). Brain-derived neurotrophic factor and epidermal growth factor activate neuronal m-calpain via mitogen-activated protein kinase-dependent phosphorylation. J Neurosci 30, 1086-1095.
34. Hawasli, A.H., Benavides, D.R., Nguyen, C., Kansy, J.W., Hayashi, K., Chambon, P., Greengard, P., Powell, C.M., Cooper, D.C., and Bibb, J.A. (2007). Cyclin-dependent kinase 5 governs learning and synaptic plasticity via control of NMDAR degradation. Nat Neurosci 10, 880-886.
35. Lu, X., Wyszynski, M., Sheng, M., and Baudry, M. (2001). Proteolysis of glutamate receptor-interacting protein by calpain in rat brain: implications for synaptic plasticity. J Neurochem 77, 1553-1560.
36. O'Hanlon, G.M., Humphreys, P.D., Goldman, R.S., Halstead, S.K., Bullens, R.W., Plomp, J.J., Ushkaryov, Y., and Willison, H.J. (2003). Calpain inhibitors protect against axonal degeneration in a model of anti-ganglioside antibody-mediated motor nerve terminal injury. Brain 126, 2497-2509.
37. Crocker, S.J., Smith, P.D., Jackson-Lewis, V., Lamba, W.R., Hayley, S.P., Grimm, E., Callaghan, S.M., Slack, R.S., Melloni, E., Przedborski, S., et al. (2003). Inhibition of calpains prevents neuronal and behavioral deficits in an MPTP mouse model of Parkinson's disease. J Neurosci 23, 4081-4091.
38. Wang, Y., Briz, V., Chishti, A., Bi, X., and Baudry, M. (2013). Distinct roles for mu-calpain and m-calpain in synaptic NMDAR-mediated neuroprotection and extrasynaptic NMDAR-mediated neurodegeneration. J Neurosci 33, 18880-18892.
39. Amini, M., Ma, C.L., Farazifard, R., Zhu, G., Zhang, Y., Vanderluit, J., Zoltewicz, J.S., Hage, F., Savitt, J.M., Lagace, D.C., et al. (2013). Conditional disruption of calpain in the CNS alters dendrite morphology, impairs LTP, and promotes neuronal survival following injury. J Neurosci 33, 5773-5784.
40. Li-Hawkins, J., Lund, E.G., Turley, S.D., and Russell, D.W. (2000). Disruption of the oxysterol 7alpha- hydroxylase gene in mice. J Biol Chem 275, 16536-16542.
41. Forman, O.P., De Risio, L., and Mellersh, C.S. (2013). Missense mutation in CAPN1 is associated with spinocerebellar ataxia in the Parson Russell Terrier dog breed. PLoS One 8, e64627.
42. Chen, H.L., Yuh, C.H., and Wu, K.K. (2010). Nestin is essential for zebrafish brain and eye development through control of progenitor cell apoptosis. PLoS One 5, e9318.
43. Hanington, P.C., Patten, S.A., Reaume, L.M., Waskiewicz, A.J., Belosevic, M., and Ali, D.W. (2008). Analysis of leukemia inhibitory factor and leukemia inhibitory factor receptor in embryonic and adult zebrafish (Danio rerio). Dev Biol 314, 250-260.
44. Denton, K.R., Lei, L., Grenier, J., Rodionov, V., Blackstone, C., and Li, X.J. (2014). Loss of spastin function results in disease-specific axonal defects in human pluripotent stem cell-based models of hereditary spastic paraplegia. Stem Cells 32, 414-423.
45. Trotta, N., Orso, G., Rossetto, M.G., Daga, A., and Broadie, K. (2004). The hereditary spastic paraplegia gene, spastin, regulates microtubule stability to modulate synaptic structure and function. Curr Biol 14, 1135-1147.

Tables

Table 1 Clinical features of the affected individuals with autosomal recessive HSP and available clinical data

	Age at onset/ examination	Lower extremity spasticity	Lower extremity weakness	Lower extremity hyperreflexia	Extensor plantar response	Abnormal bladder function	Foot deformity	Ataxia	Other symptoms and signs
Family A									
Individual V-2	20 / 31	+	+	+	+	+	+[a]	-	Dysarthria, upper extremity hyperreflexia
Family B									
Individual IV-1	35 / 47	+	+	+	+	-	-	-	Dysarthria, upper extremity hyperreflexia, sensory abnormalities, peripheral neuropathy
Individual IV-2	36 / 44	+	+	+	+	-	+[b]	+	Dysarthria, upper extremity hyperreflexia, peripheral neuropathy, gait ataxia, upper extremity ataxia, scoliosis
Individual IV-4	22 / 42	+	+	+	+	-	+[b]	-	Dysarthria, upper extremity hyperreflexia, amyotrophy.

Individual IV-5	39 / 40	+	-	+	-	-	-	+	Ocular movement abnormalities, dysarthria, upper extremity hyperreflexia and gait ataxia, amyotrophy
Individual IV-9	24 / 30	+	-	+	+	-	+[b]	-	Dysarthria, upper extremity hyperreflexia
Family C									
Individual IV-7	33 / 35	+	?	?	-	-	+[b]	-	Ankle clonus
Individual IV-13	19 / 22	+	+	+	+	+	+[b]	+	Mild gait ataxia, upper extremity hyperreflexia, bilateral ankle clonus

[a] Pes Valgus, [b] Pes Cavus

Figure 1

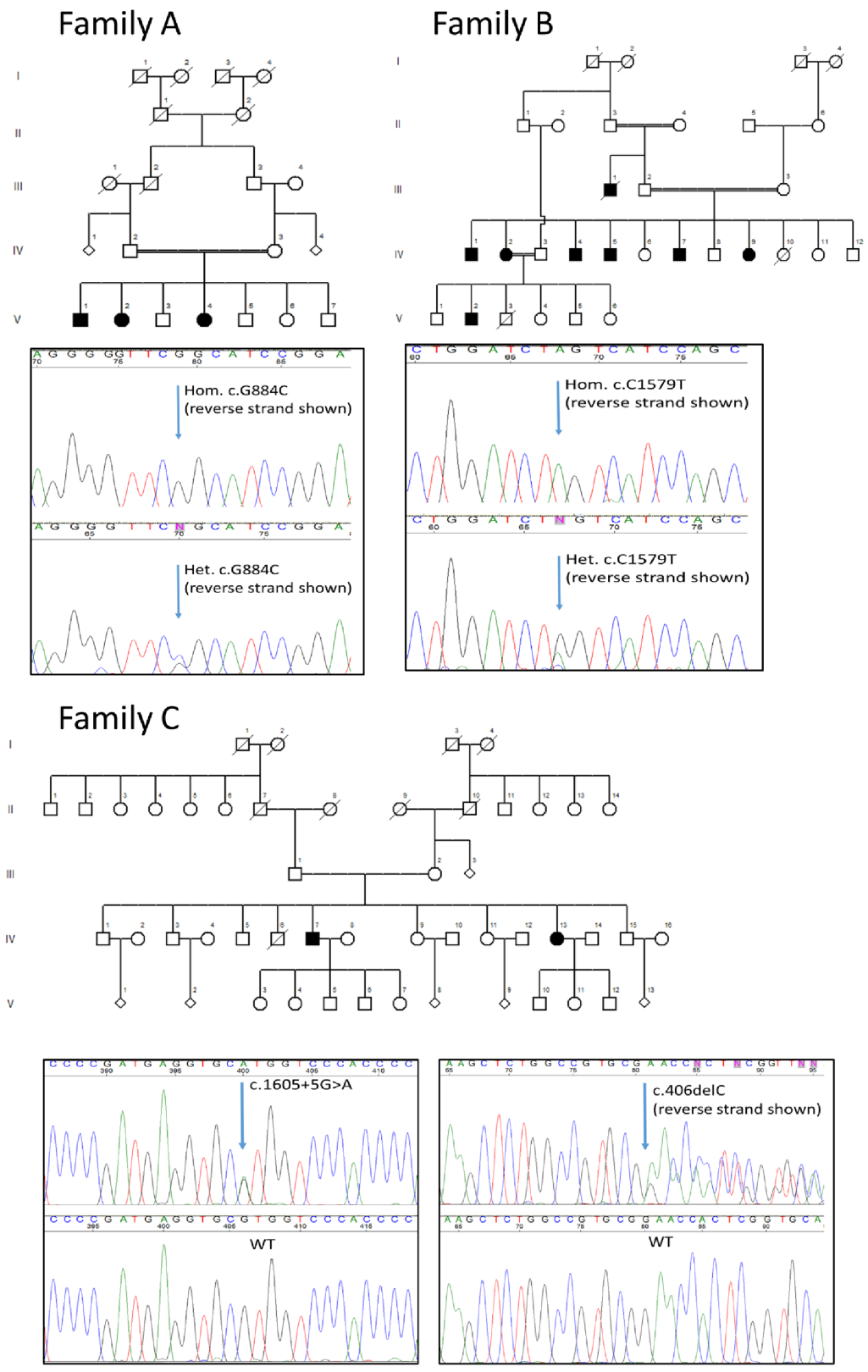
Family A
Family B
Hom. c.G884C
(reverse strand shown)
Het. c.G884C
(reverse strand shown)
Hom. c.C1579T
(reverse strand shown)
Het. c.C1579T
(reverse strand shown)
Family C
c.1605+5G>A
WT
c.406delC
(reverse strand shown)
WT

Figure 1. Pedigrees and mutations detected in three families with *CAPN1*-associated HSP.

The three affected individuals from family A were homozygous for the p.Arg295Pro substitution, and all unaffected individuals with available DNA (IV-2, IV-3, V3 and V6) were heterozygous carriers of the mutation. In family B, all four affected individuals with available DNA (IV-1, IV- 2, IV-5 and IV-9) were homozygous for the stop variant p.Gln527*, and all unaffected individuals with available DNA (III-2, III-3 and IV-11) were heterozygous carriers of the mutation. In family C, the two affected individuals were compound heterozygous for the frame-shift c.406delC (p.Pro136Argfs*40) mutation and the splicing c.1605+5G>A mutation. Four more unaffected individuals were sequenced, III-1 (father of the affected individuals), III-2 (mother), IV-9 (sister), IV-15 (brother). III-1 was heterozygous for the c.1605+5G>A mutation and non-carrier of the frameshift mutation, and III-2 was heterozygous for the c.406delC and non-carrier of the splicing mutation. IV-9 was non-carrier of both mutations, and IV-15 was carrier of the c.1605+5G>A mutation and non-carrier of the frameshift mutation.

Figure 2

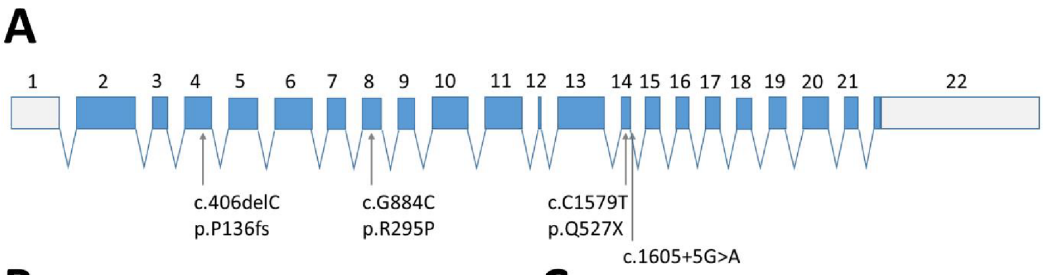

B

Mutation	Prediction
p.P136fs	Early stop codon
p.R295P	SIFT score – 0 (deleterious), Polyphen2 score – 1 (deleterious)
p.Q527X	Early stop codon
c.1605+5G>A	Intronic retention or exon skipping and early stop codon

C

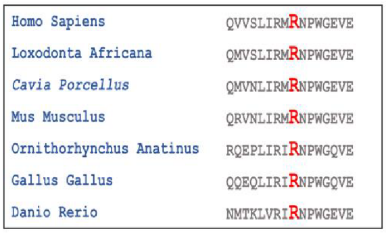

D

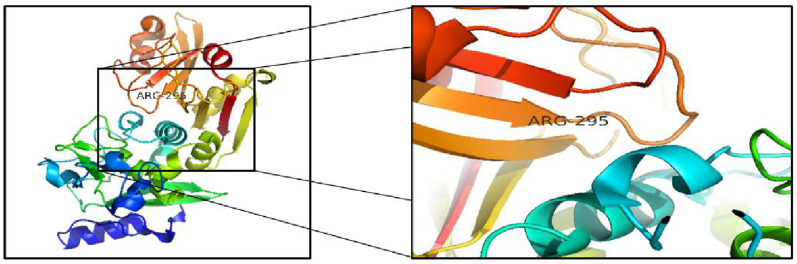

E

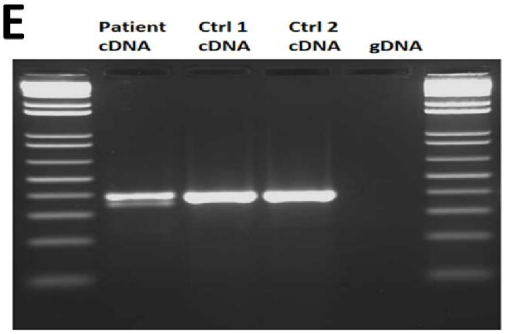

F

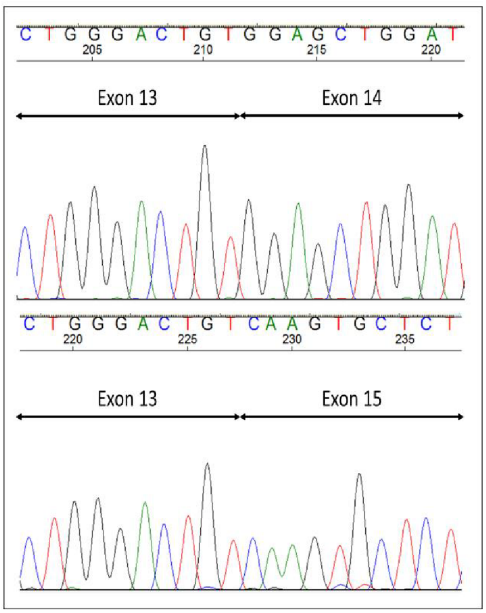

G

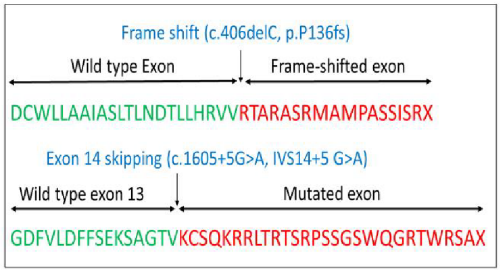

Figure 2. Characteristics and predictions of the *CAPN1* mutations

A. Structure of the *CAPN1* gene, and the locations of the four mutations identified in the current study. **B.** Functional predictions of all four mutations. **C.** Conservation of p.Arg295 in different species. With a GERP ++ score > 2, this amino acid is highly conserved. **D.** Three-dimensional model of calpain 1 and the location of the p.Arg295Pro substitution, at the end of a β strand and just before the active site at p.Asn296 (PDB #1ZCM). **E.** cDNA produced from lymphoblasts of an affected individual and two controls, around exon 14. In the left lane, two cDNA products were observed, suggesting that the c.1605+5G>A mutation affected the splicing. **F.** Sequencing of cDNA from RT-PCR of the RNA around the splicing mutation c.1605+5G>A, demonstrated that this mutation caused the skipping of exon 14. **G.** Effects of the frame-shift mutation c.406delC (p.Pro136Argfs*40, top) and the splicing mutation c.1605+5G>A (bottom) on calpain 1.

Figure 3

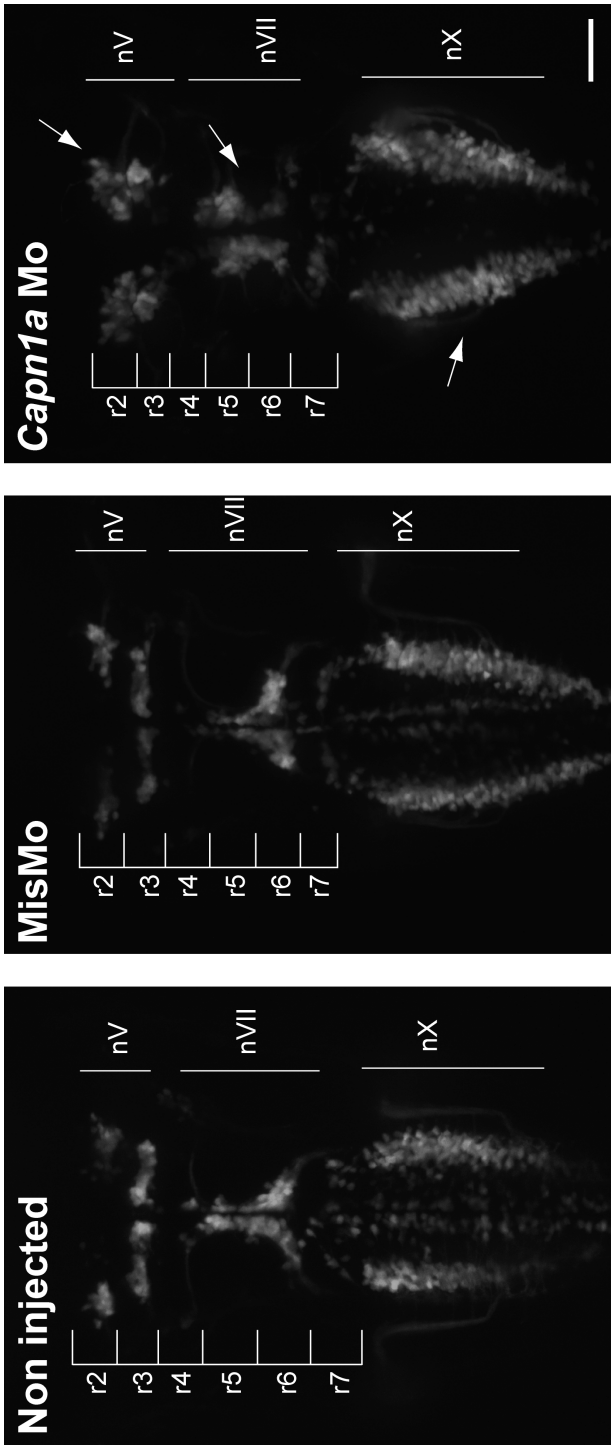

Figure 3. Branchiomotor neurons of capn1a Mo injected embryos display abnormal migration

Abnormal development and migration of both nV (trigeminal) and nVII (facial) branchiomotor neurons in 2 dpf Islet1:GFP embryos, either not injected, injected with MisMo or with capn1a Mo. Arrows indicate abnormally located cell bodies. R: rhombomere. Scale bar is 50 μm.

Figure 4

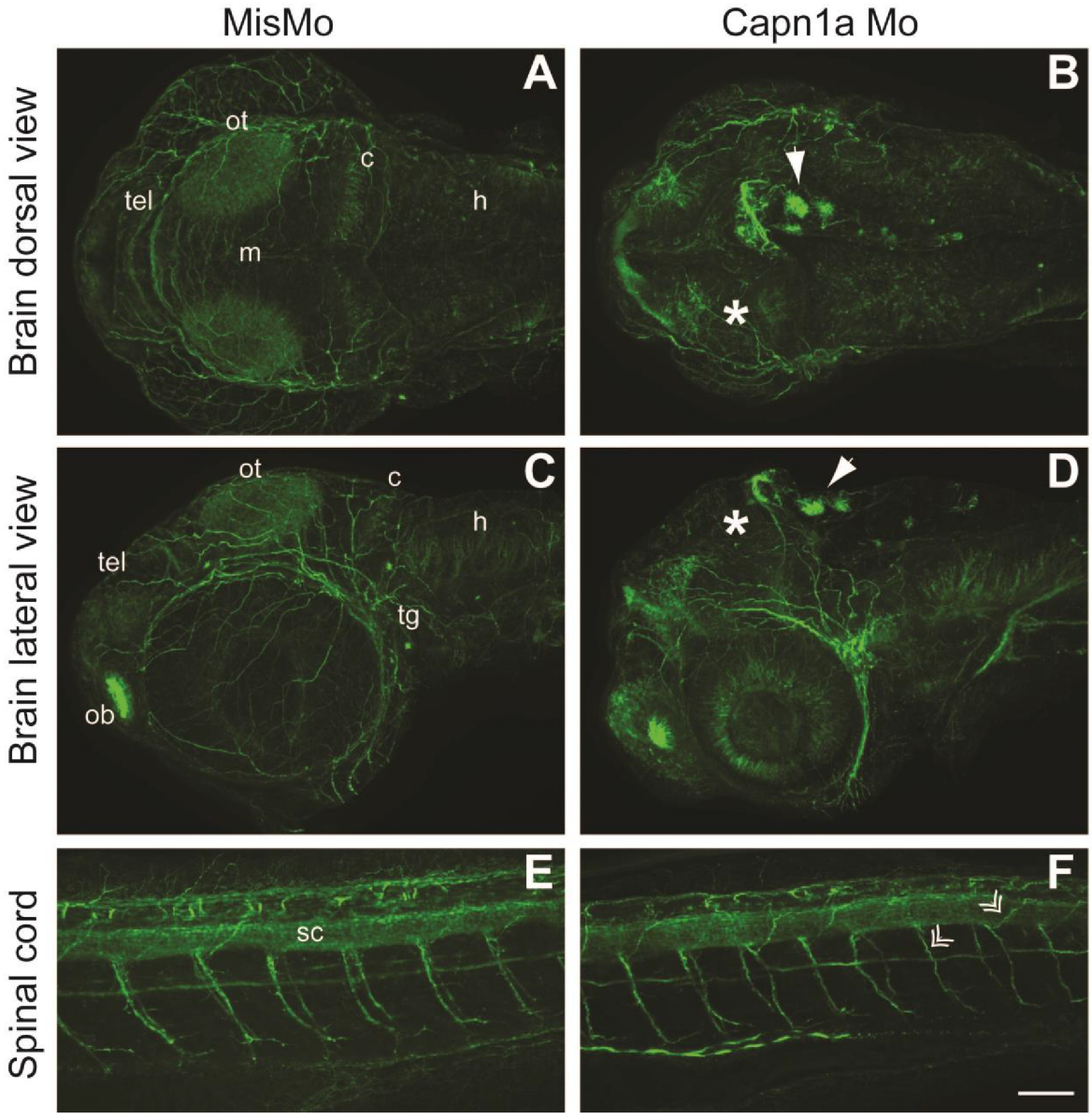
MisMo
Capn1a Mo
Brain dorsal view
Brain lateral view
Spinal cord
A
B
C
D
E
F
ot
c
tel
h
m
tg
ob
sc

Figure 4. Disorganization of the microtubule network in the brain of capn1a morphants

A., B. Z-projections of acetylated tubulin staining in the brain of MisMo (**A**) and capn1a Mo (**B**), dorsal side up. **C., D.** Z-projections of acetylated tubulin staining in the brain of MisMo (**C**) and capn1a Mo (**D**), lateral side up. **E., F.** Spinal cord of MisMo (**E**) and capn 1a Mo (**F**). The upper panel shows a dorsal view of the brain, with several anatomical structures highlighted (**A, B**). The middle panel shows a lateral view of the same fish as in the upper panels, with dorsal toward the top of the image (**C, D**). Solid white arrows show the clusters of tubulin. Asterisks (*) show the fainter staining of the optic tectum of capn1a morphants. The bottom panel show the spinal cord, along the 6 to 8 somites spanning the anus of the embryos, with dorsal toward the top of the image (**E, F**). The double arrows point toward thinner and disorganized motor neuron axons of the *capn1a* morphants. In all these images, caudal is to the left. Scale bar is 60 μm. Abbreviations: ot, optic tectum; tg trigeminal ganglion; h, hindbrain; c, cerebellum; m, midbrain; tel, telencephalon; ob, olfactory bulb; sc, spinal cord.

Supplemental note: case reports

Family A

Individual V-2

Individual V-2 presented with onset of progressive walking difficulties at the age of 20. She was initially examined by us at the age of 31 years, at the time complaining of gait difficulty and urinary frequency and incontinence. At the time of examination, the individual had spastic gait typical to HSP, however she could walk without aid. Muscle strength was 4/5 in the lower limbs, and tendon reflexes were brisk in the four limbs with bilateral Babinski sign. There was no muscle wasting, there was no sensory deficit nor were there cerebellar or extrapyramidal signs. Motor coordination and cranial nerves examinations were normal. Eye movement and fundus examinations were normal. She had moderate bilateral pes valgus with hallux valgus. Electroneuromyography (ENMG) examination was normal. The individual also suffered from mild dysarthria.

Family B.

Individual IV-1

Individual IV-1 presented with onset of spastic paraplegia at the age of 35. He experienced lower limbs weakness that predominated on the left side and he also complained of dysarthria. No balance problems were reported. He was examined at the age of 47, and according to the individual he could walk more than 5000 meters, but had difficulties in running and going down the stairs. At the time of examination, Individual IV-1 had spastic gait, paralytic dysarthria with akinetic face, proximal reduced strength in lower limbs (4/5) and brisk tendon reflexes with bilateral Babinski sign. There was no muscle wasting. He had bilateral and distal superficial hypoesthesia in both upper and lower limbs and reduced vibration sensation in lower limbs. The upper limb coordination and cranial nerves examination were normal. Eye

movement and fundus examination were normal. He had no skeletal deformities. The ENMG examination showed a moderate sensory axonal neuropathy predominating in the lower limbs, sympathetic skin reflex was normal in upper limbs and abolished in lower limbs (Table S1).

Individual IV-2

Individual IV-2 presented with onset of spastic paraplegia at the age of 36 years with lower limbs weakness and ataxic gait. She was examined at the age of 44, and at the time of examination she needed cane support for walking, that she started using at the age of 40. At examination, the individual had reduced strength in lower limbs (4/5), without muscle wasting, and with brisk tendon reflexes in all limbs with bilateral Babinski sign. She had no sensory deficit, however she had moderate upper limbs dysmetria, as well as dysarthria and moderate facial hypokinesia. The cranial nerves examination was normal, with normal eye movement and fundus examination. Cognition was normal and there were no skeletal deformities with the exception of pes cavus. Her ENMG examination showed a moderate sensory axonal neuropathy predominating in the lower limbs, sympathetic skin reflex was normal in upper limbs and abolished in lower limbs (Table S1).

Individual IV-4

Individual IV-4 presented with onset of spastic paraplegia at the age of 22 years, with lower limbs stiffness at walking that progressed to spastic gait and weakness. He was examined at the age of 42 years old. At the time of the examination, he had spastic gait, however he reported that he could walk 1000 meters unaided. The lower limbs strength was 4/5 in proximal muscles and 5/5 in distal muscles, without muscle wasting. Tendon reflexes were brisk in all limbs with bilateral Babinski sign. He had no sensory deficit, and motor coordination and cranial nerve examinations were all normal. He had dysarthria and a subtle bilateral pes varus. Spinal cord and cerebral MRI were normal. Eye movement and fundus examinations were normal.

Blood tests were performed with the following results: normal sedimentation rate, complete blood count identified a moderate leukopenia (3900/mm^3), normal serum electrolytes and hepatic tests (bilirubin, transaminases, gamma-GT), moderate hyperlipidemia (Cholesterol - 2.73 g/l, triglycerides - 2.14 g/l), normal vitamin B12, B9 and vitamin E levels, moderately reduced vitamin B1 level (86 nmol/l), normal long chain fatty acids and phytanic acid levels. Immunoelectrophoresis of proteins and ponderal levels of immunoglobulins were normal.

Individual IV-5

Individual IV-5 presented with onset of spastic paraplegia at the age of 39 years. He was examined one year later at the age of 40. At the time of examination the individual had clear spastic gait with ataxia, however he could walk without aid. He had moderate dysarthria, normal strength in all muscles, and brisk tendon reflexes in all limbs. There was no muscle wasting in lower limbs. He had normal plantar cutaneous reflexes and normal sensory examination. He had a discrete upper limbs dysmetria and bilateral nystagmus. Eye movement and fundus examinations were normal. He had no skeletal deformities.

Individual IV-9

Individual IV-9 presented with onset of spastic paraplegia at the age of 24 with lower limbs stiffness when walking. At the time of examination, she was 30 years old. She had moderate lower limbs spasticity without any motor or sensory deficit, without muscle wasting. Tendon reflexes were brisk in all limbs with bilateral Babinski sign. There was no cerebellar or extrapyramidal signs. Eye movement and fundus examinations were normal. She had moderate bilateral pes cavus. The ENMG examination was normal but sympathetic skin reflex was normal in upper limbs and abolished in lower limbs (Table S1).

Family C

Individual IV-7

Individual IV-7 presented with onset of spastic paraplegia at the age of 33, with spastic gait and discoordination. His disease was slowly progressive, with little follow up. He was examined at the age of 35, and noted to have spastic gate, discoordination, bilateral Babinski sign, and ankle clonus. Cranial nerves examination was normal, including eye movement and fundus examination. Reported results from MRI were described as mild atrophy of cervical spinal cord. Individual IV- 7 was lost of further follow-up.

Individual IV-13

Individual IV-13 presented with initial symptoms of spastic paraplegia at the age of 19, with mild lower limbs discoordination and weakness. At the first neurological examination, at the age of 22 years, she had normal motor examination with the exception of bilateral weakness (4/5) of the iliopsoas muscles. There was no muscle wasting. Sensory examination was normal. The gait was waddling, and she could not perform heel walk, and was unable to rise from a crouched position. Funduscopic examination and cranial nerves examination including eye movements were normal. Ten months prior to the first examination, she had CSF examination, myelogram and head CT, all of which were within the normal limit except for a slightly prominent sulci observed on the CT. At the time of recruitment, she was 31 years old, and presented with lower limbs spasticity, ataxic gait, poor balance and frequent tripping. Reflexes of the upper limbs were brisk and the lower limbs were spastic, with positive bilateral Babinski sign. Strength was 4/5 in both legs, and sensation was normal in both upper and lower limbs. She complained on urinary urgency and frequency, with stress incontinence, which deteriorated in the 3 years prior to the exam, and she also had pes cavus.

Supplemental figures and legends

Figure S1 - *clp-1*(RNAi) produces motor phenotypes and axonal degeneration in *C. elegans*

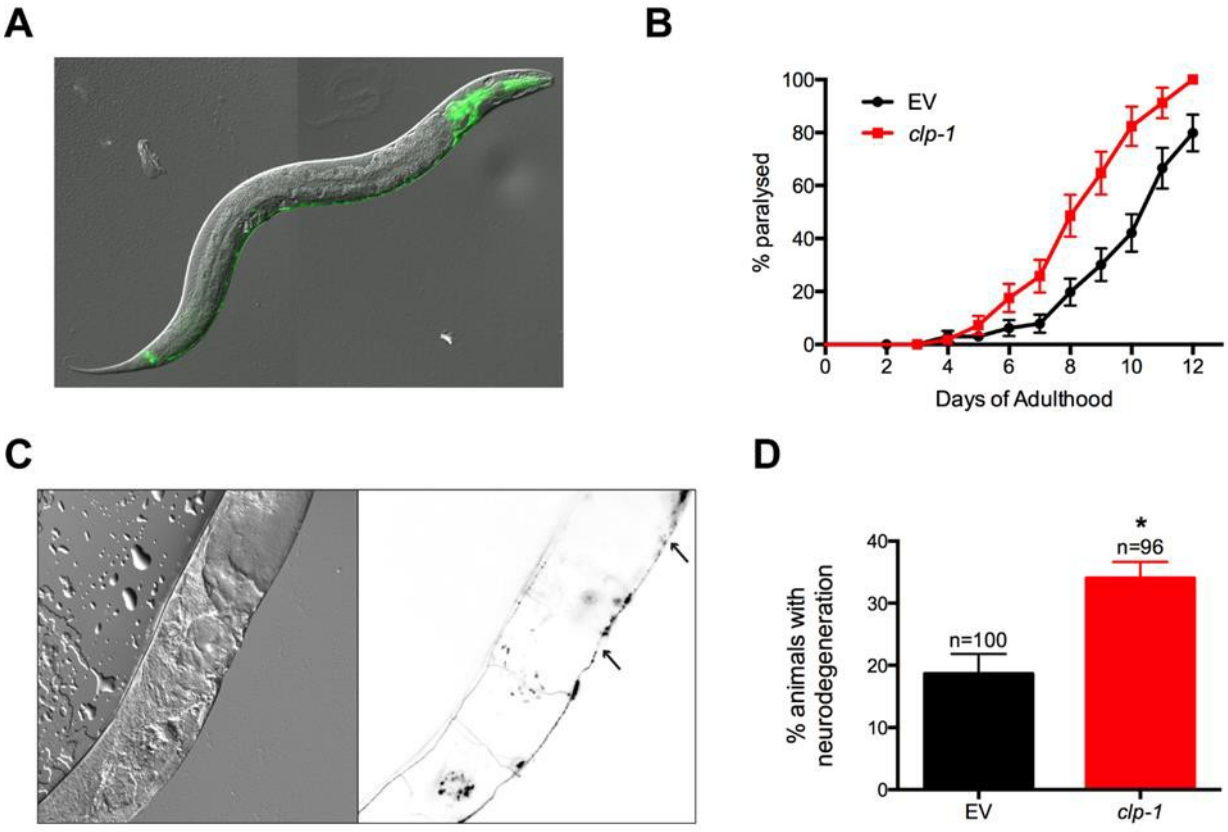

Figure S1 legend

clp-1*(RNAi) produces motor phenotypes and axonal degeneration in *C. elegans

The *C. elegans clp-1* encodes an orthologue of human calpain, and to investigate the contribution of *clp-1* to neuronal function, RNAi was used to knockdown the expression of endogenous *clp-1* in *C. elegans*. The *C. elegans strains* - XE137518 wpIs36 [unc-47p::mCherry] I; wpSi1 [unc- 47p::rde-1::SL2::sid-1 + Cbr-unc-119(+)] II; eri-1(mg366) IV;

rde-1(ne219) V; lin-15B(n744) X] were used for RNA interference (RNAi) assays. GABAergic neurons were visualized through and RNAi sensitivity only in GABAergic motor neurons was conveyed via wpSi1. Visualization of clp-1 expression was done using the transgenic GFP reporter strain BC1465819 dpy-5(e907) I; sEx14658 [rCes C06G4.2b::GFP + pCeh361]. *RNAi procedures* - (RNAi)-treated strains were fed E. coli (HT115) containing an empty vector (EV) or clp-1(RNAi). RNAi clones were from the ORFeome RNAi library (Open Biosystems). RNAi experiments were performed at 20°C. Worms were grown on Nematode Growth Media enriched with 1 mM isopropyl-ß-D- thiogalactopyranoside. RNAi neurodegeneration tests were performed using the strain XE1375. Eggs were placed on plates with RNAi until day 5 of adulthood. Worms were transferred on fresh plates every 2 days. *Neurodegeneration assays* - For scoring of neuronal processes for gaps or breakage, XE1375 transgenic animals were selected at day 5 of adulthood for visualization of motor neuron processes in vivo. Animals were immobilized in 60% glycerol and mounted on slides with 2% agarose pads. mCherry was visualized at 585 nm using a Zeiss Axio Imager M2 microscope, using the Zen Pro 2012 software. Approximately 100 worms were scored per condition and each experiment was performed in triplicates. The mean and standard error of the mean were calculated for each trial and 2-tailed t tests were used for statistical analysis. Prism 5 (GraphPad Software) was used for all statistical analyses.

A. *clp-1*::GFP reporter shows expression in the pharynx, nerve ring, and along the ventral nerve cord. **B.** RNAi knockdown of the expression of endogenous *clp-1* in *C. elegans*. Worms treated with *clp-1*(RNAi) had motility defects, culminating in an age-dependent paralysis phenotype, which occurred at a higher frequency than control worms treated with empty vector (EV). RNAi *clp-1*(RNAi) (*clp-1*, n=62) enhances paralysis in a strain sensitized to RNAi only within the nervous system compared to empty vector (EV) controls (EV, n=72). Error bars represent SEM,

***P<0.001, log-rank (Mantel-Cox)-test. **C.** Visualization of neurodegeneration observed as gaps or breaks along neuronal processes (arrows) in a worm (*left*, differential interference contrast, *right*, inverted image from mCherry-fluorescence) in the nervous system exposed to *clp-1*(RNAi). *clp-1* (RNAi) treatment resulted in degeneration, observed as gaps or breaks along axonal processes and this occurred at a greater rate than compared to EV RNAi control

worms **D.** Quantification of neurodegeneration in worms treated with EV (n=100) or *clp-1*(RNAi) (n=96) during development and examined at day 5 of adulthood. *P<0.05, unpaired t-test. Error bars represent SEM. Overall, these data suggest that *clp-1* protects the nervous system against dysfunction and degeneration.

Figure S2 - Pan neuronal expression of *calpain B* RNAi leads to defects in negative geotaxis in *Drosophila*.

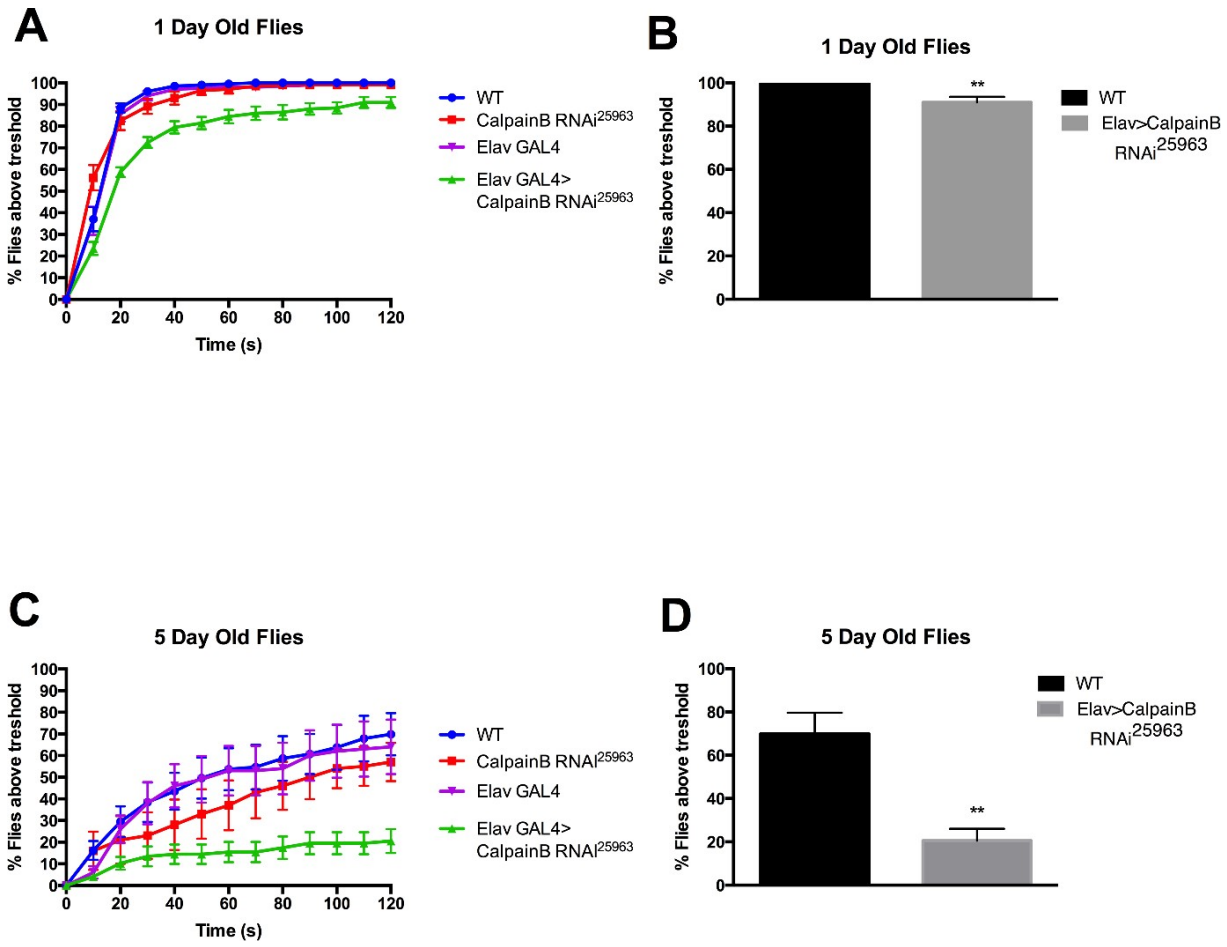

Figure S2 legend

Drosophila contains 3 paralogues of *CAPN1*. *Calpain B* has the highest homology with 45% blast identity versus 40% for *calpain A* and 28% for *calpain C* (Geneseer). Transgenic Drosophila containing the RNAi construct 25963 against Calpain B were obtained from the Vienna Drosophila Resource Center (VDRC). Pan-neuronal expression of the RNAi transgene was obtained by crossing the RNAi stocks to Elav-GAL4 homozygous flies. The flies were raised at 25ºC. One day-old or 5 day-old flies were used for the climbing assay. Briefly, groups of 20 homogenous flies are tested at the time for their ability to climb in a glass

cylinder above the 190mL line of a 250mL cylinder. The flies were filmed and then the percentage of flies that climbed above the target line was plotted every 10 seconds, and results were plotted using Prism 5 (GraphPad Software). SigmaPlot 11.0 integrated with SigmaStat 3.1 was used to assess data groupings for significance. Statistical analyses used one-way ANOVA and Chi-square.

A. *Drosophila* transgenic for both the pan-neuronal driver ElavGAL4 and the responder UAS-calpain B RNAi present significant defect in their ability to climb above a reference target line when compared to the appropriate genetic controls (Elav GAL4 or UAS CalpainB RNAi. **B.** Climbing ability at 120 second for WT and Elav>CalpainB RNAi 25963 is significantly different (N=10, p=0.0064 t-test). **C.** Similarly, flies aged for 5 days show a more severe defect in climbing when compared to the same genetic controls. **D.** This defect is significant (N=5, p=0.0063 t-test).

Figure S3 - Pan neuronal expression of calpain B RNAi leads to defects in neuromuscular junction neurons.

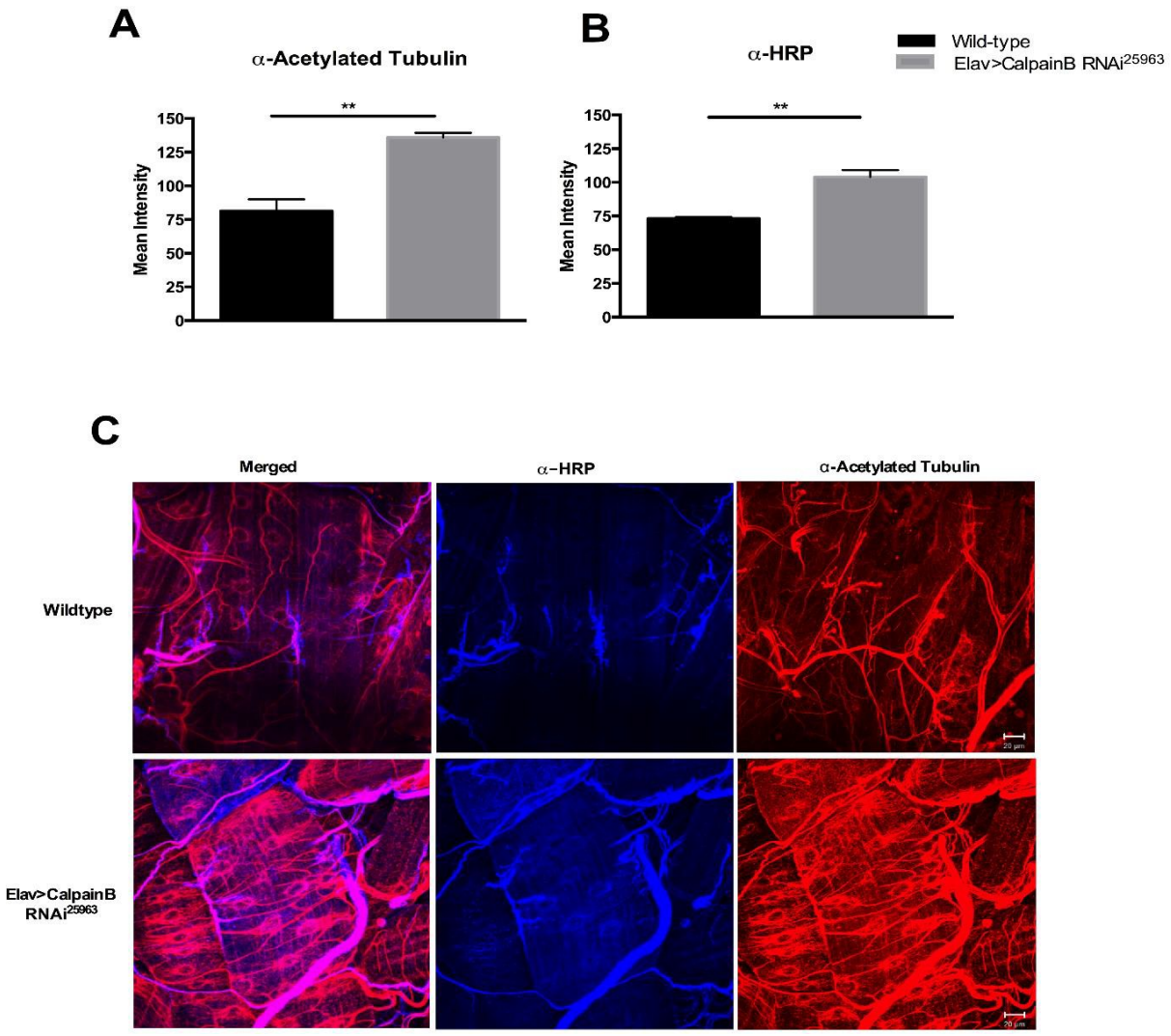

Figure S3 legend

Defects in axons were observed in transgenic flies expressing calpain B with the pan-neuronal driver Elav. Axons appeared of larger diameter and with increased level of acetylated tubulin. Increased acetylated tubulin is associated with hyperstabilization of microtubules and has been associated with *SPAST* mutations previously. Drosophila confocal imaging of the 3rd instar

neuromuscular junction was performed on third instar larvae. Antibodies against acetylated tubulin (Sigma T7451-200UL) and HRP (ThermoFisher PA1-26409) were utilized at a concentration of 1:1000. JacksonImmuno secondary antibodies Cy3 anti-mouse (115-165-003) and Cy5 anti-rabbit (JacksonIummuno 711-175-152) were purchased from Cedarlane and utilized at a concentration of 1:200.

Confocal imaging was performed using Zeiss LSM 700. Graph were made using data from mean intensity of the region of interest with Prism 5 (GraphPad Software). Image analysis was completed using ImageJ.

A. We observed a significant increase in the level of acetylated tubulin in the axons and muscles of the neuromuscular junction of larva expressing pan neuronally Calpain B RNAi. (N=3, P=0.0045, t-test). **B.** In addition, we observed that axons were larger on HRP immunohistochemistry suggesting larger fibers (N=3, P= 0.0039, t-test) **C.** Representative immunohistochemistry for the wild-type and pan-neuronal expressing Calpain RNAi larva. Interestingly, the acetylated tubulin were elevated and covered the entire diameter of large fibers compared to controls.

Figure S4 - Clusters of acetylated tubulin are present in capn1a morphants zebrafish

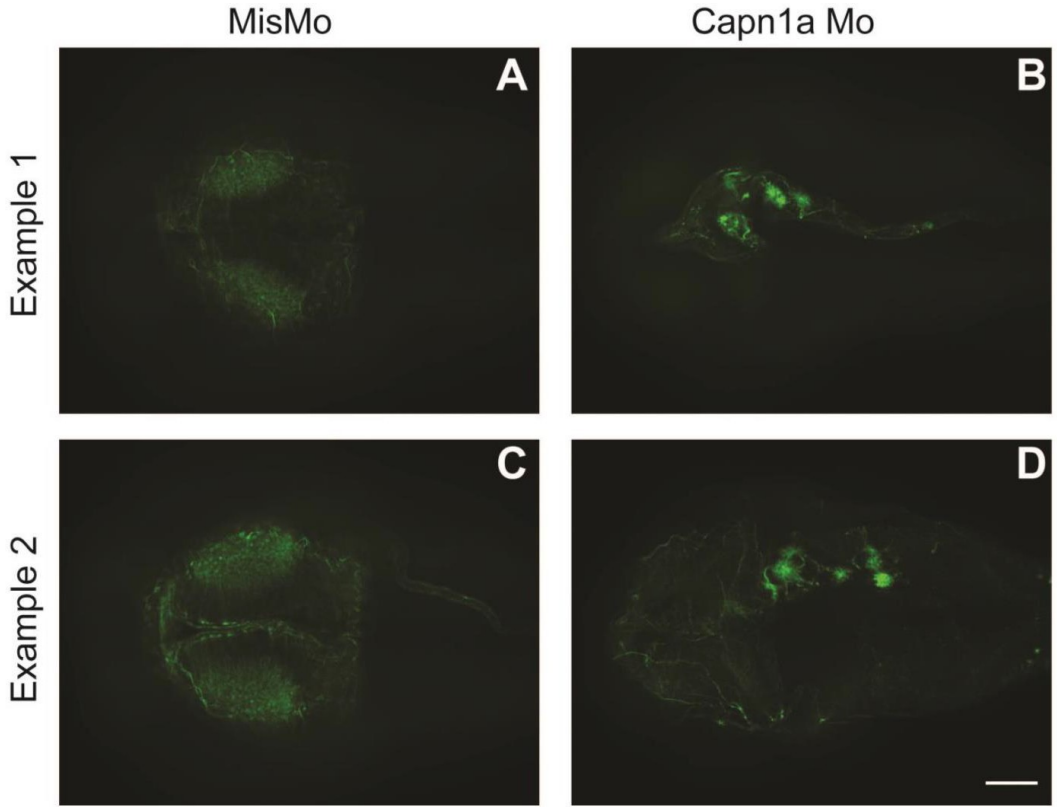

Figure S4 legend

Single slice images of acetylated tubulin staining in the brain of MisMo (**A, C**) and *capn1a* Mo (**B, D**) injected embryos. Images from 2 different embryos are shown for each condition, in order to show the variable clusters of acetylated tubulin observed in capn 1a morphants (**B, D**). Slices from the approximate same region of the brain are shown for the mismatch morphants (**A, C**). Scale bar is 60 μm.

Figure S5. *Capn1a* morpholino induces morphological defects and abnormal development in *Danio rerio*

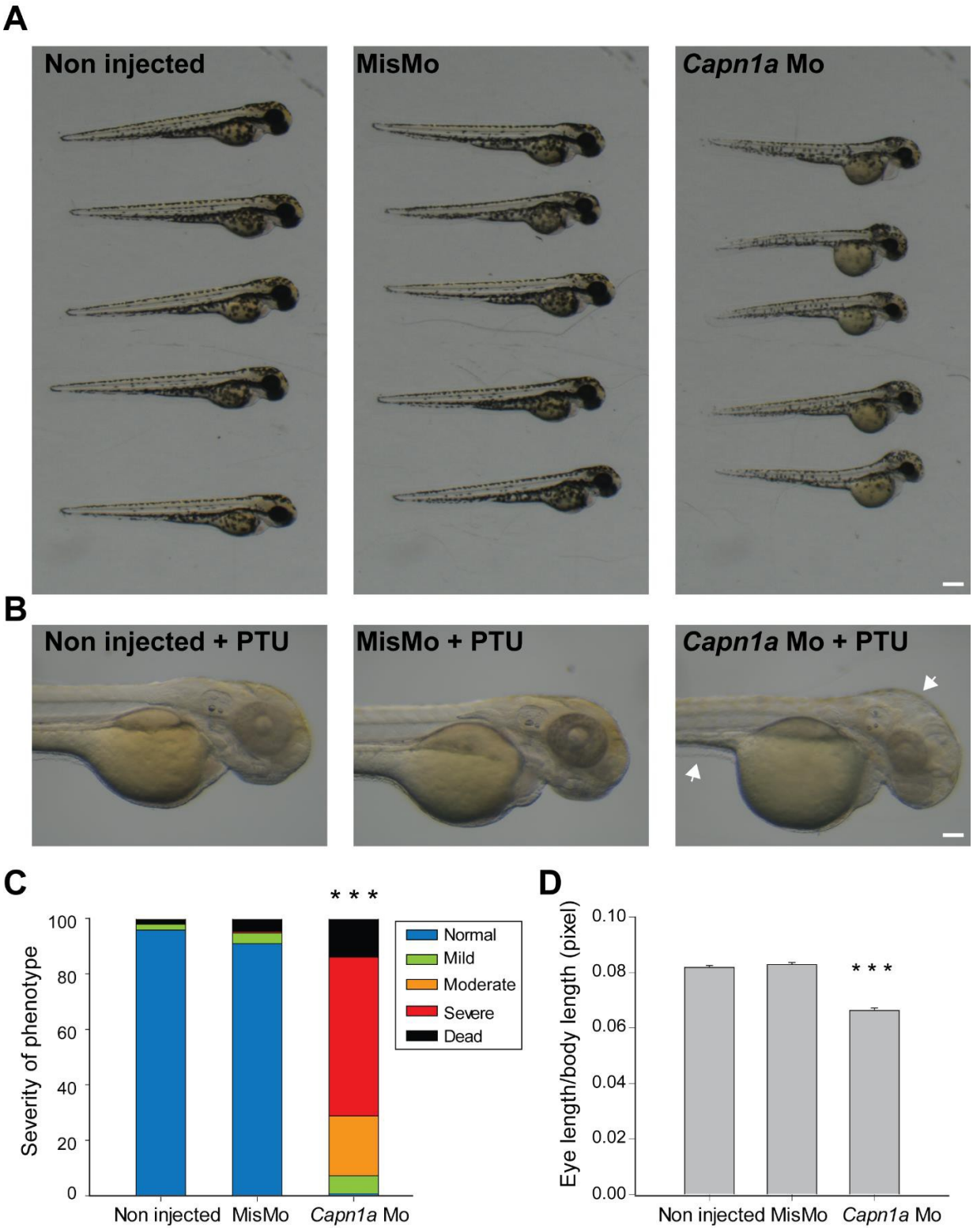

Figure S5 legend

Knockdown of zebrafish calpain1a and calpain 1b was achieved using morpholino oligonucleotides targeting the translation initiation site (*capn1a* Mo 5'-GAGATCCCGCCGTATGAGAACATGC-3'; *capn1b* Mo 5'-TCGACACACCTCCAATTGAAAACAT-3' Gene Tools, LLC). As an injection control, a mismatched *capn1a* morpholino with a five nucleotides substitution was used (MisMo 5'-GAcATCCaGCCcTATGAcAACATcC-3'). The morpholinos were diluted in deionized water with 0.05% Fast Green vital dye (Sigma) and 5 ng per embryo was pulse-injected into 1-4 cell stage embryos using a Picospritzer III pressure ejector. For this study, either AB-Tu wild-type or Islet1:GFP transgenic embryos were used. Embryos were kept until 5 days post-fertilization and the phenotype was quantified as follows: normal - no abnormal features or developmental delay; mild - absence of swim bladder; moderate - absence of swim bladder and presence of inflated pericardium; severe - absence of swim bladder, severely inflated pericardium with fluid accumulation around the yolk sac and extension. Eye phenotype assessment was performed using ImageJ 1.43m (NIH); the eye length was measured in the longitudinal plan, and divided by the length of the body, measured from the tip of the tail, until the frontal-most part of the head. Six hours post-fertilization embryos were treated with 0.2mM 1-phenyl 2-thiourea (PTU) until imaged, in order to prevent pigmentation from appearing. Two days post fertilization (dpf) embryos were anesthetized in 0.04% tricaine (Sigma) and mounted in 3% methylcellulose on a depression slide. The hindbrain of these embryos was visualized with a 10× water-immersion lens. Acetylated tubulin staining was performed as previously published. Briefly, 2 dpf embryos previously treated with PTU were fixed in Dent's fixative (80% methanol, 20% DMSO) overnight at 4 °C and washed 3X 10 minutes in 1% PBST. Embryos were blocked for one hour at room temperature in PBST with 2% BSA and 2% normal goat serum, followed by an overnight incubation at 4°C with anti- acetylated tubulin monoclonal antibody (Sigma) in block (1:500). The next day, the embryos were washed 3X 10 minutes in PBST, then blocked for 1 hour, followed by a 4 hours incubation with a goat anti-mouse secondary antibody conjugated with Alex Fluor 488 (1:1,000). Embryos were then washed in PBST overnight, cleared in 80% glycerol and deyolked before being mounted either dorsal up, or on the side and imaged with a 10X air objective. Embryos were imaged with a Quorum

Technologies spinning disk confocal microscope with a CSU10B (Yokogawa) spinning head mounted on an Olympus BX61W1 fluorescence microscope and connected to a Hamamatsu ORCA-ER camera and acquired using Volocity software (Improvision). The images were then processed using ImageJ 1.43m (NIH). Z-projections of confocal images are shown, except when otherwise specified.

A. Morphological features of 2 days post fertilization (dpf) embryos either not injected, injected with a mismatch morpholino (MisMo), or with a morpholino against *calpain 1a* (*Capn1a* Mo). Five representative embryos are shown for each condition. Scale bar is 250 μm. **B.** Non injected, MisMo injected and capn1a Mo injected embryos were treated with 1-phenyl 2-thiourea (PTU) to prevent pigmentation from developing. Arrows indicate defects in the head (hydrocephalus) and yolk sac extension. Scale bar is 50 μm. **C.** Quantification of severity of phenotype displayed at 5 dpf by non-injected (n=189), MisMo injected (n=209) and *capn1a* Mo (n=236) larvae.
***$p<0.001$, chi-square test. **C.** Ratio of the eye longitudinal length with the body length of 2 dpf non injected (0.0818, n=91), MisMo injected (0.0829, n=60) and *capn1a* Mo (0.0663, n=79) embryos. ***$p<0.001$, one-way ANOVA. Error bars represent standard error.

Figure S6 - Western-blot analysis of calpain 1 expression levels in zebrafish

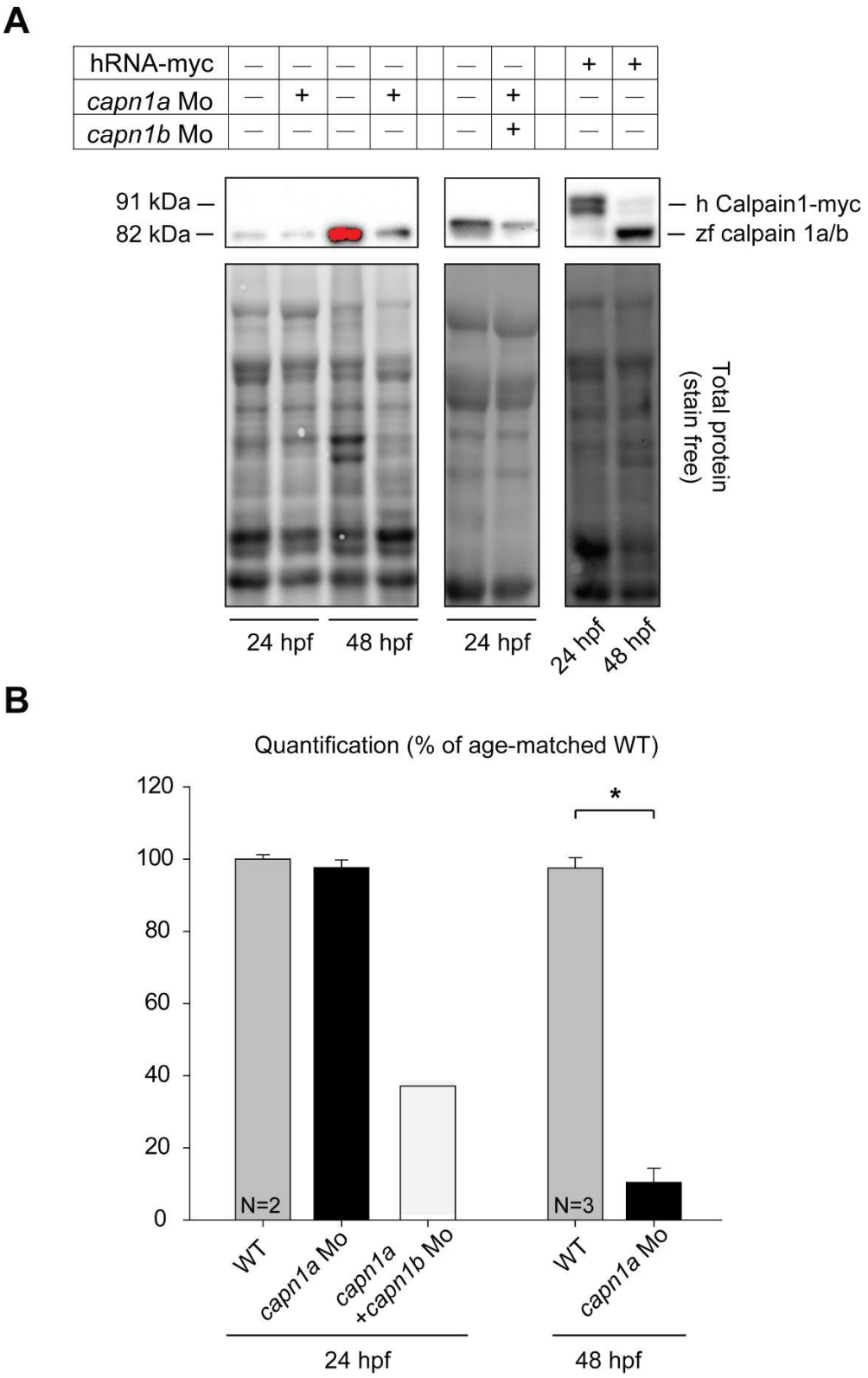

Figure S6 legend

About 30 embryos at 24 and 48 hours post-fertilization were lysed in ice-cold RIPA buffer (150 mM NaCl, 50 mM Tris pH 7.5, 1 % Triton X-100, 0.1 % SDS, 1 % Na deoxycholate, 0.1 % protease inhibitor), maintained on ice and homogenized with a hand-held pestle. The lysates were centrifuged for 10 minutes at 10,000 rpm at 4°C and the supernatant was collected. Protein concentration was established using Bio-Rad DC Protein Assay and 60 µg of proteins were loaded in 2X Lämmli buffer after boiling the samples for 5 minutes at 95°C. TGX Stain-Free FastCast acrylamide Kit (Bio-Rad) was used to make 10% Tris-glycine. After electrophoresis, the gels were activated by exposure to UV for one minute, and transferred to either regular or low-fluorescence PVDF membrane (Bio-Rad). After transfer, total proteins on membranes were detected by UV. Membranes were then blocked for one hour using 5 % fat free milk in PBST. The primary antibody (Calpain 1, 1:1000, Novus Biological NB120-3589) was incubated overnight at 4°C in 5 % fat free milk in PBST. After washing 3x 5 minutes in PBST, the membrane was incubated with an anti- mouse IgG, HRP conjugated (1:5000, Jackson Immuno) in 5 % fat free milk in PBST for one hour at room temperature, and then washed 3x 5 minutes. Membranes were exposed to Clarity enhanced chemiluminescence (ECL, Bio-Rad) for 5 minutes at room temperature and visualized using a ChemiDoc MP (Bio-Rad). Detection and quantification of band intensities was conducted using Image Lab 5.2 software (Bio-Rad). Bands were normalized to total protein by dividing the intensity of the band by the intensity of the total proteins from the same samples on the same blot, and the ratio was expressed as percentage of the age-matched wild-type control. Student's t-test was used to compare samples with their age-matched control. A value of $p < 0.05$ was considered statistically significant. **A.** Western blot analysis of calpain 1 in zebrafish at 24 hours post-fertilization (hpf) and 48 hpf without or with capn1a Mo knock down (first panel, the 48 hpf wild- type condition is saturated on purpose. This exposure time is not used for quantification); without or with a double knock down of capn1a and capn1b (second panel); and following injection of 500 pg of human CAPN1 mRNA with 6x myc-tags, at 24 and 48 hpf (third panel, hRNA-myc). Total protein visualized by the stain-free technology is shown in the lower panel. **B.** Quantification of the western blots shown in A. The results are expressed as mean +/- SEM, * $p<0.05$. h: human; zf: zebrafish; hpf: hours post-fertilization; WT: wild-type.

Supplemental tables

Table S1 – primers used for amplification and sequencing of *CAPN1* mutations

Variant	Forward	Reverse	Tm (c)	Length (bp)
p.Pro136Argfs*40	AACCCCAGATTCTCCCTAGC	GCAGGTATTGTGGGTCATCC	61	273
c.1605+5G>A	CTGGAGTCTGGGTCTGGG	ACTCAGGGGACAGGACACC	61	527
p.Gln527*	CTGGAGTCTGGGTCTGGG	ACTCAGGGGACAGGACACC	61	527
p.Arg295Pro	AAGAGAATTGAATTGCTTGAACC	CGAGCAGAAATGTCGGG	61	316

c, Celsius; bp, base-pares

Table S2 – Genetic data on exome sequencing results

Family	Family A	Family B	Family C
Number of individuals sequenced	3	4	2
Average coverage	133X	130X	121X
All variants	215843	250171	168177
Coding/splicing [a]	37430	39414	28903
NS/SS/Indels [b]	16637	5400	15161
MAF 1KG [c]	2425	1841	2275
MAF EVS [d]	538	465	1815
Absent from In-house database	158	276	377
Common to affected	27	25	133
Genes with homozygous/compound heterozygous mutations	2	1	3
Deleterious [e]	1	1	1

[a] Filtering out variants that are not in the coding sequences or in the 6 base-pairs before and after the exon.

[b] Filtering out synonymous variants and including only non-synonymous/stop (NS), splice site (SS) and insertions and deletions (Indels).

[c] Including variants that had minor allele frequency (MAF) < 0.005 in the 1000 genome project (1KG) database.

[d] Including variants that had minor allele frequency (MAF) < 0.005 in the exome variant server (EVS) database.

[e] Predicted to be deleterious and conserved by SIFT, PolyPhen 2, MutationTaster, PhyloP and GERP++.

Table S3 - Nerve conduction study data

	Family B Individual IV-1	**Family B Individual IV-2**	**Family B Individual IV-9**	**Family A Individual V-2**	**Normal limits**
Median nerve	L 3,5	L 3,6	L 3,1	NA	
DML (ms)	9,4	9,1	9,6		< 4
CMAP amplitude	60	62	58		>4,8
(mV) MNCV m/s	28,8	23,3	23,7		> 47
FWL (ms)					<33
Ulnar nerve	R 3,1	R 2,4	R 2,8	NA	
DML (ms)	8,1	11,5	11,2		<3,2
CMAP amplitude	58	63	60		>4,8
(mV) MNCV m/s	28,6	25	25,8		> 47
FWL (ms)					<33
Peroneal nerve	L 6,3	L 5,6	R 4,9	R 3,8	
DML (ms)	2,5	2,8	6,9	1,9	<6,5
CMAP amplitude	43	49	50	48,5	>2
(mV) MNCV m/s	52,7	47,7	46,9	40,6	>40
FWL (ms)					<52
Tibial nerve	R 5	R 3,6	NA	NA	
DML (ms)	4,3	5,3			<6
CMAP amplitude	46	50			>3,5
(mV) MNCV m/s	50,5	45,2			>40
FWL (ms)					<52
Median nerve	R 26,3	L 31	L 30	NA	
SNAP amplitude (uV)	NA	47	50		>12
SCV (m/s)					>40
Ulnar nerve	R 11,8	R 12	R 16	NA	
SNAP amplitude (uV)	NA	55	NA		>8
SCV (m/s)					>40
Sural nerve	R 5,6 L 3,8	R 5,3 L 5,4	R 26 L 26	R 16 L 21	
SNAP amplitude (uV)	38 39	40 41	32 33	45 36	>10
SCV (m/s)					>35
Upper limbs	L	L R	L R	NA	
Latency (s)	1,7	1,39 1,35	1,23 1,38		Positive
Lower limbs	L	L R	L R	NA	
Latency (s)	NO	NO NO	NO NO		Positive

DML: distal motor latency; CMAP: compound muscle action potential; MNCV: motor nerve conduction velocity; FWL: F wave latency; SNAP: sensory nerve action potential; SCV: sensory conduction velocity; NA: not available; NO: not obtained; R: right; L: left.

Chapter 4: Transcriptomic Analysis of Zebrafish TDP-43 Transgenic Lines

Alexandra Lissouba, Meijiang Liao, Edor Kabashi and Pierre Drapeau

Manuscript accepted in *Frontiers on Molecular Neuroscience,* 29/11/2018

Authors contribution

I am the first author of this manuscript.

As such, I designed all of the experiments with PD, realized all the experiments except the initial injection of the transgenic lines, analyzed the results and produced all the figures. I wrote the manuscript with PD.

Manuscript

Transcriptomic Analysis of Zebrafish TDP-43 Transgenic Lines

Alexandra Lissouba[1], Meijiang Liao[2], Edor Kabashi[3,4], Pierre Drapeau[2]*

[1] Department of Pathology and Cell Biology and Research Center of the University of Montréal Hospital Center, University of Montreal, Montréal, QC, Canada

[2] Department of Neurosciences and Research Center of the University of Montreal Hospital Center, University of Montreal, Montréal, QC, Canada

[3]Sorbonne Université Paris VI, UMR CNRS 1127, UPMC INSERM U 1127, CNRS UMR 7225, Institut du Cerveau et de la Moelle épinière – ICM, Paris, France

[4]Institut Imagine, UMR INSERM 1163, Université Paris Descartes, Hospital Necker-Enfants, Paris, France

***Correspondence:**

Dr. Pierre Drapeau

p.drapeau@umontreal.ca

Keywords: Amyotrophic lateral sclerosis, ALS, Zebrafish, TDP-43, *TARDBP*.

Abstract

Amyotrophic lateral sclerosis (ALS) is a late-onset progressive neurodegenerative disorder that affects both upper and lower motor neurons, leading to muscle atrophy with spasticity and eventual death in 3 to 5 years after the disease onset. More than 50 mutations linked to ALS have been found in the gene *TARDBP*, encoding the protein TDP-43 that is the predominant component of neuronal inclusions in ALS. TDP-43 is an RNA binding protein with glycine-rich domains that binds to more than 6,000 RNAs in the human brain. However, ALS-related mutations do not appear to affect the function of these genes, indicating that a toxic gain-of-function may occur. We generated transgenic zebrafish lines expressing human TDP-43, either the wild-type form or the ALS-causative G348C mutation identified in a subset of ALS patients, with the transgene expression driven by an inducible heat shock promoter in order to bypass a potential early mortality. The expression of the mutant but not the wild-type human TDP-43 in zebrafish embryos induced a reduction of the locomotor activity in response to touch compared to controls and moderate axonopathy of the motor neurons of the spinal cord, with premature branching of the main axonal branch, recapitulating previous results obtained by mRNA injections. We used these lines to investigate transcriptomic changes due to the presence of mutant TDP-43 using RNA sequencing and have found 159 genes that are differentially expressed compared to control, with 67 genes up-regulated and 92 genes down-regulated. These transcriptomic changes are in line with recent transcriptomic data obtained in mouse models, indicating that these zebrafish transgenic lines are adequate to further study TDP-43-related ALS.

Introduction

Amyotrophic lateral sclerosis (ALS) is a devastating motor neuron disorder characterized by the loss of both upper motor neurons, located in the motor cortex and lower motor neurons, located in the anterior horn of the spinal cord and in the brainstem. The disease onset is around 50-60 years of age and is first recognized as muscle weakness, atrophy and eventual death due to respiratory failure, with a median survival of 2-3 years. ALS is part of a clinical continuum with fronto-temporal dementia (FTD), with overlapping genes and clinical features between the two diseases. Most ALS cases appear to be sporadic in nature (sporadic ALS - sALS) and around 10% of patients having a familial history of the disease (familial ALS -fALS) (Chio et al., 2013; Swinnen and Robberecht, 2014; Hardiman et al., 2017). Several genes have been implicated in ALS including *TARDBP*, coding for the protein TDP-43 (Taylor et al., 2016; Therrien et al., 2016).

TDP-43 is a predominantly nuclear protein, but was first linked to ALS and FTD as the main protein found in the ubiquitin-positive cytoplasmic inclusions in the neurons, including motor neurons, of ALS and of FTD patients, with a clearance of its usual nuclear localization (Arai et al., 2006; Neumann et al., 2006). Following this discovery, mutations in *TARDBP* were identified in around 5% of fALS cases, 1% of sALS cases and 1% of FTD cases (Kabashi et al., 2008; Sreedharan et al., 2008; Caroppo et al., 2016). TDP-43 has several physiological functions mainly in regulating RNAs, as it is involved in most steps of RNA metabolism, including transcription, splicing, transport and stability (Gao et al., 2018). TDP-43 is known to bind to at least 6000 mRNAs in the murine brain and to modify the expression level of at least 600 mRNAs (Polymenidou et al., 2011), and as such it was hypothesized that mutant TDP-43 may induce differentially expressed genes and isoforms, which may be part of the pathogenicity of ALS.

Several animal models of ALS based on mutations of TDP-43 have been generated, from mouse models to yeast, including zebrafish (Patten et al., 2014; Van Damme et al., 2017), but how ALS-causing mutations of TDP-43 induce the pathophysiological changes seen in ALS patients is still poorly understood. The TDP-43 transgenic mouse models highly overexpress

the mutant human TDP-43 protein compared to the endogenous Tdp-43 and result in a very aggressive early onset phenotype with premature lethality (Wegorzewska et al., 2009; Stallings et al., 2010; Xu et al., 2010; Xu et al., 2011). On the other hand, the mice overexpressing an amount of mutant TDP-43 closer to the physiological level display only minor motor deficiencies and have a phenotype that resembles more closely an FTD ones than an ALS one (Swarup et al., 2011; Arnold et al., 2013). Additionally, in most cases, overexpression of the wild-type TDP-43 protein leads to similar defects as the mutated forms, thus preventing the discrimination between the overexpression of a transgene in general and the overexpression of mutant TDP-43 in particular. Recently, a new Tdp-43 mouse model was generated using CRISPR/Cas9 technology to knock-in an endogenous *Tardbp* mutation similar to the human Q331K mutation (White et al., 2018). While these mice presented with motor and cognitive defects, the phenotype did not evolve to paralysis or death after 24 months, thus leading again to a phenotype closer to FTD than ALS.

The overexpression of human mutant TDP-43 but not of wild-type TDP-43 at low doses in zebrafish embryos by mRNA overexpression has been shown to result in reduced locomotion and aberrant motor neuron axons, with abnormal synaptic transmission (Kabashi et al., 2010; Laird et al., 2010; Kabashi et al., 2011; Vaccaro et al., 2012; Armstrong and Drapeau, 2013; Vaccaro et al., 2013; Patten et al., 2017). However, these models express only transiently the human protein and the high level of expression may vary with the quality of the mRNA injections, adding variability to the models. To palliate this issue, we aimed to generate stable transgenic TDP-43 zebrafish lines expressing human TDP-43 with ALS-causing mutations in order to study the disease using zebrafish in a more accurate fashion. Thus, we have generated two transgenic zebrafish lines expressing either human wild-type TDP-43 or human TDP-43 bearing the G348C mutation in ALS and characterized the locomotor activity and the axonal defects of these lines. We also identified differentially expressed genes due to the presence of mutant TDP-43. Using these lines, we performed an unbiased transcriptomic analysis comparing whole transcriptome from zebrafish expressing mutant TDP-43 to control and we identified candidate genes that may be involved in TDP-43 pathogenicity.

Material and methods

Ethics statement

This study was approved by the Canadian Council for Animal Care and conducted at the Research Center of the University of Montreal Hospital Center (CRCHUM).

Fish husbandry

Wild-type zebrafish (*Danio rerio*) were maintained at 28.5°C and kept under a 12/12 hour light/dark cycles at the animal facility of the Centre Hospitalier de Montréal research center, Montréal, Canada. They were bred according to standard procedure (Westerfield, 1995) and staged as previously described (Kimmel et al., 1995).

Generation of the transgenic lines and heat shock procedure

The pCS2-TDP43-Myc and pCS2-TDP43-G348C-Myc plasmids were generously shared by Dr. Guy Rouleau (McGill University). They respectively contain the human wild type *TARDBP* cDNA and the human *TARDBP* cDNA bearing the G1176T change encoding for the G348C mutation. Six sequences coding for the myc tag were added to the 3' end of the sequences. The Tol2Kit was used to generate the two pDest-Tol2CG2-hsp70-TDP43-Myc and pDest-Tol2CG2-hsp70-TDP43-Myc vectors. 25 ng/µl of these vectors were injected in one-cell stage zebrafish embryos with 25 ng/µl of the Tol2 transposase mRNA with 0.05% Fast Green (Sigma). The injections were done using a Picospritzer III pressure ejector (General Valve, Fairfield, NJ, USA). Approximately 300 embryos were injected for each line and less than 40% expressed eGFP in the heart. These embryos were selected and raised to adulthood as the F0 founders. For the TDP-43^{WT} line, 25 F0 fish reached sexual maturity and 11 of them transmitted the transgene to their progeny when outcrossed with wild type AB zebrafish, as identified by eGFP expression in the heart. The percentage of transgene transmission for these F0 founders varied from 0.69% to 33.54%. We selected the two F0 fish with the highest transgene transmission rate (28.44% and 33.54%) to raise the F1 generations. The adult F1 TDP-43^{WT} fish were then outcrossed to identify the rate of transgene transmission and estimate the copy number of the transgene. The transmission rate of one of the TDP-43^{WT} lines followed normal mendelian ratios for a single insertion, with 50% of the progeny inheriting the transgene and we decided to only work with this line. 32 TDP-43^{G348C} F0 fish

reached adulthood and only 7 of them transmitted the transgene to their progeny, at a rate of 0.78% to 29.42%. Due to the low percentages, only the two F0 fish transmitting with the highest frequency per line (17.95% and 29.42%) were selected to raise their progeny until adulthood, to create the two independent lines A-TDP-43^{G348C} and B-TDP-43^{G348C}. The adult F1 fish were then outcrossed to identify the rate of transgene transmission and both TDP-43^{G348C} lines displayed mendelian ratios of transgene transmission, with around 50% of transgene transmission.

For the heat shock procedure, 20 hpf embryos were transferred to glass tubes with system water. The tubes were then placed in a pre-heated incubator at 38.5°C for 60 minutes at a 60 RPM agitation. Embryos were then put back at 28.5°C and dechorionated at 25 hpf.

Western blot

Western blots were performed as previously described (Gan-Or et al., 2016). Briefly, about 30 embryos for each condition were lysed in ice-cold RIPA buffer (150 mM NaCl, 50 mM Tris pH 7.5, 1% Triton X-100, 0.1% SDS, 1% Na deoxycholate, 0.1% protease inhibitor), maintained on ice and homogenized with a hand-held pestle. The lysates were centrifuged for 10 minutes at 10,000 rpm at 4°C and the supernatants were collected. Protein concentration was established using Bio-Rad DC Protein Assay and 60 µg of proteins were loaded in 2X Lämmli buffer after boiling the samples for 5 minutes at 95°C. TGX Stain-Free FastCast acrylamide Kit (Bio-Rad) was used to make 10% Tris-glycine. After electrophoresis, the gels were activated by exposure to UV for one minute, and transferred to either regular or low-fluorescence PVDF membrane (Bio-Rad). After transfer, total proteins on membranes were detected by UV. Membranes were then blocked for one hour using 5% fat free milk in PBST. The primary antibody (anti-myc, 1:5,000) was incubated overnight at 4°C in 5% fat free milk in PBST. After washing 3x 5 minutes in PBST, the membrane was incubated with an anti-mouse IgG, HRP conjugated (1:5,000, Jackson Immuno) in 5 % fat free milk in PBST for one hour at room temperature, and then washed 3x 5 minutes. Membranes were exposed to Clarity enhanced chemiluminescence (ECL, Bio-Rad) for 5 minutes at room temperature and visualized using a ChemiDoc MP (Bio-Rad). Detection and quantification of band intensities was conducted using Image Lab 5.2 software (Bio-Rad).

Immunohistochemistry

Whole-mount immunohistochemistry was done like previously described (Dzieciolowska et al., 2017). Briefly, 2 dpf embryos were fixed in 4% paraformaldehyde overnight at 4°C. Following fixation, the embryos were rinsed several times over the course of an hour with phosphate buffered saline and incubated in 1 mg/ml collagenase in PBS for 40 minutes. The collagenase was washed off over one hour with PBS and the embryos were then incubated with Triton X-100 (PBST) for 30 minutes. Following this step, the embryos were incubated in fresh block solution prepared from PBS containing goat serum, bovine serum albumin, dimethyl sulfide (DMSO) and Triton X-100, for 1 hour at room temperature and then treated with a solution containing a primary antibody against pre-synaptic synaptotagmin 1 (znp-1) (1:100; Molecular Probes) overnight at 4°C. Samples were then washed in PBST and incubated in block solution containing a secondary antibody (Alexa Fluor 488, 1:1000; Invitrogen) for 6 hour at 4°C. Before imaging, larvae were transferred to a solution containing 70% glycerol and mounted the following day on a slide. The embryos were visualized using a Quorum Technologies spinning disk confocal microscope with a CSU10B (Yokogawa) spinning head mounted on an Olympus BX61W1 fluorescence microscope and connected to a Hamamatsu ORCA-ER camera. Images were acquired using Volocity software (Improvision) and analyzed using ImageJ (NIH).

Touch-evoked escape response

Locomotor activity was assessed by lightly touching the tail of the zebrafish embryos with a light forceps. The embryos were placed at the center of a 150 mm diameter petri dish filled with system water that was kept at 28.5C by a heating plate. Swimming was recorded from above at 30 Hz (Grasshopper 2 camera, Point Gray Research) and swim duration, swim distance and maximum swim velocity were quantified off line using the Manual Tracking plug-in for ImageJ (NIH).

RNA-sequencing

Total RNA from around 100 RNAlater-fixed embryos (Ambion) was extracted using RNAsolv reagent (Omega Biotek) following the manufacturer's standard protocol. RNA extraction was made using between 5.19–9.75 × 105 cells by RNAsolv reagent manufacturer's protocol (Omega Biotek). Absence of contamination with chemicals was assessed by nanodrop using 260/280 and 260/230 ratios. Quantification of total RNA was made by nanodrop and 0.1 to 1.44 g of total RNA was used for sequencing. Quality of total RNA was assessed with the BioAnalyzer Nano (Agilent).

Library preparation was done with the Truseq RNA (Illumina). 18 PCR cycles was required to amplify cDNA libraries. Libraries were quantified by nanodrop and BioAnalyzer. All librairies were diluted to 10 nM and normalized with the Miseq SR50 v2. Libraries were pooled to equimolar concentration and multiplexed by six samples per lane. Sequencing was performed with the Illumina Hiseq2000 using the SBS Reagent Kit v3 (100 cycles, paired-end) with 1.6 nM of the pooled library. Cluster density was targeted at around 800 k clusters/mm2. Around 70 million reads were generated for each sample. Library preparation and sequencing was done at the Institute for Research in Immunology and Cancer's Platform (University of Montreal). About 95% of high quality reads were mapped onto GRCz10 version of the zebrafish genome (gene annotation from Ensembl version 87) using STAR version 2.5.1b.

Differential gene expression analysis was assessed by DeSeq package using R software. Differential gene expression was filtered on a False Discovery Rate (or adjusted p-value) < 0.05.

qRT-PCR

Quantitative RT-PCR (qRT-PCR) primers for each gene were designed using the Universal Probe Library tool from Roche. Total RNA was extracted from FACS-purified NSCs using RNAsolv reagent (Omega Biotek) and chloroform followed by isopropanol precipitation. Reverse transcription was performed from 1 µg of total RNA using the superscript VILO reverse transcription mix (Invitrogen). Quantitative PCR was performed on 2 µL of 1:10-diluted cDNA using SYBR Green I master (Roche) on a LightCycler 80 thermocycler. *polr2d* gene (ENSDART00000108718) was used as a reference gene for ddCt quantification.

Results

Generation of transgenic TDP-43 zebrafish

In order to study the effects of mutant TDP-43, we have generated transgenic zebrafish lines expressing stably either human wild-type TDP-43 (TDP-43^{WT}) or bearing the G348C mutations found in ALS patients from a French-Canadian population (TDP-43^{G348C}) (Kabashi et al., 2008). The transgenic lines were generated using the human TDP-43 cDNA to which 6 myc tags were fused to the C-terminus of the protein. Since previous work showed that the presence of mutant TDP-43 in the early stages of development of the zebrafish lead to adverse effects (Kabashi et al., 2010; Laird et al., 2010; Kabashi et al., 2011; Vaccaro et al., 2012; Armstrong and Drapeau, 2013; Vaccaro et al., 2013; Patten et al., 2017), we decided to use an inducible promoter, the zebrafish heat shock protein 70 like promoter (*hsp70l*), to temporally control the expression of the transgene. The transgene constructs also contained eGFP driven by the cardiac myosin light chain 2 (*cmlc2*) promoter used as a reporter gene in order to easily identify transgenic embryos with green hearts (**Figure 1A**).

The constructs were injected in 1-4 cell stage embryos (F0) and the fish were raised until adulthood. The adult F0 fish were outcrossed with wild-type fish and their progeny was screened for the presence of fluorescent hearts, to select the ones having integrated the transgenes in their germline. We selected the two F0 fish with the highest transmission rate for both lines to raise the F1. These F1 fish were outcrossed with wild-type to estimate the transgene copy number by the transgene transmission rate. While both TDP-43^{G348C} lines had an approximate 50% transmission rate of the transgene, only one of the TDP-43^{WT} line transmitted the transgene following mendelian ratios and only this line was kept for further experiments. We selected the TDP-43^{G348C} line (B) that had the closest level of expression to the TDP-43WT line (**Supplementary Figure S1**). The F2 offsprings were raised to adulthood and used to establish the lines for the following experiments.

In order to express the transgene, a 60 minutes heat shock at 38.5°C (10°C above the temperature at which they are raised) is done when the embryos are 20 hours post fertilization

(hpf). Only normal looking embryos are selected at 48 hpf for experiments (**Figure 1B**). To establish the expression of the transgenes by Western blot, we used an anti-myc antibody. No transgenic protein was detectable before the heat shock, thus validating the integrity of the *hsp70l* promoter. However, upon heat shock the TDP-43^{WT} and TDP-43^{G348C} transgenes were detectable at around 60 kDa, which corresponds to the molecular weight of the TDP-43 protein with the linker and the 6 myc tags (**Figure 1C**). Interestingly, we observed the TDP43^{WT} expression level was systematically lower than that of TDP-43^{G348C}. Moreover, several bands were also observed in the TDP-43^{G348C} line, indicating the presence of C-terminus TDP-43 fragments, consistent with what is seen in human patients and in mouse studies (Stallings et al., 2010; Swarup et al., 2011; Xu et al., 2011; Gao et al., 2018) (**Figure 1C**).

Locomotor defects induced by the TDP-43^{G348C} transgene

We then verified if the stable expression of TDP-43^{G348C} upon heat shock was associated with locomotor defects, as it was observed in previous studies by transient expression. We elicited the touch-evoked response by lightly touching the tail of 48 hpf embryos with a blunt forceps. The swim distance, swim duration and the maximum swim velocity were analysed using the swim traces obtained by tracking the embryos following the touch (**Figure 2A**). While heat shock of wild type embryos or expressing TDP-43^{WT} had no influence on locomotion compared to wild type, the expression of TDP-43^{G348C} led to a strong reduction of the swim distance, the swim duration and the maximum swim velocity compared to controls (**Figure 2B**), indicating that the motor neuron axonal defects had a strong impact on the physiology as seen by the severe negative influence on the locomotion of the TDP-43^{G348C} embryos, as was previously reported (Kabashi et al., 2010; Laird et al., 2010; Kabashi et al., 2011; Vaccaro et al., 2012; Armstrong and Drapeau, 2013; Vaccaro et al., 2013; Patten et al., 2017).

Human mutant TDP-43 induces motor neuron axonopathy

As locomotor defects were observed, we investigated whether they reflected axonal motor neuron defects by immunohistochemistry using an antibody against the pre-synaptic marker

znp-1. When TDP-43^{G348C} was expressed, the majority of motor neuron axons exhibited several defects, including overbranching of the main axonal branch, absence of secondary branching or abnormal innervation of nearby myotome (**Figure 3A**). The axonal defects were classified as mainly moderate (**Figure 3C**) using a classification scale based on the visual interpretation of the axonal appearance, adapted from McWhorter et al (**Figure 3B**)(McWhorter et al., 2008). The overexpression of the TDP-43^{WT} transgene, or the heat shock of wild-type embryos did not induce specific defects, indicating that it was the specifically the presence of mutant TDP-43 rather than the heat shock or the presence of a foreign gene that was responsible for the defects obtained with TDP-43^{G348C}. This is consistent with previous zebrafish models overexpressing mutant TDP-43 (Kabashi et al., 2010; Laird et al., 2010; Kabashi et al., 2011; Vaccaro et al., 2012; Armstrong and Drapeau, 2013; Vaccaro et al., 2013; Patten et al., 2017). Altogether, these data validate the relevance of our stable expressing transgenic zebrafish lines since they display a clinically-relevant pathogenicity associated with the G348C mutation.

Transcriptomic analysis of TDP-43^{G348C} embryos and qRT-PCR validation

Given that TDP-43 is an RNA-binding protein involved in RNA metabolism (Gao et al., 2018), we next sought to investigate whether transcriptomic modifications were caused by the expression of TDP-43^{G348C}. While TDP-43 is involved in mRNA splicing, it is also involved in mRNA stability and the depletion of Tdp-43 causes around 600 mRNAs to have altered expression levels in mice (Polymenidou et al., 2011). Thus, we used RNA-sequencing to look at differentially regulated genes due to TDP-43^{G348C} expression. Since the human TDP-43^{WT} line following heat shock presented no obvious phenotype compared to wild-type zebrafish with heat shock, and since the expression level of human TDP-43^{WT} was lowered than human TDP-43^{G348C} with an equal heat shock, we hypothesized that using human TDP-43^{WT} as a control may give us differentially expressed genes based on the expression level of the transgenes rather than solely based on the presence of the mutation. We thus decided to use the wild type zebrafish heat shock condition as a control in order to compensate for the effect of the heat shock.

More than 70 million reads were sequenced and analysed for either TDP-43^{G348C} heat shock or wild type heat shock and more than 95% were mapped to the GRCz10 version of the zebrafish genome (gene annotation from Ensembl version 87). We used DESeq to analyze the differentially expressed genes amongst the 32,267 genes analyzed between the two conditions. Filtering on a *p*-value < 0.05 we found 159 differentially expressed genes, with 67 up-regulated and 92 down-regulated. In order to have a more stringent cut-off, we used a |log2FC| greater than one, corresponding to a minimal two-fold up-regulation or down-regulation. This cut-off decreased the number of differentially expressed genes to 148 (65 up-regulated and 83 down-regulated). An even more stringent cut-off of |log2FC| greater than two, corresponding to a minimal four-fold up- or down- regulation, led to only 59 genes that were differentially regulated, with 27 up-regulated and 32 down-regulated (**Figure 4A**). A volcano plot representing these data is shown in **Figure 4B** with data in, blue, orange or black for cut-offs of |log2FC| greater than two or one or for $p < 0.05$, respectively. The list of significantly differentially expressed genes can be found in the **supplementary Table S1**.

These results show that the expression of a G348C mutant TDP-43 is associated with broad changes in the transcriptome. While no common pathways could be found between the 159 genes with $p < 0.05$, some of these changes can be associated with potential pathophysiological mechanisms of ALS and TDP-43 mutations. Thus the human orthologs of some of the differentially expressed genes have been linked to several neuromuscular disorders, including ALS and muscular dystrophy, such as *CLCN2*, *ELOVL4*, *ELOVL5*, *PEA15*, *LBH*, *PAMR1* and *MSTO1* (references in **Table 1**). Other genes can be linked to pathways that are perturbed in ALS, such as calcium signaling (*icn2*, *smdt1a*, *pvalb4*, *pvalb9* and *adcy1b*), or mitochondria and oxidative stress (*msto1*, *smdt1a* and *mt2*). Also of interest, some of the genes identified are unknown, such as *ponzr3*, *ponzr4* or *ftr86*, which may indicate new pathogenic mechanisms of ALS (references in **Table 1**).

In order to validate these results, we selected 12 of the differentially expressed genes to measure their expression levels by qRT-PCR in all of our conditions, including TDP-43^{WT} heat shock (**Figure 5 A-L**). All mRNA expression levels positively correlated with the RNA-sequencing data, even though significance was not always reached (**Figure 5 D, E, F, G, J, K**), probably due to variability in the level of mRNA expression (**Figure 5 D, F, I** and **J**).

Discussion

In this report, we have generated inducible transgenic zebrafish lines expressing human TDP-43, either wild type or bearing the ALS-causing mutation G348C. We have characterized the phenotype induced by the expression of the mutant TDP-43^{G348C} and have used this line to study transcriptomic variations induced by ALS-causing mutant TDP-43.

Overexpressing mutant TDP-43 but not wild-type at 21 hpf, during a critical period for motor neuron development (Myers et al., 1986), induced a reduction of the locomotor activity in response to touch with reduced swim distance, time and velocity compared to controls. These swimming defects were correlated with moderate axonopathy of the motor neurons of the spinal cord, with premature branching of the main axonal branch and branching defects in the secondary branches. These results recapitulate the phenotype obtained by overexpression of mutant TDP-43 mRNA by our group and others (Kabashi et al., 2008; Kabashi et al., 2010; Laird et al., 2010; Vaccaro et al., 2012; Armstrong and Drapeau, 2013; Vaccaro et al., 2013; Patten et al., 2017), thus validating our transgenic lines as genetic models of TDP-43-related ALS that can be used to better understand the pathophysiology of TDP-43 pathogenicity in ALS

Interestingly, a stronger transgene expression was systematically reached for TDP-43^{G348C} compared to TDP-43^{WT}. It was shown to be the case in mouse models as well, including in the transgenic mouse model expressing the same G348C mutation from Swarup and colleagues (Igaz et al., 2011; Swarup et al., 2011) and may be explained by a higher stability of the mutant protein. It is unlikely to be the result of a deficiency in TDP-43 autoregulation due to the G348C mutations, since we generated our transgenic lines using cDNA lacking the TDP-43 3'UTR necessary for its autoregulation (Ayala et al., 2011). However, the fact that we observed multiple bands by western blot when TDP-43^{G348C} was expressed may indicate a dysfunction in its normal degradation, thus impacting the turnover of the protein. An additional possibility inherent to the Tol2 system used to generate these transgenic lines is that the TDP-43^{G348C} line may have integrated concatemers of the transgene at a single insertion

point, thus leading to a higher expression level of the transgene compared to the TDP-43^{WT} line, while still following mendelian ratios.

Since TDP-43 affects the level of many mRNAs (Polymenidou et al., 2011), we used our transgenic lines to identify differentially expressed genes at the time when we observed the TDP-43^{G348C} mutant induced phenotype. We found 159 genes misregulated compared to heat shocked wild type embryos, the majority with 2- to 4- fold differences. However, since we did not use TDP-43^{WT} expressing embryos as a control, we can not exclude that some of the transcriptomic changes identified may be due to the presence of a transgene and not specifically to the G348C TDP-43 mutant. However, we validated a subset of these genes by qRT-PCR in both transgenic lines and found concordant results, with up- or down-regulation of the selected genes specific to the expression of TDP-43^{G348C} and not TDP-43^{WT}. Testing of genetic interactions between these potential new ALS hits and TDP-43 will allow us to functionally validate these results.

White and colleagues investigated transcriptomic differences in their Tdp-43 knock-in mice (White et al., 2018). In the lumbar region of 5-months-old mice, only 31 genes were found to be differentially regulated. However, when repeating this experiment using the frontal cortices of these mice, 404 genes were differentially regulated and this number increased to 1,219 when the experiment was done in 20 months-old mice (White et al., 2018). Even though our experimental paradigms are different, with an induced early onset *versus* a slow disease course, it is interesting to note that 16 differentially expressed genes or their orthologs are in common between our two datasets. Additionally, 12 of these common genes were found when comparing our dataset to their aged mouse frontal cortex dataset. While this may be due to chance, it could also indicate that some of these transcriptomic changes may be the consequences of the phenotype, rather than its cause (**supplementary Table S1**). Our results presented here indicate that these zebrafish transgenic lines are promising tools to better understand TDP-43 pathophysiology and will complement other existing models.

Conflict of Interest

The authors declare that the research was conducted in the absence of any commercial or financial relationships that could be construed as a potential conflict of interest.

Author Contributions

EK and ML generated the transgenic lines. AL designed and interpreted the experiments. AL and PD wrote the manuscript. All authors reviewed the manuscript.

Funding

AL was funded by ALS Canada. PD is funded by CIHR. EK is funded by an ERC Consolidator Grant ALS-Networks.

Acknowledgments

We thank Dr. Edna Brustein and Dr. Nathalie Champagne for their help generating the transgenic lines and Dr. Guy Rouleau for his gifts of the plasmids used in generating the lines. We also thank Marina Drits and Guy Laliberté for help in taking care of the fish as well as Dr. Eric Samarut and Dr. Kessen Patten for their advice on the paper.

Data Availability Statement

The raw data supporting the conclusions of this manuscript will be made available by the authors, without undue reservation, to any qualified researcher.

References

Arai, T., Hasegawa, M., Akiyama, H., Ikeda, K., Nonaka, T., Mori, H., et al. (2006). TDP-43 is a component of ubiquitin-positive tau-negative inclusions in frontotemporal lobar degeneration and amyotrophic lateral sclerosis. *Biochem Biophys Res Commun* 351(3)**,** 602-611. doi: 10.1016/j.bbrc.2006.10.093.

Armstrong, G.A., and Drapeau, P. (2013). Calcium channel agonists protect against neuromuscular dysfunction in a genetic model of TDP-43 mutation in ALS. *J Neurosci* 33(4)**,** 1741-1752. doi: 10.1523/JNEUROSCI.4003-12.2013.

Arnold, E.S., Ling, S.C., Huelga, S.C., Lagier-Tourenne, C., Polymenidou, M., Ditsworth, D., et al. (2013). ALS-linked TDP-43 mutations produce aberrant RNA splicing and adult-onset motor neuron disease without aggregation or loss of nuclear TDP-43. *Proc Natl Acad Sci U S A* 110(8)**,** E736-745. doi: 10.1073/pnas.1222809110.

Ayala, Y.M., De Conti, L., Avendano-Vazquez, S.E., Dhir, A., Romano, M., D'Ambrogio, A., et al. (2011). TDP-43 regulates its mRNA levels through a negative feedback loop. *EMBO J* 30(2)**,** 277-288. doi: 10.1038/emboj.2010.310.

Cadieux-Dion, M., Turcotte-Gauthier, M., Noreau, A., Martin, C., Meloche, C., Gravel, M., et al. (2014). Expanding the clinical phenotype associated with ELOVL4 mutation: study of a large French-Canadian family with autosomal dominant spinocerebellar ataxia and erythrokeratodermia. *JAMA Neurol* 71(4)**,** 470-475. doi: 10.1001/jamaneurol.2013.6337.

Caroppo, P., Camuzat, A., Guillot-Noel, L., Thomas-Anterion, C., Couratier, P., Wong, T.H., et al. (2016). Defining the spectrum of frontotemporal dementias associated with TARDBP mutations. *Neurol Genet* 2(3)**,** e80. doi: 10.1212/NXG.0000000000000080.

Chio, A., Logroscino, G., Traynor, B.J., Collins, J., Simeone, J.C., Goldstein, L.A., et al. (2013). Global epidemiology of amyotrophic lateral sclerosis: a systematic review of the published literature. *Neuroepidemiology* 41(2)**,** 118-130. doi: 10.1159/000351153.

Depienne, C., Bugiani, M., Dupuits, C., Galanaud, D., Touitou, V., Postma, N., et al. (2013). Brain white matter oedema due to ClC-2 chloride channel deficiency: an observational analytical study. *Lancet Neurol* 12(7)**,** 659-668. doi: 10.1016/S1474-4422(13)70053-X.

Di Gregorio, E., Borroni, B., Giorgio, E., Lacerenza, D., Ferrero, M., Lo Buono, N., et al. (2014). ELOVL5 mutations cause spinocerebellar ataxia 38. *Am J Hum Genet* 95(2)**,** 209-217. doi: 10.1016/j.ajhg.2014.07.001.

Dzieciolowska, S., Drapeau, P., and Armstrong, G.A.B. (2017). Augmented quantal release of acetylcholine at the vertebrate neuromuscular junction following tdp-43 depletion. *PLoS One* 12(5)**,** e0177005. doi: 10.1371/journal.pone.0177005.

Gal, A., Balicza, P., Weaver, D., Naghdi, S., Joseph, S.K., Varnai, P., et al. (2017). MSTO1 is a cytoplasmic pro-mitochondrial fusion protein, whose mutation induces myopathy and ataxia in humans. *EMBO Mol Med* 9(7)**,** 967-984. doi: 10.15252/emmm.201607058.

Gan-Or, Z., Bouslam, N., Birouk, N., Lissouba, A., Chambers, D.B., Veriepe, J., et al. (2016). Mutations in CAPN1 Cause Autosomal-Recessive Hereditary Spastic Paraplegia. *Am J Hum Genet* 98(5)**,** 1038-1046. doi: 10.1016/j.ajhg.2016.04.002.

Gao, J., Wang, L., Huntley, M.L., Perry, G., and Wang, X. (2018). Pathomechanisms of TDP-43 in neurodegeneration. *J Neurochem*. doi: 10.1111/jnc.14327.

Hardiman, O., Al-Chalabi, A., Chio, A., Corr, E.M., Logroscino, G., Robberecht, W., et al. (2017). Amyotrophic lateral sclerosis. *Nat Rev Dis Primers* 3**,** 17071. doi: 10.1038/nrdp.2017.71.

Igaz, L.M., Kwong, L.K., Lee, E.B., Chen-Plotkin, A., Swanson, E., Unger, T., et al. (2011). Dysregulation of the ALS-associated gene TDP-43 leads to neuronal death and degeneration in mice. *J Clin Invest* 121(2)**,** 726-738. doi: 10.1172/JCI44867.

Iwama, K., Takaori, T., Fukushima, A., Tohyama, J., Ishiyama, A., Ohba, C., et al. (2018). Novel recessive mutations in MSTO1 cause cerebellar atrophy with pigmentary retinopathy. *J Hum Genet* 63(3)**,** 263-270. doi: 10.1038/s10038-017-0405-8.

Kabashi, E., Bercier, V., Lissouba, A., Liao, M., Brustein, E., Rouleau, G.A., et al. (2011). FUS and TARDBP but not SOD1 interact in genetic models of amyotrophic lateral sclerosis. *PLoS Genet* 7(8)**,** e1002214. doi: 10.1371/journal.pgen.1002214.

Kabashi, E., Lin, L., Tradewell, M.L., Dion, P.A., Bercier, V., Bourgouin, P., et al. (2010). Gain and loss of function of ALS-related mutations of TARDBP (TDP-43) cause motor deficits in vivo. *Hum Mol Genet* 19(4)**,** 671-683. doi: 10.1093/hmg/ddp534.

Kabashi, E., Valdmanis, P.N., Dion, P., Spiegelman, D., McConkey, B.J., Vande Velde, C., et al. (2008). TARDBP mutations in individuals with sporadic and familial amyotrophic lateral sclerosis. *Nat Genet* 40(5)**,** 572-574. doi: 10.1038/ng.132.

Kimmel, C.B., Ballard, W.W., Kimmel, S.R., Ullmann, B., and Schilling, T.F. (1995). Stages of embryonic development of the zebrafish. *Dev Dyn* 203(3)**,** 253-310. doi: 10.1002/aja.1002030302.

Kraemer, A.M., Saraiva, L.R., and Korsching, S.I. (2008). Structural and functional diversification in the teleost S100 family of calcium-binding proteins. *BMC Evol Biol* 8**,** 48. doi: 10.1186/1471-2148-8-48.

Laird, A.S., Van Hoecke, A., De Muynck, L., Timmers, M., Van den Bosch, L., Van Damme, P., et al. (2010). Progranulin is neurotrophic in vivo and protects against a mutant TDP-43 induced axonopathy. *PLoS One* 5(10)**,** e13368. doi: 10.1371/journal.pone.0013368.

Luo, K., Li, Y., Xia, L., Hu, W., Gao, W., Guo, L., et al. (2017). Analysis of the expression patterns of the novel large multigene TRIM gene family (finTRIM) in zebrafish. *Fish Shellfish Immunol* 66**,** 224-230. doi: 10.1016/j.fsi.2017.04.024.

McWhorter, M.L., Boon, K.L., Horan, E.S., Burghes, A.H., and Beattie, C.E. (2008). The SMN binding protein Gemin2 is not involved in motor axon outgrowth. *Dev Neurobiol* 68(2)**,** 182-194. doi: 10.1002/dneu.20582.

Monies, D., Abouelhoda, M., AlSayed, M., Alhassnan, Z., Alotaibi, M., Kayyali, H., et al. (2017). The landscape of genetic diseases in Saudi Arabia based on the first 1000 diagnostic panels and exomes. *Hum Genet* 136(8)**,** 921-939. doi: 10.1007/s00439-017-1821-8.

Myers, P.Z., Eisen, J.S., and Westerfield, M. (1986). Development and axonal outgrowth of identified motoneurons in the zebrafish. *J Neurosci* 6(8)**,** 2278-2289.

Nakayama, Y., Nara, N., Kawakita, Y., Takeshima, Y., Arakawa, M., Katoh, M., et al. (2004). Cloning of cDNA encoding a regeneration-associated muscle protease whose expression is attenuated in cell lines derived from Duchenne muscular dystrophy patients. *Am J Pathol* 164(5)**,** 1773-1782. doi: 10.1016/S0002-9440(10)63735-2.

Nasca, A., Scotton, C., Zaharieva, I., Neri, M., Selvatici, R., Magnusson, O.T., et al. (2017). Recessive mutations in MSTO1 cause mitochondrial dynamics impairment, leading to myopathy and ataxia. *Hum Mutat* 38(8)**,** 970-977. doi: 10.1002/humu.23262.

Neumann, M., Sampathu, D.M., Kwong, L.K., Truax, A.C., Micsenyi, M.C., Chou, T.T., et al. (2006). Ubiquitinated TDP-43 in frontotemporal lobar degeneration and amyotrophic lateral sclerosis. *Science* 314(5796)**,** 130-133. doi: 10.1126/science.1134108.

Nihei, K., McKee, A.C., and Kowall, N.W. (1993). Patterns of neuronal degeneration in the motor cortex of amyotrophic lateral sclerosis patients. *Acta Neuropathol* 86(1)**,** 55-64.

Ozaki, K., Doi, H., Mitsui, J., Sato, N., Iikuni, Y., Majima, T., et al. (2015). A Novel Mutation in ELOVL4 Leading to Spinocerebellar Ataxia (SCA) With the Hot Cross Bun Sign but Lacking Erythrokeratodermia: A Broadened Spectrum of SCA34. *JAMA Neurol* 72(7)**,** 797-805. doi: 10.1001/jamaneurol.2015.0610.

Patten, S.A., Aggad, D., Martinez, J., Tremblay, E., Petrillo, J., Armstrong, G.A., et al. (2017). Neuroleptics as therapeutic compounds stabilizing neuromuscular transmission in amyotrophic lateral sclerosis. *JCI Insight* 2(22). doi: 10.1172/jci.insight.97152.

Patten, S.A., Armstrong, G.A., Lissouba, A., Kabashi, E., Parker, J.A., and Drapeau, P. (2014). Fishing for causes and cures of motor neuron disorders. *Dis Model Mech* 7(7)**,** 799-809. doi: 10.1242/dmm.015719.

Perruolo, G., Viggiano, D., Fiory, F., Cassese, A., Nigro, C., Liotti, A., et al. (2016). Parkinson-like phenotype in insulin-resistant PED/PEA-15 transgenic mice. *Sci Rep* 6**,** 29967. doi: 10.1038/srep29967.

Polymenidou, M., Lagier-Tourenne, C., Hutt, K.R., Huelga, S.C., Moran, J., Liang, T.Y., et al. (2011). Long pre-mRNA depletion and RNA missplicing contribute to neuronal vulnerability from loss of TDP-43. *Nat Neurosci* 14(4)**,** 459-468. doi: 10.1038/nn.2779.

Sancak, Y., Markhard, A.L., Kitami, T., Kovacs-Bogdan, E., Kamer, K.J., Udeshi, N.D., et al. (2013). EMRE is an essential component of the mitochondrial calcium uniporter complex. *Science* 342(6164)**,** 1379-1382. doi: 10.1126/science.1242993.

Scholl, U.I., Stolting, G., Schewe, J., Thiel, A., Tan, H., Nelson-Williams, C., et al. (2018). CLCN2 chloride channel mutations in familial hyperaldosteronism type II. *Nat Genet* 50(3)**,** 349-354. doi: 10.1038/s41588-018-0048-5.

Sethna, F., Feng, W., Ding, Q., Robison, A.J., Feng, Y., and Wang, H. (2017). Enhanced expression of ADCY1 underlies aberrant neuronal signalling and behaviour in a syndromic autism model. *Nat Commun* 8**,** 14359. doi: 10.1038/ncomms14359.

Shimazu, T., Hirschey, M.D., Newman, J., He, W., Shirakawa, K., Le Moan, N., et al. (2013). Suppression of oxidative stress by beta-hydroxybutyrate, an endogenous histone deacetylase inhibitor. *Science* 339(6116)**,** 211-214. doi: 10.1126/science.1227166.

Sreedharan, J., Blair, I.P., Tripathi, V.B., Hu, X., Vance, C., Rogelj, B., et al. (2008). TDP-43 mutations in familial and sporadic amyotrophic lateral sclerosis. *Science* 319(5870)**,** 1668-1672. doi: 10.1126/science.1154584.

Stallings, N.R., Puttaparthi, K., Luther, C.M., Burns, D.K., and Elliott, J.L. (2010). Progressive motor weakness in transgenic mice expressing human TDP-43. *Neurobiol Dis* 40(2)**,** 404-414. doi: 10.1016/j.nbd.2010.06.017.

Swarup, V., Phaneuf, D., Bareil, C., Robertson, J., Rouleau, G.A., Kriz, J., et al. (2011). Pathological hallmarks of amyotrophic lateral sclerosis/frontotemporal lobar degeneration in transgenic mice produced with TDP-43 genomic fragments. *Brain* 134(Pt 9)**,** 2610-2626. doi: 10.1093/brain/awr159.

Swinnen, B., and Robberecht, W. (2014). The phenotypic variability of amyotrophic lateral sclerosis. *Nat Rev Neurol* 10(11)**,** 661-670. doi: 10.1038/nrneurol.2014.184.

Taetzsch, T., Tenga, M.J., and Valdez, G. (2017). Muscle Fibers Secrete FGFBP1 to Slow Degeneration of Neuromuscular Synapses during Aging and Progression of ALS. *J Neurosci* 37(1)**,** 70-82. doi: 10.1523/JNEUROSCI.2992-16.2016.

Taylor, J.P., Brown, R.H., Jr., and Cleveland, D.W. (2016). Decoding ALS: from genes to mechanism. *Nature* 539(7628)**,** 197-206. doi: 10.1038/nature20413.

Therrien, M., Dion, P.A., and Rouleau, G.A. (2016). ALS: Recent Developments from Genetics Studies. *Curr Neurol Neurosci Rep* 16(6)**,** 59. doi: 10.1007/s11910-016-0658-1.

Vaccaro, A., Patten, S.A., Aggad, D., Julien, C., Maios, C., Kabashi, E., et al. (2013). Pharmacological reduction of ER stress protects against TDP-43 neuronal toxicity in vivo. *Neurobiol Dis* 55**,** 64-75. doi: 10.1016/j.nbd.2013.03.015.

Vaccaro, A., Patten, S.A., Ciura, S., Maios, C., Therrien, M., Drapeau, P., et al. (2012). Methylene blue protects against TDP-43 and FUS neuronal toxicity in C. elegans and D. rerio. *PLoS One* 7(7)**,** e42117. doi: 10.1371/journal.pone.0042117.

Valdez, G., Heyer, M.P., Feng, G., and Sanes, J.R. (2014). The role of muscle microRNAs in repairing the neuromuscular junction. *PLoS One* 9(3)**,** e93140. doi: 10.1371/journal.pone.0093140.

Van Damme, P., Robberecht, W., and Van Den Bosch, L. (2017). Modelling amyotrophic lateral sclerosis: progress and possibilities. *Dis Model Mech* 10(5)**,** 537-549. doi: 10.1242/dmm.029058.

Wegorzewska, I., Bell, S., Cairns, N.J., Miller, T.M., and Baloh, R.H. (2009). TDP-43 mutant transgenic mice develop features of ALS and frontotemporal lobar degeneration. *Proc Natl Acad Sci U S A* 106(44)**,** 18809-18814. doi: 10.1073/pnas.0908767106.

Westerfield, M. (1995). *The zebrafish book : a guide for the laboratory use of zebrafish (Danio rerio)*. [Eugene, OR]: Institute of Neuroscience, University of Oregon.

White, M.A., Kim, E., Duffy, A., Adalbert, R., Phillips, B.U., Peters, O.M., et al. (2018). TDP-43 gains function due to perturbed autoregulation in a Tardbp knock-in mouse model of ALS-FTD. *Nat Neurosci* 21(4)**,** 552-563. doi: 10.1038/s41593-018-0113-5.

Xu, Y.F., Gendron, T.F., Zhang, Y.J., Lin, W.L., D'Alton, S., Sheng, H., et al. (2010). Wild-type human TDP-43 expression causes TDP-43 phosphorylation, mitochondrial aggregation, motor deficits, and early mortality in transgenic mice. *J Neurosci* 30(32)**,** 10851-10859. doi: 10.1523/JNEUROSCI.1630-10.2010.

Xu, Y.F., Zhang, Y.J., Lin, W.L., Cao, X., Stetler, C., Dickson, D.W., et al. (2011). Expression of mutant TDP-43 induces neuronal dysfunction in transgenic mice. *Mol Neurodegener* 6**,** 73. doi: 10.1186/1750-1326-6-73.

Yamaguchi-Kabata, Y., Morihara, T., Ohara, T., Ninomiya, T., Takahashi, A., Akatsu, H., et al. (2018). Integrated analysis of human genetic association study and mouse transcriptome suggests LBH and SHF genes as novel susceptible genes for amyloid-beta accumulation in Alzheimer's disease. *Hum Genet*. doi: 10.1007/s00439-018-1906-z.

Yamanaka, Y., Kitano, A., Takao, K., Prasansuklab, A., Mushiroda, T., Yamazaki, K., et al. (2011). Inactivation of fibroblast growth factor binding protein 3 causes anxiety-related behaviors. *Mol Cell Neurosci* 46(1)**,** 200-212. doi: 10.1016/j.mcn.2010.09.003.

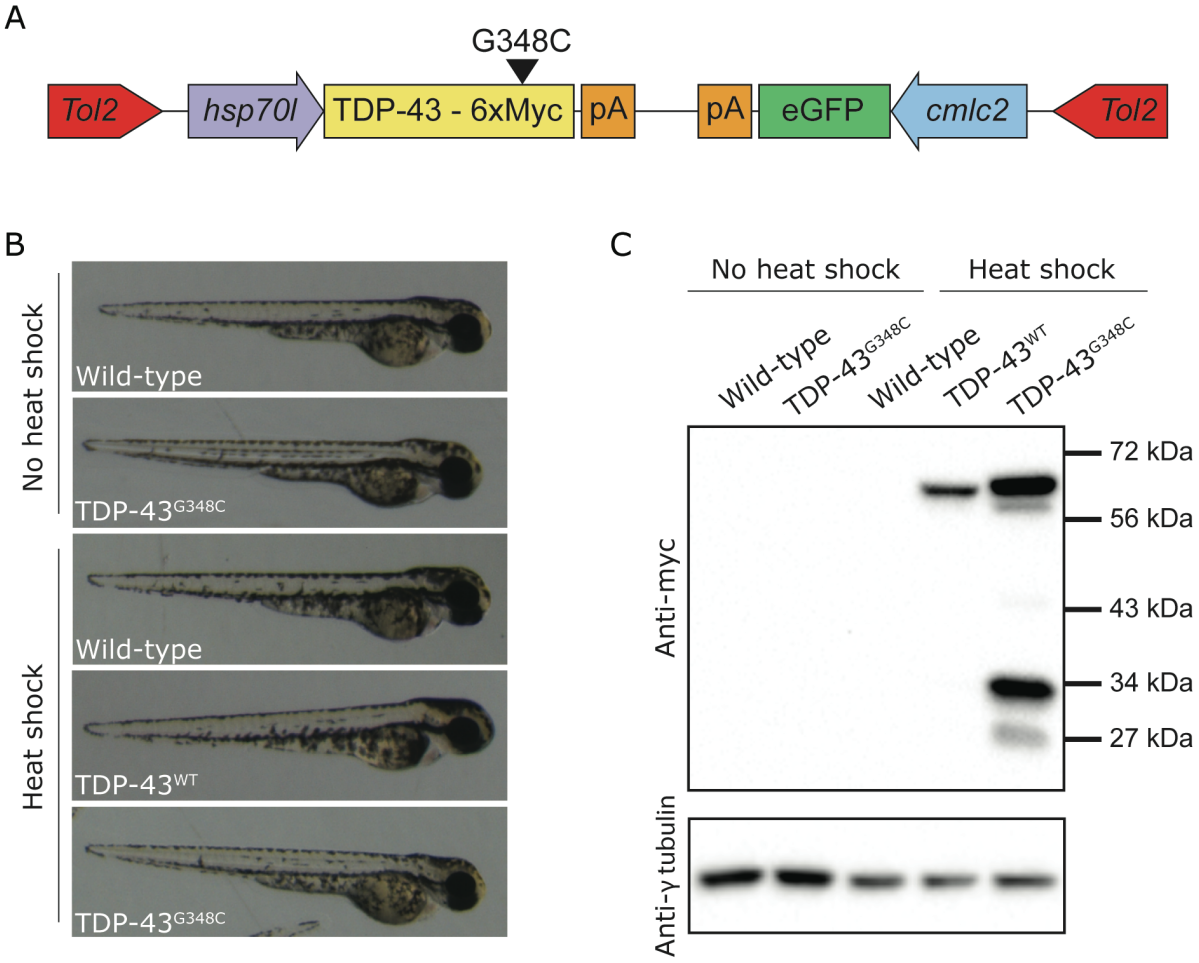

Figure 1. Generation of zebrafish transgenic lines expressing wild type and mutant human TDP-43

(**A**) The transgene constructs consist of the human wild type (TDP-43^{WT}) or the G348C mutant TDP-43 (TDP-43^{G348C}) cDNA fused with 6 myc-tag under the control of the hsp70-like promoter (*hsp70l*). The constructs also contained eGFP driven by the cardiac myosin light chain (*cmlc2*) promoter. (**B**) Representative picture of the embryos used for all experiments. (**C**) Western blot showing expression of the human transgene in 2 days post-fertilization (dpf) embryos following a one hour heat shock at 38.5°C using an anti-myc antibody.

.

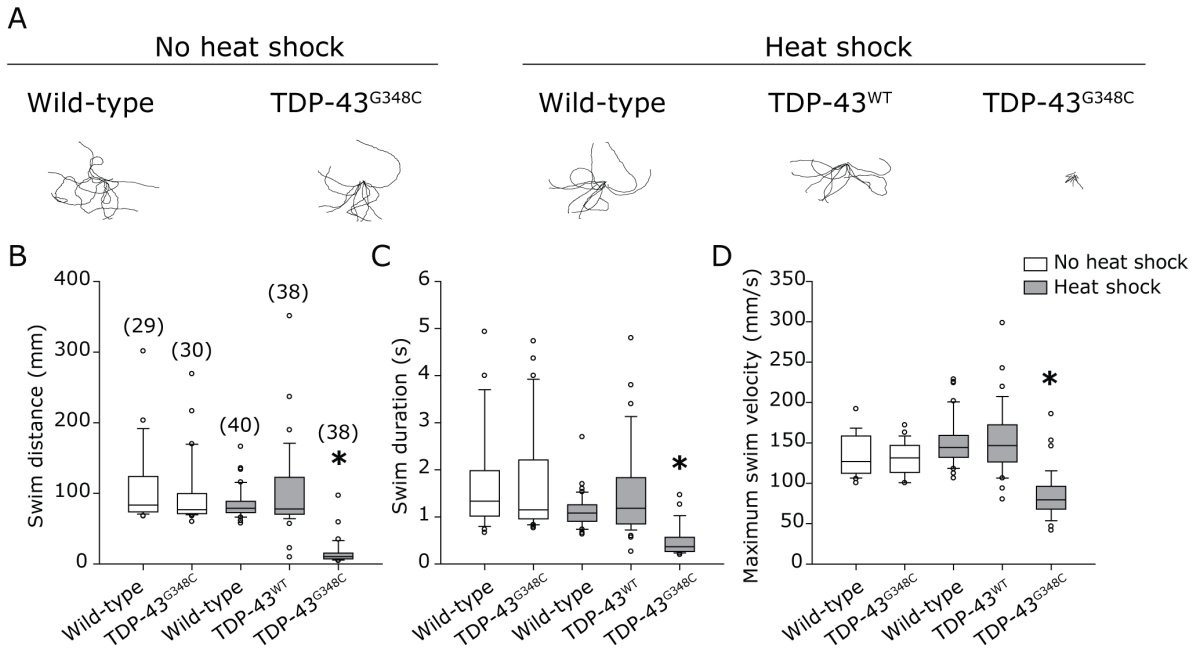

Figure 2. Zebrafish embryos expressing TDP-43^{G348C} display an abnormal touch-evoked locomotion at 2 dpf

(**A**) Overlay of 10 representative swim traces obtained after lightly touching the tail of 2 dpf embryos with a blunt forceps. Embryos expressing TDP-43^{G348C} exhibited a significantly reduced swim distance (**B**), swim duration (**C**) and maximum swim velocity (**D**), compared to embryos expressing TDP-43^{WT} or not expressing any transgene. All experiments were done in triplicate; the total number of embryos used is indicated in brackets. Kruskal-Wallis one-way analysis on variance on ranks was performed and pairwise multiple comparison procedures were done according to Dunn's method. * p-value < 0.05.

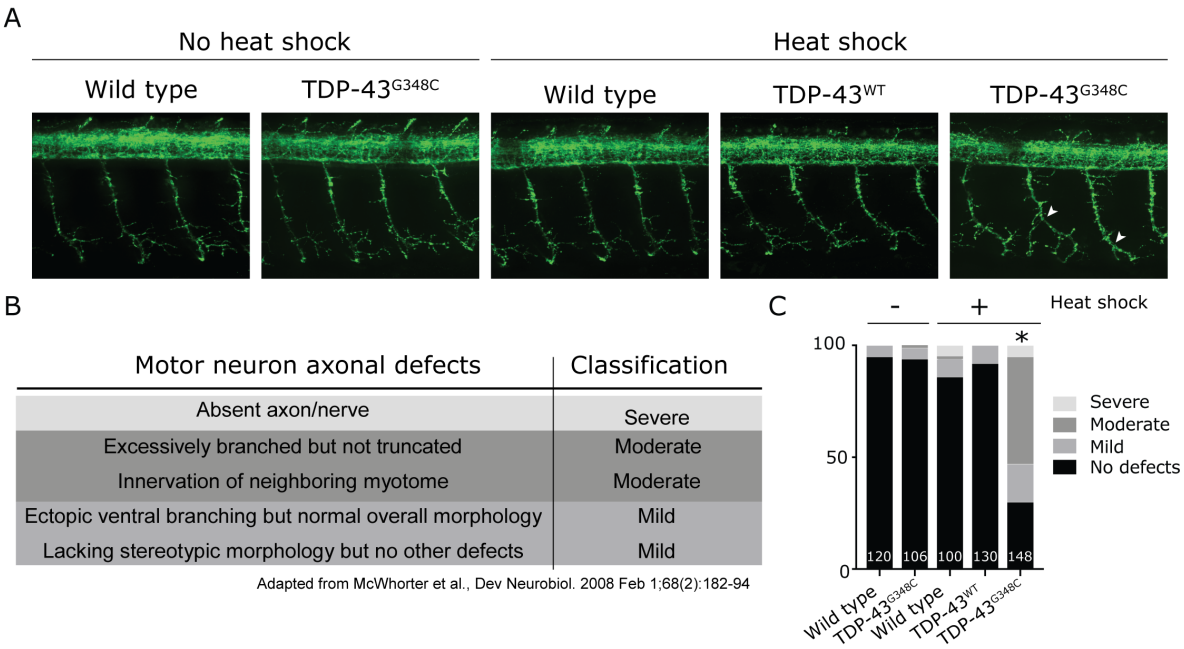

Figure 3. Abnormal development of motor neuron axons in zebrafish expressing TDP-43^{G348C}

(**A**) Immunohistochemistry against znp-1 in 2 dpf whole-mount embryos. The 3-to-4 somites spanning the anus are shown with the axons of the motor neuron expanding down from the spinal cord. White arrow heads indicate abnormal premature branching of the main axonal branch and absence of secondary branching in transgenic embryos expressing TDP-43^{G348C}, compared to embryos expressing TDP-43^{WT} or not expressing any transgene. (**B**) Classification criteria used for the quantification of defects. (**C**) Quantification of axonal defects based on the classification found in (**B**). The total number of axons analysed is indicated; The 3 axons spanning the anus were analyzed in at least 30 embryos over the course of three experiments. Chi-square analysis was performed between the different conditions, * p-value < 0.05.

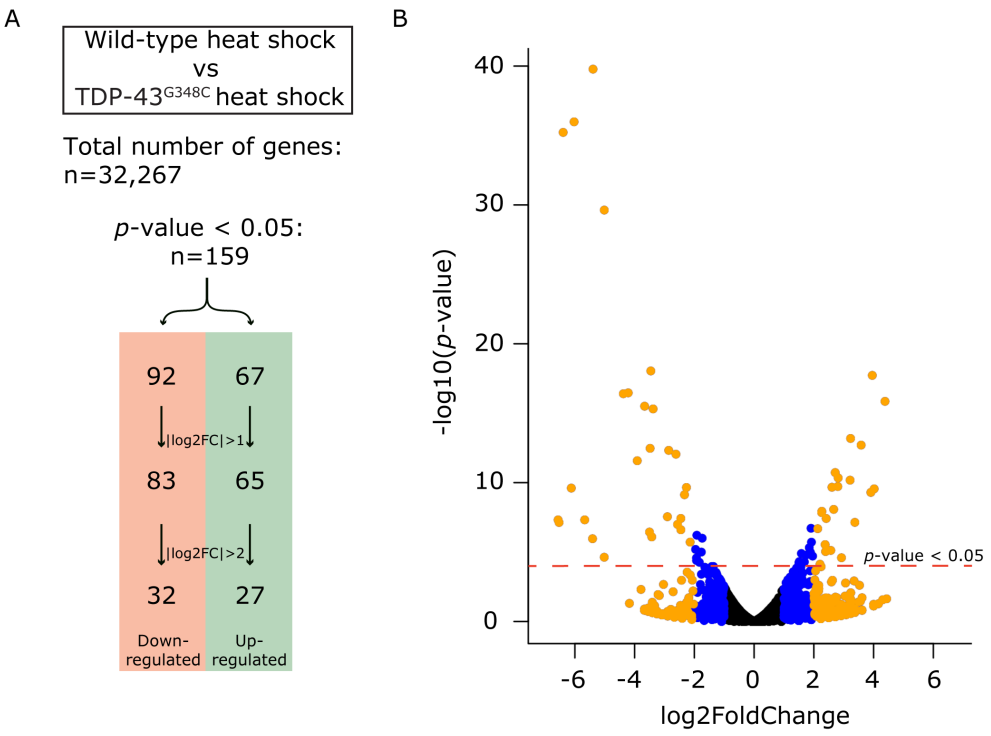

Figure 4. Differential expression analysis obtained by RNA-sequencing

(**A**) In order to compensate for the effect of the heat shock, we compared the expression of genes between the wild-type heat shock and the TDP-43^{G348C} heat shock conditions. Out of the 32,267 genes identified, 159 genes (67 up-regulated and 92 down-regulated) had a significant differential expression (p-value < 0.05). This number could be reduced by using a more stringent cut-off of either a |log2FC| > 1 (148 genes, 65 up-regulated and 83 down-regulated) or |log2FC| > 2 (59 genes, 27 up-regulated and 32 down-regulated). (**B**) Volcano plot showing all of the 32,267 genes. The dotted red line indicate the level of significance with p-value < 0.05. The blue dots show the genes with a |log2FC| comprised between 1 and 2. The orange dots show the genes with |log2FC| > 2.

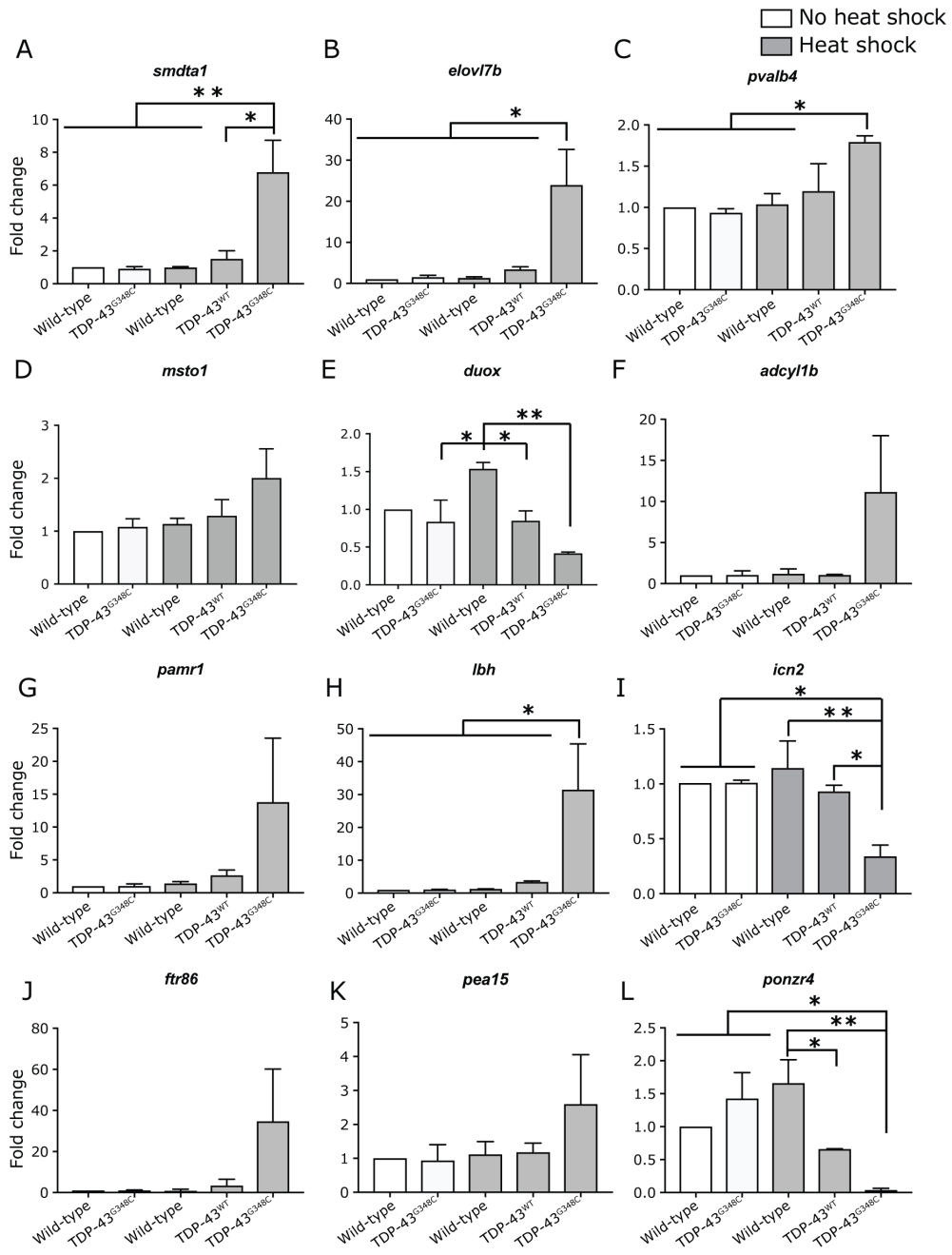

Figure 5. Validation of differentially expressed genes by RT-qPCR

(**A-L**) Expression level of 12 selected genes was tested in duplicate by RT-qPCR in all of the conditions. One-way ANOVA with Tukey's multiple comparisons test was performed. * *p*-value < 0.05, ** *p*-value < 0.01 and error bars are standard deviation.

Table 1. Genes of interest from the RNA-sequencing data

Genes of interest amongst the differentially expressed genes, upon expression of human mutant TDP-43. The full list of differentially expressed genes can be found in **supplementary Table S1 (Annexe 7)**.

Table 1. Genes of interest from the RNA-sequencing data

Gene name	Log2 FC	Gene description	Comments	References
clcn2b	1.45	Chloride channel, voltage-sensitive 2b	Disease (*CLCN2*: leukoencephalopathy with ataxia; familial hyperaldosteronism type 2); ion channels	(Depienne et al., 2013; Scholl et al., 2018)
elovl7b	2.27	ELOVL fatty acid elongase 7b	Disease (*ELOVL4*: SCA-34; *ELOVL5*: SCA-38); ER-membrane proteins	(Cadieux-Dion et al., 2014; Di Gregorio et al., 2014; Ozaki et al., 2015)
pvalb9	-1.08	Parvalbumin 9	Disease (*PVALB*: ALS); calcium signaling	(Nihei et al., 1993)
pvalb4	1.13	Parvalbumin 4		
fgfbp2b	1	Fibroblast growth factor binding protein 2b	Disease (*FGFBP1*: ALS); *FGFBP1*: NMJ; *FGFBP3*: anxiety	(Yamanaka et al., 2011; Valdez et al., 2014; Taetzsch et al., 2017)
smdt1a	1.89	Single-pass membrane protein with aspartate-rich tail 1a	Disease (*SMDT1*: Limb-girdle muscular dystrophy); mitochondria; calcium signaling	(Sancak et al., 2013; Monies et al., 2017)
pea15	1.56	Proliferation and apoptosis adaptor protein 15	Disease (Parkinson-like disorder)	(Perruolo et al., 2016)
lbh	3.96	Limb bud and heart development	Disease (Alzheimer's disease)	(Yamaguchi-Kabata et al., 2018)
pamr1	2.72	Peptidase domain containing associated with muscle regeneration 1	Disease (Duchenne muscular dystrophy)	(Nakayama et al., 2004)
msto1	1.28	Misato 1, mitochondrial distribution and morphology regulator	Disease (mitochondrial myopathy and ataxia; cerebellar atrophy with pigmentary retinopathy); mitochondria	(Gal et al., 2017; Nasca et al., 2017; Iwama et al., 2018)
adcy1b	2.03	Adenylate cyclase 1b	Calcium signaling (neurone specific, calmodulin-sensitive)	(Sethna et al., 2017)
icn2	-1.74	Ictacalcin 2	Calcium signaling	(Kraemer et al., 2008)
mt2	-1.27	Metallothionein 2	Oxidative stress	(Shimazu et al., 2013)
ftr86	1.41	FinTRIM family, member 86	Unknown, possible antiviral activity	(Luo et al., 2017)
ponzr4	-2.56	Plac8 onzin related protein 4	Unknown	

Supplementary Figure S1

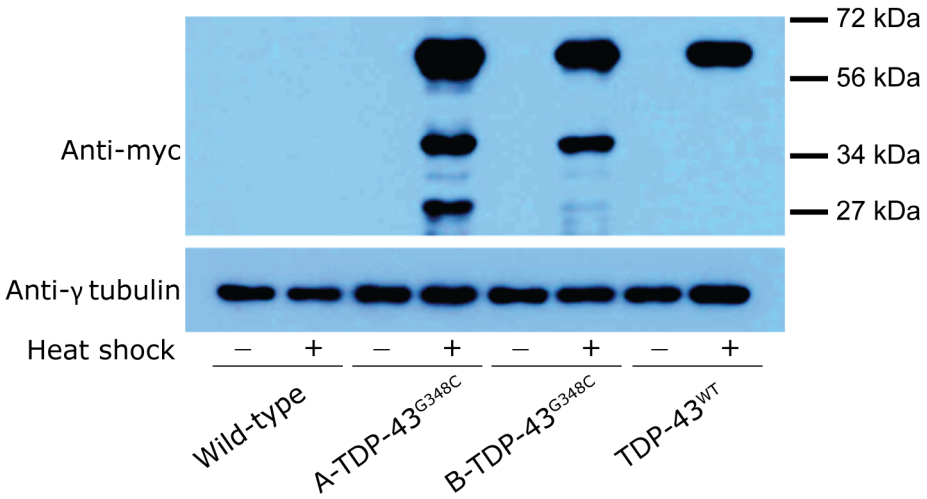

Figure S1. Western blot showing the expression of the human transgenes at 2 days post fertilization without (-) or with (+) a one hour heat shock at 38.5°C. The conditions shown are wild-type embryos, embryos from one independent TDP-43^{G348C} line (A-TDP-43^{G348C}), a second independent TDP-43^{G348C} line (B-TDP-43^{G348C}) and from the TDP-43^{WT} line.

Chapter 5: Homology directed knockin of point mutations in the zebrafish *tardbp* and *fus* genes in ALS using the CRISPR/Cas9 system

Gary A.B. Armstrong*, Meijiang Liao*, Zhipeng You, **Alexandra Lissouba**, Brian E. Chen, Pierre Drapeau

PLoS One. 2016 Mar 1;11(3):e0150188,
Doi: 10.1371/journal.pone.0150188

Authors contribution

*Both authors contributed equally to this work.

For this article, I contributed to the screening process of the knockout and knock-in lines of *fus* and helped analyse the results. I reviewed the manuscript.

Manuscript

Homology directed knockin of point mutations in the zebrafish *tardbp* and *fus* genes in ALS using the CRISPR/Cas9 system

Short title: Homology directed knockin of point mutations in zebrafish

Gary A.B. Armstrong[1]*, Meijiang Liao[1]*, Zhipeng You[1], Alexandra Lissouba [1], Brian E. Chen[2], Pierre Drapeau[1]

*Both authors contributed equally to this work.

[1]Department of Neurosciences,
Research Centre of the University of Montréal Hospital Centre,
Montréal, Québec, Canada

[2]Department of Neurology and Neurosurgery,
Research Institute of the McGill University Health Centre and Centre for Research in Neuroscience,
Montréal, Québec, Canada

Key words: Genome editing, site directed mutagenesis, TDP-43, FUS, ALS, homology directed repair, CRISPR/Cas9, single stranded oligonucleotide template

Abstract

The methodology for site-directed editing of single nucleotides in the vertebrate genome is of considerable interest for research in biology and medicine. The clustered regularly interspaced short palindromic repeats (CRISPR)/CRISPR-associated protein 9 type II (Cas9) system has emerged as a simple and inexpensive tool for editing genomic loci of interest in a variety of animal models. In zebrafish, error-prone non- homologous end joining (NHEJ) has been used as a simple method to disrupt gene function. We sought to develop a method to easily create site-specific SNPs in the zebrafish genome. Here, we report simple methodologies for using CRISPR/Cas9- mediated homology directed repair using single-stranded oligodeoxynucleotide donor templates (ssODN) for site-directed single nucleotide editing, for the first time in two disease-related genes, *tardbp* and *fus*.

Introduction

In humans, mutations in *TARDBP* (coding for TDP-43, a major protein component of inclusions in many neurodegenerative diseases) or *FUS* cause the progressive disease amyotrophic lateral sclerosis (ALS) and in rare cases frontotemporal lobar degeneration (FTLD) (1-5). The majority of these mutations are missense mutations caused by base pair substitutions clustered in regions highly conserved across vertebrates. Many transgenic models have been generated but knockin of point mutations has not been reported, yet would provide the most disease- relevant models. ALS-associated mutations in *TARDBP* are commonly found in the C- terminal glycine-rich region and in the C-terminal of *FUS* encoding a nuclear localization signal (5). We have previously demonstrated that expression of mutant human *TARDBP*^{A382T} or *FUS*^{R521H} mRNA causes motor deficits and aberrant motor axon projections in larval zebrafish (6, 7). However, these transient human mRNA expression models as well as other loss-of-function (early lethality) models (8, 9) limit investigations to the first few days of zebrafish development and do not address gain-of-function disease phenotypes as may be the case for ALS which manifests clinically in midlife. Ideally, one would like to introduce these specific point mutations in the genes of interest and follow the resulting phenotypes over a long time course.

Editing of the zebrafish genome, using TALEN- or CRISPR/Cas9-based homology-dependent repair (HDR), has been previously used to incorporate sequences (though not point mutations) encoding a restriction site or a modified *loxP* site in two different loci (10) or and convert eGFP into Gal4 transgenic lines (11). A similar method using the CRISPR/Cas9 system has been used in *C. elegans* (12), *Drosophila* (13) and mice (14) to introduce defined point mutations, but as of yet not in zebrafish. We sought to develop a general CRISPR/Cas9 methodology in zebrafish that permits the generation of knockin lines, in our case with the corresponding disease-causing point mutations in humans, zebrafish *tardbp*^{A379T} (*TARDBP*^{A382T}) and *fus*^{R536H} (*FUS*^{R521H}), as these are among the first mutations to be identified in patients with ALS (1, 3, 4). Moreover, gene and amino acid sequence homology at these loci are highly conserved between humans and zebrafish (Figure 1A,B).

Materials and Methods

Zebrafish husbandry and ethical considerations

Wild type TL adult zebrafish (*Danio rerio*) were maintained at 25 ˚C under a 12/12 hour light/dark cycle in a colony at the animal research facility at the Centre Hospitalier de l'Université de Montréal Research Centre (CRCHUM) located in Montréal Québec, Canada. Embryos and larvae were raised at 28.5 ˚C under at 12/12 hour light/dark cycle. Genomes of entire 48 hour old embryos were extracted in order to measure genomic indels. The Animal Care Committee of the University of Montreal Research Centre approved all experiments.

Synthesis of Cas9 mRNA and gRNAs

Synthesis of zebrafish-optimized nls-zCas9-nls mRNA was done using previously described methods (15) and the pCS2-nCas9n was a gift from Wenbiao Chen (Addgene plasmid # 47929). Briefly, the nls-zCas9-nls template was linearized with NotI and synthesized using the mMESSAGE mMACHINE SP6 kit (Ambion/Invitrogen) followed by a phenol-chloroform extraction and ethanol precipitation. The pT7-gRNA was a gift from Wenbiao Chen (Addgene plasmid # 46759). The pT7-gRNA was linearized with BamHI and RNA was transcribed using the MEGAshortscript T7 kit (Ambion/Invitrogen) and extracted and precipitated using the same methods for nls-zCas9-nls mRNA.
The sequences of the designed gRNAs are as follows:
tardbp: GGCAGCAGCTCAGCTGCTCT (forward strand, targeting exon 6);

fus: TAGTAAGGGCGGTCTCTG (reverse strand, targeting exon 15).

Donor templates

Single-stranded oligodeoxynucleotide donor templates (ssODN) were designed with the following sequences and synthesized by Invitrogen:

tardbp template: GGCAGCAGCTCAGCTACTCTCGG

fus template: CCACAGACATGACCACAGAGACCGCCCTTACTA

tardbp template with silent mutations: CCAAACATATAGCTCGGCTAACAGCAATTACG GCAGCAGCTCAGCCACTTTGGGTTGGGGCACCGGCTCTAACTCGGGCGCTGCCA GTGCTGGCTTTAAC

Micro-injection of embryos

A solution containing either the Cas9 mRNA (200 ng/µl) and gRNA (30 ng/µl) or Cas9 (200 ng/µl) and gRNA (30 ng/µl) and ssODN (60 ng/µl) were injected into one-cell stage zebrafish eggs. A total volume of 1.5 nl was injected into each embryo.

Restriction fragment length polymorphism assay

Genomic DNA was extracted from individual 48 hpf larvae using the REDExtract-N- AMP Tissue PCR kit (Sigma-Aldrich) and used as a template for PCR using the following primer sets:

tardbp-forward: CAGTACGGAGAGGTCACAGACG
tardbp-reverse: CACGCTAGGAATACCGACAC
fus-forward: CCTGGAAAGATGGACTCGAGGTG
fus-reverse: TAGTACTAAGGTGGCCTAACCGC

Amplified PCR products of 752 and 409 base pairs for *tardbp* and *fus* were digested with PvuII or MwoI for *tardbp* and *fus* amplicons respectively. Digested PCR amplicons generated bands of 609 and 143 base pairs for *tardbp* and 274 and 135 for *fus.* Indels were identified based upon the loss of restriction sites and confirmed by sequencing of homozygous amplicons using an Applied Biosystems 3730xl DNA Analyzer (Thermo Fisher Scientific).

Results

CRISPR/Cas9-mediated NHEJ failed to generate single nucleotide substitutions

In an initial series of experiments we explored the feasibility of generating point mutations using CRISPR/Cas9-mediated NHEJ in the zebrafish *tardbp* and *fus* genes. A gRNA targeting the glycine-rich C-terminal portion of the *tardbp* gene and another targeting the nuclear localization sequence of the *fus* gene were selected based upon low sequence homology to other genomic regions and position of the protospacer adjacent motif (PAM) close to the sites of the disease-causing point mutations (Figure 2**A**,**B**). Microinjection of the gRNA and Cas9 mRNA at the one-cell embryo stage was performed using standard techniques (15). Adult (F0) zebrafish were crossed with wild type animals and F1 larvae were screened at 48 hours post-fertilization (hpf) for genomic modifications at the target loci. PCR amplicons containing the target loci were analyzed using restriction fragment length polymorphism (RFLP) to determine the presence of mutations. The restriction enzymes, PvuII and MwoI for *tardbp* and *fus,* respectively, were selected based upon their potential for identifying single nucleotide substitutions that corresponded to the desired point mutations (Figure 2**C**,**D**). Twelve of 58 adult F0 *tardbp*-targeted zebrafish successfully transmitted indels to their F1 progeny representing a 21% efficiency in germline transmission. For the *fus*-targeted F0 adults, 8 of 46 transmitted unique indels (17% efficiency) to their F1 progeny. Individual *tardbp* and *fus* founders displayed differing indel transmission rates (Table 1). Outcrossed F1 zebrafish were raised to adulthood and incrosses were performed and homozygous larval PCR amplicons were sequenced. Seven lines that targeted *tardbp* resulted in deletions, 3 lines had insertions and 2 lines had a combination of insertions and deletions (Figure 2**E**). Similar indel distributions for our *fus*-targeted lines were observed: 3 lines had deletions, 3 lines had insertions and 2 lines had both insertions and deletions encompassing our target site (Figure 2**F**). Although CRISPR/Cas9- mediated NHEJ reliably generated indels, none of our derived lines resulted in the generation of single nucleotide substitutions.

Homology-dependent repair following CRISPR/Cas9 DNA double-stranded cuts introduced the desired single nucleotide substitutions

To address the feasibility of using HDR to introduce point mutations of interest, we designed ssODN template sequences containing point mutations, which were then co-injected with gRNA and Cas9 mRNA. Flanking the G to A point mutation in the ssODN *tardbp* template were 15 base pair homology arms on the 5' and 7 base pairs on the 3' sides (Figure 3**A**). We designed a template that spanned the same region targeted by the gRNA as this is where DNA cleavage was expected to occur. The likelihood that the gRNA would also target the template was of concern. However single nucleotide mismatches near the PAM site in the gRNA have been reported to be less effective at generating double-stranded DNA breaks (16). We thus speculated that the ssODN template containing the G to A point mutation 5 base pairs from the PAM sequence might not be recognized by the gRNA. A total of 46 adult zebrafish were raised and outcrossed with wild type animals and F1 larvae were screened using RFLP. Fourteen of 46 adults successfully transmitted (30% efficiency) indels to their F1 progeny but only 1 of these adult zebrafish transmitted the proper edited sequence encoding the zebrafish *tardbp*^{A379T} point mutation (Figure3**B**,**C**).

We also designed an ssODN template sequence for HDR integration of the *fus*^{R536H} missense mutation. Flanking the G to A point mutation in this ssODN template were 14 and 18 base pair 5' and 3' homology arms (Figure **3B**). Unlike the *tardbp* ssODN template that spanned the gRNA target site, the point mutation in the *fus* ssODN template was contained in the PAM sequence located at the nucleotide adjacent to the gRNA sequence. A successful integration of our point mutation would not change the PAM sequence from NGG and it was of concern that subsequent DNA cleavage would occur following template integration. Despite this possibility we were able to generate our point mutation of interest. A total of 47 F0 zebrafish were raised and crossed with wild type animals to test for HRD heritable integration of the point mutation encoding the *fus*^{R536H}. Twelve of 47 F0 zebrafish transmitted indels to their F1 progeny (26% efficiency) but only 1 of these adult fish successfully transmitted the G to A point mutation to its progeny (Figure 3**E**,**F**).

Despite the successful generation of our point mutations in the experiments in which we co-injected ssODN templates, this does not rule out the possibility that these mutations were a result of the random repair by NHEJ and not HDR. To investigate if HDR could be responsible for integration of a template we designed a *tardbp* template bearing four silent mutations flanked by 46 and 53 base pair 5' and 3' arms from the A379T mutation of interest as this set of mutations could only be generated by HDR and not randomly e.g. by NHEJ (Figure 4**A**). A total of 77 F0 zebrafish were raised and crossed with wild type animals to test for HRD heritable integration of the template. We were able to detect this integration in 3 heterozygous F1 larvae from separate F0 founders (Figure 4**B**), confirming editing by HDR using this template. This represents a 4% efficiency for heritable transmission of the template containing 5 mutations.

Discussion

Taking advantage of the HDR pathway we were able to generate defined missense mutations in the zebrafish *tardbp* and *fus* genes that are analogous to those in their human orthologs associated with ALS. We also demonstrated that donor templates containing defined point mutations, within the gRNA target site, can be utilized to knockin point mutations despite the increased likelihood that the gRNA would recognize the ssODN template sequences. This may account for the low efficiencies for heritable integration of defined point mutations. However, similar experiments in mice suggest that donor templates that are closer to the gRNA target site more frequently incorporate defined point mutations when compared to gRNAs targeting sequences further from the target site (14). We also examined two templates, one 23 and the other 100 base pairs in length for HDR-mediated integration at the *tardbp* gRNA target site. Although a single F0 founder (1/46) was identified for the smaller template *vs.* 3/77 F0 founders for the longer template, further investigations pertaining to the optimization of template integration with respect to template length and location to the PAM sequence would be useful. Furthermore, the efficiency of HDR would also be limited by the overall efficiency of Cas9-mediated cleavage at the gRNA target site. Here we report efficiencies of 21% and 17% Cas9-mediated cleavage for our *tardbp* and *fus* gRNA target sites and we speculate that if these efficiencies were higher better integration of our template would have occurred.

NHEJ repairs double-stranded DNA breaks often with indels at the cleaved DNA site. CRISPR/Cas9-mediated NHEJ can be used to disrupt gene function either by targeted removal of start codons, frameshifts, or the generation of premature stop codons, effectively generating loss-of-function knockout models. These are useful for exploring the fundamental aspects of altered cellular biology but are of limited value for modeling phenotypes not caused by loss-of-function. The ability to generate point mutations at predefined loci by HDR using the CRISPR/Cas9 system has several advantages. First, traditional transgenesis relies upon the knockin of cDNA, often under the control of a non-endogenous promoter. Differing levels of protein expression and variations in the promoter expression patterns can impact the

phenotype and possibly lead to erroneous results. Furthermore, expression of the endogenous gene usually continues in the presence of the transgenic allele. Some proteins such as TDP-43 and FUS autoregulate their expression, necessitating careful measurements of transgenic and endogenous protein levels. Moreover, limited conclusions can be drawn from experiments where a human gene, with reduced homology to the ortholog, is expressed in a phylogenetically removed species. The CRISPR/Cas9-mediated cleavage and HDR ssODN template knockin avoids these limitations by editing the endogenous gene. Second, unlike the labour and time intensive mouse ES cell-derived mutant lines, in zebrafish genomic insertion efficiencies can be determined within two days and stable transmission can be determined when sexually mature adults are outcrossed (2-3 months).

In conclusion, we have established a simple experimental methodology for introducing defined point mutations in the zebrafish genome by editing specific loci. We demonstrated that NHEJ using gRNAs targeting either *tardbp* or *fus* failed to generate single nucleotide substitutions at our desired targets despite having gRNA target sites near the nucleotide of interest. However, co-injection of an ssODN template was sufficient to knockin the desired point mutation encoding two missense mutations (*tardbp*^{A379T} and *fus*^{R536H}) relevant to ALS and for the first time in models of these genetic disorders. These lines need however to be out-crossed over several generations to eliminate any potential off-target mutations. We believe that this technique will be useful for the creation of other disease models and in general for editing point mutations in the zebrafish genome.

Acknowledgments

We thank G. Laliberté and M Drits for animal care.

Figure 1

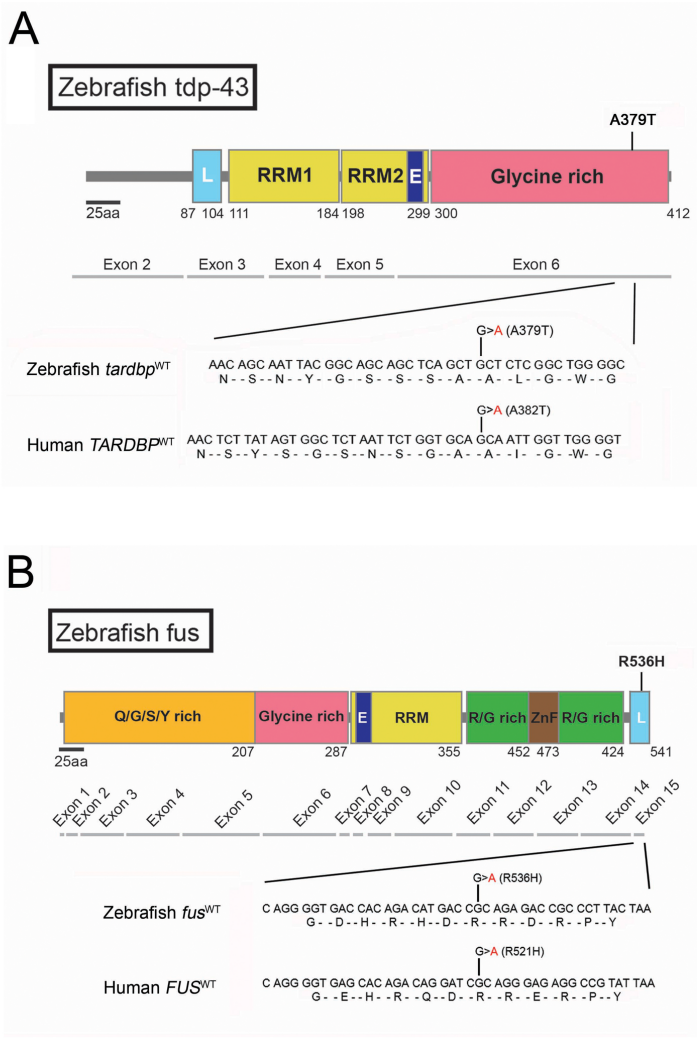
A
Zebrafish tdp-43
A379T
L
RRM1
RRM2
E
Glycine rich
25aa
87 104 111
184 198
299 300
412
Exon 2
Exon 3
Exon 4
Exon 5
Exon 6
G>A (A379T)
Zebrafish tardbp^WT
AAC AGC AAT TAC GGC AGC AGC TCA GCT GCT CTC GGC TGG GGC
N - - S - - N - - Y - - G - - S - - S - - S - - A - - A - - L - - G - - W - - G
G>A (A382T)
Human TARDBP^WT
AAC TCT TAT AGT GGC TCT AAT TCT GGT GCA GCA ATT GGT TGG GGT
N - - S - - Y - - S - - G - - S - - N - - S - - G - - A - - A - - I - - G - - W - - G
B
Zebrafish fus
R536H
Q/G/S/Y rich
Glycine rich
E
RRM
R/G rich
ZnF
R/G rich
L
25aa
207
287
355
452 473
424
541
Exon 1
Exon 2
Exon 3
Exon 4
Exon 5
Exon 6
Exon 7
Exon 8
Exon 9
Exon 10
Exon 11
Exon 12
Exon 13
Exon 14
Exon 15
G>A (R536H)
Zebrafish fus^WT
C AGG GGT GAC CAC AGA CAT GAC CGC AGA GAC CGC CCT TAC TAA
G - - D - - H - - R - - H - - D - - R - - R - - D - - R - - P - - Y
G>A (R521H)
Human FUS^WT
C AGG GGT GAG CAC AGA CAG GAT CGC AGG GAG AGG CCG TAT TAA
G - - E - - H - - R - - Q - - D - - R - - R - - E - - R - - P - - Y

Figure 1: *HDR knockin of point mutations in zebrafish using the CRISPR/Cas9 system with ssODN templates.*

Schematic representation of zebrafish tdp-43 (**A**) and fus (**B**) and locations of point mutations encoding missense mutations generated by HDR (top). L, nuclear localization sequences; E, nuclear export sequences; RRM, RNA recognition motifs; ZnF, zinc finger motif. Exon coding sequences (middle). Comparisons of zebrafish gRNA target sites with human coding sequences (bottom). Note the high amino acid sequence homologies between human and zebrafish proteins. ALS-causing point mutations (red) encoding missense mutations *TARDBP*^{A382T} and *FUS*^{R521H} are indicated in the human sequences and analogous point mutations are noted in the zebrafish genes (*tardbp*^{A379T} and *fus*^{R536H}).

Figure 2

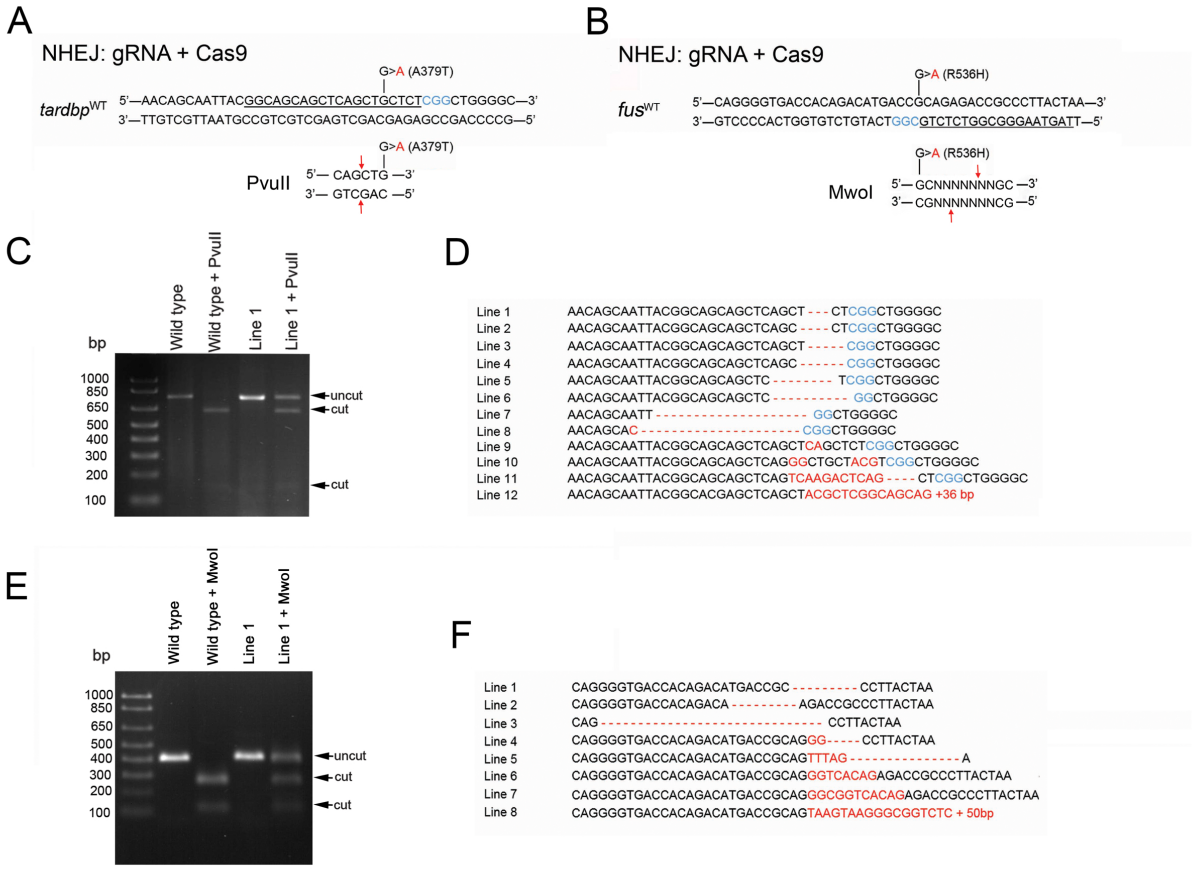
A
NHEJ: gRNA + Cas9
G>A (A379T)
tardbpWT 5'—AACAGCAATTACGGCAGCAGCTCAGCTGCTCTCGGCTGGGGC—3'
3'—TTGTCGTTAATGCCGTCGTCGAGTCGACGAGAGCCGACCCCG—5'
G>A (A379T)
PvuII 5'— CAGCTG —3'
3'— GTCGAC —5'
B
NHEJ: gRNA + Cas9
G>A (R536H)
fusWT 5'—CAGGGGTGACCACAGACATGACCGCAGAGACCGCCCTTACTAA—3'
3'—GTCCCCACTGGTGTCTGTACTGGCGTCTCTGGCGGGAATGATT—5'
G>A (R536H)
MwoI 5'— GCNNNNNNNGC —3'
3'— CGNNNNNNNCG —5'
C
bp
Wild type
Wild type + PvuII
Line 1
Line 1 + PvuII
1000
850
650
500
400
300
200
100
uncut
cut
cut
D
Line 1 AACAGCAATTACGGCAGCAGCTCAGCT - - - CTCGGCTGGGGC
Line 2 AACAGCAATTACGGCAGCAGCTCAGC - - - - CTCGGCTGGGGC
Line 3 AACAGCAATTACGGCAGCAGCTCAGCT - - - - - CGGCTGGGGC
Line 4 AACAGCAATTACGGCAGCAGCTCAGC - - - - - - CGGCTGGGGC
Line 5 AACAGCAATTACGGCAGCAGCTC - - - - - - - - TCGGCTGGGGC
Line 6 AACAGCAATTACGGCAGCAGCTC - - - - - - - - - - GGCTGGGGC
Line 7 AACAGCAATT - GGCTGGGGC
Line 8 AACAGCAC - CGGCTGGGGC
Line 9 AACAGCAATTACGGCAGCAGCTCAGCTCAGCTCTCGGCTGGGGC
Line 10 AACAGCAATTACGGCAGCAGCTCAGGGCTGCTACGTCGGCTGGGGC
Line 11 AACAGCAATTACGGCAGCAGCTCAGTCAAGACTCAG - - - - CTCGGCTGGGGC
Line 12 AACAGCAATTACGGCACGAGCTCAGCTACGCTCGGCAGCAG +36 bp
E
bp
Wild type
Wild type + MwoI
Line 1
Line 1 + MwoI
1000
850
650
500
400
300
200
100
uncut
cut
cut
F
Line 1 CAGGGGTGACCACAGACATGACCGC - - - - - - - - - CCTTACTAA
Line 2 CAGGGGTGACCACAGACA - - - - - - - - - AGACCGCCCTTACTAA
Line 3 CAG - CCTTACTAA
Line 4 CAGGGGTGACCACAGACATGACCGCAGGG - - - - - CCTTACTAA
Line 5 CAGGGGTGACCACAGACATGACCGCAGTTTAG - - - - - - - - - - - - - - A
Line 6 CAGGGGTGACCACAGACATGACCGCAGGGTCACAGAGACCGCCCTTACTAA
Line 7 CAGGGGTGACCACAGACATGACCGCAGGGCGGTCACAGAGACCGCCCTTACTAA
Line 8 CAGGGGTGACCACAGACATGACCGCAGTAAGTAAGGGCGGTCTC + 50bp

Figure 2: *NHEJ reliably generated indels at target site but failed to generate point mutations.*

Design of gRNAs targeting our regions of interest in the zebrafish *tardbp* (**A**) and *fus* (**B**) were generated and co-injected with Cas9 into the one cell stage fertilized egg. gRNA target sites are underlined and PAM sequences are denoted in blue. Germline transmission of mutations was assessed by RFLP analysis. PCR amplicons for *tardbp* and *fus* were designed to contain unique restriction enzyme sites (PvuII and MwoI for *tardbp* and *fus* respectively) that would fail to cut *tardbp*^{A379T} and *fus*^{R536H} mutant amplicons. **C**, Example gel electrophoresis of PCR amplicons of wild type and an example heterozygotes mutant *tardbp* line. Note the partial cut in our mutant line digested with PvuII **D**, Sequencing of homozygous F2 larval amplicons for *tardbp*. **E**, Example gel electrophoresis of PCR amplicons of wild type and an example heterozygotes mutant *fus* line. Note the partial cut in our mutant line digested with MwoI **F**, Sequence results of homozygous F2 larval amplicons for our *fus* mutant lines. None of our generated lines were single point mutations suggesting that CRISPR/Cas9- medated NHEJ was not a desirable method for generating specific point mutations.

Figure 3

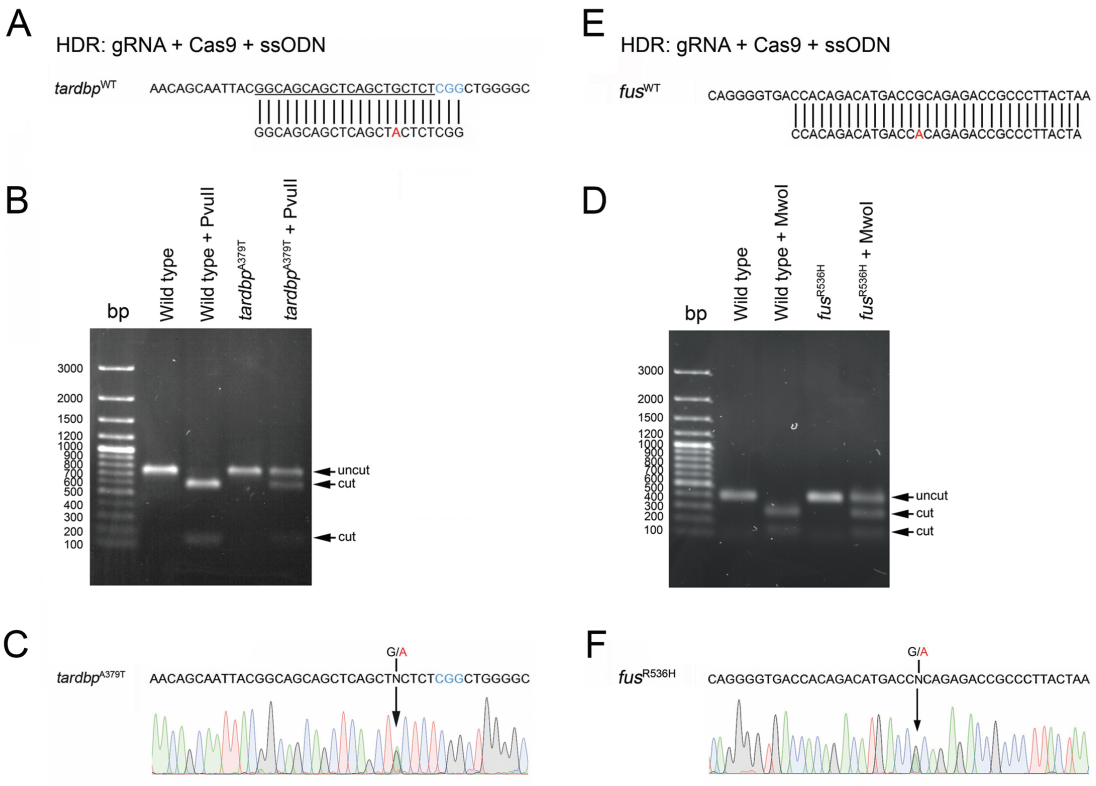
A
HDR: gRNA + Cas9 + ssODN
tardbp^WT
AACAGCAATTACGGCAGCAGCTCAGCTGCTCTCGGCTGGGGC
GGCAGCAGCTCAGCTACTCTCGG
E
HDR: gRNA + Cas9 + ssODN
fus^WT
CAGGGGTGACCACAGACATGACCGCAGAGACCGCCCTTACTAA
CCACAGACATGACCACAGAGACCGCCCTTACTA
B
bp
Wild type
Wild type + PvuII
tardbp^A379T
tardbp^A379T + PvuII
3000
2000
1500
1200
1000
900
800
700
600
500
400
300
200
100
uncut
cut
cut
D
bp
Wild type
Wild type + MwoI
fus^R536H
fus^R536H + MwoI
3000
2000
1500
1200
1000
900
800
700
600
500
400
300
200
100
uncut
cut
cut
C
tardbp^A379T
G/A
AACAGCAATTACGGCAGCAGCTCAGCTNCTCTCGGCTGGGGC
F
fus^R536H
G/A
CAGGGGTGACCACAGACATGACCNCAGAGACCGCCCTTACTAA

Figure 3. *Generation of point mutations encoding tardbp^{A379T} and fus^{R536H} was achieved by HDR.*

Co-injection of our gRNA, Cas9 and an ssODN template encoding our desired point mutations encoding *tardbp*^{A379T} (**A**) and *fus*^{R536H} (**E**) was made into one cell stage embryos. gRNA target sites are underlined and PAM sequences are denoted in blue. We identified a line in each batch of raised *tardbp* and *fus* F0 fish that transmitted an indel, identified by RFLP (**B** and **D**) that integrated and transmitted to F1 progeny the *tardbp*^{A379T} (**C**) and *fus*^{R536H} (**F**) missense point mutations identified following sequencing. Corresponding electropherograms of heterozygous F1 progeny indicating our desired point mutations (arrowheads).

Figure 4

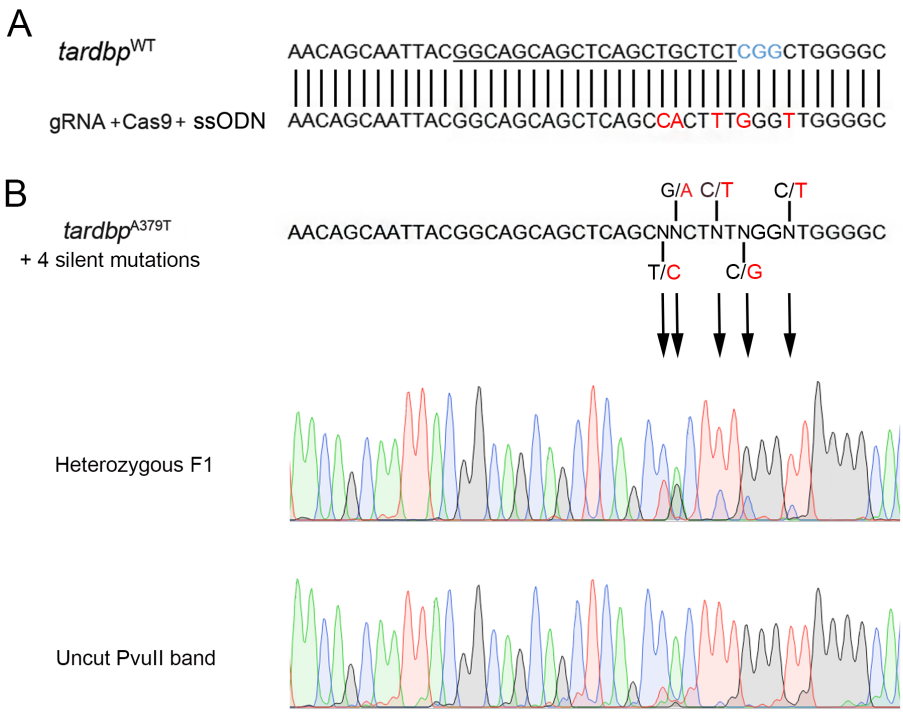
A
tardbp^WT
AACAGCAATTACGGCAGCAGCTCAGCTGCTCTCGGCTGGGGC
gRNA +Cas9+ ssODN
AACAGCAATTACGGCAGCAGCTCAGCCACTTTGGGTTGGGGC
B
tardbp^A379T
+ 4 silent mutations
G/A C/T C/T
AACAGCAATTACGGCAGCAGCTCAGCNNCTNTNGGNTGGGGC
T/C C/G
Heterozygous F1
Uncut PvuII band

Figure 4: *HDR ssODN template integration was confirmed by the inclusion of multiple silent around the tardbp^{A379T} point mutation.*

Confirmation of ssODN integration was achieved by co-injection of an ssODN template containing our point mutation of interest and 4 silent point mutations (red nucleotides; **A** shown for the region flanking the mutation) and was successfully transmitted to F1 progeny; note the double peaks in the electropherogram of heterozygous F1 progeny (top electropherograms; **B**). We also sequenced the undigested PvuII band and confirmed the integrated template (bottom electropherogram).

Table 1. lndel transmission from FO founders to F1 progeny

	Fraction		Fraction
tardbp		***fus***	
Line 1	6/12	Line 1	3/11
Line 2	2/7	Line 2	1/7
Line 3	2/13	Line 3	4/14
Line 4	2/14	Line4	3/7
Line 5	1/14	Line 5	2/7
Line 6	4/7	Line 6	2/7
Line 7	1/7	Line 7	10/14
Line 8	1/7	Line 8	1/14
Line 9	1/7		
Line 10	2/24		
Line 11	1/7		
Li e	3/		

References

1. Kabashi E, Valdmanis PN, Dion P, Spiegelman D, McConkey BJ, Vande Velde C, et al. TARDBP mutations in individuals with sporadic and familial amyotrophic lateral sclerosis. Nat Genet. 2008;40(5):572-4.
2. Sreedharan J, Blair IP, Tripathi VB, Hu X, Vance C, Rogelj B, et al. TDP-43 Mutations in Familial and Sporadic Amyotrophic Lateral Sclerosis. Science. 2008;319(5870):1668-72.
3. Vance C, Rogelj B, Hortobágyi T, De Vos KJ, Nishimura AL, Sreedharan J, et al. Mutations in FUS, an RNA Processing Protein, Cause Familial Amyotrophic Lateral Sclerosis Type 6. Science. 2009;323(5918):1208-11.
4. Kwiatkowski TJ, Bosco DA, LeClerc AL, Tamrazian E, Vanderburg CR, Russ C, et al. Mutations in the FUS/TLS Gene on Chromosome 16 Cause Familial Amyotrophic Lateral Sclerosis. Science. 2009;323(5918):1205-8.
5. Da Cruz S, Cleveland DW. Understanding the role of TDP-43 and FUS/TLS in ALS and beyond. Current Opinion in Neurobiology. 2011;21(6):904-19.
6. Kabashi E, Lin L, Tradewell ML, Dion PA, Bercier V, Bourgouin P, et al. Gain and loss of function of ALS-related mutations of TARDBP (TDP-43) cause motor deficits in vivo. Human Molecular Genetics. 2010;19(4):671-83.
7. Kabashi E, Bercier V, Lissouba A, Liao M, Brustein E, Rouleau GA, et al. FUS and TARDBP but not SOD1 interact in genetic models of amyotrophic lateral sclerosis. PLoS Genet. 2011;7(8):e1002214.
8. Schmid B, Hruscha A, Hogl S, Banzhaf-Strathmann J, Strecker K, van der Zee J, et al. Loss of ALS- associated TDP-43 in zebrafish causes muscle degeneration, vascular dysfunction, and reduced motor neuron axon outgrowth. Proceedings of the National Academy of Sciences. 2013;110(13):4986-91.
9. Hewamadduma CAA, Grierson AJ, Ma TP, Pan L, Moens CB, Ingham PW, et al. Tardbpl splicing rescues motor neuron and axonal development in a mutant tardbp zebrafish. Human Molecular Genetics. 2013;22(12):2376-86.
10. Bedell VM, Wang Y, Campbell JM, Poshusta TL, Starker CG, Krug Ii RG, et al. In vivo genome editing using a high-efficiency TALEN system. Nature. 2012;491(7422):114-8.
11. Auer TO, Duroure K, De Cian A, Concordet J-P, Del Bene F. Highly efficient CRISPR/Cas9- mediated knock-in in zebrafish by homology-independent DNA repair. Genome Research. 2013.
12. Zhao P, Zhang Z, Ke H, Yue Y, Xue D. Oligonucleotide-based targeted gene editing in C. elegans via the CRISPR/Cas9 system. Cell Res. 2014;24(2):247-50.
13. Port F, Chen H-M, Lee T, Bullock SL. Optimized CRISPR/Cas tools for efficient germline and somatic genome engineering in Drosophila. Proceedings of the National Academy of Sciences. 2014;111(29):E2967-E76.
14. Inui M, Miyado M, Igarashi M, Tamano M, Kubo A, Yamashita S, et al. Rapid generation of mouse models with defined point mutations by the CRISPR/Cas9 system. Sci Rep. 2014;4.
15. Jao L-E, Wente SR, Chen W. Efficient multiplex biallelic zebrafish genome editing using a CRISPR nuclease system. Proceedings of the National Academy of

Sciences. 2013;110(34):13904-9.
16. Hsu PD, Scott DA, Weinstein JA, Ran FA, Konermann S, Agarwala V, et al. DNA targeting specificity of RNA-guided Cas9 nucleases. Nat Biotech. 2013;31(9):827-32.

Chapter 6: Discussion

Summary of results

HSP

In the two articles presented in **Chapter 2** and **Chapter 3** ([491, 492]), we have shown that the zebrafish can be used to advance knowledge and therapeutic avenues for HSP. The first article used a previously published morpholino [138-141] to model SPG4 in zebrafish. We replicated previous results, as embryos with spastin knockdown had abnormal acetylated tubulin networks in the spinal cord, and defects in motor neuron axonal projections with hydrocephaly, impaired yolk-sac extension and general morphological abnormalities. Additionally, these embryos exhibited increased reactive oxygen species (ROS). We next built on this model to investigate ER stress as a new potential pathophysiological pathway related to *SPAST* loss-of-function and demonstrated that ER-stress modulators could be used as potential new therapeutics, as they were able to partially rescue the phenotypes observed in the zebrafish, including the oxidative stress. We have thus implicated a new pathological mechanism linked to SPG4 as well as a new therapeutic avenue [491].

In the second article, following identification of mutations in *CAPN1* in three non-related families with HSP, we used the zebrafish to validate *in vivo* the pathophysiology of Calpain 1 loss-of-function. Knockdown of *capn1a* in zebrafish embryos induced migration and positioning defects of branchiomotor neurons and disorganized microtubule network predominantly in the brain, with large clusters of acetylated-tubulin (see **video1.mov**, **video2.mov**, **video3.mov** and **video4.mov** not included in the published article. Legend in **Annexe 6**), and to a lesser extant in the spinal cord. Further investigations will be necessary to understand the pathophysiological mechanism of this new HSP gene responsible for SPG76 [492].

In both articles, experiments from our collaborators with *C. elegans* and *Drosophila* models provided valuable complementary experiments to our zebrafish model. However, the discussion will focus on the experiments from the zebrafish model.

ALS

In the two articles presented in **Chapter 4** and **Chapter 5** ([478]), we generated new zebrafish models that can be used to study the pathophysiology of mutant TDP-43 or FUS and provide new insights into ALS pathogenicity.

In the first manuscript, we generated two transgenic lines expressing human TDP-43, either the wild-type form, or bearing the G348C mutation found in a subset of ALS patients, using an inducible heat shock promoter to bypass a potential early mortality. The expression of the mutant but not the wild-type human TDP-43 in zebrafish embryo induced locomotor defects as well as motor neuron axonal defects, recapitulating previous results obtained by mRNA injections. We have used this line to investigate transcriptomic changes due to the presence of mutant TDP-43 and have found 159 genes that are misregulated compared to control.

In the second article, we have generated the first point mutations knock-in in the zebrafish *tardbp* and *fus* genes using the CRISPR/Cas9 technology by coinjecting the gRNA with single-stranded oligodeoxynucleotide donor templates. This technique allowed us to introduce the equivalent of the ALS-causative TDP-43^{A382T} and FUS^{R521H} mutations [478]. These lines will be able to further our understanding of the pathophysiological mechanisms of mutant TDP-43 and FUS in a more physiological manner.

Discussion of the HSP studies

Spastin loss-of-function induces ER stress

In our article, we showed that loss of spastin in zebrafish, *C. elegans* and *Drosophila* leads to increased ROS production, as visualized by dichlorofluorescein diacetate (DCF-DA). Treatment with four ER stress modulators prevented this oxidative stress, indicating that the increase of ROS production was due to ER stress.

ER stress

The ER is a major organelle with roles in protein synthesis, folding and sorting. In pathophysiological conditions the ER homeostasis may be disrupted by the abnormal accumulation of unfolded or misfolded protein, leading to a condition called ER stress, which initiates the unfolded protein response (UPR) [493]. The role of the UPR is to preserve the cell by restoring proper homeostasis in the ER and in the cell and this adaptive response initially promotes cell survival. However, this response may sometimes not be enough to restore proper homeostasis and may itself become detrimental to the cell overtime, due to chronic activation of the UPR, which then switches to activation of pro-apoptotic signalling. This phenomenon is thought to be involved in the pathogenicity or at least in the pathophysiology of many diseases, including MNDs [494-496].

I will briefly introduce the UPR and the links between ER stress and oxidative stress, in order to discuss our results.

Unfolded protein response (UPR)

The UPR initiates three mechanisms in order to resolve the ER stress: (1) an increase in the levels of the protein involved in folding in order to increase protein folding capacity; (2) an increase in the level of the proteins involved in the ER-associated degradation (ERAD) pathway in order to clear the ER of irremediably misfolded proteins; and (3) decreased protein synthesis in general in order to decrease the ER protein load [493]. These mechanisms are mediated by the collaboration of three ER transmembrane proteins that act as stress sensors: activating factor 6 (ATF6), PKR-like endoplasmic reticulum kinase (PERK) and inositol-requiring enzyme 1α (IRE1α) [497]. In physiological conditions, they are inhibited by the ER chaperone BiP/GRP78, which binds to their luminal domain. In the context of ER stress, BiP/GRP78 preferentially binds to unfolded proteins in the ER lumen instead of the stress sensors, thus activating these ER signalling pathways [498]. Chronic ER stress and upregulation of the UPR has been implicated in several neurodegenerative disorders such as Alzheimer's disease and ALS[499, 500].

Our group with collaborators previously showed that expression of ALS-causative mutant TDP-43 or FUS (Fused in Sarcoma) in zebrafish and in *C. elegans* led to an increase in

oxidative stress and ER stress [480, 485]. Treatment with known ER stress modulators Methylene blue, Salubrinal and Guanabenz, as well as Phenazine, a structurally related compound, were able to reduce oxidative stress as well as the swimming deficits and abnormal spinal motor neuron axonal projections found in the zebrafish model. Additionally, genetic work using *C. elegans* confirmed that these four compounds affect ER stress through different branches of the UPR, either the IRE1α pathway (Methylene blue and Phenazine), the PERK pathway (Guanabenz and Phenazine) or the ATF6 pathway (Guanabenz). Interestingly, while Salubrinal is known to increase activation of eIF2α by inhibiting its phosphatases, this effect was not abolished by inactivating the PERK pathway, thus demonstrating that the effect of Salubrinal on eIF2α activity may not be through the UPR, but through a general stress response [480, 485].

In our study, we have for the first time shown that the use of ER stress modulators can partially rescue the phenotypes induced by spastin loss-of-function, indicating that ER stress is a pathophysiological mechanism involved in SPG4. While this is the first time that ER stress is being investigated as a mechanism in SPG4, its involvement should not come as a surprise, since several studies have previously linked ER stress to non-SPG4 HSP.

HSP and ER stress

Animal models and cell lines have been used to study the response to ER stressors for different HSP-linked proteins.

SPG33 is caused by mutations in Protrudin, a protein located at the tubular ER [501]. Neuro2A cells expressing an HSP-related mutant form of Protrudin display ER stress in basal conditions and have an increased response to ER stress inducers [502]. REEP1 is a protein located at the ER and the mitochondria and *REEP1* mutations cause SPG31 [68]. In plants, the REEP1 ortholog is required to tolerate stress [503] and *Drosophila* lacking REEP1 exhibit a lower resistance to tunicamycin-induced ER stress [504]. Mutations in *ATL1* (Atlastin-1) cause SPG3A [60]. Atlastin-1 is a protein located at ER tubules and interestingly, if plants lack the *ATL1* ortholog, they exhibit a reduced induction of UPR genes following ER stress induction by tunicamycin compared to control [505]. Reticulon-2 is also a protein located at the ER and mutations in Reticulon-2 cause SPG12 [506]. *Drosophila* lacking the ortholog of

Reticulon-2 have a higher basal level of spliced mRNA of XBP1, a marker of ER stress [507]. Mutations in *NIPA1* (SPG6) lead to a partial accumulation of the mutant protein in the ER, ER stress and activation of the UPR. Additionally, expression of mutant but not wild-type NIPA1 in *C. elegans* induced progressive motor paralysis, which was rescued when abolishing the UPR by using an xbp-1 mutant strain [508, 509]. The gain-of-function mutations N88S and S90L in the *BSCL2* gene have been associated with a rare autosomal dominant complicated form of HSP, SPG17 [510, 511]. This gene encodes the protein Seipin, an ER-membrane resident glycoprotein expressed in cortical neurons in the cerebral cortex and in motor neurons in the spinal cord [512, 513]. The N88S and S90L muations lead to misfolded Seipin accumulating in the ER lumen and causing ER stress in cultured cells [511-513].

Thus, several HSP genes linked to the ER seem to either activate the UPR, or modify the normal response to ER stress. Several of these genes are located in the ER, similar to the M1 isoform of spastin, thus underscoring that ER dysfunction is a pathophysiological mechanism involved in different forms of HSP.

In our study, we also identified oxidative stress as a consequence of spastin loss-of-function. However, this could be secondary to the ER stress, as both are linked.

ER stress and oxidative stress

ER stress often leads to an increase in ROS, which in excess can lead to oxidative stress and several mechanisms involved in the ER stress response are responsible for this increase. The ER is a highly oxidized environment, which is necessary for proper protein folding and ROS are produced in the ER lumen during the formation of the disulphide bonds by the ERO1α and the PDI (protein disulphide isomerase) proteins [496, 514]. The ER has limited antioxidant protection under basal conditions and the risk of oxidative stress increases with protein load [514]. During ER stress, both PDI and ERO1α are upregulated in order to increase the proper folding of proteins and ROS production also increases as a result [515, 516]. Mitochondria also produce ROS during ATP production [517]. During ER stress, ERO1α activates IP3R-mediated calcium leakage from the ER into the mitochondria [496, 518]. This calcium uptake stimulates energy production, which leads to increased ROS as a

byproduct [519]. Importantly, this oxidative stress can in turn increase the UPR response, in a feed-forward loop [514, 520].

Since the oxidative stress was prevented by the four ER stress modulators, we conclude that this increase in ROS is mainly a consequence of the ER stress. Indeed, one study investigating muscle biopsies from HSP patients found no evidence of mitochondrial dysfunction in SPG4 patients [521]. However, it is still possible that spastin loss-of-function leads to oxidative stress by other mechanisms.

Interestingly, a series of studies using olfactory cell lines derived from nine SPG4 patients showed reduced levels of acetylated α-tubulin, impaired transport of peroxisomes, presence of oxidative stress and an increased sensitivity to hydrogen peroxide compared to control cells, presumably due to an inefficient redox regulation at the distal end of the axons [522-524]. Epothilone D, a tubulin-binding drug that increases the number of stable microtubules was used to restore the levels of acetylated α-tubulin, which consequently also rescued the peroxisome trafficking abnormalities and the increased sensitivity to hydrogen peroxide [523, 524]. While they do not show whether basal oxidative stress is reduced following the use of epothilone D [524], they do show that oxidative stress can be found at basal condition in SPG4 patient cells, and that it seems to be secondary to defects in microtubules, leading to abnormalities in peroxisome trafficking. However, as they have not investigated if ER stress was present, it is unknown if the peroxisome defects were concomitant with ER stress and thus whether the oxidative stress could be also secondary to ER stress, as it is in our models. Indeed, a functional ER is necessary for proper peroxisomal formation and maintenance [525].

While we now know that spastin loss-of-function induces ER stress, how and why this ER stress is induced needs to be investigated. Several possibilities are open, given what we know about spastin's functions. Indeed, microtubule dysfunctions may induce ER stress, as this is in fact one of the mechanisms used in cancer treatment. Molecules that target microtubule dynamics are used in cancer to prevent cancer cells from dividing. Amongst these, the vinca alkoids lead to microtubule depolarization, whereas the taxanes block the depolarization of microtubules and the use of these molecules leads to ER stress [526-529]. Interestingly, neuroblastoma cells were more sensitive than breast cancer cells to these

treatments [530], which underscores the fact that neuronal cells seem to be more sensitive to ER stress [495].

However, as mentioned in the introduction, the M1 isoform of spastin is located in the membrane of the tubular ER. It is thus possible that the ER stress may originate from the loss of this isoform in particular.

Limitations of the model

A pathophysiological mechanism due to a toxic gain-of-function of mutant spastin is a possibility that has been gaining more attention in recent years, in part due to the fact that presently, no correlation has been found between the level of spastin protein present and the severity of the disease [155, 159], in addition to the possibility of clinical variability in families harbouring the same spastin mutation [160], as is detailed in a review by Solowska and Baas [124].

Two elements for this challenge to the loss-of-function hypothesis are of particular interest to us: first, the fact that, except for the zebrafish, the loss of spastin does not cause developmental defects in the CNS, despite a higher necessity for microtubule severing during development; and second, the fact that the M1 isoform of spastin, an ER-membrane protein, may be more toxic than the M87 isoform, in addition to the fact that putative truncated M1 spastin may still be present in some SPG4 cases [124].

Developmental defects

In humans, even though the age of onset of SPG4 may sometimes be during childhood, no developmental defects have been found. Similarly, in the two spastin mouse models, no developmental defects are observed, and indeed the motor phenotype developed in these models is very mild and occurs only in homozygous cases, contrary to what happens in human [164-166]. Additionally, when *Drosophila* spastin (Dspastin) is ubiquitously depleted, the larvae exhibit low eclosion rates of around 20% and the ones surviving die very early after the eclosion, thus preventing the development of an adult-onset phenotype [143]. However, depletion of Dspastin only in the CNS prevents the pre-eclosion mortality and the flies develop an adult onset age-dependent motor deficit [142, 144]. These results raise the question

about the specificity of the phenotype obtained in zebrafish embryos with a ubiquitous spastin knockdown. However, several explanations concerning this difference are possible.

Functional compensation

In rodents, p60-katanin, another microtubule severing enzyme, is present at a higher level than spastin during development, while its levels reduce drastically at adulthood [116]. It is thus possible that p60-katanin compensates for the loss of rodent spastin during development in the two mouse models [164-166]. Zebrafish also express p60-katanin during development and its knockdown leads to axonal outgrowth defects and abnormal growth cone motility similarly to spastin knockdown [140]. Interestingly, when both spastin and katanin are knocked-down using sub-optimal morpholino concentration, a synergistic effect is obtained with a stronger phenotype than when only one of these is depleted [140], indicating that spastin and katanin have partially overlapping functions. It is now well known that not all morpholino phenotypes can be reproduced in mutant lines [463]. In some cases, this is due to the fact that the observed morpholino phenotype was in fact resulting from non-specific off-target effects, not related to the specific mRNA being knockdown [463]. However, in other cases, it is due to compensation mechanisms that only occur in stable mutant lines and not with a transient knockdown [464]. This is a highly probable hypothesis for the differences between the zebrafish models and the rodent and *Drosophila* models in term of developmental phenotype. An important next step in order to validate the results obtained in the zebrafish are thus to generate a zebrafish spastin knockout. This will also confirm that the ER stress phenotype observed in our studies is indeed due to the lack of spastin and not to the use of morpholinos. However, ER stress is also observed in the *C. elegans* and *Drosophila* models, which were both stable spastin knockout or knockdown, giving us confidence in the results obtained in our zebrafish model.

Spastin knockout vs mutant spastin

As mentioned in Solowska and Baas review [124], the current animal models do not fully mirror SPG4. One possibility is that by concentrating on the loss-of-function of spastin, the potential effect of missense mutations or truncated spastin proteins is not investigated. A very interesting hypothesis is that the pathogenic M1 isoform could be more important than

the M87 isoform in the pathogenesis of SPG4. Amongst the possibilities underlining this hypothesis is the fact that in rodents, while M87 is the main spastin isoform at all stages of development, M1 is almost absent in the developing rodent but accounts for 20-25% of total spastin in adult spinal cord (but not the cerebral cortex or the hippocampus for example) [116]. When truncated SPG4 mutant M1 or M87 spastin are overexpressed in cell lines, truncated mutant M1 accumulates to greater levels than M87 and is more toxic to neurite outgrowth [531]. M87 spastin has better microtubule severing abilities, but M1 spastin seems to have different function than M87, as it is present at the tubular ER membrane and interacts with different ER membrane proteins that also have a role in shaping ER tubules and several of them are also mutated in HSP, such as Atlastin-1, REEP1, Reticulon-2 and Protrudin [69, 117, 506, 532]. While, as detailed previously, there are possible explanations as to how the loss of the microtubule severing function of spastin may lead to ER stress, we can not neglect the fact the loss of M1 spastin at the ER may be a cause in and of itself of the ER stress. Additionally, M1 spastin while located at the ER membrane can also interact with microtubules through its MBTD and AAA domains. In SPG4 with truncated spastin mutations or with a loss-of-function of the AAA domain due to missense mutations, M1 spastin may still be located at the ER membrane, but unable to carry out its physiological functions, which may induce ER stress. One way to answer this question would be to knock-in missense and nonsense mutations in the zebrafish *spast* gene similar to the ones identified in SPG4 patients to investigate whether they would have the same phenotype and pathophysiological hallmarks as *spast* knockout. These models may better reflect the disease, as they will allow for a possible adult-onset of the motor deficits and the potential accumulation of the truncated spastin.

Calpain 1 as a new complex SPG gene

In the second article of this chapter, our group and colleagues identified a new HSP causative-gene, *CAPN1*, coding for the protein Calpain 1. I will briefly introduce what is already known about Calpain 1 in health and disease and discuss potential pathological mechanisms and how they compare with what is already known in HSP.

The calpain system

Calpain 1 is part of the calpain system, a group of intracellular calcium-dependant cysteine proteases from the papain family (EC 3.4.22.17; Clan CA, family C02). The calpain proteases cleave their substrates creating protein fragments that often acquire novel functions and as such, calpains have a modulatory and regulatory function, rather than a degradation function [533, 534]. Calpains were first identified in 1964 [535] and in human, 15 different calpain genes have now been identified, including the two conventional calpains, calpain 1 and calpain 2, also known as μ-calpain and m-calpain respectively, due to the concentration of calcium necessary for their activation: μ-calpain requires micromolar concentration of calcium (EC50 = 5-10 μM) whereas m-calpain requires millimolar concentration of calcium (EC50 = 0.2-0.5 mM) [536] . Two small regulatory subunits (*CAPNS1* and *CAPNS2*) and Calpastatin (*CAST*), a specific endogenous inhibitor of calpain are also part of the calpain system [533, 534, 537].

Calpain 1 in human and zebrafish

Similar to the human calpain system, the zebrafish calpain system has several members, although most have only been minimally studied. Fifteen calpain genes have been identified and their mRNA expression profile was analyzed in adult zebrafish [538]. Amongst these, four genes correspond to the two conventional human calpain subunits: *capn1a* and its paralog *capn1b* are orthologs of *CAPN1* and *capn2a* and its paralog *capn2b* are orthologs of *CAPN2*. Two *CASPN1* orthologs are also present in zebrafish, *caspn1a* and *caspn1b*, although no studies have been done to determine if the zebrafish conventional calpains also form heterodimers with the small regulatory subunits. Zebrafish *capn1a*, *capn1b*, *capn2a* and *capn2b* are highly similar, having a 95% similarity between each paralogs and up to 90% similarity between capn1a/1b and capn2a/2b [539]. Currently, no studies have been done to identify the *in vitro* calcium concentration requirements to activate these different zebrafish calpain enzymes. In the zebrafish, mRNA expression profiles and *in situ* were done in the embryo by Lepage and Bruce, while MacQueen and Wilcox studied semi-quantitative mRNA expression in adult zebrafish [538, 539]. *Capn1a* and *capn1b* have a ubiquitous expression pattern at shield stage, and at one dpf, both are expressed in the brain, while *capn1b* was also

expressed in the myotome. By two dpf, their expressions is restricted to the anterior part of the embryo with diffuse brain staining. Interestingly, *capn1b* showed a stronger expression in two small clusters of hindbrain neurons [539].

The zebrafish conventional calpains are closely related to the human ones, as they are 88% to 91% similar [539]. The protein sequence alignement of CAPN1 and capn1a and capn1b is found in **Annexe 2**.

Functions

Calpains partially hydrolyze their substrates, with the finality being not of degradation, but of modulation of the functions of existing proteins and their newly cleaved fragments. The vast number of substrates that has been identified for μ-calpain and m-calpain, as well as their ubiquitous expression highlights the numerous possible functions of these proteases. Indeed, calpains 1 and 2 are known to be involved in signal transduction [540], synaptic plasticity [541], cell cycle regulation [542], platelet functions [543] apoptosis [544] and cell spreading and migration [545]. Interestingly, the substrates specificity for μ-calpain and m-calpain are almost indistinguishable with more than a hundred identified [546, 547]. Thus, mutations in *CAPN1* leading a loss-of-function may have severe consequences in many different cellular processus.

Microtubule network dysfunction

In our zebrafish model, we identified broad developmental abnormalities, in particular abnormal development and migration of branchiomotor neurons, as well a general disorganization of the microtubules in the brain (**video1.mov** and **video2.mov** versus **video3.mov** and **video4.mov**), and to a lesser extent in the spinal cord. These underscore an additional potential pathophysiological mechanism for calpain 1 loss-of-function, in term of cytoskeletal remodelling and cell migration, which go hand-in-hand.

Indeed, calpains in general and μ-calpain and m-calpain in particular have been involved in cell migration and motility, as several proteins involved in these processes are calpain substrates, such as β2-integrin [548], talin [549] and focal adhesion kinase (FAK) [550] and their proteolytic cleavages by calpain are necessary for axonal guidance [551].

Additionally, μ-calpain also has at least an indirect role in microtubule dynamics, as tubulin itself is a calpain substrate, as are several microtubules regulatory proteins such as MAP1A, MAP1B, MAP2 and Tau [552-555]. Tau binding to microtubules is in part regulated by its phosphorylation state, which is mediated by several kinases and some of them are calpain substrates, such as Cdk5 and GSK3β [556]. Additionally, GSK3β also phosphorylates MAP1B, especially in growing axons [557, 558]. Interestingly, a double knockout mouse for both Tau and MAP1B showed suppressed axonal development and microtubule disorganization as well as a delay in migration [559], which is similar to results we found in our zebrafish knockdown model.

As such, the lack of calpain1 may potentially lead to abnormal microtubule and cytoskeleton dynamics, resulting in migration and axonal elongation deficits. This pathophysiological mechanism is already at play in other HSP cases such as SPG4, as discussed previously.

Calpain 1 mutations in disease

While we have for the first time linked *CAPN1* to HSP, *CAPN1* missense mutation had previously been identified as causing spinocerebellar ataxia in Jack Russel Terrier [560]. This C115Y missense mutation affects the cysteine residue of the catalytic triad, which is responsible for the protease function of μ-calpain and it is thus hypothesized to be a loss-of-function mutation.

Very shortly after our report, the Baudry laboratory published an article describing four families in which affected members had progressive spastic ataxia due to mutations in *CAPN1* predicted to lead to a loss-of-function of CAPN1 [561]. Since then, several additional reports have been made of *CAPN1* mutations leading to spastic paraplegia [562], ataxia [563] or both [564, 565]. In total as of now, 22 individuals from 12 families have been identified with *CAPN1* mutations, all of them predicted to be detrimental to the function of CAPN1 [492, 561-565], validating our first results.

HSP versus cerebellar ataxias

However, in most of these patients, mild cerebellar atrophy was present, as well as several cerebellar findings such as ataxia and dysarthria [492, 561-565]. When the spasticity was found to be predominant, the individuals were classified under HSP and the ataxic signs were classified as part of the complicated signs associated with the HSP. These results raise the question as to whether the dysfunctions due to the loss of CAPN1 should really be classified as part of HSP, or whether they should be classified as cerebellar ataxias. Another possibility is that the distinction between these two disorders is only artificial when talking about complicated HSP with additional cerebellar signs [566, 567]. While axonopathy of the long axons of the corticospinal tract is the hallmark of HSP, cerebellar Purkinje cells and spinocerebellar tracts degeneration are characteristic of cerebellar ataxias, thus CAPN1 loss-of-function may affect both of these pathways and the ubiquitous nature of CAPN1 allows for this possibility.

Indeed, while the *Capn1* knockout mice were initial thought to have no gross CNS developmental abnormalities and only platelets dysfunction [568], Wang and colleagues reported that these mice displayed mild ataxia due to an abnormal cerebellar development with enhanced apoptosis of the cerebellar granule cells leading to their reduced density and impairment of the synaptic transmission to Purkinje cells [561].

It would thus be interesting to compare with zebrafish models to investigate whether similar defects will be observed. In zebrafish, differentiation of cerebellar neurons starts at 3 dpf and a layer structure appears at 5 dpf [569], but additional development occurs during the larval and juvenile stages [570]. Since morpholino effects are limited in time due to dilution of the antisense oligonucleotides, a stable knockout line would be preferable to study the effects of zebrafish calpain 1 loss, while allowing us to observe a potential adult-onset phenotype.

Paralogs and orthologs complicate matters

While we observed that knockdown of *capn1a* induced a developmental phenotype, an ATG morpholino against *capn1b* had no effect. The two genes have mostly overlapping expression patterns in the developing embryo, and both have a high similarity to human *CAPN1* [539]. However, our morpholino results seem to indicate that *capn1a* is of a foremost

importance in CNS development compared to *capn1b*. In zebrafish the antibody against calpain 1 does not allow us to distinguish between capn1a and capn1b, as both subunits are recognized by the antibody and have a similar 82 kDa molecular weight. The expression level of calpain 1a/b at 24 hpf is low but increases dramatically at 24 hpf [492]. Interestingly, the *capn1a* morpholino had almost no effect on the expression level of calpain 1a/b at 24 hpf, but led to a dramatic reduction at 48 hpf. It is thus possible that at 24 hpf, the main calpain1 isoform in the zebrafish is calpain 1b. Indeed, if we do a double knockdown of both *capn1a* and *capn1b*, we see a stronger reduction in the expression level of calpain 1a/b. In order to better study the consequences of calpain 1 loss-of-function, the stable zebrafish model should thus be a knockout of both *capn1a* and *capn1b.* It should be noted that genetic compensation also occurs in mouse models and is at play in the *Capn1* knockout mice, as increase in activity of not only m-calpain but also of caspase 3 and caspase 7 were observed in young knockout mice, but not in old ones [571], which may explain the very mild phenotype of these mice.

Discussion of the ALS studies

How do our transgenic lines compare to what is found in the literature

Many animal models of TDP-43 dysfunction have been generated, either through depletions of the animal TDP-43 in order to model a possible loss-of-function, or through expression of wild-type or mutant human TDP-43 in order to model a possible gain-of-function. As TDP-43 is a highly regulated protein with many functions, both its depletion and its overexpression usually lead to a moderate-to-severe phenotype in the different models used. However, variability is seen in the different models, probably resulting from the different experimental paradigms that were chosen for any given study. I will go over some of the choices that we've made for the design of our transgenic models and compare them to choices others have made to generate transgenic animals expressing mutant TDP-43. For brevity purposes, I will only discuss transgenic models overexpressing TDP-43 with ALS-related mutations and their TDP-43 wild-type controls.

Choice of promoter

When generating transgenic lines, the choice of promoter is crucial in order to have a stable expression of the transgene in an adequate spatial and temporal manner. A first choice must be made between a ubiquitous or a cell specific promoter as well as between a constitutively active or an inducible promoter. The different ALS-related TDP-43 models that have been generated in mouse, *Drosophila* or *C. elegans* have used a combination of these two choices. In our case, we opted for the heat shock protein-like (*hsp70l*) promoter, an inducible and ubiquitous promoter [572]. Our reasoning was to try to reproduce as closely as possible the human situation where TDP-43 is ubiquitously expressed, while avoiding the risk of an early embryonic lethality, as the overexpression of mutant human TDP-43 in zebrafish embryo by mRNA injection leads to early developmental defects.

The choice of promoter in zebrafish models

Recently, another group generated a transgenic zebrafish line expressing the wild-type human TDP-43 protein in motor neurons [573]. They show that TDP-43^{WT} is located mainly in the nucleus of motor neuron and that upon UV-induced injury and in the absence of microglial cells, the TDP-43^{WT} protein becomes more cytoplasmic and can sometimes be seen in the axons of the motor neurons. However, they do not describe whether overexpression of TDP-43^{WT} induces a phenotype in these fish [573].

The choice of promoter for rodent models

Most mutant TDP-43 transgenic mouse models with a constitutive promoter use either the mouse Prion promoter [574-578], which induces a high expression of the transgene in the brain, mainly in the cerebellum and in the spinal cord, but not in non-neuronal tissues such as the heart, liver, lungs or kidney [579]; or the neuronal Thy-1.2 murine promoter [580], which is active starting one week after birth, avoiding potential developmental effect of the mutant TDP-43 [581]. These mice usually have a high level of the transgene, more than 2.5 times the level of endogenous Tdp-43 and sometimes as high as 10 times higher and display a severe phenotype with early onset leading to paralysis or death in 0.5 to 5 months [574-577].

The transgenic mouse lines generated by Arnold and colleagues have a lower level of transgene expression, around 1.5 to 3 times the endogenous level, with only the highest expressing mutant line displaying age dependent motor deficits with motor neuron loss and motor neuron axonal degeneration [578]. And a transgenic mouse model generated by the Julien laboratory used BAC transgenesis in order to use not only the endogenous human *TARDBP* promoter but also its regulatory elements, making it a true ubiquitous and constitutive promoter [582]. These mice, either the wild-type or the mutant transgenic, had a three-fold overexpression of the transgene compared to the endogenous Tdp-43, and developed cognitive deficits in a time-dependent manner, as well as age-dependent motor deficits starting at 42 weeks [582].

The choice of promoter for *Drosophila* models

In Drosphila, overexpression of mutant and wild-type TDP-43 transgenes in a ubiquitous manner induces premature lethality of all the transgenic flies, including the ones expressing wild-type TDP-43 [583]. When the transgenes are expressed in a tissue-specific manner, either through a pan-neuronal promoter [583, 584], or by targeting specific neuronal tissues such as the retina [583, 585-587], motor neurons [227, 583-585, 588], glial cells [588] or sensory neurons [589], overexpression of mutant TDP-43 is deleterious to the tissues with age-progressive neuronal degeneration, motor deficits if expressed in a pan-neuronal or motor neuron specific manner and with decreased survival if expressed in a pan-neuronal fashion. However, the defects were the same when wild-type TDP-43 was overexpressed.

As such, in mouse and *Drosophila* transgenic models, human TDP-43 is overexpressed to high levels and leads to early lethality. These excessively high expression levels may account for why wild-type TDP-43 is also (albeit less) toxic in these models compared to our zebrafish transgenic lines.

The choice of promoter for *C. elegans* models

Similar to *Drosophila* models, the transgenic *C. elegans* lines overexpressing mutant TDP-43 use tissue-specific promoters, either pan-neuronal [590, 591], or targeting specifically the GABAergic neurons [592]. Contrary to the mouse or *Drosophila* models, the wild-type

TDP-43 transgenic *C. elegans* do not develop motor deficits or neurodegeneration [590-592]. Interestingly, the loss of tdp-1, the *C. elegans* ortholog of TDP-43 is viable with only minor defects [593], whereas the loss of tbph, the *Drosophila* ortholog of TDP-43, or of mouse Tdp-43 are as detrimental as the overexpression of mutant or wild-type TDP-43 [593-595], as it is for zebrafish [447, 471].

The transgenic lines that we have developed are thus one of the rare ones to use a ubiquitous promoter. One of the risks is premature lethality and the impossibility to generate the following generation of animals. For this reason, we used an inducible promoter, allowing us to time the onset of the transgene expression. In this paper, as a proof of concept and to verify if we could replicate previous results obtained by our groups and others with mRNA injections, we expressed the transgene early in development in order to have a motor phenotype at 2 dpf. Additional use of these lines will allow us to time the onset of the transgene expression in a way that can better recapitulate ALS, by expressing small doses of the transgene during the lifetime of the zebrafish, from embryo until adulthood by heat shocking the fish regularly. It would be interesting to confirm whether timing of the onset of the transgene expression is important for disease development, as was previously postulated [596]. These experiment will also enable us to test whether reversal of the disease is possible by preventing mutant TDP-43 to be expressed after disease onset, as it was shown in inducible rodent models overexpressing either TDP-43$^{\Delta NLS}$, TDP-43^{A315T} or TDP-43^{M337V} [597-599].

TDP-43 expression level and autoregulation

One thing that is striking amongst all these animal models is how tightly TDP-43 is regulated and that overexpression of its wild-type version will lead to very similar motor defects and degeneration, except in one mouse model, even though splicing changes in the CNS occurred due to overexpression of both wild-type and mutant TDP-43 [578]. In our case, expression of wild-type TDP-43 did not cause a motor phenotype and although we have not used that line for RNA-sequencing, the qRT-PCR validations on selected genes seem to indicate that the differential gene expressions we observed in the case of mutant TDP-43 expression are specific to the presence of the mutation. However, a stronger expression of the mutant TDP-43 transgene was systematically obtained compared to wild-type TDP-43, as is

seen in some mouse models [582, 600]. Several hypotheses are possible to explain this phenomenon, such as an increased, perhaps toxic, stabilisation of mutant TDP-43 compared to wild-type TDP-43 [601, 602]. An additional possibility would be a feed-forward loop due to the use of the *hsp70l* promoter. We now know that TDP-43 is involved in the stress response and that mutant TDP-43 leads to increased ER and oxidative stress, which in turn leads to an increase in hsp70. This last step may also induce up-regulation of the *hsp70l* promoter we are using to express human TDP-43, thus increasing even more the levels of mutant TDP-43. Interestingly, while not statistically significant, a trend can be seen of increased *hsp70l* expression in the embryos expressing mutant TDP-43 (**Annexe 5**).

Transcriptomic changes

Since TDP-43 is involved in RNA metabolism and its absence leads to transcriptomic changes [271], we investigated whether the G348C mutation will lead to abnormally expressed genes due to a perturbation of TDP-43 function. We identified 159 genes whose expression level was significantly altered, amongst which 59 had a more than 4-fold difference compared to a wild-type embryo with heat shock (**Annxe 6**). This is to our knowledge the first time that the differences of genes expression level due to TDP-43 mutations is done in a transgenic model.

Previously, Arnold and colleagues investigated the splicing changes occurring in their mouse transgenic models [578]. They evaluated splicing differences in the spinal cord between their TDP-43^{WT} and their TDP-43^{Q331K} mice using microarrays and found more than 4,000 alternative splicing events in both conditions. Additionally, concentrating only on alternative cassette exons, 1,060 of these events are common to both TDP-43^{WT} and TDP-43^{Q331K}, out of 1,454 and 1,479 events respectively [578]. Thus, these changes may be due, at least in part, to the presence of a transgene in general, rather than specifically to mutations in TDP-43. While we have only looked at differentially expressed genes, it would be interesting to reproduce this experiment in our model and compare results.

This raises another point of discussion, as we have used whole-embryos for our transcriptomic data, rather than doing a tissue-specific analysis. By doing so, we are concentrating only on the genes with the highest expressional change and may miss subtle

differences in gene expression that could be tissue- or even cell-specific. While generating our transgenic lines using the Gal4/UAS system may have facilitated this process, we could also easily cross our hemizygous transgenic fish with homozygous fish expressing tissue-specific fluorescence that can be FACS-sorted to select only the cells of interest, as was done recently by our group [603].

However, as mentioned in the discussion of the article, the fact that we have several genes in common with the transcriptomic analysis done on the recently generated CRISPR/Cas9 line is encouraging (**Annexe 7**) [604]. Another endogenous *Tdp-43* CRISPR/Cas9 knock-in line was recently generated in order to validate a gain-of-function of mutant Tdp-43 in splicing, the skipping of constitutive exons [605], but they have not listed differentially expressed genes in their paper.

Absence of motoneuron loss

One of the limitations of the transgenic lines we have developed is the absence of motoneuron loss following expression of mutant TDP-43, as ALS is a neurodegenerative disorder leading to the loss of the motoneurons. One possibility to explain that despite axonal defects motoneurons are not lost, is the timeline used in the study. As we were replicating results previously obtained in the zebrafish through the injection of human mutant TDP-43 [466, 480, 484, 485, 489], we overexpressed a large amount of the transgenic mutant protein in a short amount of time and evaluated the results of this overexpression in a very short time frame of 24 hours between the start of the overexpression and the evaluation of the defects. While this is a sufficient time for swimming defects to develop, it may not be enough time for motoneurons to be lost due to the presence of the mutant protein. As such, it will be important to change the protocol of transgene expression, in order to express smaller amounts of mutant TDP-43 over a longer period of time and see if this will elicit motoneuron loss as is seen in other mouse models of ALS caused by mutant TDP-43 [574-580, 582].

Precise genome editing, the generation of new animal models

In the second paper of this section, we present the first knock-ins of a point mutation in the genome of the zebrafish by homologous recombination. We successfully generated two

lines, one with the introduction of the A379T mutation in the *tardbp* gene, equivalent to the TDP-43^{A382T} ALS-causing mutation in human; and one with the introduction of the R536H in the fus gene, equivalent to the FUS^{R521H} ALS-causing mutation in human. The phenotypes of these lines are currently being characterized in the Armstrong laboratory (McGill University). To note, we have recently developed a pipeline for screening CRISPR/Cas9 lines using high-resolution melting, simplifying the process ([606] found in **Annexe 8**).

Knockout of *tardbp* or *fus* has been previously done in zebrafish, using different methods such as zinc-finger nucleases [471], TILLING [447] or CRISPR/Cas9 [476, 477]. However, this is the first time that ALS-related point mutations are introduced in zebrafish genes.

As the phenotypes of knock-in mutations in the mouse *Tardbp* and *Fus* gene have recently been described, I will start by summarizing their findings.

Knock-in of ALS-related point mutations in the mouse *Tardbp* gene

Two new mouse models generated by introducing ALS-related point mutations in the *Tardbp* gene have been published recently, both of them with the equivalent of the human TDP-43^{Q331K} mutation [604, 605]. The knock-in mice generated by White and colleague display only minor age-dependent motor deficits starting at 4 months, with no motor neuron degeneration and no NMJ denervation at 5 and 18-to-20 months of age [604]. However, these mice display several behavioural deficits, such as executive dysfunction and memory impairment, which are symptoms of FTD. Thus, similarly to the transgenic mouse developed by the Julien laboratory, these mice mimic FTD more than ALS [582, 604].

In order to study the toxic gain-of-function due to the Q331K mutation, they performed RNA sequencing on different tissues (spinal cord vs frontal cortices), at different stages of diease (pre-symptomatic vs phenotype) and between different mice with or without a strong FTD phenotype. They found disease-state dependent transcriptomic changes, with 1,136 differentially expressed genes in older animals compared to only 404 in younger ones, as well as differences between the spinal cord and frontal cortex gene expression.

Their results underscore the importance of doing cell-specific but also time-specific transcriptomic analysis in order to understand the pathophysiological mechanism of mutant

TDP-43 dysfunction. Understanding how this time-dependant degradation of TDP-43 RNA metabolism functions occur will be primordial to our understanding of ALS and how to better design therapeutic treatments. Interestingly, several identical genes, or genes from the same family were found differentially regulated in their study as well as in our transgenic model, indicating that mutant TDP-43 pathological pathways are conserved between the mouse and the zebrafish (**Annexe 7**).

The second model created the Q331K knock-in line in order to validate results they have obtained from ENU-generated mice with an endogenous M232K mutation in the C-terminus domain. These mice developed a mild age-dependent motor phenotype but no paralysis or death at up to 24 months. Using these mice, they identified through RNA-sequencing of the spinal cord of one-year old mice 523 significantly differently spliced exons compared to wild-type. By further analyzing their data, they uncovered a new function of mutant Tdp-43 as it causes a novel splicing event, the skipping of constitutive exons in 44 genes. Interestingly, this skipping of constitutive exons concerns *Ankrd42*, which was also shown to be down-regulated in White paper [604] and an homolog in zebrafish, *ankrd9* is also down-regulated. It would be interesting to investigate whether *Ankrd42* and *ankrd9* have similar functions and how they relate to TDP-43 pathogenesis.

In both studies, they investigated not only differentially expressed genes but also alternative splicing events. Indeed, as TDP-43 is involved in mRNA splicing, this is a follow up experiments that we have to do with our transgenic lines.

Knock-in of ALS-related point mutations in the mouse *Fus* gene

One group recently generated a *Fus* knock-in mutant mouse line with the p.G466VfsX14 ALS-causative mutation [607]. In human, this mutation causes the skipping of exon 14 and the out-of-frame translation of exon 15 with a premature stop codon after 14 residues. In order to generate a similar protein in the mouse, the team knocked-in the equivalent A to G mutation, but also the human exon 15 in order to obtain the same frameshift, as the mouse lacks the same premature stop codon, leading to a longer out-of-frame exon 15. Thus it is a “humanized” endogenous mutated $Fus^{\Delta 14}$ protein that is expressed in these animals. The heterozygous mice had an age-dependent progressive motor phenotype

with mild motor neuron degeneration starting at 12 months and a modest survival reduction starting at 19 months. They carried a transcriptomic analysis on the lumber spinal cord of 3 months old and 12 months old heterozygous $Fus^{\Delta 14}$ and compared the differentially expressed genes compared to the wild-type littermates. Interestingly, and similarly to the results obtained by White and colleagues, very few mRNAs were misregulated at pre-symptomatic stages, with only 3 genes identified for Devoy and colleagues [607]. However, 1,289 genes were misregulated in the spinal cord of the 12 months-old heterozygous $Fus^{\Delta 14}$.

Previous work from our group identified that FUS and TDP-43 are part of the same genetic pathway, with FUS being downstream of TDP-43, as overexpression of wild-type FUS (but not mutant FUS) can partially rescue the loss of tdp-43 in zebrafish, whereas $TARDBP^{WT}$ failed to rescue loss of fus. Additionally, depletion of Fus leads to a reduction level of 610 genes, out of which 112 are also TDP-43 targets [270]. It is thus interesting to compare transcriptomics data from TDP-43 and FUS models to identify commonly misregulated pathways, as they may bring new understanding of the pathogenicity of both *TARDBP* and *FUS* mutations in ALS. As such, it is very exciting to note several misregulated genes in common not only between the datasets from the mouse Tdp-43 knock-in, but also with our dataset. While Devoy and colleagues identified only 3 misregulated genes in the 3 months-old spinal cord two of these, *Pgm5* and *Cyp3a13* are also found down-regulated in the mutant Tdp-43 mouse, *Pgm5* in the aged cortex and *Cyp3a13* in the 5 months-old cortex. However, when comparing the genes differentially regulated in the 12 months-old spinal cord of mutant Fus mouse, the homologs of 9 misregulated genes from our dataset are also misregulated in our zebrafish TDP-43 transgenic line, amongst which 5 are also misregulated in the Tdp-43 mutant mouse (**Annexe 7**). There are at least two possibilities for these genes: either their expressions are modified in response to the neurodegenerative processes occurring due to mutations in TDP-43 and FUS and they are "innocent" bystanders, not linked to the pathogenicity of the disease; or they are actively involved in the neurodegenerative process and the pathogenicity of ALS as consequences of misregulated RNA processing due to mutations in TDP-43 and FUS. Understanding where the genes we have identified fit within these two possibilities will allow us to deepen our understanding of ALS and increase our possibility of developing adequate treatments.

The *tardbp* paralog question

While these mutant mouse models are encouraging for the future of our zebrafish mutant lines, one question remains regarding how *tardbpl*, the zebrafish paralog of *tardbp* will behave in our knock-in lines. We know that when *tardbp* is knocked-down or knocked-out, *tardbpl*-spliced variant is up-regulated and can compensate for the loss of *tardbp*. It will be interesting to verify whether this up-regulation also happens with mutant tdp-43, and if it does, when: constitutively, or only when the fish develops a phenotype? Interestingly, this particularity of the zebrafish may help us answer one question that we still have regarding the physiological consequences of TDP-43 mutations. Indeed, an up-regulation of the *tardbpl*-spliced variant may suggest that the mutation induces a loss-of-function of tdp-43, whereas the absence of the up-regulation would point towards a toxic gain-of-function, which the knock-in mouse models suggest [604, 605].

Perspectives

Over the course of this thesis, I have used the zebrafish as a model to further study two MNDs, HSP and ALS., however much still remains to be done:

Through the two studies on HSP, we have uncovered a potential new pathophysiological mechanism of HSP linked to mutations in spastin (**Chapter 2**) and a new gene linked to HSP, *CAPN1* (**Chapter 3**). By identifying ER stress as a new consequence of spastin loss-of-function, we found new therapeutic targets and compounds for SPG4. Guanabenz, one of the compounds used in this study (**Chapter 2** and [491]) is currently under consideration to be used in clinical trial against HSP (personal communication from Dr. Guy Rouleau). However, we still need to understand the exact cause of ER stress in our HSP model in order to identify and target upstream elements linking spastin to ER stress. To do so, a better understanding of the role of M1 spastin is primordial. A first step to investigate the pathogenicity of truncated M1 would be to express it in the zebrafish, either the human protein by mRNA injection or the zebrafish one by generating knock-in lines with specific nonsense mutations found in SPG4 patients and see if this leads to ER stress. Additionally, we need to investigate in details which ER processes are particularly disturbed in HSP models. This can

be done via *in vivo* imaging using different zebrafish lines with fluorescent markers for subcellular structure such as the the microtubules [608], but also the Golgi apparatus [609] or by using fluorescent ER stress indicators [610] or calcium indicators expressed in specific cell lines [611]. Alternatively, culture of zebrafish motor neurons can allow for a better resolution to observe these processes in a cell-specific manner.

While several possibilities are open as the pathophysiological mechanisms of *CAPN1* mutations, spastin, and CAPN1 may have overlapping mechanisms, for instance, through perturbation of the microtubule network and of the cytoskeleton, affecting cell migration. It would be interesting to further study the abnormal clusters of acetylated α-tubulin that occur in our *capn1a* knockdown model, to investigate which other post-translational modifications are specific for these clusters and whether nocodazole, or other microtubules depolymerisation agents can reverse this phenotype. Interestingly, *CAPN1* mutations are found in patients with HSP and cerebellar ataxia, or whose symptoms are harder to discriminate between these two disorders, highlighting the heterogeneity of the different HSP and the difficulty of classifying disorders. Generating zebrafish *capn1a* and *capn1b* double knockout lines will allow us to have a clearer picture of SPG76 and investigate cerebellar dysfunctions that may arise in this disease. The use of zebrafish lines with cerebellum specific promoters [612] can be used to follow in vivo how the loss of calpain 1 affects the development of the cerebellum.

In this thesis, three new zebrafish ALS models were developed. They can be used to enhance our understanding of ALS-causing mutations related to two important ALS genes namely *TARDBP* and *FUS*. The inducible transgenic line (**Chapter 4**) provides a valuable tool to temporally control the expression of mutant TDP-43 and to investigate how timing and expression levels of mutant TDP-43 impact motor neurons and other cell-types in the pathogenicity of ALS; whereas the knock-in of ALS-causing mutations in *tardbp* and *fus* (**Chapter 5** and [478]) can be used to recapitulate ALS in a more physiological setting. However, the knock-in lines require further characterization prior to be used as models to shed light on the pathophysiological functions of TDP-43 and FUS mutations.

Using transgenic lines expressing fluorescent markers in different disease-relevant cell types, we can investigate the specific transcriptomic changes occuring in different cell populations. Ultimately, these future experiments can provide a comparison of how motor

neurons, glial and muscles are affected by the mutant TDP-43 or FUS at different disease stages. Furthermore, although transcriptomic changes are important, we also need to investigate how these changes translate at the protein levels through cell specific proteomic studies.

One key aspect of ALS pathophysiological mechanism is changes at the synaptic levels. The zebrafish is an ideal model to identify pre-symptomatic and early-stage synaptic abnormalities that may arise due to mutant TDP-43 or FUS expression ([484, 490]). Identifying early markers of the disease is primordial in order to develop drugs that will not only delay disease progression, but also act early enough to be able to delay disease onset or even prevent it. Zebrafish embryos and larvae are ideal models to perform medium-to-large scale screening of small molecules to identify targets that act on the exact mechanism that we would have previously uncover.

Overall, our zebrafish models of HSP and ALS can enable further investigations that will potentially enable the identification of new important pathophysiological mechanisms that can be used to design optimal therapeutics for treating these two disorders They are thus powerful tools for translational research in accelerating therapeutic developments for HSP and ALS.

General conclusion

In this thesis, I have used the zebrafish to study two of the main MNDs, HSP and ALS. ER stress was identified as a new pathological mechanism involved in SPG4 and the pathological loss-of-function of a new HSP gene, *CAPN1* (SPG76) was validated functionally in vivo. New zebrafish models to study ALS were also generated and the zebrafish line overexpressing a human mutant TDP-43 but not wild-type shows aberrant motor behavioural and axonal phenotypes. Furthermore, transcriptomic changes were identified in this model, and the findings are consistent with reports using mouse models. In the new CRISPR/Cas9 era, new zebrafish lines expressing specific ALS-causative point mutation in their endogenous genes through knock-in approaches were successfully generated. These models require further characterization but they can prove to be valuable disease-relevant models to study ALS pathogenesis.

The observation of ER stress due to spastin loss-of-function that can be restored with compounds previously tested on zebrafish models of ALS [480, 485], indicate that similar pathological mechanisms are at play between the two MNDs. These new developments will allow us to deepen our understanding of ALS and HSP and to have the proper tools in order to design and test new therapeutic avenues, as the zebrafish has proved itself to be a great model for molecule screening.

Our group, in collaboration with Dr. Alex Parker of the Université de Montréal, has recently demonstrated that a pipeline consisting of *C. elegans* and zebrafish models of ALS could be used to identify small molecules that can rescue the ALS-like phenotypes [486]. A first large screen was performed using the *C. elegans* model and the hits were further validated in zebrafish, with the most potent hit, Pimozide, tested in a mouse model, to finally being used in a small clinical trial on ALS patients. Thus our new models can be tools to identify new therapeutics. In this new area of CRISPR/Cas9 technology, we could foresee a future where zebrafish could be used for personalized medicine, as zebrafish models could be made for a single patient, mimicking their specific genetic conditions. This could be done not for only one causative gene, as we have done in the fourth study [478], but to integrate known genetic risk factors, as well as environmental exposure that will be specific to a single patient. Therapeutic

compounds could be tested at different ages of development and this would allow us to identify compounds that could reverse the specific pathophysiological changes at different disease stages, thus providing personalized treatment that could be adapted to the evolution of the disease, maximizing their beneficial effects. While this future is still far away, this thesis is a first stepping-stone to the moment where we may find treatments for these currently incurable diseases.

References

1. Bell, C., *Case of partial wasting of the muscles of the upper extremities*, in *The nervous system of the human body*. 1836. p. 432-434.
2. Duchenne, G.-B.-A., *Recherches faites a l'aide du galvanisme sur l'état de la contractilité et de la sensibilité électro-musculaires dans les paralyses des membres supérieurs*. Compt. rend. Acad. sc., 1849. **29**: p. 667-670.
3. Aran, F.-A., *Recherches sur une maladie non encore décrité de système musculaire (atrophie musculaire progressive)*. Arch. gén. méd., 1850. **24**: p. 4-35.
4. Cruveilhier, J., *Sur la paralysie musculaire progressive atrophique.* Bull Acad Méd, 1853: p. 490-502; 546-83.
5. Chancellor, A.M., J.D. Mitchell, and R.J. Swingler, *The first description of idiopathic progressive bulbar palsy.* J Neurol Neurosurg Psychiatry, 1993. **56**(12): p. 1270.
6. Duchenne, G.-B.-A., *Paralysie musculaire progressive de la langue, du voile du palais et des lèvres, affection non encore décrite comme espèce morbide distincte.* Arch. gén. méd., 1860. **16**: p. 283-296.
7. Charcot, J.-M., *Sclérose des cordons latéraux de la moelle épinière chez une femme hystérique atteinte de contracture permanente des quatres membres.* Bull Soc Med Hop Paris, 1865: p. 24-35.
8. Charcot, J.-M., *Sclérose latérale amyotrophique*. Oeuvres complètes. Vol. 2. 1874, Paris: Bureau du Progrès Médicale.
9. Erb, W.H., *Über einen wenig bekannten spinalen Symptomen-Complex.* Klin. Wchnschr, 1875. **12**: p. 357-359.
10. Kahler, O., *Über die progressiven spinaler Amyotrophien.* Ztschr. f. Heilk, 1884. **5**: p. 169.
11. Kahler, O. and A. Pick, *Beiträge zur Pathologie und pathologischer Anatomie des zentralen Nervensystems.* Ztschr. f. Nervenh, 1884. **5**: p. 169.
12. Strümpell, A., *Beiträge zur Pathologie des Rückenmarks.* Arch Psychiatr Nervenkr, 1880. **10**(3): p. 676-717.
13. Lorrain, M., *Contribution à l'étude de la paraplégie spasmodique familiale : travail de la clinique des maladies du système nerveux à la Salpêtrière*. 1898: Thèse de Paris.
14. Werdnig, G., *Zwei frühinfantile hereditäre Fälle von progressiver Muskelatrophie unter dem Bilde der Dystrophie, aber auf neurotischer Grundlage.* Arch Psychiatrie Nervenkrankheiten, 1891. **22**: p. 436-480.
15. Hoffman, J., *Über familiere progressive spinale muskelatrophie* Arch Psych Berlin, 1892. **24**: p. 644-646.
16. Brain, W.R., *Diseases of the nervous system*. 1933, London, England: Oxford University Press.
17. de Carvalho, M. and M. Swash, *Lower motor neuron dysfunction in ALS.* Clin Neurophysiol, 2016. **127**(7): p. 2670-81.
18. Blackstone, C., *Cellular pathways of hereditary spastic paraplegia.* Annu Rev Neurosci, 2012. **35**: p. 25-47.

19. Brooks, B.R., et al., *El Escorial revisited: revised criteria for the diagnosis of amyotrophic lateral sclerosis.* Amyotroph Lateral Scler Other Motor Neuron Disord, 2000. **1**(5): p. 293-9.
20. Swash, M., *Why are upper motor neuron signs difficult to elicit in amyotrophic lateral sclerosis?* J Neurol Neurosurg Psychiatry, 2012. **83**(6): p. 659-62.
21. Rosler, K.M., et al., *Quantification of upper motor neuron loss in amyotrophic lateral sclerosis.* Clin Neurophysiol, 2000. **111**(12): p. 2208-18.
22. Paganoni, S., et al., *Diagnostic timelines and delays in diagnosing amyotrophic lateral sclerosis (ALS).* Amyotroph Lateral Scler Frontotemporal Degener, 2014. **15**(5-6): p. 453-6.
23. Harding, A.E., *Classification of the hereditary ataxias and paraplegias.* Lancet, 1983. **1**(8334): p. 1151-5.
24. Fink, J.K., *Hereditary spastic paraplegia: clinico-pathologic features and emerging molecular mechanisms.* Acta Neuropathol, 2013. **126**(3): p. 307-28.
25. Lo Giudice, T., et al., *Hereditary spastic paraplegia: clinical-genetic characteristics and evolving molecular mechanisms.* Exp Neurol, 2014. **261**: p. 518-39.
26. Fink, J.K., *Hereditary spastic paraplegia: clinical principles and genetic advances.* Semin Neurol, 2014. **34**(3): p. 293-305.
27. Klebe, S., G. Stevanin, and C. Depienne, *Clinical and genetic heterogeneity in hereditary spastic paraplegias: from SPG1 to SPG72 and still counting.* Rev Neurol (Paris), 2015. **171**(6-7): p. 505-30.
28. Tesson, C., J. Koht, and G. Stevanin, *Delving into the complexity of hereditary spastic paraplegias: how unexpected phenotypes and inheritance modes are revolutionizing their nosology.* Hum Genet, 2015. **134**(6): p. 511-38.
29. Faber, I., et al., *Hereditary spastic paraplegia from 1880 to 2017: an historical review.* Arq Neuropsiquiatr, 2017. **75**(11): p. 813-818.
30. Ruano, L., et al., *The global epidemiology of hereditary ataxia and spastic paraplegia: a systematic review of prevalence studies.* Neuroepidemiology, 2014. **42**(3): p. 174-83.
31. de Souza, P.V.S., et al., *Hereditary Spastic Paraplegia: Clinical and Genetic Hallmarks.* Cerebellum, 2017. **16**(2): p. 525-551.
32. Schule, R., et al., *Hereditary spastic paraplegia: Clinicogenetic lessons from 608 patients.* Ann Neurol, 2016. **79**(4): p. 646-58.
33. Parodi, L., et al., *Hereditary spastic paraplegia: More than an upper motor neuron disease.* Rev Neurol (Paris), 2017. **173**(5): p. 352-360.
34. Schule, R., et al., *The Spastic Paraplegia Rating Scale (SPRS): a reliable and valid measure of disease severity.* Neurology, 2006. **67**(3): p. 430-4.
35. Chrestian, N., et al., *Clinical and genetic study of hereditary spastic paraplegia in Canada.* Neurol Genet, 2017. **3**(1): p. e122.
36. Deluca, G.C., G.C. Ebers, and M.M. Esiri, *The extent of axonal loss in the long tracts in hereditary spastic paraplegia.* Neuropathol Appl Neurobiol, 2004. **30**(6): p. 576-84.
37. Harding, A.E., *Hereditary spastic paraplegias.* Semin Neurol, 1993. **13**(4): p. 333-6.
38. White, K.D., et al., *Clinical and pathologic findings in hereditary spastic paraparesis with spastin mutation.* Neurology, 2000. **55**(1): p. 89-94.
39. Tallaksen, C.M., et al., *Subtle cognitive impairment but no dementia in patients with spastin mutations.* Arch Neurol, 2003. **60**(8): p. 1113-8.

40. Chamard, L., et al., *Cognitive Impairment Involving Social Cognition in SPG4 Hereditary Spastic Paraplegia.* Behav Neurol, 2016. **2016**: p. 6423461.
41. Depienne, C., et al., *Spastin mutations are frequent in sporadic spastic paraparesis and their spectrum is different from that observed in familial cases.* J Med Genet, 2006. **43**(3): p. 259-65.
42. Brugman, F., et al., *Paraplegin mutations in sporadic adult-onset upper motor neuron syndromes.* Neurology, 2008. **71**(19): p. 1500-5.
43. Saugier-Veber, P., et al., *X-linked spastic paraplegia and Pelizaeus-Merzbacher disease are allelic disorders at the proteolipid protein locus.* Nat Genet, 1994. **6**(3): p. 257-62.
44. Jouet, M., et al., *X-linked spastic paraplegia (SPG1), MASA syndrome and X-linked hydrocephalus result from mutations in the L1 gene.* Nat Genet, 1994. **7**(3): p. 402-7.
45. Hazan, J., et al., *Spastin, a new AAA protein, is altered in the most frequent form of autosomal dominant spastic paraplegia.* Nat Genet, 1999. **23**(3): p. 296-303.
46. Souza, P.V.S., et al., *New genetic causes for complex hereditary spastic paraplegia.* J Neurol Sci, 2017. **379**: p. 283-292.
47. Novarino, G., et al., *Exome sequencing links corticospinal motor neuron disease to common neurodegenerative disorders.* Science, 2014. **343**(6170): p. 506-511.
48. Morais, S., et al., *Massive sequencing of 70 genes reveals a myriad of missing genes or mechanisms to be uncovered in hereditary spastic paraplegias.* Eur J Hum Genet, 2017. **25**(11): p. 1217-1228.
49. Burguez, D., et al., *Clinical and molecular characterization of hereditary spastic paraplegias: A next-generation sequencing panel approach.* J Neurol Sci, 2017. **383**: p. 18-25.
50. Steinmuller, R., et al., *Evidence of a third locus in X-linked recessive spastic paraplegia.* Hum Genet, 1997. **100**(2): p. 287-9.
51. Schwartz, C.E., et al., *Allan-Herndon-Dudley syndrome and the monocarboxylate transporter 8 (MCT8) gene.* Am J Hum Genet, 2005. **77**(1): p. 41-53.
52. Macedo-Souza, L.I., et al., *Reevaluation of a large family defines a new locus for X-linked recessive pure spastic paraplegia (SPG34) on chromosome Xq25.* Neurogenetics, 2008. **9**(3): p. 225-6.
53. Khan, T.N., et al., *Evidence for autosomal recessive inheritance in SPG3A caused by homozygosity for a novel ATL1 missense mutation.* Eur J Hum Genet, 2014. **22**(10): p. 1180-4.
54. Esteves, T., et al., *Loss of association of REEP2 with membranes leads to hereditary spastic paraplegia.* Am J Hum Genet, 2014. **94**(2): p. 268-77.
55. Caballero Oteyza, A., et al., *Motor protein mutations cause a new form of hereditary spastic paraplegia.* Neurology, 2014. **82**(22): p. 2007-16.
56. Hodgkinson, C.A., et al., *A novel form of autosomal recessive pure hereditary spastic paraplegia maps to chromosome 13q14.* Neurology, 2002. **59**(12): p. 1905-9.
57. Durr, A., et al., *Atlastin1 mutations are frequent in young-onset autosomal dominant spastic paraplegia.* Arch Neurol, 2004. **61**(12): p. 1867-72.
58. Namekawa, M., et al., *SPG3A is the most frequent cause of hereditary spastic paraplegia with onset before age 10 years.* Neurology, 2006. **66**(1): p. 112-4.

59. Rainier, S., et al., *Hereditary spastic paraplegia linked to chromosome 14q11-q21: reduction of the SPG3 locus interval from 5.3 to 2.7 cM.* J Med Genet, 2001. **38**(11): p. E39.
60. Zhao, X., et al., *Mutations in a newly identified GTPase gene cause autosomal dominant hereditary spastic paraplegia.* Nat Genet, 2001. **29**(3): p. 326-31.
61. Byrnes, L.J. and H. Sondermann, *Structural basis for the nucleotide-dependent dimerization of the large G protein atlastin-1/SPG3A.* Proc Natl Acad Sci U S A, 2011. **108**(6): p. 2216-21.
62. Muriel, M.P., et al., *Atlastin-1, the dynamin-like GTPase responsible for spastic paraplegia SPG3A, remodels lipid membranes and may form tubules and vesicles in the endoplasmic reticulum.* J Neurochem, 2009. **110**(5): p. 1607-16.
63. Namekawa, M., et al., *Mutations in the SPG3A gene encoding the GTPase atlastin interfere with vesicle trafficking in the ER/Golgi interface and Golgi morphogenesis.* Mol Cell Neurosci, 2007. **35**(1): p. 1-13.
64. Rismanchi, N., et al., *Atlastin GTPases are required for Golgi apparatus and ER morphogenesis.* Hum Mol Genet, 2008. **17**(11): p. 1591-604.
65. Beetz, C., et al., *REEP1 mutation spectrum and genotype/phenotype correlation in hereditary spastic paraplegia type 31.* Brain, 2008. **131**(Pt 4): p. 1078-86.
66. Goizet, C., et al., *REEP1 mutations in SPG31: frequency, mutational spectrum, and potential association with mitochondrial morpho-functional dysfunction.* Hum Mutat, 2011. **32**(10): p. 1118-27.
67. Hewamadduma, C., et al., *New pedigrees and novel mutation expand the phenotype of REEP1-associated hereditary spastic paraplegia (HSP).* Neurogenetics, 2009. **10**(2): p. 105-10.
68. Zuchner, S., et al., *Mutations in the novel mitochondrial protein REEP1 cause hereditary spastic paraplegia type 31.* Am J Hum Genet, 2006. **79**(2): p. 365-9.
69. Park, S.H., et al., *Hereditary spastic paraplegia proteins REEP1, spastin, and atlastin-1 coordinate microtubule interactions with the tubular ER network.* J Clin Invest, 2010. **120**(4): p. 1097-110.
70. Lim, Y., et al., *Hereditary spastic paraplegia-linked REEP1 modulates endoplasmic reticulum/mitochondria contacts.* Ann Neurol, 2015. **78**(5): p. 679-96.
71. Beetz, C., et al., *A spastic paraplegia mouse model reveals REEP1-dependent ER shaping.* J Clin Invest, 2013. **123**(10): p. 4273-82.
72. Schule, R., et al., *SPG10 is a rare cause of spastic paraplegia in European families.* J Neurol Neurosurg Psychiatry, 2008. **79**(5): p. 584-7.
73. Reid, E., et al., *A new locus for autosomal dominant "pure" hereditary spastic paraplegia mapping to chromosome 12q13, and evidence for further genetic heterogeneity.* Am J Hum Genet, 1999. **65**(3): p. 757-63.
74. Goizet, C., et al., *Complicated forms of autosomal dominant hereditary spastic paraplegia are frequent in SPG10.* Hum Mutat, 2009. **30**(2): p. E376-85.
75. Collongues, N., et al., *Novel SPG10 mutation associated with dysautonomia, spinal cord atrophy, and skin biopsy abnormality.* Eur J Neurol, 2013. **20**(2): p. 398-401.
76. Blair, M.A., S. Ma, and P. Hedera, *Mutation in KIF5A can also cause adult-onset hereditary spastic paraplegia.* Neurogenetics, 2006. **7**(1): p. 47-50.
77. Ebbing, B., et al., *Effect of spastic paraplegia mutations in KIF5A kinesin on transport activity.* Hum Mol Genet, 2008. **17**(9): p. 1245-52.

78. Boukhris, A., et al., *Hereditary spastic paraplegia with mental impairment and thin corpus callosum in Tunisia: SPG11, SPG15, and further genetic heterogeneity.* Arch Neurol, 2008. **65**(3): p. 393-402.
79. Pippucci, T., et al., *Autosomal recessive hereditary spastic paraplegia with thin corpus callosum: a novel mutation in the SPG11 gene and further evidence for genetic heterogeneity.* Eur J Neurol, 2009. **16**(1): p. 121-6.
80. Schule, R., et al., *Frequency and phenotype of SPG11 and SPG15 in complicated hereditary spastic paraplegia.* J Neurol Neurosurg Psychiatry, 2009. **80**(12): p. 1402-4.
81. Siri, L., et al., *Cognitive profile in spastic paraplegia with thin corpus callosum and mutations in SPG11.* Neuropediatrics, 2010. **41**(1): p. 35-8.
82. Stevanin, G., et al., *Mutations in SPG11 are frequent in autosomal recessive spastic paraplegia with thin corpus callosum, cognitive decline and lower motor neuron degeneration.* Brain, 2008. **131**(Pt 3): p. 772-84.
83. Stevanin, G., et al., *Spastic paraplegia with thin corpus callosum: description of 20 new families, refinement of the SPG11 locus, candidate gene analysis and evidence of genetic heterogeneity.* Neurogenetics, 2006. **7**(3): p. 149-56.
84. Stevanin, G., et al., *Mutations in SPG11, encoding spatacsin, are a major cause of spastic paraplegia with thin corpus callosum.* Nat Genet, 2007. **39**(3): p. 366-72.
85. Murmu, R.P., et al., *Cellular distribution and subcellular localization of spatacsin and spastizin, two proteins involved in hereditary spastic paraplegia.* Mol Cell Neurosci, 2011. **47**(3): p. 191-202.
86. Branchu, J., et al., *Loss of spatacsin function alters lysosomal lipid clearance leading to upper and lower motor neuron degeneration.* Neurobiol Dis, 2017. **102**: p. 21-37.
87. Chang, J., S. Lee, and C. Blackstone, *Spastic paraplegia proteins spastizin and spatacsin mediate autophagic lysosome reformation.* J Clin Invest, 2014. **124**(12): p. 5249-62.
88. Hirst, J., et al., *Interaction between AP-5 and the hereditary spastic paraplegia proteins SPG11 and SPG15.* Mol Biol Cell, 2013. **24**(16): p. 2558-69.
89. Renvoise, B., et al., *Lysosomal abnormalities in hereditary spastic paraplegia types SPG15 and SPG11.* Ann Clin Transl Neurol, 2014. **1**(6): p. 379-389.
90. Arnoldi, A., et al., *Clinical phenotype variability in patients with hereditary spastic paraplegia type 5 associated with CYP7B1 mutations.* Clin Genet, 2012. **81**(2): p. 150-7.
91. Goizet, C., et al., *CYP7B1 mutations in pure and complex forms of hereditary spastic paraplegia type 5.* Brain, 2009. **132**(Pt 6): p. 1589-600.
92. Tsaousidou, M.K., et al., *Sequence alterations within CYP7B1 implicate defective cholesterol homeostasis in motor-neuron degeneration.* Am J Hum Genet, 2008. **82**(2): p. 510-5.
93. Biancheri, R., et al., *White matter lesions in spastic paraplegia with mutations in SPG5/CYP7B1.* Neuromuscul Disord, 2009. **19**(1): p. 62-5.
94. Schule, R., et al., *Analysis of CYP7B1 in non-consanguineous cases of hereditary spastic paraplegia.* Neurogenetics, 2009. **10**(2): p. 97-104.
95. Schule, R., et al., *Marked accumulation of 27-hydroxycholesterol in SPG5 patients with hereditary spastic paresis.* J Lipid Res, 2010. **51**(4): p. 819-23.

96. Casari, G., et al., *Spastic paraplegia and OXPHOS impairment caused by mutations in paraplegin, a nuclear-encoded mitochondrial metalloprotease.* Cell, 1998. **93**(6): p. 973-83.
97. De Michele, G., et al., *A new locus for autosomal recessive hereditary spastic paraplegia maps to chromosome 16q24.3.* Am J Hum Genet, 1998. **63**(1): p. 135-9.
98. Elleuch, N., et al., *Mutation analysis of the paraplegin gene (SPG7) in patients with hereditary spastic paraplegia.* Neurology, 2006. **66**(5): p. 654-9.
99. Klebe, S., et al., *Spastic paraplegia gene 7 in patients with spasticity and/or optic neuropathy.* Brain, 2012. **135**(Pt 10): p. 2980-93.
100. Tzoulis, C., et al., *Hereditary spastic paraplegia caused by the novel mutation 1047insC in the SPG7 gene.* J Neurol, 2008. **255**(8): p. 1142-4.
101. van Gassen, K.L., et al., *Genotype-phenotype correlations in spastic paraplegia type 7: a study in a large Dutch cohort.* Brain, 2012. **135**(Pt 10): p. 2994-3004.
102. Nolden, M., et al., *The m-AAA protease defective in hereditary spastic paraplegia controls ribosome assembly in mitochondria.* Cell, 2005. **123**(2): p. 277-89.
103. Langer, T., *AAA proteases: cellular machines for degrading membrane proteins.* Trends Biochem Sci, 2000. **25**(5): p. 247-51.
104. Webb, S., V. Patterson, and M. Hutchinson, *Two families with autosomal recessive spastic paraplegia, pigmented maculopathy, and dementia.* J Neurol Neurosurg Psychiatry, 1997. **63**(5): p. 628-32.
105. Hanein, S., et al., *Identification of the SPG15 gene, encoding spastizin, as a frequent cause of complicated autosomal-recessive spastic paraplegia, including Kjellin syndrome.* Am J Hum Genet, 2008. **82**(4): p. 992-1002.
106. Goizet, C., et al., *SPG15 is the second most common cause of hereditary spastic paraplegia with thin corpus callosum.* Neurology, 2009. **73**(14): p. 1111-9.
107. Schicks, J., et al., *Atypical juvenile parkinsonism in a consanguineous SPG15 family.* Mov Disord, 2011. **26**(3): p. 564-6.
108. Kjellin, K., *Familial spastic paraplegia with amyotrophy, oligophrenia, and central retinal degeneration.* Arch Neurol, 1959. **1**: p. 133-40.
109. Denora, P.S., et al., *Spastic paraplegia with thinning of the corpus callosum and white matter abnormalities: further mutations and relative frequency in ZFYVE26/SPG15 in the Italian population.* J Neurol Sci, 2009. **277**(1-2): p. 22-5.
110. Pensato, V., et al., *Overlapping phenotypes in complex spastic paraplegias SPG11, SPG15, SPG35 and SPG48.* Brain, 2014. **137**(Pt 7): p. 1907-20.
111. Slabicki, M., et al., *A genome-scale DNA repair RNAi screen identifies SPG48 as a novel gene associated with hereditary spastic paraplegia.* PLoS Biol, 2010. **8**(6): p. e1000408.
112. Vantaggiato, C., et al., *Defective autophagy in spastizin mutated patients with hereditary spastic paraparesis type 15.* Brain, 2013. **136**(Pt 10): p. 3119-39.
113. Claudiani, P., et al., *Spastin subcellular localization is regulated through usage of different translation start sites and active export from the nucleus.* Exp Cell Res, 2005. **309**(2): p. 358-69.
114. Mancuso, G. and E.I. Rugarli, *A cryptic promoter in the first exon of the SPG4 gene directs the synthesis of the 60-kDa spastin isoform.* BMC Biol, 2008. **6**: p. 31.
115. Svenson, I.K., et al., *Identification and expression analysis of spastin gene mutations in hereditary spastic paraplegia.* Am J Hum Genet, 2001. **68**(5): p. 1077-85.

116. Solowska, J.M., et al., *Quantitative and functional analyses of spastin in the nervous system: implications for hereditary spastic paraplegia.* J Neurosci, 2008. **28**(9): p. 2147-57.
117. Sanderson, C.M., et al., *Spastin and atlastin, two proteins mutated in autosomal-dominant hereditary spastic paraplegia, are binding partners.* Hum Mol Genet, 2006. **15**(2): p. 307-18.
118. Evans, K., et al., *Interaction of two hereditary spastic paraplegia gene products, spastin and atlastin, suggests a common pathway for axonal maintenance.* Proc Natl Acad Sci U S A, 2006. **103**(28): p. 10666-71.
119. Reid, E., et al., *The hereditary spastic paraplegia protein spastin interacts with the ESCRT-III complex-associated endosomal protein CHMP1B.* Hum Mol Genet, 2005. **14**(1): p. 19-38.
120. Mannan, A.U., et al., *Spastin, the most commonly mutated protein in hereditary spastic paraplegia interacts with Reticulon 1 an endoplasmic reticulum protein.* Neurogenetics, 2006. **7**(2): p. 93-103.
121. Ciccarelli, F.D., et al., *The identification of a conserved domain in both spartin and spastin, mutated in hereditary spastic paraplegia.* Genomics, 2003. **81**(4): p. 437-41.
122. White, S.R., et al., *Recognition of C-terminal amino acids in tubulin by pore loops in Spastin is important for microtubule severing.* J Cell Biol, 2007. **176**(7): p. 995-1005.
123. Eckert, T., et al., *Spastin's microtubule-binding properties and comparison to katanin.* PLoS One, 2012. **7**(12): p. e50161.
124. Solowska, J.M. and P.W. Baas, *Hereditary spastic paraplegia SPG4: what is known and not known about the disease.* Brain, 2015. **138**(Pt 9): p. 2471-84.
125. Roll-Mecak, A. and R.D. Vale, *Structural basis of microtubule severing by the hereditary spastic paraplegia protein spastin.* Nature, 2008. **451**(7176): p. 363-7.
126. Eckert, T., et al., *Subunit Interactions and cooperativity in the microtubule-severing AAA ATPase spastin.* J Biol Chem, 2012. **287**(31): p. 26278-90.
127. Taylor, J.L., et al., *Crystal structure of the human spastin AAA domain.* J Struct Biol, 2012. **179**(2): p. 133-7.
128. Roll-Mecak, A. and R.D. Vale, *The Drosophila homologue of the hereditary spastic paraplegia protein, spastin, severs and disassembles microtubules.* Curr Biol, 2005. **15**(7): p. 650-5.
129. Evans, K.J., et al., *Linking axonal degeneration to microtubule remodeling by Spastin-mediated microtubule severing.* J Cell Biol, 2005. **168**(4): p. 599-606.
130. Errico, A., A. Ballabio, and E.I. Rugarli, *Spastin, the protein mutated in autosomal dominant hereditary spastic paraplegia, is involved in microtubule dynamics.* Hum Mol Genet, 2002. **11**(2): p. 153-63.
131. Lacroix, B., et al., *Tubulin polyglutamylation stimulates spastin-mediated microtubule severing.* J Cell Biol, 2010. **189**(6): p. 945-54.
132. Valenstein, M.L. and A. Roll-Mecak, *Graded Control of Microtubule Severing by Tubulin Glutamylation.* Cell, 2016. **164**(5): p. 911-21.
133. Goyal, U., et al., *Spastin-interacting protein NA14/SSNA1 functions in cytokinesis and axon development.* PLoS One, 2014. **9**(11): p. e112428.
134. Errico, A., et al., *Spastin interacts with the centrosomal protein NA14, and is enriched in the spindle pole, the midbody and the distal axon.* Hum Mol Genet, 2004. **13**(18): p. 2121-32.

135. Yang, D., et al., *Structural basis for midbody targeting of spastin by the ESCRT-III protein CHMP1B.* Nat Struct Mol Biol, 2008. **15**(12): p. 1278-86.
136. Guizetti, J., et al., *Cortical constriction during abscission involves helices of ESCRT-III-dependent filaments.* Science, 2011. **331**(6024): p. 1616-20.
137. Connell, J.W., et al., *Spastin couples microtubule severing to membrane traffic in completion of cytokinesis and secretion.* Traffic, 2009. **10**(1): p. 42-56.
138. Zhang, C., et al., *Role of spastin and protrudin in neurite outgrowth.* J Cell Biochem, 2012. **113**(7): p. 2296-307.
139. Wood, J.D., et al., *The microtubule-severing protein Spastin is essential for axon outgrowth in the zebrafish embryo.* Hum Mol Genet, 2006. **15**(18): p. 2763-71.
140. Butler, R., et al., *Genetic and chemical modulation of spastin-dependent axon outgrowth in zebrafish embryos indicates a role for impaired microtubule dynamics in hereditary spastic paraplegia.* Dis Model Mech, 2010. **3**(11-12): p. 743-51.
141. Allison, R., et al., *An ESCRT-spastin interaction promotes fission of recycling tubules from the endosome.* J Cell Biol, 2013. **202**(3): p. 527-43.
142. Trotta, N., et al., *The hereditary spastic paraplegia gene, spastin, regulates microtubule stability to modulate synaptic structure and function.* Curr Biol, 2004. **14**(13): p. 1135-47.
143. Sherwood, N.T., et al., *Drosophila spastin regulates synaptic microtubule networks and is required for normal motor function.* PLoS Biol, 2004. **2**(12): p. e429.
144. Orso, G., et al., *Disease-related phenotypes in a Drosophila model of hereditary spastic paraplegia are ameliorated by treatment with vinblastine.* J Clin Invest, 2005. **115**(11): p. 3026-34.
145. Qiang, L., et al., *Basic fibroblast growth factor elicits formation of interstitial axonal branches via enhanced severing of microtubules.* Mol Biol Cell, 2010. **21**(2): p. 334-44.
146. Denton, K.R., et al., *Loss of spastin function results in disease-specific axonal defects in human pluripotent stem cell-based models of hereditary spastic paraplegia.* Stem Cells, 2014. **32**(2): p. 414-23.
147. Howes, S.C., et al., *Effects of tubulin acetylation and tubulin acetyltransferase binding on microtubule structure.* Mol Biol Cell, 2014. **25**(2): p. 257-66.
148. Baas, P.W., C. Vidya Nadar, and K.A. Myers, *Axonal transport of microtubules: the long and short of it.* Traffic, 2006. **7**(5): p. 490-8.
149. Roll-Mecak, A. and R.D. Vale, *Making more microtubules by severing: a common theme of noncentrosomal microtubule arrays?* J Cell Biol, 2006. **175**(6): p. 849-51.
150. Wang, L. and A. Brown, *Rapid movement of microtubules in axons.* Curr Biol, 2002. **12**(17): p. 1496-1501.
151. Blackstone, C., C.J. O'Kane, and E. Reid, *Hereditary spastic paraplegias: membrane traffic and the motor pathway.* Nat Rev Neurosci, 2011. **12**(1): p. 31-42.
152. Lumb, J.H., et al., *The AAA ATPase spastin links microtubule severing to membrane modelling.* Biochim Biophys Acta, 2012. **1823**(1): p. 192-7.
153. Tsang, H.T., et al., *The hereditary spastic paraplegia proteins NIPA1, spastin and spartin are inhibitors of mammalian BMP signalling.* Hum Mol Genet, 2009. **18**(20): p. 3805-21.
154. Fonknechten, N., et al., *Spectrum of SPG4 mutations in autosomal dominant spastic paraplegia.* Hum Mol Genet, 2000. **9**(4): p. 637-44.

155. Shoukier, M., et al., *Expansion of mutation spectrum, determination of mutation cluster regions and predictive structural classification of SPAST mutations in hereditary spastic paraplegia.* Eur J Hum Genet, 2009. **17**(2): p. 187-94.
156. Beetz, C., et al., *High frequency of partial SPAST deletions in autosomal dominant hereditary spastic paraplegia.* Neurology, 2006. **67**(11): p. 1926-30.
157. Boone, P.M., et al., *The Alu-rich genomic architecture of SPAST predisposes to diverse and functionally distinct disease-associated CNV alleles.* Am J Hum Genet, 2014. **95**(2): p. 143-61.
158. McDermott, C.J., et al., *Clinical features of hereditary spastic paraplegia due to spastin mutation.* Neurology, 2006. **67**(1): p. 45-51.
159. Yip, A.G., et al., *Meta-analysis of age at onset in spastin-associated hereditary spastic paraplegia provides no evidence for a correlation with mutational class.* J Med Genet, 2003. **40**(9): p. e106.
160. Meijer, I.A., et al., *Spectrum of SPG4 mutations in a large collection of North American families with hereditary spastic paraplegia.* Arch Neurol, 2002. **59**(2): p. 281-6.
161. Durr, A., C. Tallaksen, and C. Depienne, *Spastic Paraplegia 4*, in *GeneReviews((R))*, M.P. Adam, et al., Editors. 1993: Seattle (WA).
162. Nielsen, J.E., et al., *Hereditary spastic paraplegia with cerebellar ataxia: a complex phenotype associated with a new SPG4 gene mutation.* Eur J Neurol, 2004. **11**(12): p. 817-24.
163. Webb, S., et al., *A family with hereditary spastic paraparesis and epilepsy.* Epilepsia, 1997. **38**(4): p. 495-9.
164. Tarrade, A., et al., *A mutation of spastin is responsible for swellings and impairment of transport in a region of axon characterized by changes in microtubule composition.* Hum Mol Genet, 2006. **15**(24): p. 3544-58.
165. Kasher, P.R., et al., *Direct evidence for axonal transport defects in a novel mouse model of mutant spastin-induced hereditary spastic paraplegia (HSP) and human HSP patients.* J Neurochem, 2009. **110**(1): p. 34-44.
166. Fassier, C., et al., *Microtubule-targeting drugs rescue axonal swellings in cortical neurons from spastin knockout mice.* Dis Model Mech, 2013. **6**(1): p. 72-83.
167. Riano, E., et al., *Pleiotropic effects of spastin on neurite growth depending on expression levels.* J Neurochem, 2009. **108**(5): p. 1277-88.
168. Havlicek, S., et al., *Gene dosage-dependent rescue of HSP neurite defects in SPG4 patients' neurons.* Hum Mol Genet, 2014. **23**(10): p. 2527-41.
169. Hardiman, O., et al., *Amyotrophic lateral sclerosis.* Nat Rev Dis Primers, 2017. **3**: p. 17071.
170. Chio, A., et al., *Global epidemiology of amyotrophic lateral sclerosis: a systematic review of the published literature.* Neuroepidemiology, 2013. **41**(2): p. 118-30.
171. Logroscino, G., et al., *Incidence of amyotrophic lateral sclerosis in Europe.* J Neurol Neurosurg Psychiatry, 2010. **81**(4): p. 385-90.
172. Chio, A., et al., *Prognostic factors in ALS: A critical review.* Amyotroph Lateral Scler, 2009. **10**(5-6): p. 310-23.
173. Gruis, K.L. and N. Lechtzin, *Respiratory therapies for amyotrophic lateral sclerosis: a primer.* Muscle Nerve, 2012. **46**(3): p. 313-31.

174. Phukan, J., et al., *The syndrome of cognitive impairment in amyotrophic lateral sclerosis: a population-based study.* J Neurol Neurosurg Psychiatry, 2012. **83**(1): p. 102-8.
175. Wagner, L., et al., *State and metropolitan area-based amyotrophic lateral sclerosis (ALS) surveillance.* Amyotroph Lateral Scler Frontotemporal Degener, 2015. **17**(1-2): p. 128-34.
176. Logroscino, G., et al., *Descriptive epidemiology of amyotrophic lateral sclerosis: new evidence and unsolved issues.* J Neurol Neurosurg Psychiatry, 2008. **79**(1): p. 6-11.
177. Johnston, C.A., et al., *Amyotrophic lateral sclerosis in an urban setting: a population based study of inner city London.* J Neurol, 2006. **253**(12): p. 1642-3.
178. Golby, R., et al., *Five-Year Incidence of Amyotrophic Lateral Sclerosis in British Columbia (2010-2015).* Can J Neurol Sci, 2016. **43**(6): p. 791-795.
179. Gaskin, J., et al., *Burden of neurological conditions in Canada.* Neurotoxicology, 2017. **61**: p. 2-10.
180. Al-Chalabi, A., et al., *Amyotrophic lateral sclerosis: moving towards a new classification system.* Lancet Neurol, 2016. **15**(11): p. 1182-94.
181. de Carvalho, M., et al., *Electrodiagnostic criteria for diagnosis of ALS.* Clin Neurophysiol, 2008. **119**(3): p. 497-503.
182. Ludolph, A., et al., *A revision of the El Escorial criteria - 2015.* Amyotroph Lateral Scler Frontotemporal Degener, 2015. **16**(5-6): p. 291-2.
183. Al-Chalabi, A. and O. Hardiman, *The epidemiology of ALS: a conspiracy of genes, environment and time.* Nat Rev Neurol, 2013. **9**(11): p. 617-28.
184. Beghi, E., et al., *The heterogeneity of amyotrophic lateral sclerosis: a possible explanation of treatment failure.* Curr Med Chem, 2007. **14**(30): p. 3185-200.
185. Chio, A., et al., *Phenotypic heterogeneity of amyotrophic lateral sclerosis: a population based study.* J Neurol Neurosurg Psychiatry, 2011. **82**(7): p. 740-6.
186. McDermott, C.J. and P.J. Shaw, *Diagnosis and management of motor neurone disease.* BMJ, 2008. **336**(7645): p. 658-62.
187. Ravits, J.M. and A.R. La Spada, *ALS motor phenotype heterogeneity, focality, and spread: deconstructing motor neuron degeneration.* Neurology, 2009. **73**(10): p. 805-11.
188. Swinnen, B. and W. Robberecht, *The phenotypic variability of amyotrophic lateral sclerosis.* Nat Rev Neurol, 2014. **10**(11): p. 661-70.
189. Elamin, M., et al., *Cognitive changes predict functional decline in ALS: a population-based longitudinal study.* Neurology, 2013. **80**(17): p. 1590-7.
190. Ferrari, R., et al., *FTD and ALS: a tale of two diseases.* Curr Alzheimer Res, 2011. **8**(3): p. 273-94.
191. Rosen, D.R., et al., *Mutations in Cu/Zn superoxide dismutase gene are associated with familial amyotrophic lateral sclerosis.* Nature, 1993. **362**(6415): p. 59-62.
192. Beghi, E., et al., *The epidemiology and treatment of ALS: focus on the heterogeneity of the disease and critical appraisal of therapeutic trials.* Amyotroph Lateral Scler, 2011. **12**(1): p. 1-10.
193. Bensimon, G., L. Lacomblez, and V. Meininger, *A controlled trial of riluzole in amyotrophic lateral sclerosis. ALS/Riluzole Study Group.* N Engl J Med, 1994. **330**(9): p. 585-91.

194. Lacomblez, L., et al., *Dose-ranging study of riluzole in amyotrophic lateral sclerosis. Amyotrophic Lateral Sclerosis/Riluzole Study Group II.* Lancet, 1996. **347**(9013): p. 1425-31.
195. Fang, T., et al., *Stage at which riluzole treatment prolongs survival in patients with amyotrophic lateral sclerosis: a retrospective analysis of data from a dose-ranging study.* Lancet Neurol, 2018. **17**(5): p. 416-422.
196. Miller, R.G., et al., *Riluzole for amyotrophic lateral sclerosis (ALS)/motor neuron disease (MND).* Cochrane Database Syst Rev, 2007(1): p. CD001447.
197. Sojka, P., P.M. Andersen, and L. Forsgren, *Effects of riluzole on symptom progression in amyotrophic lateral sclerosis.* Lancet, 1997. **349**(9046): p. 176-7.
198. Hardiman, O. and L.H. van den Berg, *Edaravone: a new treatment for ALS on the horizon?* Lancet Neurol, 2017. **16**(7): p. 490-491.
199. Jaiswal, M.K., *Riluzole and edaravone: A tale of two amyotrophic lateral sclerosis drugs.* Med Res Rev, 2018.
200. Boillee, S., C. Vande Velde, and D.W. Cleveland, *ALS: a disease of motor neurons and their nonneuronal neighbors.* Neuron, 2006. **52**(1): p. 39-59.
201. Lasiene, J. and K. Yamanaka, *Glial cells in amyotrophic lateral sclerosis.* Neurol Res Int, 2011. **2011**: p. 718987.
202. Haidet-Phillips, A.M., et al., *Astrocytes from familial and sporadic ALS patients are toxic to motor neurons.* Nat Biotechnol, 2011. **29**(9): p. 824-8.
203. Kato, S., et al., *New consensus research on neuropathological aspects of familial amyotrophic lateral sclerosis with superoxide dismutase 1 (SOD1) gene mutations: inclusions containing SOD1 in neurons and astrocytes.* Amyotroph Lateral Scler Other Motor Neuron Disord, 2000. **1**(3): p. 163-84.
204. Sun, Z., et al., *Molecular determinants and genetic modifiers of aggregation and toxicity for the ALS disease protein FUS/TLS.* PLoS Biol, 2011. **9**(4): p. e1000614.
205. Huang, E.J., et al., *Extensive FUS-immunoreactive pathology in juvenile amyotrophic lateral sclerosis with basophilic inclusions.* Brain Pathol, 2010. **20**(6): p. 1069-76.
206. Arai, T., et al., *TDP-43 is a component of ubiquitin-positive tau-negative inclusions in frontotemporal lobar degeneration and amyotrophic lateral sclerosis.* Biochem Biophys Res Commun, 2006. **351**(3): p. 602-11.
207. Neumann, M., et al., *Ubiquitinated TDP-43 in frontotemporal lobar degeneration and amyotrophic lateral sclerosis.* Science, 2006. **314**(5796): p. 130-3.
208. Schymick, J.C., K. Talbot, and B.J. Traynor, *Genetics of sporadic amyotrophic lateral sclerosis.* Hum Mol Genet, 2007. **16 Spec No. 2**: p. R233-42.
209. Wang, M.D., et al., *Identification of risk factors associated with onset and progression of amyotrophic lateral sclerosis using systematic review and meta-analysis.* Neurotoxicology, 2017. **61**: p. 101-130.
210. Mitchell, J.D. and G.D. Borasio, *Amyotrophic lateral sclerosis.* Lancet, 2007. **369**(9578): p. 2031-2041.
211. Laferriere, F. and M. Polymenidou, *Advances and challenges in understanding the multifaceted pathogenesis of amyotrophic lateral sclerosis.* Swiss Med Wkly, 2015. **145**: p. w14054.
212. Renton, A.E., A. Chio, and B.J. Traynor, *State of play in amyotrophic lateral sclerosis genetics.* Nat Neurosci, 2014. **17**(1): p. 17-23.

213. Belzil, V.V. and G.A. Rouleau, *Familial ALS: less common than we think?* J Neurol Neurosurg Psychiatry, 2012. **83**(12): p. 1133.
214. Byrne, S., et al., *Rate of familial amyotrophic lateral sclerosis: a systematic review and meta-analysis.* J Neurol Neurosurg Psychiatry, 2011. **82**(6): p. 623-7.
215. Chio, A., et al., *Genetic counselling in ALS: facts, uncertainties and clinical suggestions.* J Neurol Neurosurg Psychiatry, 2014. **85**(5): p. 478-85.
216. Ryan, M., et al., *Determining the incidence of familiality in ALS: A study of temporal trends in Ireland from 1994 to 2016.* Neurol Genet, 2018. **4**(3): p. e239.
217. Al-Chalabi, A., L.H. van den Berg, and J. Veldink, *Gene discovery in amyotrophic lateral sclerosis: implications for clinical management.* Nat Rev Neurol, 2017. **13**(2): p. 96-104.
218. Gibson, S.B., et al., *The evolving genetic risk for sporadic ALS.* Neurology, 2017. **89**(3): p. 226-233.
219. Al-Chalabi, A., et al., *An estimate of amyotrophic lateral sclerosis heritability using twin data.* J Neurol Neurosurg Psychiatry, 2010. **81**(12): p. 1324-6.
220. Sreedharan, J., et al., *TDP-43 mutations in familial and sporadic amyotrophic lateral sclerosis.* Science, 2008. **319**(5870): p. 1668-72.
221. Kabashi, E., et al., *TARDBP mutations in individuals with sporadic and familial amyotrophic lateral sclerosis.* Nat Genet, 2008. **40**(5): p. 572-4.
222. Kwiatkowski, T.J., Jr., et al., *Mutations in the FUS/TLS gene on chromosome 16 cause familial amyotrophic lateral sclerosis.* Science, 2009. **323**(5918): p. 1205-8.
223. Vance, C., et al., *Mutations in FUS, an RNA processing protein, cause familial amyotrophic lateral sclerosis type 6.* Science, 2009. **323**(5918): p. 1208-1211.
224. DeJesus-Hernandez, M., et al., *Expanded GGGGCC hexanucleotide repeat in noncoding region of C9ORF72 causes chromosome 9p-linked FTD and ALS.* Neuron, 2011. **72**(2): p. 245-56.
225. Renton, A.E., et al., *A hexanucleotide repeat expansion in C9ORF72 is the cause of chromosome 9p21-linked ALS-FTD.* Neuron, 2011. **72**(2): p. 257-68.
226. Chia, R., A. Chio, and B.J. Traynor, *Novel genes associated with amyotrophic lateral sclerosis: diagnostic and clinical implications.* Lancet Neurol, 2018. **17**(1): p. 94-102.
227. Sreedharan, J., et al., *Age-Dependent TDP-43-Mediated Motor Neuron Degeneration Requires GSK3, hat-trick, and xmas-2.* Curr Biol, 2015. **25**(16): p. 2130-6.
228. Wang, H.Y., et al., *Structural diversity and functional implications of the eukaryotic TDP gene family.* Genomics, 2004. **83**(1): p. 130-9.
229. Shiina, Y., et al., *TDP-43 dimerizes in human cells in culture.* Cell Mol Neurobiol, 2010. **30**(4): p. 641-52.
230. Buratti, E. and F.E. Baralle, *Characterization and functional implications of the RNA binding properties of nuclear factor TDP-43, a novel splicing regulator of CFTR exon 9.* J Biol Chem, 2001. **276**(39): p. 36337-43.
231. Ou, S.H., et al., *Cloning and characterization of a novel cellular protein, TDP-43, that binds to human immunodeficiency virus type 1 TAR DNA sequence motifs.* J Virol, 1995. **69**(6): p. 3584-96.
232. Mompean, M., et al., *The TDP-43 N-terminal domain structure at high resolution.* FEBS J, 2016. **283**(7): p. 1242-60.

233. Qin, H., et al., *TDP-43 N terminus encodes a novel ubiquitin-like fold and its unfolded form in equilibrium that can be shifted by binding to ssDNA.* Proc Natl Acad Sci U S A, 2014. **111**(52): p. 18619-24.
234. Ayala, Y.M., et al., *Human, Drosophila, and C.elegans TDP43: nucleic acid binding properties and splicing regulatory function.* J Mol Biol, 2005. **348**(3): p. 575-88.
235. Kuo, P.H., et al., *Structural insights into TDP-43 in nucleic-acid binding and domain interactions.* Nucleic Acids Res, 2009. **37**(6): p. 1799-808.
236. Ayala, Y.M., et al., *Structural determinants of the cellular localization and shuttling of TDP-43.* J Cell Sci, 2008. **121**(Pt 22): p. 3778-85.
237. Budini, M., F.E. Baralle, and E. Buratti, *Targeting TDP-43 in neurodegenerative diseases.* Expert Opin Ther Targets, 2014. **18**(6): p. 617-32.
238. Buratti, E., et al., *TDP-43 binds heterogeneous nuclear ribonucleoprotein A/B through its C-terminal tail: an important region for the inhibition of cystic fibrosis transmembrane conductance regulator exon 9 splicing.* J Biol Chem, 2005. **280**(45): p. 37572-84.
239. Cushman, R., et al., *Ethical, legal and social issues for personal health records and applications.* J Biomed Inform, 2010. **43**(5 Suppl): p. S51-5.
240. D'Ambrogio, A., et al., *Functional mapping of the interaction between TDP-43 and hnRNP A2 in vivo.* Nucleic Acids Res, 2009. **37**(12): p. 4116-26.
241. Hasegawa, M., et al., *Phosphorylated TDP-43 in frontotemporal lobar degeneration and amyotrophic lateral sclerosis.* Ann Neurol, 2008. **64**(1): p. 60-70.
242. Nishimoto, Y., et al., *Characterization of alternative isoforms and inclusion body of the TAR DNA-binding protein-43.* J Biol Chem, 2010. **285**(1): p. 608-19.
243. Xiao, S., et al., *Low molecular weight species of TDP-43 generated by abnormal splicing form inclusions in amyotrophic lateral sclerosis and result in motor neuron death.* Acta Neuropathol, 2015. **130**(1): p. 49-61.
244. Zhang, Y.J., et al., *Aberrant cleavage of TDP-43 enhances aggregation and cellular toxicity.* Proc Natl Acad Sci U S A, 2009. **106**(18): p. 7607-12.
245. Barmada, S.J., et al., *Cytoplasmic mislocalization of TDP-43 is toxic to neurons and enhanced by a mutation associated with familial amyotrophic lateral sclerosis.* J Neurosci, 2010. **30**(2): p. 639-49.
246. Winton, M.J., et al., *A90V TDP-43 variant results in the aberrant localization of TDP-43 in vitro.* FEBS Lett, 2008. **582**(15): p. 2252-6.
247. Winton, M.J., et al., *Disturbance of nuclear and cytoplasmic TAR DNA-binding protein (TDP-43) induces disease-like redistribution, sequestration, and aggregate formation.* J Biol Chem, 2008. **283**(19): p. 13302-9.
248. Strong, M.J., et al., *TDP43 is a human low molecular weight neurofilament (hNFL) mRNA-binding protein.* Mol Cell Neurosci, 2007. **35**(2): p. 320-7.
249. Lagier-Tourenne, C. and D.W. Cleveland, *Rethinking ALS: the FUS about TDP-43.* Cell, 2009. **136**(6): p. 1001-4.
250. Calvio, C., et al., *Identification of hnRNP P2 as TLS/FUS using electrospray mass spectrometry.* RNA, 1995. **1**(7): p. 724-33.
251. Morohoshi, F., et al., *Genomic structure of the human RBP56/hTAFII68 and FUS/TLS genes.* Gene, 1998. **221**(2): p. 191-8.

252. Andersson, M.K., et al., *The multifunctional FUS, EWS and TAF15 proto-oncoproteins show cell type-specific expression patterns and involvement in cell spreading and stress response.* BMC Cell Biol, 2008. **9**: p. 37.
253. Abhyankar, M.M., C. Urekar, and P.P. Reddi, *A novel CpG-free vertebrate insulator silences the testis-specific SP-10 gene in somatic tissues: role for TDP-43 in insulator function.* J Biol Chem, 2007. **282**(50): p. 36143-54.
254. Zinszner, H., R. Albalat, and D. Ron, *A novel effector domain from the RNA-binding protein TLS or EWS is required for oncogenic transformation by CHOP.* Genes Dev, 1994. **8**(21): p. 2513-26.
255. Yang, L., et al., *Self-assembled FUS binds active chromatin and regulates gene transcription.* Proc Natl Acad Sci U S A, 2014. **111**(50): p. 17809-14.
256. Prasad, D.D., et al., *TLS/FUS fusion domain of TLS/FUS-erg chimeric protein resulting from the t(16;21) chromosomal translocation in human myeloid leukemia functions as a transcriptional activation domain.* Oncogene, 1994. **9**(12): p. 3717-29.
257. Panagopoulos, I., et al., *Fusion of the FUS gene with ERG in acute myeloid leukemia with t(16;21)(p11;q22).* Genes Chromosomes Cancer, 1994. **11**(4): p. 256-62.
258. Tan, A.Y. and J.L. Manley, *TLS inhibits RNA polymerase III transcription.* Mol Cell Biol, 2010. **30**(1): p. 186-96.
259. Uranishi, H., et al., *Involvement of the pro-oncoprotein TLS (translocated in liposarcoma) in nuclear factor-kappa B p65-mediated transcription as a coactivator.* J Biol Chem, 2001. **276**(16): p. 13395-401.
260. Baechtold, H., et al., *Human 75-kDa DNA-pairing protein is identical to the pro-oncoprotein TLS/FUS and is able to promote D-loop formation.* J Biol Chem, 1999. **274**(48): p. 34337-42.
261. Wang, W.Y., et al., *Interaction of FUS and HDAC1 regulates DNA damage response and repair in neurons.* Nat Neurosci, 2013. **16**(10): p. 1383-91.
262. Rulten, S.L., et al., *PARP-1 dependent recruitment of the amyotrophic lateral sclerosis-associated protein FUS/TLS to sites of oxidative DNA damage.* Nucleic Acids Res, 2014. **42**(1): p. 307-14.
263. Mastrocola, A.S., et al., *The RNA-binding protein fused in sarcoma (FUS) functions downstream of poly(ADP-ribose) polymerase (PARP) in response to DNA damage.* J Biol Chem, 2013. **288**(34): p. 24731-41.
264. Buratti, E., et al., *Nuclear factor TDP-43 and SR proteins promote in vitro and in vivo CFTR exon 9 skipping.* EMBO J, 2001. **20**(7): p. 1774-84.
265. Mercado, P.A., et al., *Depletion of TDP 43 overrides the need for exonic and intronic splicing enhancers in the human apoA-II gene.* Nucleic Acids Res, 2005. **33**(18): p. 6000-10.
266. Bose, J.K., et al., *TDP-43 overexpression enhances exon 7 inclusion during the survival of motor neuron pre-mRNA splicing.* J Biol Chem, 2008. **283**(43): p. 28852-9.
267. Gerbino, V., et al., *Mislocalised FUS mutants stall spliceosomal snRNPs in the cytoplasm.* Neurobiol Dis, 2013. **55**: p. 120-8.
268. Yamazaki, T., et al., *FUS-SMN protein interactions link the motor neuron diseases ALS and SMA.* Cell Rep, 2012. **2**(4): p. 799-806.
269. Kim, S.H., et al., *Amyotrophic lateral sclerosis-associated proteins TDP-43 and FUS/TLS function in a common biochemical complex to co-regulate HDAC6 mRNA.* J Biol Chem, 2010. **285**(44): p. 34097-105.

270. Lagier-Tourenne, C., et al., *Divergent roles of ALS-linked proteins FUS/TLS and TDP-43 intersect in processing long pre-mRNAs.* Nat Neurosci, 2012. **15**(11): p. 1488-97.
271. Polymenidou, M., et al., *Long pre-mRNA depletion and RNA missplicing contribute to neuronal vulnerability from loss of TDP-43.* Nat Neurosci, 2011. **14**(4): p. 459-68.
272. Sephton, C.F., et al., *TDP-43 is a developmentally regulated protein essential for early embryonic development.* J Biol Chem, 2010. **285**(9): p. 6826-34.
273. Tollervey, J.R., et al., *Characterizing the RNA targets and position-dependent splicing regulation by TDP-43.* Nat Neurosci, 2011. **14**(4): p. 452-8.
274. Xiao, S., et al., *RNA targets of TDP-43 identified by UV-CLIP are deregulated in ALS.* Mol Cell Neurosci, 2011. **47**(3): p. 167-80.
275. Sephton, C.F., et al., *Identification of neuronal RNA targets of TDP-43-containing ribonucleoprotein complexes.* J Biol Chem, 2011. **286**(2): p. 1204-15.
276. Ayala, Y.M., et al., *TDP-43 regulates its mRNA levels through a negative feedback loop.* EMBO J, 2011. **30**(2): p. 277-88.
277. Rogelj, B., et al., *Widespread binding of FUS along nascent RNA regulates alternative splicing in the brain.* Sci Rep, 2012. **2**: p. 603.
278. Colombrita, C., et al., *From transcriptomic to protein level changes in TDP-43 and FUS loss-of-function cell models.* Biochim Biophys Acta, 2015. **1849**(12): p. 1398-410.
279. Hoell, J.I., et al., *RNA targets of wild-type and mutant FET family proteins.* Nat Struct Mol Biol, 2011. **18**(12): p. 1428-31.
280. Honda, D., et al., *The ALS/FTLD-related RNA-binding proteins TDP-43 and FUS have common downstream RNA targets in cortical neurons.* FEBS Open Bio, 2013. **4**: p. 1-10.
281. Ishigaki, S., et al., *Position-dependent FUS-RNA interactions regulate alternative splicing events and transcriptions.* Sci Rep, 2012. **2**: p. 529.
282. Nakaya, T., et al., *FUS regulates genes coding for RNA-binding proteins in neurons by binding to their highly conserved introns.* RNA, 2013. **19**(4): p. 498-509.
283. van Blitterswijk, M., et al., *Characterization of FUS mutations in amyotrophic lateral sclerosis using RNA-Seq.* PLoS One, 2013. **8**(4): p. e60788.
284. Orozco, D. and D. Edbauer, *FUS-mediated alternative splicing in the nervous system: consequences for ALS and FTLD.* J Mol Med (Berl), 2013. **91**(12): p. 1343-54.
285. Zhou, Y., et al., *ALS-associated FUS mutations result in compromised FUS alternative splicing and autoregulation.* PLoS Genet, 2013. **9**(10): p. e1003895.
286. Tan, Q., et al., *Extensive cryptic splicing upon loss of RBM17 and TDP43 in neurodegeneration models.* Hum Mol Genet, 2016. **25**(23): p. 5083-5093.
287. Humphrey, J., et al., *Quantitative analysis of cryptic splicing associated with TDP-43 depletion.* BMC Med Genomics, 2017. **10**(1): p. 38.
288. Ling, J.P., et al., *TDP-43 repression of nonconserved cryptic exons is compromised in ALS-FTD.* Science, 2015. **349**(6248): p. 650-5.
289. Jeong, Y.H., et al., *Tdp-43 cryptic exons are highly variable between cell types.* Mol Neurodegener, 2017. **12**(1): p. 13.
290. Lagier-Tourenne, C. and D.W. Cleveland, *Neurodegeneration: An expansion in ALS genetics.* Nature, 2010. **466**(7310): p. 1052-3.
291. Buratti, E., et al., *Nuclear factor TDP-43 can affect selected microRNA levels.* FEBS J, 2010. **277**(10): p. 2268-81.

292. Gregory, R.I., et al., *The Microprocessor complex mediates the genesis of microRNAs.* Nature, 2004. **432**(7014): p. 235-40.
293. Di Carlo, V., et al., *TDP-43 regulates the microprocessor complex activity during in vitro neuronal differentiation.* Mol Neurobiol, 2013. **48**(3): p. 952-63.
294. Morlando, M., et al., *FUS stimulates microRNA biogenesis by facilitating co-transcriptional Drosha recruitment.* EMBO J, 2012. **31**(24): p. 4502-10.
295. Dini Modigliani, S., et al., *An ALS-associated mutation in the FUS 3'-UTR disrupts a microRNA-FUS regulatory circuitry.* Nat Commun, 2014. **5**: p. 4335.
296. Volkening, K., et al., *Tar DNA binding protein of 43 kDa (TDP-43), 14-3-3 proteins and copper/zinc superoxide dismutase (SOD1) interact to modulate NFL mRNA stability. Implications for altered RNA processing in amyotrophic lateral sclerosis (ALS).* Brain Res, 2009. **1305**: p. 168-82.
297. Udagawa, T., et al., *FUS regulates AMPA receptor function and FTLD/ALS-associated behaviour via GluA1 mRNA stabilization.* Nat Commun, 2015. **6**: p. 7098.
298. Coyne, A.N., et al., *Futsch/MAP1B mRNA is a translational target of TDP-43 and is neuroprotective in a Drosophila model of amyotrophic lateral sclerosis.* J Neurosci, 2014. **34**(48): p. 15962-74.
299. Ishiguro, A., et al., *TDP-43 binds and transports G-quadruplex-containing mRNAs into neurites for local translation.* Genes Cells, 2016. **21**(5): p. 466-81.
300. Narayanan, R.K., et al., *Identification of RNA bound to the TDP-43 ribonucleoprotein complex in the adult mouse brain.* Amyotroph Lateral Scler Frontotemporal Degener, 2013. **14**(4): p. 252-60.
301. Wang, I.F., et al., *TDP-43, the signature protein of FTLD-U, is a neuronal activity-responsive factor.* J Neurochem, 2008. **105**(3): p. 797-806.
302. Alami, N.H., et al., *Axonal transport of TDP-43 mRNA granules is impaired by ALS-causing mutations.* Neuron, 2014. **81**(3): p. 536-543.
303. Belly, A., et al., *Delocalization of the multifunctional RNA splicing factor TLS/FUS in hippocampal neurones: exclusion from the nucleus and accumulation in dendritic granules and spine heads.* Neurosci Lett, 2005. **379**(3): p. 152-7.
304. Fujii, R. and T. Takumi, *TLS facilitates transport of mRNA encoding an actin-stabilizing protein to dendritic spines.* J Cell Sci, 2005. **118**(Pt 24): p. 5755-65.
305. Muresan, V. and Z. Ladescu Muresan, *Shared Molecular Mechanisms in Alzheimer's Disease and Amyotrophic Lateral Sclerosis: Neurofilament-Dependent Transport of sAPP, FUS, TDP-43 and SOD1, with Endoplasmic Reticulum-Like Tubules.* Neurodegener Dis, 2016. **16**(1-2): p. 55-61.
306. Yoshimura, A., et al., *Myosin-Va facilitates the accumulation of mRNA/protein complex in dendritic spines.* Curr Biol, 2006. **16**(23): p. 2345-51.
307. Izumikawa, K., et al., *TDP-43 stabilises the processing intermediates of mitochondrial transcripts.* Sci Rep, 2017. **7**(1): p. 7709.
308. Wang, W., et al., *The inhibition of TDP-43 mitochondrial localization blocks its neuronal toxicity.* Nat Med, 2016. **22**(8): p. 869-78.
309. Anderson, P. and N. Kedersha, *RNA granules: post-transcriptional and epigenetic modulators of gene expression.* Nat Rev Mol Cell Biol, 2009. **10**(6): p. 430-6.
310. Buchan, J.R. and R. Parker, *Eukaryotic stress granules: the ins and outs of translation.* Mol Cell, 2009. **36**(6): p. 932-41.

311. Aulas, A., S. Stabile, and C. Vande Velde, *Endogenous TDP-43, but not FUS, contributes to stress granule assembly via G3BP.* Mol Neurodegener, 2012. **7**: p. 54.
312. Khalfallah, Y., et al., *TDP-43 regulation of stress granule dynamics in neurodegenerative disease-relevant cell types.* Sci Rep, 2018. **8**(1): p. 7551.
313. McDonald, K.K., et al., *TAR DNA-binding protein 43 (TDP-43) regulates stress granule dynamics via differential regulation of G3BP and TIA-1.* Hum Mol Genet, 2011. **20**(7): p. 1400-10.
314. Colombrita, C., et al., *TDP-43 is recruited to stress granules in conditions of oxidative insult.* J Neurochem, 2009. **111**(4): p. 1051-61.
315. Liu-Yesucevitz, L., et al., *Tar DNA binding protein-43 (TDP-43) associates with stress granules: analysis of cultured cells and pathological brain tissue.* PLoS One, 2010. **5**(10): p. e13250.
316. Moisse, K., et al., *Cytosolic TDP-43 expression following axotomy is associated with caspase 3 activation in NFL-/- mice: support for a role for TDP-43 in the physiological response to neuronal injury.* Brain Res, 2009. **1296**: p. 176-86.
317. Bosco, D.A., et al., *Mutant FUS proteins that cause amyotrophic lateral sclerosis incorporate into stress granules.* Hum Mol Genet, 2010. **19**(21): p. 4160-75.
318. Daigle, J.G., et al., *RNA-binding ability of FUS regulates neurodegeneration, cytoplasmic mislocalization and incorporation into stress granules associated with FUS carrying ALS-linked mutations.* Hum Mol Genet, 2013. **22**(6): p. 1193-205.
319. Dormann, D., et al., *ALS-associated fused in sarcoma (FUS) mutations disrupt Transportin-mediated nuclear import.* EMBO J, 2010. **29**(16): p. 2841-57.
320. Sama, R.R., et al., *FUS/TLS assembles into stress granules and is a prosurvival factor during hyperosmolar stress.* J Cell Physiol, 2013. **228**(11): p. 2222-31.
321. Bentmann, E., et al., *Requirements for stress granule recruitment of fused in sarcoma (FUS) and TAR DNA-binding protein of 43 kDa (TDP-43).* J Biol Chem, 2012. **287**(27): p. 23079-94.
322. Geser, F., et al., *Pathological TDP-43 in parkinsonism-dementia complex and amyotrophic lateral sclerosis of Guam.* Acta Neuropathol, 2008. **115**(1): p. 133-45.
323. Giordana, M.T., et al., *TDP-43 redistribution is an early event in sporadic amyotrophic lateral sclerosis.* Brain Pathol, 2010. **20**(2): p. 351-60.
324. Pamphlett, R., et al., *TDP-43 neuropathology is similar in sporadic amyotrophic lateral sclerosis with or without TDP-43 mutations.* Neuropathol Appl Neurobiol, 2009. **35**(2): p. 222-5.
325. Van Deerlin, V.M., et al., *TARDBP mutations in amyotrophic lateral sclerosis with TDP-43 neuropathology: a genetic and histopathological analysis.* Lancet Neurol, 2008. **7**(5): p. 409-16.
326. Yokoseki, A., et al., *TDP-43 mutation in familial amyotrophic lateral sclerosis.* Ann Neurol, 2008. **63**(4): p. 538-42.
327. Dickson, D.W., *TDP-43 immunoreactivity in neurodegenerative disorders: disease versus mechanism specificity.* Acta Neuropathol, 2008. **115**(1): p. 147-9.
328. Igaz, L.M., et al., *Enrichment of C-terminal fragments in TAR DNA-binding protein-43 cytoplasmic inclusions in brain but not in spinal cord of frontotemporal lobar degeneration and amyotrophic lateral sclerosis.* Am J Pathol, 2008. **173**(1): p. 182-94.

329. Mackenzie, I.R., et al., *Pathological TDP-43 distinguishes sporadic amyotrophic lateral sclerosis from amyotrophic lateral sclerosis with SOD1 mutations.* Ann Neurol, 2007. **61**(5): p. 427-34.
330. Neumann, M., et al., *TDP-43 proteinopathy in frontotemporal lobar degeneration and amyotrophic lateral sclerosis: protein misfolding diseases without amyloidosis.* Arch Neurol, 2007. **64**(10): p. 1388-94.
331. Arai, T., et al., *Phosphorylated and cleaved TDP-43 in ALS, FTLD and other neurodegenerative disorders and in cellular models of TDP-43 proteinopathy.* Neuropathology, 2010. **30**(2): p. 170-81.
332. Neumann, M., *Molecular neuropathology of TDP-43 proteinopathies.* Int J Mol Sci, 2009. **10**(1): p. 232-46.
333. Kwong, L.K., et al., *TDP-43 proteinopathies: neurodegenerative protein misfolding diseases without amyloidosis.* Neurosignals, 2008. **16**(1): p. 41-51.
334. Blair, I.P., et al., *FUS mutations in amyotrophic lateral sclerosis: clinical, pathological, neurophysiological and genetic analysis.* J Neurol Neurosurg Psychiatry, 2010. **81**(6): p. 639-45.
335. Tan, C.F., et al., *TDP-43 immunoreactivity in neuronal inclusions in familial amyotrophic lateral sclerosis with or without SOD1 gene mutation.* Acta Neuropathol, 2007. **113**(5): p. 535-42.
336. Mackenzie, I.R., R. Rademakers, and M. Neumann, *TDP-43 and FUS in amyotrophic lateral sclerosis and frontotemporal dementia.* Lancet Neurol, 2010. **9**(10): p. 995-1007.
337. Amador-Ortiz, C., et al., *TDP-43 immunoreactivity in hippocampal sclerosis and Alzheimer's disease.* Ann Neurol, 2007. **61**(5): p. 435-45.
338. Higashi, S., et al., *Concurrence of TDP-43, tau and alpha-synuclein pathology in brains of Alzheimer's disease and dementia with Lewy bodies.* Brain Res, 2007. **1184**: p. 284-94.
339. King, A., et al., *Abnormal TDP-43 expression is identified in the neocortex in cases of dementia pugilistica, but is mainly confined to the limbic system when identified in high and moderate stages of Alzheimer's disease.* Neuropathology, 2010. **30**(4): p. 408-19.
340. Nakashima-Yasuda, H., et al., *Co-morbidity of TDP-43 proteinopathy in Lewy body related diseases.* Acta Neuropathol, 2007. **114**(3): p. 221-9.
341. Schwab, C., et al., *Colocalization of transactivation-responsive DNA-binding protein 43 and huntingtin in inclusions of Huntington disease.* J Neuropathol Exp Neurol, 2008. **67**(12): p. 1159-65.
342. Geser, F., et al., *Pathological 43-kDa transactivation response DNA-binding protein in older adults with and without severe mental illness.* Arch Neurol, 2010. **67**(10): p. 1238-50.
343. Caroppo, P., et al., *Defining the spectrum of frontotemporal dementias associated with TARDBP mutations.* Neurol Genet, 2016. **2**(3): p. e80.
344. Gitcho, M.A., et al., *TDP-43 A315T mutation in familial motor neuron disease.* Ann Neurol, 2008. **63**(4): p. 535-8.
345. Benajiba, L., et al., *TARDBP mutations in motoneuron disease with frontotemporal lobar degeneration.* Ann Neurol, 2009. **65**(4): p. 470-3.

346. Millecamps, S., et al., *SOD1, ANG, VAPB, TARDBP, and FUS mutations in familial amyotrophic lateral sclerosis: genotype-phenotype correlations.* J Med Genet, 2010. **47**(8): p. 554-60.
347. Borghero, G., et al., *Genetic architecture of ALS in Sardinia.* Neurobiol Aging, 2014. **35**(12): p. 2882 e7-2882 e12.
348. Buratti, E., *Functional Significance of TDP-43 Mutations in Disease.* Adv Genet, 2015. **91**: p. 1-53.
349. Daoud, H., et al., *Contribution of TARDBP mutations to sporadic amyotrophic lateral sclerosis.* J Med Genet, 2009. **46**(2): p. 112-4.
350. Kirby, J., et al., *Broad clinical phenotypes associated with TAR-DNA binding protein (TARDBP) mutations in amyotrophic lateral sclerosis.* Neurogenetics, 2010. **11**(2): p. 217-25.
351. Moreno, F., et al., *A novel mutation P112H in the TARDBP gene associated with frontotemporal lobar degeneration without motor neuron disease and abundant neuritic amyloid plaques.* Acta Neuropathol Commun, 2015. **3**: p. 19.
352. Maurel, C., et al., *Mutation in the RRM2 domain of TDP-43 in Amyotrophic Lateral Sclerosis with rapid progression associated with ubiquitin positive aggregates in cultured motor neurons.* Amyotroph Lateral Scler Frontotemporal Degener, 2018. **19**(1-2): p. 149-151.
353. Chiang, C.H., et al., *Structural analysis of disease-related TDP-43 D169G mutation: linking enhanced stability and caspase cleavage efficiency to protein accumulation.* Sci Rep, 2016. **6**: p. 21581.
354. Kuo, P.H., et al., *The crystal structure of TDP-43 RRM1-DNA complex reveals the specific recognition for UG- and TG-rich nucleic acids.* Nucleic Acids Res, 2014. **42**(7): p. 4712-22.
355. Deng, H.X., et al., *FUS-immunoreactive inclusions are a common feature in sporadic and non-SOD1 familial amyotrophic lateral sclerosis.* Ann Neurol, 2010. **67**(6): p. 739-48.
356. Gao, F.B., S. Almeida, and R. Lopez-Gonzalez, *Dysregulated molecular pathways in amyotrophic lateral sclerosis-frontotemporal dementia spectrum disorder.* EMBO J, 2017. **36**(20): p. 2931-2950.
357. Mackenzie, I.R., et al., *Pathological heterogeneity in amyotrophic lateral sclerosis with FUS mutations: two distinct patterns correlating with disease severity and mutation.* Acta Neuropathol, 2011. **122**(1): p. 87-98.
358. Neumann, M., et al., *Abundant FUS-immunoreactive pathology in neuronal intermediate filament inclusion disease.* Acta Neuropathol, 2009. **118**(5): p. 605-16.
359. Ticozzi, N., et al., *Analysis of FUS gene mutation in familial amyotrophic lateral sclerosis within an Italian cohort.* Neurology, 2009. **73**(15): p. 1180-5.
360. Doi, H., et al., *The RNA-binding protein FUS/TLS is a common aggregate-interacting protein in polyglutamine diseases.* Neurosci Res, 2010. **66**(1): p. 131-3.
361. Woulfe, J., D.A. Gray, and I.R. Mackenzie, *FUS-immunoreactive intranuclear inclusions in neurodegenerative disease.* Brain Pathol, 2010. **20**(3): p. 589-97.
362. Deng, H., K. Gao, and J. Jankovic, *The role of FUS gene variants in neurodegenerative diseases.* Nat Rev Neurol, 2014. **10**(6): p. 337-48.

363. Suzuki, N., et al., *FUS/TLS-immunoreactive neuronal and glial cell inclusions increase with disease duration in familial amyotrophic lateral sclerosis with an R521C FUS/TLS mutation.* J Neuropathol Exp Neurol, 2012. **71**(9): p. 779-88.
364. Baumer, D., et al., *Juvenile ALS with basophilic inclusions is a FUS proteinopathy with FUS mutations.* Neurology, 2010. **75**(7): p. 611-8.
365. Lattante, S., G.A. Rouleau, and E. Kabashi, *TARDBP and FUS mutations associated with amyotrophic lateral sclerosis: summary and update.* Hum Mutat, 2013. **34**(6): p. 812-26.
366. Millecamps, S., et al., *Phenotype difference between ALS patients with expanded repeats in C9ORF72 and patients with mutations in other ALS-related genes.* J Med Genet, 2012. **49**(4): p. 258-63.
367. Hewitt, C., et al., *Novel FUS/TLS mutations and pathology in familial and sporadic amyotrophic lateral sclerosis.* Arch Neurol, 2010. **67**(4): p. 455-61.
368. Sabatelli, M., et al., *Mutations in the 3' untranslated region of FUS causing FUS overexpression are associated with amyotrophic lateral sclerosis.* Hum Mol Genet, 2013. **22**(23): p. 4748-55.
369. Hamilton, F., *An account of the fishes found in the river Ganges and its branches*. 1822, Edinburgh & London.
370. Spence, R., et al., *The behaviour and ecology of the zebrafish, Danio rerio.* Biol Rev Camb Philos Soc, 2008. **83**(1): p. 13-34.
371. Haffter, P. and C. Nusslein-Volhard, *Large scale genetics in a small vertebrate, the zebrafish.* Int J Dev Biol, 1996. **40**(1): p. 221-7.
372. Nasevicius, A. and S.C. Ekker, *Effective targeted gene 'knockdown' in zebrafish.* Nat Genet, 2000. **26**(2): p. 216-20.
373. Hales, K.G., et al., *Genetics on the Fly: A Primer on the Drosophila Model System.* Genetics, 2015. **201**(3): p. 815-42.
374. Markaki, M. and N. Tavernarakis, *Modeling human diseases in Caenorhabditis elegans.* Biotechnol J, 2010. **5**(12): p. 1261-76.
375. Detrich, H.W., 3rd and D.A. Yergeau, *Comparative genomics in erythropoietic gene discovery: synergisms between the Antarctic icefishes and the zebrafish.* Methods Cell Biol, 2004. **77**: p. 475-503.
376. Hisaoka, K.K., *The effects of 2-acetylaminofluorene on the embryonic development of the zebrafish. II. Histochemical studies.* Cancer Res, 1958. **18**(6): p. 664-7.
377. Agranoff, B.W. and P.D. Klinger, *PUROMYCIN EFFECT ON MEMORY FIXATION IN THE GOLDFISH.* Science, 1964. **146**(3646): p. 952-3.
378. Skidmore, J.F., *Resistance to zinc sulphate of the zebrafish (Brachydanio rerio Hamilton-Buchanan) at different phases of its life history.* Ann Appl Biol, 1965. **56**(1): p. 47-53.
379. Harvey, B. and O. Zakutnyaya, *Russian Space Probes: Scientific Discoveries and Future Missions*. 2011: Springer Praxis Books / Space Exploration.
380. Dubinin, N.P., et al., *Biological experiments on the orbital station Salyut 4.* Life Sci Space Res, 1977. **15**: p. 267-72.
381. Vaulina, E.N., et al., *Biological investigations on the orbital station "Salyut-5".* Life Sci Space Res, 1979. **17**: p. 241-6.
382. Streisinger, G., et al., *Production of clones of homozygous diploid zebra fish (Brachydanio rerio).* Nature, 1981. **291**(5813): p. 293-6.

383. Walker, C. and G. Streisinger, *Induction of Mutations by gamma-Rays in Pregonial Germ Cells of Zebrafish Embryos.* Genetics, 1983. **103**(1): p. 125-36.
384. Stuart, G.W., J.V. McMurray, and M. Westerfield, *Replication, integration and stable germ-line transmission of foreign sequences injected into early zebrafish embryos.* Development, 1988. **103**(2): p. 403-12.
385. Streisinger, G., et al., *Segregation analyses and gene-centromere distances in zebrafish.* Genetics, 1986. **112**(2): p. 311-9.
386. Etchin, J., J.P. Kanki, and A.T. Look, *Zebrafish as a model for the study of human cancer.* Methods Cell Biol, 2011. **105**: p. 309-37.
387. Bakkers, J., *Zebrafish as a model to study cardiac development and human cardiac disease.* Cardiovasc Res, 2011. **91**(2): p. 279-88.
388. Cui, C., et al., *Infectious disease modeling and innate immune function in zebrafish embryos.* Methods Cell Biol, 2011. **105**: p. 273-308.
389. Bibliowicz, J., R.K. Tittle, and J.M. Gross, *Toward a better understanding of human eye disease insights from the zebrafish, Danio rerio.* Prog Mol Biol Transl Sci, 2011. **100**: p. 287-330.
390. Lieschke, G.J. and P.D. Currie, *Animal models of human disease: zebrafish swim into view.* Nat Rev Genet, 2007. **8**(5): p. 353-67.
391. Brennan, C.H., *Zebrafish behavioural assays of translational relevance for the study of psychiatric disease.* Rev Neurosci, 2011. **22**(1): p. 37-48.
392. Patten, S.A., et al., *Fishing for causes and cures of motor neuron disorders.* Dis Model Mech, 2014. **7**(7): p. 799-809.
393. Beattie, C.E., *Control of motor axon guidance in the zebrafish embryo.* Brain Res Bull, 2000. **53**(5): p. 489-500.
394. Drapeau, P., et al., *Development of the locomotor network in zebrafish.* Prog Neurobiol, 2002. **68**(2): p. 85-111.
395. Kimmel, C.B., et al., *Stages of embryonic development of the zebrafish.* Dev Dyn, 1995. **203**(3): p. 253-310.
396. Fetcho, J.R., S. Higashijima, and D.L. McLean, *Zebrafish and motor control over the last decade.* Brain Res Rev, 2008. **57**(1): p. 86-93.
397. Parichy, D.M., et al., *Normal table of postembryonic zebrafish development: staging by externally visible anatomy of the living fish.* Dev Dyn, 2009. **238**(12): p. 2975-3015.
398. Singleman, C. and N.G. Holtzman, *Growth and maturation in the zebrafish, Danio rerio: a staging tool for teaching and research.* Zebrafish, 2014. **11**(4): p. 396-406.
399. Wilson, C., *Aspects of larval rearing.* ILAR J, 2012. **53**(2): p. 169-78.
400. Orger, M.B. and G.G. de Polavieja, *Zebrafish Behavior: Opportunities and Challenges.* Annu Rev Neurosci, 2017. **40**: p. 125-147.
401. Gilbert, N., et al., *Formation of facultative heterochromatin in the absence of HP1.* EMBO J, 2003. **22**(20): p. 5540-50.
402. Bernhardt, R.R., et al., *Identification of spinal neurons in the embryonic and larval zebrafish.* J Comp Neurol, 1990. **302**(3): p. 603-16.
403. Kuwada, J.Y., R.R. Bernhardt, and N. Nguyen, *Development of spinal neurons and tracts in the zebrafish embryo.* J Comp Neurol, 1990. **302**(3): p. 617-28.
404. Eisen, J.S., P.Z. Myers, and M. Westerfield, *Pathway selection by growth cones of identified motoneurones in live zebra fish embryos.* Nature, 1986. **320**(6059): p. 269-71.

405. Kimmel, C.B., R.M. Warga, and D.A. Kane, *Cell cycles and clonal strings during formation of the zebrafish central nervous system.* Development, 1994. **120**(2): p. 265-76.
406. Myers, P.Z., J.S. Eisen, and M. Westerfield, *Development and axonal outgrowth of identified motoneurons in the zebrafish.* J Neurosci, 1986. **6**(8): p. 2278-89.
407. Fetcho, J.R. and D.M. O'Malley, *Visualization of active neural circuitry in the spinal cord of intact zebrafish.* J Neurophysiol, 1995. **73**(1): p. 399-406.
408. McLean, D.L., et al., *A topographic map of recruitment in spinal cord.* Nature, 2007. **446**(7131): p. 71-5.
409. Eisen, J.S., S.H. Pike, and B. Romancier, *An identified motoneuron with variable fates in embryonic zebrafish.* J Neurosci, 1990. **10**(1): p. 34-43.
410. Eisen, J.S., *The role of interactions in determining cell fate of two identified motoneurons in the embryonic zebrafish.* Neuron, 1992. **8**(2): p. 231-40.
411. Eisen, J.S. and E. Melancon, *Interactions with identified muscle cells break motoneuron equivalence in embryonic zebrafish.* Nat Neurosci, 2001. **4**(11): p. 1065-70.
412. Pike, S.H., E.F. Melancon, and J.S. Eisen, *Pathfinding by zebrafish motoneurons in the absence of normal pioneer axons.* Development, 1992. **114**(4): p. 825-31.
413. Eisen, J.S., *Development of motoneuronal phenotype.* Annu Rev Neurosci, 1994. **17**: p. 1-30.
414. Liu, D.W. and M. Westerfield, *Function of identified motoneurones and co-ordination of primary and secondary motor systems during zebra fish swimming.* J Physiol, 1988. **403**: p. 73-89.
415. Buss, R.R. and P. Drapeau, *Synaptic drive to motoneurons during fictive swimming in the developing zebrafish.* J Neurophysiol, 2001. **86**(1): p. 197-210.
416. Fetcho, J.R., *The spinal motor system in early vertebrates and some of its evolutionary changes.* Brain Behav Evol, 1992. **40**(2-3): p. 82-97.
417. Coutelle, O., et al., *Hedgehog signalling is required for maintenance of myf5 and myoD expression and timely terminal differentiation in zebrafish adaxial myogenesis.* Dev Biol, 2001. **236**(1): p. 136-50.
418. Devoto, S.H., et al., *Identification of separate slow and fast muscle precursor cells in vivo, prior to somite formation.* Development, 1996. **122**(11): p. 3371-80.
419. Weinberg, E.S., et al., *Developmental regulation of zebrafish MyoD in wild-type, no tail and spadetail embryos.* Development, 1996. **122**(1): p. 271-80.
420. Roy, S., C. Wolff, and P.W. Ingham, *The u-boot mutation identifies a Hedgehog-regulated myogenic switch for fiber-type diversification in the zebrafish embryo.* Genes Dev, 2001. **15**(12): p. 1563-76.
421. Stellabotte, F., et al., *Dynamic somite cell rearrangements lead to distinct waves of myotome growth.* Development, 2007. **134**(7): p. 1253-7.
422. Saint-Amant, L. and P. Drapeau, *Synchronization of an embryonic network of identified spinal interneurons solely by electrical coupling.* Neuron, 2001. **31**(6): p. 1035-46.
423. Saint-Amant, L. and P. Drapeau, *Motoneuron activity patterns related to the earliest behavior of the zebrafish embryo.* J Neurosci, 2000. **20**(11): p. 3964-72.
424. Saint-Amant, L. and P. Drapeau, *Time course of the development of motor behaviors in the zebrafish embryo.* J Neurobiol, 1998. **37**(4): p. 622-32.

425. Naganawa, Y. and H. Hirata, *Developmental transition of touch response from slow muscle-mediated coilings to fast muscle-mediated burst swimming in zebrafish.* Dev Biol, 2011. **355**(2): p. 194-204.
426. Westerfield, M., J.V. McMurray, and J.S. Eisen, *Identified motoneurons and their innervation of axial muscles in the zebrafish.* J Neurosci, 1986. **6**(8): p. 2267-77.
427. Lefebvre, J.L., et al., *Increased neuromuscular activity causes axonal defects and muscular degeneration.* Development, 2004. **131**(11): p. 2605-18.
428. Liu, D.W. and M. Westerfield, *Clustering of muscle acetylcholine receptors requires motoneurons in live embryos, but not in cell culture.* J Neurosci, 1992. **12**(5): p. 1859-66.
429. Westerfield, M., et al., *Pathfinding and synapse formation in a zebrafish mutant lacking functional acetylcholine receptors.* Neuron, 1990. **4**(6): p. 867-74.
430. Behra, M., et al., *Acetylcholinesterase is required for neuronal and muscular development in the zebrafish embryo.* Nat Neurosci, 2002. **5**(2): p. 111-8.
431. Pietri, T., et al., *Glutamate drives the touch response through a rostral loop in the spinal cord of zebrafish embryos.* Dev Neurobiol, 2009. **69**(12): p. 780-95.
432. Hirata, H., et al., *Connexin 39.9 protein is necessary for coordinated activation of slow-twitch muscle and normal behavior in zebrafish.* J Biol Chem, 2012. **287**(2): p. 1080-9.
433. Knogler, L.D., et al., *A hybrid electrical/chemical circuit in the spinal cord generates a transient embryonic motor behavior.* J Neurosci, 2014. **34**(29): p. 9644-55.
434. Postlethwait, J.H., et al., *A genetic linkage map for the zebrafish.* Science, 1994. **264**(5159): p. 699-703.
435. Johnson, S.L., et al., *Identification of RAPD primers that reveal extensive polymorphisms between laboratory strains of zebrafish.* Genomics, 1994. **19**(1): p. 152-6.
436. Howe, K., et al., *The zebrafish reference genome sequence and its relationship to the human genome.* Nature, 2013. **496**(7446): p. 498-503.
437. Christoffels, A., et al., *Fugu genome analysis provides evidence for a whole-genome duplication early during the evolution of ray-finned fishes.* Mol Biol Evol, 2004. **21**(6): p. 1146-51.
438. Meyer, A. and M. Schartl, *Gene and genome duplications in vertebrates: the one-to-four (-to-eight in fish) rule and the evolution of novel gene functions.* Curr Opin Cell Biol, 1999. **11**(6): p. 699-704.
439. Vandepoele, K., et al., *Major events in the genome evolution of vertebrates: paranome age and size differ considerably between ray-finned fishes and land vertebrates.* Proc Natl Acad Sci U S A, 2004. **101**(6): p. 1638-43.
440. Lu, J., et al., *Profiling of gene duplication patterns of sequenced teleost genomes: evidence for rapid lineage-specific genome expansion mediated by recent tandem duplications.* BMC Genomics, 2012. **13**: p. 246.
441. Venter, J.C., et al., *The sequence of the human genome.* Science, 2001. **291**(5507): p. 1304-51.
442. Pertea, M. and S.L. Salzberg, *Between a chicken and a grape: estimating the number of human genes.* Genome Biol, 2010. **11**(5): p. 206.
443. McCallum, C.M., et al., *Targeted screening for induced mutations.* Nat Biotechnol, 2000. **18**(4): p. 455-7.

444. Colbert, T., et al., *High-throughput screening for induced point mutations.* Plant Physiol, 2001. **126**(2): p. 480-4.
445. Wienholds, E., et al., *Target-selected inactivation of the zebrafish rag1 gene.* Science, 2002. **297**(5578): p. 99-102.
446. Wienholds, E., et al., *Efficient target-selected mutagenesis in zebrafish.* Genome Res, 2003. **13**(12): p. 2700-7.
447. Hewamadduma, C.A., et al., *Tardbpl splicing rescues motor neuron and axonal development in a mutant tardbp zebrafish.* Hum Mol Genet, 2013. **22**(12): p. 2376-86.
448. Kawakami, K. and A. Shima, *Identification of the Tol2 transposase of the medaka fish Oryzias latipes that catalyzes excision of a nonautonomous Tol2 element in zebrafish Danio rerio.* Gene, 1999. **240**(1): p. 239-44.
449. Kawakami, K., A. Shima, and N. Kawakami, *Identification of a functional transposase of the Tol2 element, an Ac-like element from the Japanese medaka fish, and its transposition in the zebrafish germ lineage.* Proc Natl Acad Sci U S A, 2000. **97**(21): p. 11403-8.
450. Koga, A., et al., *Transposable element in fish.* Nature, 1996. **383**(6595): p. 30.
451. Urasaki, A., G. Morvan, and K. Kawakami, *Functional dissection of the Tol2 transposable element identified the minimal cis-sequence and a highly repetitive sequence in the subterminal region essential for transposition.* Genetics, 2006. **174**(2): p. 639-49.
452. Kwan, K.M., et al., *The Tol2kit: a multisite gateway-based construction kit for Tol2 transposon transgenesis constructs.* Dev Dyn, 2007. **236**(11): p. 3088-99.
453. Villefranc, J.A., J. Amigo, and N.D. Lawson, *Gateway compatible vectors for analysis of gene function in the zebrafish.* Dev Dyn, 2007. **236**(11): p. 3077-87.
454. Huang, C.J., et al., *Germ-line transmission of a myocardium-specific GFP transgene reveals critical regulatory elements in the cardiac myosin light chain 2 promoter of zebrafish.* Dev Dyn, 2003. **228**(1): p. 30-40.
455. Park, H.C., et al., *Analysis of upstream elements in the HuC promoter leads to the establishment of transgenic zebrafish with fluorescent neurons.* Dev Biol, 2000. **227**(2): p. 279-93.
456. Halloran, M.C., et al., *Laser-induced gene expression in specific cells of transgenic zebrafish.* Development, 2000. **127**(9): p. 1953-60.
457. Summerton, J., *Morpholino antisense oligomers: the case for an RNase H-independent structural type.* Biochim Biophys Acta, 1999. **1489**(1): p. 141-58.
458. Summerton, J. and D. Weller, *Morpholino antisense oligomers: design, preparation, and properties.* Antisense Nucleic Acid Drug Dev, 1997. **7**(3): p. 187-95.
459. Bill, B.R., et al., *A primer for morpholino use in zebrafish.* Zebrafish, 2009. **6**(1): p. 69-77.
460. Draper, B.W., P.A. Morcos, and C.B. Kimmel, *Inhibition of zebrafish fgf8 pre-mRNA splicing with morpholino oligos: a quantifiable method for gene knockdown.* Genesis, 2001. **30**(3): p. 154-6.
461. Eisen, J.S. and J.C. Smith, *Controlling morpholino experiments: don't stop making antisense.* Development, 2008. **135**(10): p. 1735-43.
462. Robu, M.E., et al., *p53 activation by knockdown technologies.* PLoS Genet, 2007. **3**(5): p. e78.

463. Kok, F.O., et al., *Reverse genetic screening reveals poor correlation between morpholino-induced and mutant phenotypes in zebrafish.* Dev Cell, 2015. **32**(1): p. 97-108.
464. Rossi, A., et al., *Genetic compensation induced by deleterious mutations but not gene knockdowns.* Nature, 2015. **524**(7564): p. 230-3.
465. Gros-Louis, F., et al., *Als2 mRNA splicing variants detected in KO mice rescue severe motor dysfunction phenotype in Als2 knock-down zebrafish.* Hum Mol Genet, 2008. **17**(17): p. 2691-702.
466. Kabashi, E., et al., *Gain and loss of function of ALS-related mutations of TARDBP (TDP-43) cause motor deficits in vivo.* Hum Mol Genet, 2010. **19**(4): p. 671-83.
467. Sertori, R., et al., *Genome editing in zebrafish: a practical overview.* Brief Funct Genomics, 2016. **15**(4): p. 322-30.
468. Kim, Y.G., J. Cha, and S. Chandrasegaran, *Hybrid restriction enzymes: zinc finger fusions to Fok I cleavage domain.* Proc Natl Acad Sci U S A, 1996. **93**(3): p. 1156-60.
469. Meng, X., et al., *Targeted gene inactivation in zebrafish using engineered zinc-finger nucleases.* Nat Biotechnol, 2008. **26**(6): p. 695-701.
470. Urnov, F.D., et al., *Genome editing with engineered zinc finger nucleases.* Nat Rev Genet, 2010. **11**(9): p. 636-46.
471. Schmid, B., et al., *Loss of ALS-associated TDP-43 in zebrafish causes muscle degeneration, vascular dysfunction, and reduced motor neuron axon outgrowth.* Proc Natl Acad Sci U S A, 2013. **110**(13): p. 4986-91.
472. Boch, J., et al., *Breaking the code of DNA binding specificity of TAL-type III effectors.* Science, 2009. **326**(5959): p. 1509-12.
473. Ott de Bruin, L.M., S. Volpi, and K. Musunuru, *Novel Genome-Editing Tools to Model and Correct Primary Immunodeficiencies.* Front Immunol, 2015. **6**: p. 250.
474. Jinek, M., et al., *A programmable dual-RNA-guided DNA endonuclease in adaptive bacterial immunity.* Science, 2012. **337**(6096): p. 816-21.
475. Garneau, J.E., et al., *The CRISPR/Cas bacterial immune system cleaves bacteriophage and plasmid DNA.* Nature, 2010. **468**(7320): p. 67-71.
476. Lebedeva, S., et al., *Characterization of genetic loss-of-function of Fus in zebrafish.* RNA Biol, 2017. **14**(1): p. 29-35.
477. Hruscha, A., et al., *Efficient CRISPR/Cas9 genome editing with low off-target effects in zebrafish.* Development, 2013. **140**(24): p. 4982-7.
478. Armstrong, G.A., et al., *Homology Directed Knockin of Point Mutations in the Zebrafish tardbp and fus Genes in ALS Using the CRISPR/Cas9 System.* PLoS One, 2016. **11**(3): p. e0150188.
479. Stepanova, T., et al., *Visualization of microtubule growth in cultured neurons via the use of EB3-GFP (end-binding protein 3-green fluorescent protein).* J Neurosci, 2003. **23**(7): p. 2655-64.
480. Vaccaro, A., et al., *Pharmacological reduction of ER stress protects against TDP-43 neuronal toxicity in vivo.* Neurobiol Dis, 2013. **55**: p. 64-75.
481. Laird, A.S., et al., *Progranulin is neurotrophic in vivo and protects against a mutant TDP-43 induced axonopathy.* PLoS One, 2010. **5**(10): p. e13368.
482. Chitramuthu, B.P., et al., *Neurotrophic effects of progranulin in vivo in reversing motor neuron defects caused by over or under expression of TDP-43 or FUS.* PLoS One, 2017. **12**(3): p. e0174784.

483. Van Hoecke, A., et al., *EPHA4 is a disease modifier of amyotrophic lateral sclerosis in animal models and in humans.* Nat Med, 2012. **18**(9): p. 1418-22.
484. Armstrong, G.A. and P. Drapeau, *Calcium channel agonists protect against neuromuscular dysfunction in a genetic model of TDP-43 mutation in ALS.* J Neurosci, 2013. **33**(4): p. 1741-52.
485. Vaccaro, A., et al., *Methylene blue protects against TDP-43 and FUS neuronal toxicity in C. elegans and D. rerio.* PLoS One, 2012. **7**(7): p. e42117.
486. Patten, S.A., et al., *Neuroleptics as therapeutic compounds stabilizing neuromuscular transmission in amyotrophic lateral sclerosis.* JCI Insight, 2017. **2**(22).
487. Dzieciolowska, S., P. Drapeau, and G.A.B. Armstrong, *Augmented quantal release of acetylcholine at the vertebrate neuromuscular junction following tdp-43 depletion.* PLoS One, 2017. **12**(5): p. e0177005.
488. Acosta, J.R., et al., *Mutant human FUS Is ubiquitously mislocalized and generates persistent stress granules in primary cultured transgenic zebrafish cells.* PLoS One, 2014. **9**(6): p. e90572.
489. Kabashi, E., et al., *FUS and TARDBP but not SOD1 interact in genetic models of amyotrophic lateral sclerosis.* PLoS Genet, 2011. **7**(8): p. e1002214.
490. Armstrong, G.A. and P. Drapeau, *Loss and gain of FUS function impair neuromuscular synaptic transmission in a genetic model of ALS.* Hum Mol Genet, 2013. **22**(21): p. 4282-92.
491. Julien, C., et al., *Conserved pharmacological rescue of hereditary spastic paraplegia-related phenotypes across model organisms.* Hum Mol Genet, 2016. **25**(6): p. 1088-99.
492. Gan-Or, Z., et al., *Mutations in CAPN1 Cause Autosomal-Recessive Hereditary Spastic Paraplegia.* Am J Hum Genet, 2016. **98**(5): p. 1038-1046.
493. Halperin, L., J. Jung, and M. Michalak, *The many functions of the endoplasmic reticulum chaperones and folding enzymes.* IUBMB Life, 2014. **66**(5): p. 318-26.
494. Remondelli, P. and M. Renna, *The Endoplasmic Reticulum Unfolded Protein Response in Neurodegenerative Disorders and Its Potential Therapeutic Significance.* Front Mol Neurosci, 2017. **10**: p. 187.
495. Hetz, C. and S. Saxena, *ER stress and the unfolded protein response in neurodegeneration.* Nat Rev Neurol, 2017. **13**(8): p. 477-491.
496. Morris, G., et al., *The Endoplasmic Reticulum Stress Response in Neuroprogressive Diseases: Emerging Pathophysiological Role and Translational Implications.* Mol Neurobiol, 2018.
497. Schroder, M. and R.J. Kaufman, *The mammalian unfolded protein response.* Annu Rev Biochem, 2005. **74**: p. 739-89.
498. Bravo, R., et al., *Endoplasmic reticulum: ER stress regulates mitochondrial bioenergetics.* Int J Biochem Cell Biol, 2012. **44**(1): p. 16-20.
499. Viana, R.J., A.F. Nunes, and C.M. Rodrigues, *Endoplasmic reticulum enrollment in Alzheimer's disease.* Mol Neurobiol, 2012. **46**(2): p. 522-34.
500. Tadic, V., et al., *The ER mitochondria calcium cycle and ER stress response as therapeutic targets in amyotrophic lateral sclerosis.* Front Cell Neurosci, 2014. **8**: p. 147.
501. Mannan, A.U., et al., *ZFYVE27 (SPG33), a novel spastin-binding protein, is mutated in hereditary spastic paraplegia.* Am J Hum Genet, 2006. **79**(2): p. 351-7.

502. Hashimoto, Y., et al., *Protrudin regulates endoplasmic reticulum morphology and function associated with the pathogenesis of hereditary spastic paraplegia.* J Biol Chem, 2014. **289**(19): p. 12946-61.
503. Guo, W.J. and T.H. Ho, *An abscisic acid-induced protein, HVA22, inhibits gibberellin-mediated programmed cell death in cereal aleurone cells.* Plant Physiol, 2008. **147**(4): p. 1710-22.
504. Appocher, C., R. Klima, and F. Feiguin, *Functional screening in Drosophila reveals the conserved role of REEP1 in promoting stress resistance and preventing the formation of Tau aggregates.* Hum Mol Genet, 2014. **23**(25): p. 6762-72.
505. Lai, Y.S., G. Stefano, and F. Brandizzi, *ER stress signaling requires RHD3, a functionally conserved ER-shaping GTPase.* J Cell Sci, 2014. **127**(Pt 15): p. 3227-32.
506. Montenegro, G., et al., *Mutations in the ER-shaping protein reticulon 2 cause the axon-degenerative disorder hereditary spastic paraplegia type 12.* J Clin Invest, 2012. **122**(2): p. 538-44.
507. O'Sullivan, N.C., et al., *Reticulon-like-1, the Drosophila orthologue of the hereditary spastic paraplegia gene reticulon 2, is required for organization of endoplasmic reticulum and of distal motor axons.* Hum Mol Genet, 2012. **21**(15): p. 3356-65.
508. Rainier, S., et al., *NIPA1 gene mutations cause autosomal dominant hereditary spastic paraplegia (SPG6).* Am J Hum Genet, 2003. **73**(4): p. 967-71.
509. Zhao, J., et al., *Hereditary spastic paraplegia-associated mutations in the NIPA1 gene and its Caenorhabditis elegans homolog trigger neural degeneration in vitro and in vivo through a gain-of-function mechanism.* J Neurosci, 2008. **28**(51): p. 13938-51.
510. Patel, H., et al., *The Silver syndrome variant of hereditary spastic paraplegia maps to chromosome 11q12-q14, with evidence for genetic heterogeneity within this subtype.* Am J Hum Genet, 2001. **69**(1): p. 209-15.
511. Windpassinger, C., et al., *Heterozygous missense mutations in BSCL2 are associated with distal hereditary motor neuropathy and Silver syndrome.* Nat Genet, 2004. **36**(3): p. 271-6.
512. Ito, D. and N. Suzuki, *Seipinopathy: a novel endoplasmic reticulum stress-associated disease.* Brain, 2009. **132**(Pt 1): p. 8-15.
513. Ito, D., et al., *Characterization of seipin/BSCL2, a protein associated with spastic paraplegia 17.* Neurobiol Dis, 2008. **31**(2): p. 266-77.
514. Cao, S.S. and R.J. Kaufman, *Endoplasmic reticulum stress and oxidative stress in cell fate decision and human disease.* Antioxid Redox Signal, 2014. **21**(3): p. 396-413.
515. Zeeshan, H.M., et al., *Endoplasmic Reticulum Stress and Associated ROS.* Int J Mol Sci, 2016. **17**(3): p. 327.
516. Wang, J., et al., *Redox signaling via the molecular chaperone BiP protects cells against endoplasmic reticulum-derived oxidative stress.* Elife, 2014. **3**: p. e03496.
517. Zorov, D.B., M. Juhaszova, and S.J. Sollott, *Mitochondrial reactive oxygen species (ROS) and ROS-induced ROS release.* Physiol Rev, 2014. **94**(3): p. 909-50.
518. Li, G., et al., *Role of ERO1-alpha-mediated stimulation of inositol 1,4,5-triphosphate receptor activity in endoplasmic reticulum stress-induced apoptosis.* J Cell Biol, 2009. **186**(6): p. 783-92.
519. Bravo, R., et al., *Increased ER-mitochondrial coupling promotes mitochondrial respiration and bioenergetics during early phases of ER stress.* J Cell Sci, 2011. **124**(Pt 13): p. 2143-52.

520. Malhotra, J.D. and R.J. Kaufman, *Endoplasmic reticulum stress and oxidative stress: a vicious cycle or a double-edged sword?* Antioxid Redox Signal, 2007. **9**(12): p. 2277-93.
521. McDermott, C.J., et al., *Investigation of mitochondrial function in hereditary spastic paraparesis.* Neuroreport, 2003. **14**(3): p. 485-8.
522. Abrahamsen, G., et al., *A patient-derived stem cell model of hereditary spastic paraplegia with SPAST mutations.* Dis Model Mech, 2013. **6**(2): p. 489-502.
523. Fan, Y., et al., *Low dose tubulin-binding drugs rescue peroxisome trafficking deficit in patient-derived stem cells in Hereditary Spastic Paraplegia.* Biol Open, 2014. **3**(6): p. 494-502.
524. Wali, G., et al., *Mechanism of impaired microtubule-dependent peroxisome trafficking and oxidative stress in SPAST-mutated cells from patients with Hereditary Spastic Paraplegia.* Sci Rep, 2016. **6**: p. 27004.
525. English, A.R. and G.K. Voeltz, *Endoplasmic reticulum structure and interconnections with other organelles.* Cold Spring Harb Perspect Biol, 2013. **5**(4): p. a013227.
526. Notte, A., et al., *Taxol-induced unfolded protein response activation in breast cancer cells exposed to hypoxia: ATF4 activation regulates autophagy and inhibits apoptosis.* Int J Biochem Cell Biol, 2015. **62**: p. 1-14.
527. Wang, J., et al., *Blockade of GRP78 sensitizes breast cancer cells to microtubules-interfering agents that induce the unfolded protein response.* J Cell Mol Med, 2009. **13**(9B): p. 3888-97.
528. Mhaidat, N.M., et al., *Involvement of endoplasmic reticulum stress in Docetaxel-induced JNK-dependent apoptosis of human melanoma.* Apoptosis, 2008. **13**(12): p. 1505-12.
529. Liao, P.C., et al., *Involvement of endoplasmic reticulum in paclitaxel-induced apoptosis.* J Cell Biochem, 2008. **104**(4): p. 1509-23.
530. Tanimukai, H., et al., *Paclitaxel induces neurotoxicity through endoplasmic reticulum stress.* Biochem Biophys Res Commun, 2013. **437**(1): p. 151-5.
531. Solowska, J.M., A.N. Rao, and P.W. Baas, *Truncating mutations of SPAST associated with hereditary spastic paraplegia indicate greater accumulation and toxicity of the M1 isoform of spastin.* Mol Biol Cell, 2017. **28**(13): p. 1728-1737.
532. Chang, J., S. Lee, and C. Blackstone, *Protrudin binds atlastins and endoplasmic reticulum-shaping proteins and regulates network formation.* Proc Natl Acad Sci U S A, 2013. **110**(37): p. 14954-9.
533. Sorimachi, H. and Y. Ono, *Regulation and physiological roles of the calpain system in muscular disorders.* Cardiovasc Res, 2012. **96**(1): p. 11-22.
534. Miller, D.J., et al., *Calpain-1 inhibitors for selective treatment of rheumatoid arthritis: what is the future?* Future Med Chem, 2013. **5**(17): p. 2057-74.
535. Guroff, G., *A Neutral, Calcium-Activated Proteinase from the Soluble Fraction of Rat Brain.* J Biol Chem, 1964. **239**: p. 149-55.
536. Mellgren, R.L., *Canine cardiac calcium-dependent proteases: Resolution of two forms with different requirements for calcium.* FEBS Lett, 1980. **109**(1): p. 129-33.
537. Araujo, H., A. Julio, and M. Cardoso, *Translating genetic, biochemical and structural information to the calpain view of development.* Mech Dev, 2018.

538. Macqueen, D.J. and A.H. Wilcox, *Characterization of the definitive classical calpain family of vertebrates using phylogenetic, evolutionary and expression analyses.* Open Biol, 2014. **4**: p. 130219.
539. Lepage, S.E. and A.E. Bruce, *Characterization and comparative expression of zebrafish calpain system genes during early development.* Dev Dyn, 2008. **237**(3): p. 819-29.
540. Sato, K. and S. Kawashima, *Calpain function in the modulation of signal transduction molecules.* Biol Chem, 2001. **382**(5): p. 743-51.
541. Baudry, M. and X. Bi, *Calpain-1 and Calpain-2: The Yin and Yang of Synaptic Plasticity and Neurodegeneration.* Trends Neurosci, 2016. **39**(4): p. 235-245.
542. Honda, S., et al., *Activation of m-calpain is required for chromosome alignment on the metaphase plate during mitosis.* J Biol Chem, 2004. **279**(11): p. 10615-23.
543. Randriamboavonjy, V. and I. Fleming, *All cut up! The consequences of calpain activation on platelet function.* Vascul Pharmacol, 2012. **56**(5-6): p. 210-5.
544. Smith, M.A. and R.G. Schnellmann, *Calpains, mitochondria, and apoptosis.* Cardiovasc Res, 2012. **96**(1): p. 32-7.
545. Glading, A., D.A. Lauffenburger, and A. Wells, *Cutting to the chase: calpain proteases in cell motility.* Trends Cell Biol, 2002. **12**(1): p. 46-54.
546. Goll, D.E., et al., *The calpain system.* Physiol Rev, 2003. **83**(3): p. 731-801.
547. Carafoli, E. and M. Molinari, *Calpain: a protease in search of a function?* Biochem Biophys Res Commun, 1998. **247**(2): p. 193-203.
548. Pfaff, M., X. Du, and M.H. Ginsberg, *Calpain cleavage of integrin beta cytoplasmic domains.* FEBS Lett, 1999. **460**(1): p. 17-22.
549. Kerstein, P.C., et al., *Mechanosensitive TRPC1 channels promote calpain proteolysis of talin to regulate spinal axon outgrowth.* J Neurosci, 2013. **33**(1): p. 273-85.
550. Chan, K.T., D.A. Bennin, and A. Huttenlocher, *Regulation of adhesion dynamics by calpain-mediated proteolysis of focal adhesion kinase (FAK).* J Biol Chem, 2010. **285**(15): p. 11418-26.
551. Kerstein, P.C., K.M. Patel, and T.M. Gomez, *Calpain-Mediated Proteolysis of Talin and FAK Regulates Adhesion Dynamics Necessary for Axon Guidance.* J Neurosci, 2017. **37**(6): p. 1568-1580.
552. Yang, L.S. and H. Ksiezak-Reding, *Calpain-induced proteolysis of normal human tau and tau associated with paired helical filaments.* Eur J Biochem, 1995. **233**(1): p. 9-17.
553. Santella, L., et al., *Breakdown of cytoskeletal proteins during meiosis of starfish oocytes and proteolysis induced by calpain.* Exp Cell Res, 2000. **259**(1): p. 117-26.
554. Billger, M., M. Wallin, and J.O. Karlsson, *Proteolysis of tubulin and microtubule-associated proteins 1 and 2 by calpain I and II. Difference in sensitivity of assembled and disassembled microtubules.* Cell Calcium, 1988. **9**(1): p. 33-44.
555. Fischer, I., G. Romano-Clarke, and F. Grynspan, *Calpain-mediated proteolysis of microtubule associated proteins MAP1B and MAP2 in developing brain.* Neurochem Res, 1991. **16**(8): p. 891-8.
556. Kimura, T., et al., *Phospho-Tau Bar Code: Analysis of Phosphoisotypes of Tau and Its Application to Tauopathy.* Front Neurosci, 2018. **12**: p. 44.
557. Goold, R.G., R. Owen, and P.R. Gordon-Weeks, *Glycogen synthase kinase 3beta phosphorylation of microtubule-associated protein 1B regulates the stability of microtubules in growth cones.* J Cell Sci, 1999. **112 (Pt 19)**: p. 3373-84.

558. Trivedi, N., et al., *Glycogen synthase kinase-3beta phosphorylation of MAP1B at Ser1260 and Thr1265 is spatially restricted to growing axons.* J Cell Sci, 2005. **118**(Pt 5): p. 993-1005.
559. Takei, Y., et al., *Defects in axonal elongation and neuronal migration in mice with disrupted tau and map1b genes.* J Cell Biol, 2000. **150**(5): p. 989-1000.
560. Forman, O.P., L. De Risio, and C.S. Mellersh, *Missense mutation in CAPN1 is associated with spinocerebellar ataxia in the Parson Russell Terrier dog breed.* PLoS One, 2013. **8**(5): p. e64627.
561. Wang, Y., et al., *Defects in the CAPN1 Gene Result in Alterations in Cerebellar Development and Cerebellar Ataxia in Mice and Humans.* Cell Rep, 2016. **16**(1): p. 79-91.
562. Travaglini, L., et al., *Expanding the clinical phenotype of CAPN1-associated mutations: A new case with congenital-onset pure spastic paraplegia.* J Neurol Sci, 2017. **378**: p. 210-212.
563. Kocoglu, C., et al., *Homozygous CAPN1 mutations causing a spastic-ataxia phenotype in 2 families.* Neurol Genet, 2018. **4**(1): p. e218.
564. Lambe, J., et al., *CAPN1 mutations broadening the hereditary spastic paraplegia/spinocerebellar ataxia phenotype.* Pract Neurol, 2018.
565. Tadic, V., et al., *CAPN1 mutations are associated with a syndrome of combined spasticity and ataxia.* J Neurol, 2017. **264**(5): p. 1008-1010.
566. Parodi, L., et al., *Hereditary ataxias and paraparesias: clinical and genetic update.* Curr Opin Neurol, 2018. **31**(4): p. 462-471.
567. Synofzik, M. and R. Schule, *Overcoming the divide between ataxias and spastic paraplegias: Shared phenotypes, genes, and pathways.* Mov Disord, 2017. **32**(3): p. 332-345.
568. Azam, M., et al., *Disruption of the mouse mu-calpain gene reveals an essential role in platelet function.* Mol Cell Biol, 2001. **21**(6): p. 2213-20.
569. Bae, Y.K., et al., *Anatomy of zebrafish cerebellum and screen for mutations affecting its development.* Dev Biol, 2009. **330**(2): p. 406-26.
570. Kaslin, J., et al., *Development and specification of cerebellar stem and progenitor cells in zebrafish: from embryo to adult.* Neural Dev, 2013. **8**: p. 9.
571. Kemp, C.M., et al., *The effects of Capn1 gene inactivation on skeletal muscle growth, development, and atrophy, and the compensatory role of other proteolytic systems.* J Anim Sci, 2013. **91**(7): p. 3155-67.
572. Shoji, W. and M. Sato-Maeda, *Application of heat shock promoter in transgenic zebrafish.* Dev Growth Differ, 2008. **50**(6): p. 401-6.
573. Svahn, A.J., et al., *Nucleo-cytoplasmic transport of TDP-43 studied in real time: impaired microglia function leads to axonal spreading of TDP-43 in degenerating motor neurons.* Acta Neuropathol, 2018. **136**(3): p. 445-459.
574. Wegorzewska, I., et al., *TDP-43 mutant transgenic mice develop features of ALS and frontotemporal lobar degeneration.* Proc Natl Acad Sci U S A, 2009. **106**(44): p. 18809-14.
575. Stallings, N.R., et al., *Progressive motor weakness in transgenic mice expressing human TDP-43.* Neurobiol Dis, 2010. **40**(2): p. 404-14.

576. Xu, Y.F., et al., *Wild-type human TDP-43 expression causes TDP-43 phosphorylation, mitochondrial aggregation, motor deficits, and early mortality in transgenic mice.* J Neurosci, 2010. **30**(32): p. 10851-9.
577. Xu, Y.F., et al., *Expression of mutant TDP-43 induces neuronal dysfunction in transgenic mice.* Mol Neurodegener, 2011. **6**: p. 73.
578. Arnold, E.S., et al., *ALS-linked TDP-43 mutations produce aberrant RNA splicing and adult-onset motor neuron disease without aggregation or loss of nuclear TDP-43.* Proc Natl Acad Sci U S A, 2013. **110**(8): p. E736-45.
579. Maskri, L., et al., *Influence of different promoters on the expression pattern of mutated human alpha-synuclein in transgenic mice.* Neurodegener Dis, 2004. **1**(6): p. 255-65.
580. Janssens, J., et al., *Overexpression of ALS-associated p.M337V human TDP-43 in mice worsens disease features compared to wild-type human TDP-43 mice.* Mol Neurobiol, 2013. **48**(1): p. 22-35.
581. Kollias, G., et al., *Differential regulation of a Thy-1 gene in transgenic mice.* Proc Natl Acad Sci U S A, 1987. **84**(6): p. 1492-6.
582. Swarup, V., et al., *Pathological hallmarks of amyotrophic lateral sclerosis/frontotemporal lobar degeneration in transgenic mice produced with TDP-43 genomic fragments.* Brain, 2011. **134**(Pt 9): p. 2610-26.
583. Voigt, A., et al., *TDP-43-mediated neuron loss in vivo requires RNA-binding activity.* PLoS One, 2010. **5**(8): p. e12247.
584. Miskiewicz, K., et al., *HDAC6 is a Bruchpilot deacetylase that facilitates neurotransmitter release.* Cell Rep, 2014. **8**(1): p. 94-102.
585. Estes, P.S., et al., *Wild-type and A315T mutant TDP-43 exert differential neurotoxicity in a Drosophila model of ALS.* Hum Mol Genet, 2011. **20**(12): p. 2308-21.
586. Ihara, R., et al., *RNA binding mediates neurotoxicity in the transgenic Drosophila model of TDP-43 proteinopathy.* Hum Mol Genet, 2013. **22**(22): p. 4474-84.
587. Ritson, G.P., et al., *TDP-43 mediates degeneration in a novel Drosophila model of disease caused by mutations in VCP/p97.* J Neurosci, 2010. **30**(22): p. 7729-39.
588. Estes, P.S., et al., *Motor neurons and glia exhibit specific individualized responses to TDP-43 expression in a Drosophila model of amyotrophic lateral sclerosis.* Dis Model Mech, 2013. **6**(3): p. 721-33.
589. Lu, Y., J. Ferris, and F.B. Gao, *Frontotemporal dementia and amyotrophic lateral sclerosis-associated disease protein TDP-43 promotes dendritic branching.* Mol Brain, 2009. **2**: p. 30.
590. Liachko, N.F., C.R. Guthrie, and B.C. Kraemer, *Phosphorylation promotes neurotoxicity in a Caenorhabditis elegans model of TDP-43 proteinopathy.* J Neurosci, 2010. **30**(48): p. 16208-19.
591. Zhang, T., et al., *TDP-43 neurotoxicity and protein aggregation modulated by heat shock factor and insulin/IGF-1 signaling.* Hum Mol Genet, 2011. **20**(10): p. 1952-65.
592. Vaccaro, A., et al., *Mutant TDP-43 and FUS cause age-dependent paralysis and neurodegeneration in C. elegans.* PLoS One, 2012. **7**(2): p. e31321.
593. Zhang, T., et al., *Caenorhabditis elegans RNA-processing protein TDP-1 regulates protein homeostasis and life span.* J Biol Chem, 2012. **287**(11): p. 8371-82.
594. Feiguin, F., et al., *Depletion of TDP-43 affects Drosophila motoneurons terminal synapsis and locomotive behavior.* FEBS Lett, 2009. **583**(10): p. 1586-92.

595. Wu, L.S., et al., *TDP-43, a neuro-pathosignature factor, is essential for early mouse embryogenesis.* Genesis, 2010. **48**(1): p. 56-62.
596. Cannon, A., et al., *Neuronal sensitivity to TDP-43 overexpression is dependent on timing of induction.* Acta Neuropathol, 2012. **123**(6): p. 807-23.
597. Huang, C., et al., *Mutant TDP-43 in motor neurons promotes the onset and progression of ALS in rats.* J Clin Invest, 2012. **122**(1): p. 107-18.
598. Walker, A.K., et al., *Functional recovery in new mouse models of ALS/FTLD after clearance of pathological cytoplasmic TDP-43.* Acta Neuropathol, 2015. **130**(5): p. 643-60.
599. Ke, Y.D., et al., *Short-term suppression of A315T mutant human TDP-43 expression improves functional deficits in a novel inducible transgenic mouse model of FTLD-TDP and ALS.* Acta Neuropathol, 2015. **130**(5): p. 661-78.
600. Igaz, L.M., et al., *Dysregulation of the ALS-associated gene TDP-43 leads to neuronal death and degeneration in mice.* J Clin Invest, 2011. **121**(2): p. 726-38.
601. Li, Q., et al., *The cleavage pattern of TDP-43 determines its rate of clearance and cytotoxicity.* Nat Commun, 2015. **6**: p. 6183.
602. Austin, J.A., et al., *Disease causing mutants of TDP-43 nucleic acid binding domains are resistant to aggregation and have increased stability and half-life.* Proc Natl Acad Sci U S A, 2014. **111**(11): p. 4309-14.
603. Samarut, E., A. Bekri, and P. Drapeau, *Transcriptomic Analysis of Purified Embryonic Neural Stem Cells from Zebrafish Embryos Reveals Signaling Pathways Involved in Glycine-Dependent Neurogenesis.* Front Mol Neurosci, 2016. **9**: p. 22.
604. White, M.A., et al., *TDP-43 gains function due to perturbed autoregulation in a Tardbp knock-in mouse model of ALS-FTD.* Nat Neurosci, 2018. **21**(4): p. 552-563.
605. Fratta, P., et al., *Mice with endogenous TDP-43 mutations exhibit gain of splicing function and characteristics of amyotrophic lateral sclerosis.* EMBO J, 2018. **37**(11).
606. Samarut, E., A. Lissouba, and P. Drapeau, *A simplified method for identifying early CRISPR-induced indels in zebrafish embryos using High Resolution Melting analysis.* BMC Genomics, 2016. **17**: p. 547.
607. Devoy, A., et al., *Humanized mutant FUS drives progressive motor neuron degeneration without aggregation in 'FUSDelta14' knockin mice.* Brain, 2017. **140**(11): p. 2797-2805.
608. Tran, L.D., et al., *Dynamic microtubules at the vegetal cortex predict the embryonic axis in zebrafish.* Development, 2012. **139**(19): p. 3644-52.
609. Gerhart, S.V., et al., *The Cx43-like connexin protein Cx40.8 is differentially localized during fin ontogeny and fin regeneration.* PLoS One, 2012. **7**(2): p. e31364.
610. Li, J., et al., *A transgenic zebrafish model for monitoring xbp1 splicing and endoplasmic reticulum stress in vivo.* Mech Dev, 2015. **137**: p. 33-44.
611. Kim, D.H., et al., *Pan-neuronal calcium imaging with cellular resolution in freely swimming zebrafish.* Nat Methods, 2017. **14**(11): p. 1107-1114.
612. Takeuchi, M., et al., *Establishment of Gal4 transgenic zebrafish lines for analysis of development of cerebellar neural circuitry.* Dev Biol, 2015. **397**(1): p. 1-17.
613. Aulas, A. and C. Vande Velde, *Alterations in stress granule dynamics driven by TDP-43 and FUS: a link to pathological inclusions in ALS?* Front Cell Neurosci, 2015. **9**: p. 423.

Annexe 1: Protein sequence alignement between human and zebrafish spastin

The protein sequences are from Ensembl and the alignement was done with MUSCLE. The different domains of the protein are color-coded similarly to the schematic structure of the protein. The domains are indicated as presented by [124].

Sequence alignement between human and zebrafish spastin

The human M87 and zebrafish M61 are marked by a red box
The darker green shade indicates the hydrophobic region

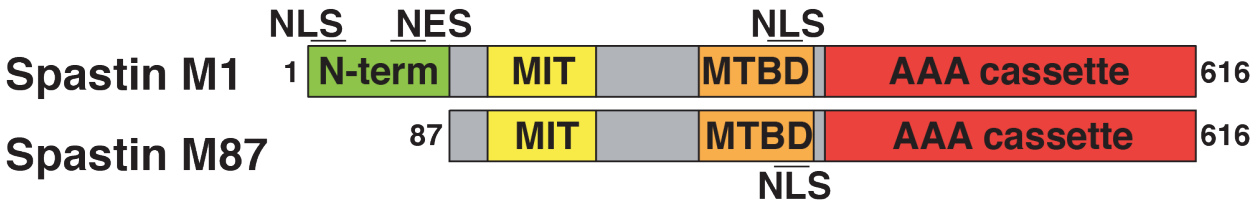

Annexe 2: Protein sequence alignement between human CAPN1 and zebrafish capn1a and capn1b

The protein sequences are from Ensembl and the alignement was done with MUSCLE. The different domains of the protein are color-coded similarly to the schematic structure of the protein. The domains are indicated as presented on www.calpain.net.

Sequence alignement between human CAPN1 and zebrafish capn1a and capn1b

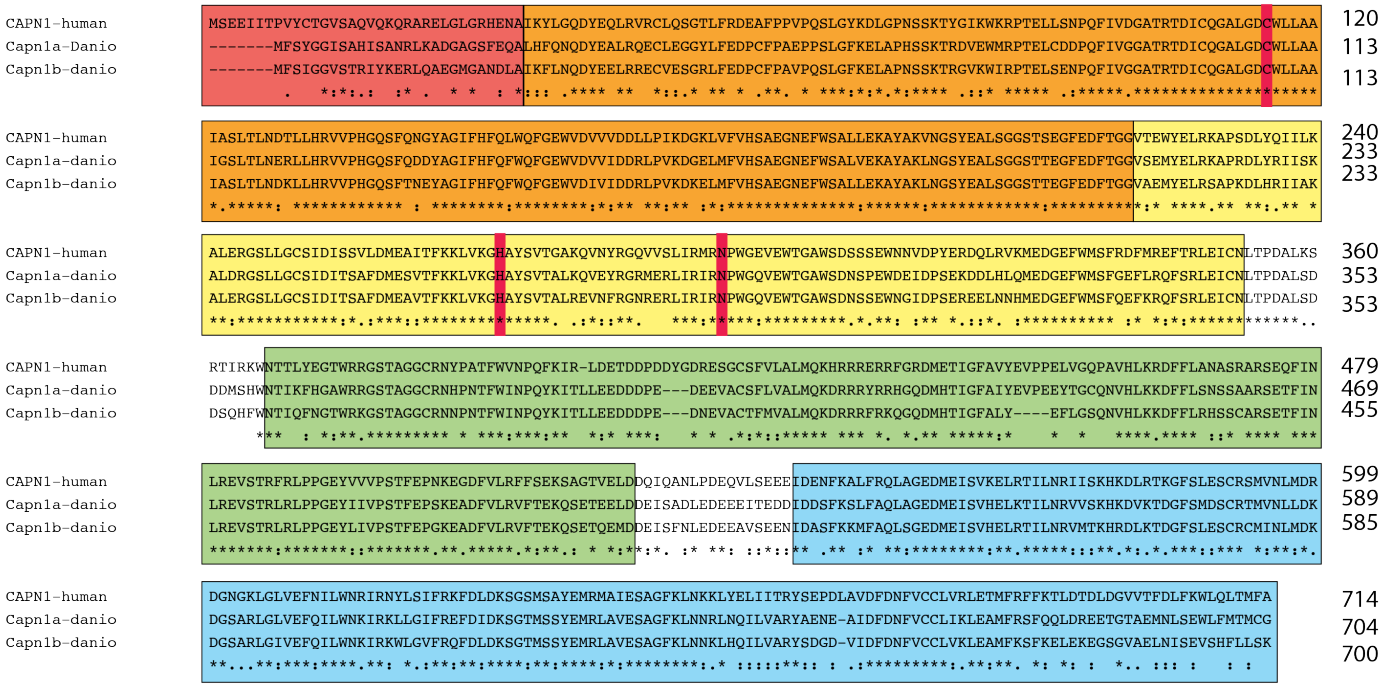

Calpain 1 (CAPN1)

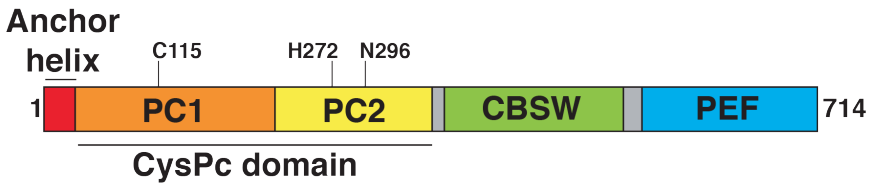

Amino acids forming the catalytic triad are in red

Annexe 3: Protein sequence alignement between human and zebrafish TDP-43

The protein sequences are from Ensembl and the alignement was done with MUSCLE. The different domains of the protein are color-coded similarly to the schematic structure of the protein. The domains are indicated as presented by [613].

Sequence alignement between human and zebrafish TDP-43

```
TDP-43_human    MSE-YIRVTEDENDEPIEIPSEDDGTVLLSTVTAQFPGACGLRYRNPVSQCMRGVRLVEGILHAPDAGWGNLVYVVNYPK-----DNKRKMDETDASSAVKVKRAVQKTSDLIVLGLPWK  114
tdp-43_Danio    MAEMYIRVAEEENEEPMEIPSEDDGTVLLSTVSAQFPGACGLRFRSPVSQCMRGVRLVDGILHAPENGWGNLVYVVNYPKETVLPDNKRKMDEIDASSATKIKRGDQKTSDLIVLGLPWK  120
                *:* ****:*:**:**:***************:**********:*.***********:******: *************     ******** *****.*:**. **********

TDP-43_human    TTEQDLKEYFSTFGEVLMVQVKKDLKTGHSKGFGFVRFTEYETQVKVMSQRHMIDGRWCDCKLPNSKQSQDEPLRSRKVFVGRCTEDMTEDELREFFSQYGDVMDVFIPKPFRAFAFVTF  234
tdp-43_danio    TSEQDLKDYFGTFGEVIMVQVKRDVKTGNSKGFGFVRFGDWETQSKVMTQRHMIDGRWCDCKLPNSKQGIDEPMRSRKVFVGRCTEDMTADELRQFFMQYGEVTDVFIPKPFRAFAFVTF  240
                *:*****:**.*****:*****.*:***:********* ::*** ***:**************.******. ***:************** ****:** ***:* ***************

TDP-43_human    ADDQIAQSLCGEDLIIKGISVHISNAEPKHNSNRQ-LERSGRFGGNPGGFGNQGGFGNSRGGGAGLGNNQGSNMGGGMNFGAFSINPAMMAAAQAALQSSWGMMGMLASQQNQSGPSGNN  353
tdp-43_danio    ADDQVAAALCGEDLIIKGVSVHISNAEPKHNNTRQMMERAGRFGNGFGGQGFAGSRSNMGGGGGGSSSSLG-------NFGNFNLNPAMMAAAQAALQSSWGMMGMLA-QQNQSGTSGTS  352
                ****:* :**********:**********...** :**:****.. ** *  *. .*  ***.* ... *      *** *.:********************** ******.**..

TDP-43_human    QNQGNMQREPNQAFGSGNNSYSGSNSGAAIGWGSASNAGSGS-GFNGGFGSSMDSKSSGWGM  414
tdp-43_danio    TSGTSSSRDQAQTYSSANSNY--GSSSAALGWGTGSNSGAASAGFNSSFGSSMESKSSGWGM  412
                .  . .*:  *::.*.*..*  ..*.**:***:.**:*:.* ***..*****:********
```

The shaded red indicates the G348 that is mutated in ALS (G348C) and expressed in the transgenic line.

The shaded blue indicates the A382/A379 that is mutated in ALS (A382T) and in our mutant tardbp line (A379T)

Annexe 4: Protein sequence alignement between human and zebrafish FUS

The protein sequences are from Ensembl and the alignement was done with MUSCLE. The different domains of the protein are color-coded similarly to the schematic structure of the protein. The domains are indicated as presented by [613].

Sequence alignement between human and zebrafish FUS

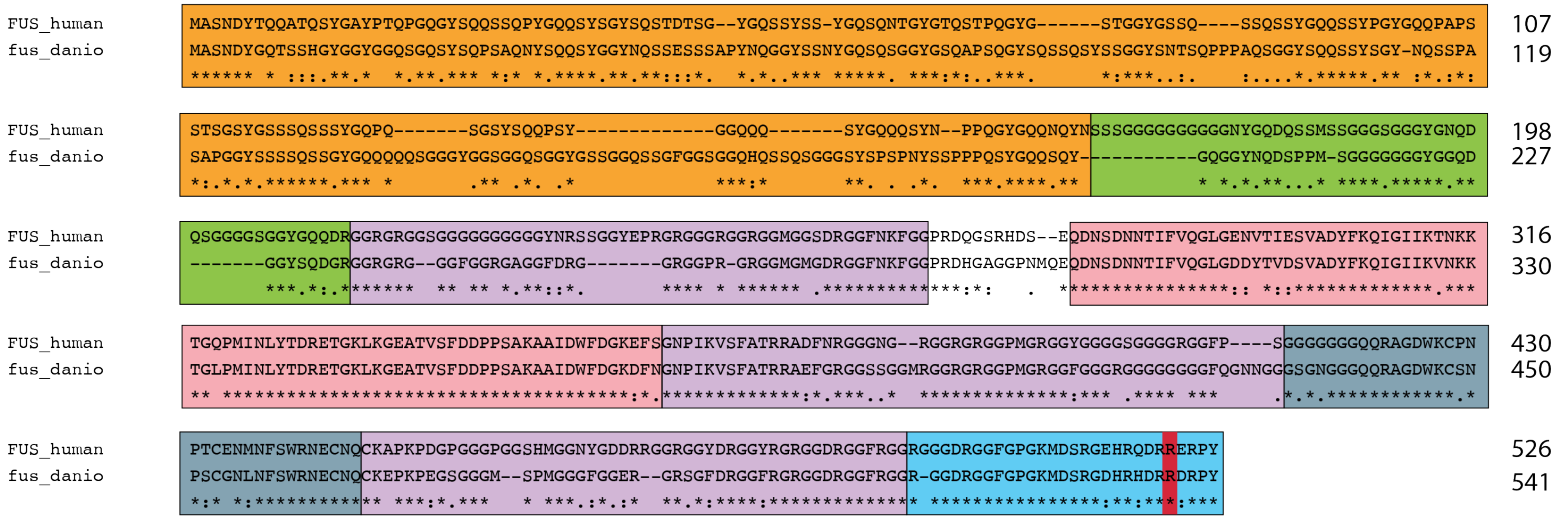

The shaded red indicates the R521/R536 that is mutated in ALS (R521H) and in our mutant fus line (R536H)

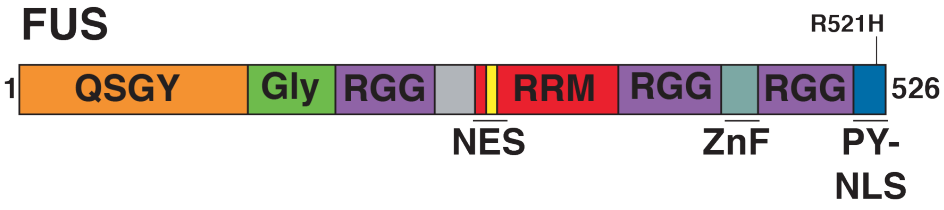

Annexe 5: *Hsp70l* mRNA

One possibility to exlain the higher level of expression of TDP-43^{G348C} compared to TDP-43^{WT} is that the h*sp70l* promoter is upregulated in the mutant line as a consequence of increased stress in presence of TDP-43^{G348C}. To test this hypothesis, we have measured *hsp70l* mRNA in all of our conditions. While not significant, a trend of up-regulation of *hsp70l* mRNA can be seen only in the presence of mutant TDP-43.

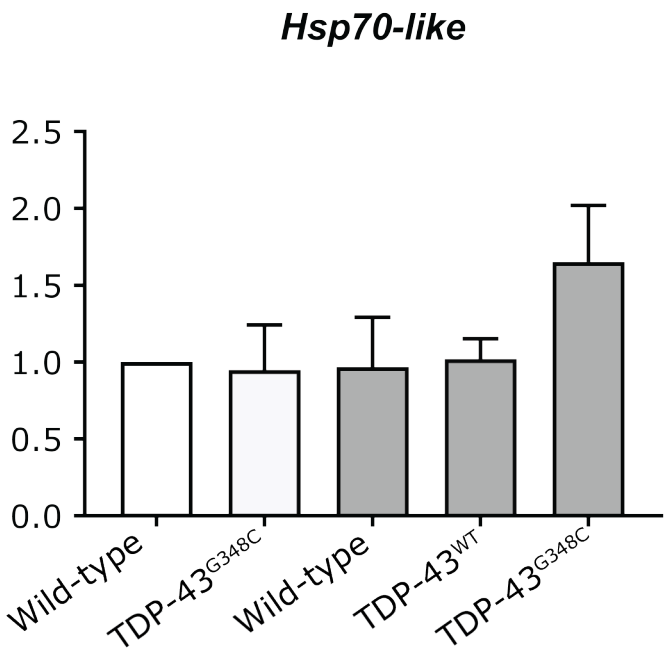

Figure 7. ***Hsp70l* mRNA measured by qRT-PCR**

Measurements of *hsp70l* mRNA by qRT-PCR. An up-regulation trend can be seen in the embryos expressing TDP-43^{G348C} but not in those expressing TDP-43^{WT}, possibly explaining the increased expression of TDP-43^{G348C} due to an up-regulation of the *hsp70l* promoter.

Annexe 6: Legends to the additional videos for Chapter 3

Acetylated tubulin staining was performed as described in **Chapter 3** [492] on 2 dpf embryos injected with a morpholino against capn1a or a mismatched morpholino. The embryos were imaged either dorsal up, or on the side and imaged with a 10x air objective.
The movies presented as additional materials are videos going through the Z-stacks of imaged acetylated tubulin staining. The embryos are either dorsal up, caudal left (**video1.mov** and **video3.mov**), or on the side, caudal left (**video2.mov** and **video4.mov**) and the Z-stack is starting from the ventral most part of the embryo. The last slide of the video is a Z-projection with max intensity. Images from these videos were taken for Figure 4 and supplemental Figure S4 presented in **Chapter 3** [492].

Video1.mov and **Video2.mov** show a representative embryo injected with the mismatch morpholino dorsal up or on the side, respectively.
Video3.mov and **video4.mov** show a representative embryo injected with the morpholino against capn1a dorsal up or on the side, respectively.

Annexe 7: Differentially expressed genes from transgenic line transcriptomic data

Table I. Supplementary Table from the article "Generation of zebrafish TDP-43 transgenic lines"

Differentially expressed genes upon expression of human mutant TDP-43**.** We found 159 differentially expressed genes in embryos expressing human mutant TDP-43 compared to heat-shock wild-type embryos by filtering with a *p*-value < 0.05. 67 genes are up-regulated (green cells) and 92 genes are down-regulated (red cells). The log2 fold change (log2FC), the p value and the base mean values from the DESeq analysis have been provided for each gene.

Differentially expressed genes from White et al., [604] (in blue) or Devoy et al., [607] (in red) that have homologs in common with our list were added to the Table for comparison. If a gene is present in both datasets they are shaded in purple.

Gene stable ID	Gene name	Log2 fold change	Gene description	Differentially expressed homolog(s) in White et al. (Mouse Tdp-43 knock-in) [604]			Differentially expressed homolog(s) in Devoy et al. (Mouse Fus knock-in) [607]	
				Gene name	Dataset	Direction of change	Gene name	Direction of change
ENSDARG00000028396	fkbp5	-1.08	FK506 binding protein 5 [Source:ZFIN;Acc:ZDB-GENE-030616-630]	Fkbp5	cortex	down-regulated	Fkbp3	down-regulated
ENSDARG00000100513	rps27l	1.41	ribosomal protein S27 like [Source:ZFIN;Acc:ZDB-GENE-060331-65]	Rps27	cortex MB	up-regulated in MB+; downregulated in MB-	Rps27; Rps27l; Rps27a	down-regulated
ENSDARG00000102474	dusp16	1.27	dual specificity phosphatase 16 [Source:ZFIN;Acc:ZDB-GENE-040426-2360]	Dusp15	aged cortex	up-regulated	Dusp12	down-regulated
				Dusp27	aged cortex	up-regulated	Dusp28	down-regulated
ENSDARG00000028804	ankrd9	-1.42	ankyrin repeat domain 9 [Source:ZFIN;Acc:ZDB-GENE-041114-3]	Ankrd42; Ankrd46; Ankrd55	aged cortex	down-regulated	Ankrd37; Ankrd49	down-regulated
				Ankrd11; Ankrd12; Ankrd13b; Ankrd17; Ankrd24; Ankrd52	cortex MB	down-regulated in MB+; up-regulated in MB-	Ankrd34a	up-regulated
ENSDARG00000088634	adcy1b	2.03	adenylate cyclase 1b [Source:ZFIN;Acc:ZDB-	Adcy4	aged cortex	up-regulated	Adcy9	up-regulated

			GENE-100805-1]				Adcy7	up-regulated
							Adcy1	up-regulated
ENSDARG00000007576	crybb1l1	-0.95	crystallin, beta B1, like 1 [Source:ZFIN;Acc:ZDB-GENE-100112-3]	Crybb1	aged cortex	up-regulated	N/A	
ENSDARG00000011998	bfsp2	-1.04	beaded filament structural protein 2, phakinin [Source:ZFIN;Acc:ZDB-GENE-041212-58]	Bfsp2	aged cortex	up-regulated	N/A	
ENSDARG00000016412	agt	1.56	angiotensinogen [Source:ZFIN;Acc:ZDB-GENE-030131-1205]	Agt	aged cortex	up-regulated	N/A	
ENSDARG00000030215	matn1	1.31	matrilin 1 [Source:ZFIN;Acc:ZDB-GENE-050307-3]	Matn4	aged cortex	up-regulated	N/A	
ENSDARG00000036237	slc27a2a	-1.36	solute carrier family 27 (fatty acid transporter), member 2a [Source:ZFIN;Acc:ZDB-GENE-050706-104]	Slc27a1	aged cortex	up-regulated	N/A	
ENSDARG00000038056	fgfbp2b	1	fibroblast growth factor binding protein 2b [Source:ZFIN;Acc:ZDB-GENE-070410-95]	Fgfbp3	cortex MB	up-regulated in MB+; down-regulated in MB-	N/A	
ENSDARG00000041623	mt2	-1.27	metallothionein 2 [Source:ZFIN;Acc:ZDB-GENE-030131-4174]	Mt2	cortex MB	up-regulated in MB+; down-regulated in MB-	N/A	
ENSDARG00000104550	clcn2b	1.45	chloride channel, voltage-sensitive 2b [Source:ZFIN;Acc:ZDB-GENE-151006-1]	Clcn5	aged cortex	down-regulated	N/A	

ENSDARG00000024433	pvalb4	1.13	parvalbumin 4 [Source:ZFIN;Acc:ZDB-GENE-040625-48]	Pvalb	cortex	down-regulated	N/A	
				Pvalb	aged cortex	down-regulated	N/A	
ENSDARG00000071601	pvalb9	-1.08	parvalbumin 9 [Source:ZFIN;Acc:ZDB-GENE-030805-4]	Pvalb	aged cortex	down-regulated	N/A	
				Pvalb	cortex	down-regulated	N/A	
ENSDARG00000100185	elovl7b	2.27	ELOVL fatty acid elongase 7b [Source:ZFIN;Acc:ZDB-GENE-030131-5485]	Elovl1	aged cortex	up-regulated	N/A	
				Elovl2	cortex and aged cortex	up-regulated	N/A	
				Elovl7	cortex MB	up-regulated in MB+; downregulated in MB-	N/A	
ENSDARG00000071877	dhrs7cb	-1.92	dehydrogenase/reductase (SDR family) member 7Cb [Source:ZFIN;Acc:ZDB-GENE-050522-226]	N/A			Dhrs7b	down-regulated
ENSDARG00000103934	megf8	1.88	multiple EGF-like-domains 8 [Source:ZFIN;Acc:ZDB-GENE-090730-1]	N/A			Megf9	down-regulated
ENSDARG00000095826	smdt1a	1.89	single-pass membrane protein with aspartate-rich tail 1a [Source:ZFIN;Acc:ZDB-GENE-110411-114]	N/A			SMDT1	Down-regulation
ENSDARG00000006427	fabp2	-1.41	fatty acid binding protein 2, intestinal [Source:ZFIN;Acc:ZDB-GENE-991019-5]	N/A			Fabp3; Fabp5; Fabp7	down-regulated

ENSDARG00000103398	fabp1b.2	2.06	fatty acid binding protein 1b, liver, tandem duplicate 2 [Source:ZFIN;Acc:ZDB-GENE-100318-6]	N/A			Fabp3; Fabp5; Fabp7	down-regulated
ENSDARG00000002193	rho	1.5	rhodopsin [Source:ZFIN;Acc:ZDB-GENE-990415-271]	N/A			N/A	
ENSDARG00000003203	rhcga	-3.43	Rh family, C glycoprotein a [Source:ZFIN;Acc:ZDB-GENE-070424-81]	N/A			N/A	
ENSDARG00000004748	zgc:100868	1.51	zgc:100868 [Source:ZFIN;Acc:ZDB-GENE-040801-33]	N/A			N/A	
ENSDARG00000006588	zgc:111983	1.39	zgc:111983 [Source:ZFIN;Acc:ZDB-GENE-050417-335]	N/A			N/A	
ENSDARG00000007715	lgsn	-1.19	lengsin, lens protein with glutamine synthetase domain [Source:ZFIN;Acc:ZDB-GENE-060312-26]	N/A			N/A	
ENSDARG00000011983	zgc:136908	-1.38	zgc:136908 [Source:ZFIN;Acc:ZDB-GENE-060312-22]	N/A			N/A	
ENSDARG00000013430	bhmt	-1.01	betaine-homocysteine methyltransferase [Source:ZFIN;Acc:ZDB-GENE-030131-947]	N/A			N/A	
ENSDARG00000015654	ca15a	-2.45	carbonic anhydrase XVa [Source:ZFIN;Acc:ZDB-GENE-070424-7]	N/A			N/A	
ENSDARG00000016343	zgc:92518	-1.49	zgc:92518 [Source:ZFIN;Acc:ZDB-GENE-040718-53]	N/A			N/A	
ENSDARG00000017274	opn1sw2	3.91	opsin 1 (cone pigments), short-wave-sensitive 2 [Source:ZFIN;Acc:ZDB-GENE-990604-40]	N/A			N/A	

ENSDARG00000017624	krt4	-0.94	keratin 4 [Source:ZFIN;Acc:ZDB-GENE-000607-83]	N/A			N/A	
ENSDARG00000018881	apobec2a	-1.22	apolipoprotein B mRNA editing enzyme, catalytic polypeptide-like 2a [Source:ZFIN;Acc:ZDB-GENE-050306-15]	N/A			N/A	
ENSDARG00000019122	he1.2	-3.48	hatching enzyme 1, tandem dupliate 2 [Source:ZFIN;Acc:ZDB-GENE-030131-2100]	N/A			N/A	
ENSDARG00000020866	apoa4b.2	-1.05	apolipoprotein A-IV b, tandem duplicate 2 [Source:ZFIN;Acc:ZDB-GENE-030131-3143]	N/A			N/A	
ENSDARG00000023656	he1.1	-3.46	hatching enzyme 1, tandem duplicate 1 [Source:ZFIN;Acc:ZDB-GENE-021211-3]	N/A			N/A	
ENSDARG00000024381	msto1	1.28	misato 1, mitochondrial distribution and morphology regulator [Source:ZFIN;Acc:ZDB-GENE-030131-6238]	N/A			N/A	
ENSDARG00000025703	dmgdh	-1.03	dimethylglycine dehydrogenase [Source:ZFIN;Acc:ZDB-GENE-080227-8]	N/A			N/A	
ENSDARG00000026759	ldlrb	1.42	low density lipoprotein receptor b [Source:ZFIN;Acc:ZDB-GENE-040426-1254]	N/A			N/A	
ENSDARG00000028663	tek	1.68	TEK tyrosine kinase, endothelial [Source:ZFIN;Acc:ZDB-GENE-990415-56]	N/A			N/A	

ENSDARG00000030349	cryba2a	-1.03	crystallin, beta A2a [Source:ZFIN;Acc:ZDB-GENE-040625-8]	N/A			N/A	
ENSDARG00000036832	cyt1l	-0.96	type I cytokeratin, enveloping layer, like [Source:ZFIN;Acc:ZDB-GENE-061026-4]	N/A			N/A	
ENSDARG00000041119	ceacam1	-1.76	carcinoembryonic antigen-related cell adhesion molecule 1 [Source:ZFIN;Acc:ZDB-GENE-010724-14]	N/A			N/A	
ENSDARG00000041589	adprhl1	2.21	ADP-ribosylhydrolase like 1 [Source:ZFIN;Acc:ZDB-GENE-041010-126]	N/A			N/A	
ENSDARG00000042529	gnat2	1.6	guanine nucleotide binding protein (G protein), alpha transducing activity polypeptide 2 [Source:ZFIN;Acc:ZDB-GENE-011128-10]	N/A			N/A	
ENSDARG00000044861	opn1lw2	2.61	opsin 1 (cone pigments), long-wave-sensitive, 2 [Source:ZFIN;Acc:ZDB-GENE-040718-141]	N/A			N/A	
ENSDARG00000045015	cyp27b1	-2.24	cytochrome P450, family 27, subfamily B, polypeptide 1 [Source:ZFIN;Acc:ZDB-GENE-111005-2]	N/A			N/A	
ENSDARG00000045677	opn1sw1	3.58	opsin 1 (cone pigments), short-wave-sensitive 1 [Source:ZFIN;Acc:ZDB-GENE-991109-25]	N/A			N/A	
ENSDARG00000045768	cry1aa	1.14	cryptochrome circadian clock 1aa [Source:ZFIN;Acc:ZDB-GENE-010426-2]	N/A			N/A	

ENSDARG00000051762	CABZ01080568.1	1.12		N/A			N/A	
ENSDARG00000053345	si:dkey-56i24.1	-2.43	si:dkey-56i24.1 [Source:ZFIN;Acc:ZDB-GENE-081105-8]	N/A			N/A	
ENSDARG00000053973	fetub	0.93	fetuin B [Source:ZFIN;Acc:ZDB-GENE-050208-4]	N/A			N/A	
ENSDARG00000055192	zgc:136930	-0.99	zgc:136930 [Source:ZFIN;Acc:ZDB-GENE-060312-16]	N/A			N/A	
ENSDARG00000055514	icn2	-1.74	ictacalcin 2 [Source:ZFIN;Acc:ZDB-GENE-070822-9]	N/A			N/A	
ENSDARG00000055527	cmn	-0.96	calymmin [Source:ZFIN;Acc:ZDB-GENE-000208-9]	N/A			N/A	
ENSDARG00000056248	si:dkey-183i3.5	-1.12	si:dkey-183i3.5 [Source:ZFIN;Acc:ZDB-GENE-030131-8568]	N/A			N/A	
ENSDARG00000056511	arr3a	2.13	arrestin 3a, retinal (X-arrestin) [Source:ZFIN;Acc:ZDB-GENE-040718-102]	N/A			N/A	
ENSDARG00000056836	si:ch211-125o16.4	-1.25	si:ch211-125o16.4 [Source:ZFIN;Acc:ZDB-GENE-131120-100]	N/A			N/A	
ENSDARG00000057460	crygm2d13	-1.1	crystallin, gamma M2d13 [Source:ZFIN;Acc:ZDB-GENE-040718-105]	N/A			N/A	
ENSDARG00000060549	ecel1	3.23	endothelin converting enzyme-like 1 [Source:ZFIN;Acc:ZDB-GENE-130530-692]	N/A			N/A	
ENSDARG00000060797	pfkmb	-1	phosphofructokinase, muscle b [Source:ZFIN;Acc:ZDB-GENE-081114-1]	N/A			N/A	

ENSDARG00000062632	duox	-2.45	dual oxidase [Source:ZFIN;Acc:ZDB-GENE-091117-14]	N/A			N/A	
ENSDARG00000062788	irg1l	2.26	immunoresponsive gene 1, like [Source:ZFIN;Acc:ZDB-GENE-061103-301]	N/A			N/A	
ENSDARG00000068947	si:ch211-264e16.1	-1.83	si:ch211-264e16.1 [Source:ZFIN;Acc:ZDB-GENE-060503-226]	N/A			N/A	
ENSDARG00000069192	zgc:163030	-1.53	zgc:163030 [Source:ZFIN;Acc:ZDB-GENE-060810-77]	N/A			N/A	
ENSDARG00000069817	crygm2d17	-1.15	crystallin, gamma M2d17 [Source:ZFIN;Acc:ZDB-GENE-070720-9]	N/A			N/A	
ENSDARG00000069826	crygm2d15	-1.26	crystallin, gamma M2d15 [Source:ZFIN;Acc:ZDB-GENE-040718-322]	N/A			N/A	
ENSDARG00000071250	tmem79a	2.57	transmembrane protein 79a [Source:ZFIN;Acc:ZDB-GENE-060503-538]	N/A			N/A	
ENSDARG00000071558	fblim1	2.41	filamin binding LIM protein 1 [Source:ZFIN;Acc:ZDB-GENE-061013-662]	N/A			N/A	
ENSDARG00000073750	crygm2d9	-1.15	crystallin, gamma M2d9 [Source:ZFIN;Acc:ZDB-GENE-081105-81]	N/A			N/A	
ENSDARG00000073874	crygm2d6	-1.14	crystallin, gamma M2d6 [Source:ZFIN;Acc:ZDB-GENE-040625-145]	N/A			N/A	
ENSDARG00000074306	ctslb	-4.21	cathepsin Lb [Source:ZFIN;Acc:ZDB-GENE-980526-285]	N/A			N/A	
ENSDARG00000075191	oacyl	-1.37	O-acyltransferase like [Source:ZFIN;Acc:ZDB-GENE-090710-2]	N/A			N/A	
ENSDARG00000075527	zgc:174154	-3.5	zgc:174154 [Source:ZFIN;Acc:ZDB-GENE-071004-116]	N/A			N/A	

ENSDARG00000076221	zgc:198419	-2.9	zgc:198419 [Source:ZFIN;Acc:ZDB-GENE-030131-7540]	N/A			N/A	
ENSDARG00000076294	klb	-2.07	klotho beta [Source:ZFIN;Acc:ZDB-GENE-110909-4]	N/A			N/A	
ENSDARG00000076572	crygm2d7	-1.19	crystallin, gamma M2d7 [Source:ZFIN;Acc:ZDB-GENE-060918-5]	N/A			N/A	
ENSDARG00000076693	crygm2d19	-0.97	ID no longer valid	N/A			N/A	
ENSDARG00000076839	ftr86	1.41	finTRIM family, member 86 [Source:ZFIN;Acc:ZDB-GENE-060929-108]	N/A			N/A	
ENSDARG00000077169	si:ch211-153b23.4	1.63	si:ch211-153b23.4 [Source:ZFIN;Acc:ZDB-GENE-030131-7332]	N/A			N/A	
ENSDARG00000079064	CABZ01079080.1	1.37		N/A			N/A	
ENSDARG00000079771	pea15	1.56	proliferation and apoptosis adaptor protein 15 [Source:ZFIN;Acc:ZDB-GENE-170119-2]	N/A			N/A	
ENSDARG00000080337	NC_002333.4	-2.26		N/A			N/A	
ENSDARG00000081218	RF00002	-6.39		N/A			N/A	
ENSDARG00000081270	rn7sk	-4.38	RNA, 7SK small nuclear [Source:ZFIN;Acc:ZDB-GENE-090323-1]	N/A			N/A	
ENSDARG00000082321	RF00004	-5.02		N/A			N/A	

ENSDARG00000082753	NC_002333.17	-2.62		N/A			N/A	
ENSDARG00000086356	CABZ01078944.1	2.82	ID no longer valid	N/A			N/A	
ENSDARG00000086912	crygm2d18	-1.23	ID no longer valid	N/A			N/A	
ENSDARG00000086917	crygm2d2	-0.98	crystallin, gamma M2d2 [Source:ZFIN;Acc:ZDB-GENE-060918-1]	N/A			N/A	
ENSDARG00000087164	crygm2d4	-1.03	crystallin, gamma M2d4 [Source:ZFIN;Acc:ZDB-GENE-060918-3]	N/A			N/A	
ENSDARG00000087301	crygm2d14	-1.37	crystallin, gamma M2d14 [Source:ZFIN;Acc:ZDB-GENE-070822-20]	N/A			N/A	
ENSDARG00000087324	crygm2d1	-1.01	crystallin, gamma M2d1 [Source:ZFIN;Acc:ZDB-GENE-050522-395]	N/A			N/A	
ENSDARG00000087337	wu:fi09b08	-5.41	ID no longer valid	N/A			N/A	
ENSDARG00000087377	lbh	3.96	limb bud and heart development, new ID: ENSDARG00000111701; ZFIN ID: ZDB-GENE-040426-1613	N/A			N/A	
ENSDARG00000087440	ponzr4	-2.56	plac8 onzin related protein 4 [Source:ZFIN;Acc:ZDB-GENE-050411-6]	N/A			N/A	
ENSDARG00000087641	cdh26.2	-1.93	cadherin 26, tandem duplicate 2 [Source:ZFIN;Acc:ZDB-GENE-100922-183]	N/A			N/A	
ENSDARG00000087732	RF00017	-6.02		N/A			N/A	

ENSDARG00000087843	cntn1a	1.85	contactin 1a [Source:ZFIN;Acc:ZDB-GENE-030427-1]	N/A			N/A	
ENSDARG00000087953	wu:fi09b08	-6.12	ID no longer valid	N/A			N/A	
ENSDARG00000088589	ponzr3	-2.14	plac8 onzin related protein 3 [Source:ZFIN;Acc:ZDB-GENE-050506-38]	N/A			N/A	
ENSDARG00000088687	crygm2d17	-1.19	ID no longer valid	N/A			N/A	
ENSDARG00000089382	zgc:158463	-5.39	zgc:158463 [Source:ZFIN;Acc:ZDB-GENE-070410-9]	N/A			N/A	
ENSDARG00000089617	RF00009	-6.56		N/A			N/A	
ENSDARG00000089750	si:dkey-26g8.5	-1.93	si:dkey-26g8.5 [Source:ZFIN;Acc:ZDB-GENE-121214-19]	N/A			N/A	
ENSDARG00000089806	si:dkey-239j18.3	-3.66	si:dkey-239j18.3 [Source:ZFIN;Acc:ZDB-GENE-121214-39]	N/A			N/A	
ENSDARG00000091148	crygm2d20	-1.17	crystallin, gamma M2d20 [Source:ZFIN;Acc:ZDB-GENE-070424-32]	N/A			N/A	
ENSDARG00000091618	cltcl1	1.25	clathrin, heavy chain-like 1 [Source:ZFIN;Acc:ZDB-GENE-130530-1029]	N/A			N/A	
ENSDARG00000091996	si:ch211-117m20.5	-1.27	si:ch211-117m20.5 [Source:ZFIN;Acc:ZDB-GENE-030131-12]	N/A			N/A	
ENSDARG00000093120	si:dkey-117m1.4	1.91	si:dkey-117m1.4 [Source:ZFIN;Acc:ZDB-GENE-090313-177]	N/A			N/A	
ENSDARG00000093318	si:dkey-57a22.15	-2.14	si:dkey-57a22.15 [Source:ZFIN;Acc:ZDB-GENE-081104-427]	N/A			N/A	

ENSDARG00000093480	pamr1	2.72	peptidase domain containing associated with muscle regeneration 1 [Source:ZFIN;Acc:ZDB-GENE-100422-12]	N/A			N/A	
ENSDARG00000093584	zgc:193505	-1.14	zgc:193505 [Source:ZFIN;Acc:ZDB-GENE-030131-7103]	N/A			N/A	
ENSDARG00000094210	zgc:109934	-1.96	zgc:109934 [Source:ZFIN;Acc:ZDB-GENE-050522-428]	N/A			N/A	
ENSDARG00000094559	zgc:174855	-3.38	zgc:174855 [Source:ZFIN;Acc:ZDB-GENE-071004-74]	N/A			N/A	
ENSDARG00000095744	si:dkey-269i1.4	-3.91	si:dkey-269i1.4 [Source:ZFIN;Acc:ZDB-GENE-121214-37]	N/A			N/A	
ENSDARG00000095850	CU672266.1	1.96		N/A			N/A	
ENSDARG00000096403	CT027638.1	0		N/A			N/A	
ENSDARG00000096454	ap1m2	1.92	adaptor-related protein complex 1, mu 2 subunit [Source:ZFIN;Acc:ZDB-GENE-041114-20]	N/A			N/A	
ENSDARG00000096712	si:dkey-193p11.2	-1.59	si:dkey-193p11.2 [Source:ZFIN;Acc:ZDB-GENE-030131-8407]	N/A			N/A	
ENSDARG00000096727	CT737227.1	-1.65		N/A			N/A	
ENSDARG00000097008	opn1mw1	4.02	opsin 1 (cone pigments), medium-wave-sensitive, 1 [Source:ZFIN;Acc:ZDB-GENE-990604-42]	N/A			N/A	

ENSDARG00000097523	si:ch73-364h19.1	2.39	si:ch73-364h19.1 [Source:ZFIN;Acc:ZDB-GENE-031010-45]	N/A			N/A	
ENSDARG00000098011	BX000438.2	-1.58		N/A			N/A	
ENSDARG00000098994	CR352263.1	1.21		N/A			N/A	
ENSDARG00000099362	CABZ01088346.1	-1.49		N/A			N/A	
ENSDARG00000099420	nme2b.2	1.07	NME/NM23 nucleoside diphosphate kinase 2b, tandem duplicate 2 [Source:ZFIN;Acc:ZDB-GENE-000210-33]	N/A			N/A	
ENSDARG00000099425	CABZ01073265.1	1.14	complement factor I [Source:NCBI gene;Acc:557557]	N/A			N/A	
ENSDARG00000100181	lamp1a	1.73	lysosomal associated membrane protein 1a [Source:ZFIN;Acc:ZDB-GENE-030131-3708]	N/A			N/A	
ENSDARG00000100266	si:dkey-77p23.6	-6.53	ID no longer valid	N/A			N/A	
ENSDARG00000100353	si:ch1073-398f15.1	-1.76	si:ch1073-398f15.1 [Source:ZFIN;Acc:ZDB-GENE-141212-388]	N/A			N/A	
ENSDARG00000100582	si:ch211-195b11.3	-1.11	si:ch211-195b11.3 [Source:ZFIN;Acc:ZDB-GENE-141222-6]	N/A			N/A	
ENSDARG00000100660	si:ch73-252i11.1	3.37	si:ch73-252i11.1 [Source:ZFIN;Acc:ZDB-GENE-141210-7]	N/A			N/A	
ENSDARG00000100833	si:dkey-269i1.4	-2.86	si:dkey-269i1.4 [Source:ZFIN;Acc:ZDB-GENE-121214-37]	N/A			N/A	

ENSDARG00000100904	CABZ01109021.1	2.93		N/A			N/A	
ENSDARG00000100957	CABZ01113883.1	1.65	ID no longer valid	N/A			N/A	
ENSDARG00000101200	zgc:112964	-1.18	zgc:112964 [Source:ZFIN;Acc:ZDB-GENE-050306-47]	N/A			N/A	
ENSDARG00000101324	apoa1b	-0.98	apolipoprotein A-Ib [Source:ZFIN;Acc:ZDB-GENE-050302-172]	N/A			N/A	
ENSDARG00000101840	U3	-5.67	ID no longer valid	N/A			N/A	
ENSDARG00000102207	zgc:86738	-1.26	zgc:86738 [Source:ZFIN;Acc:ZDB-GENE-040625-151]	N/A			N/A	
ENSDARG00000102300	ca9	-1.34	carbonic anhydrase IX [Source:ZFIN;Acc:ZDB-GENE-080818-5]	N/A			N/A	
ENSDARG00000102364	si:dkey-202l22.6	-2.33	si:dkey-202l22.6 [Source:ZFIN;Acc:ZDB-GENE-131121-181]	N/A			N/A	
ENSDARG00000102421	acp7	1.88	acid phosphatase 7, tartrate resistant (putative) [Source:ZFIN;Acc:ZDB-GENE-070615-9]	N/A			N/A	
ENSDARG00000102907	CABZ01072043.1	2.8	ID no longer valid	N/A			N/A	
ENSDARG00000103069	LSAMP	1.6	limbic system associated membrane protein [Source:HGNC Symbol;Acc:HGNC:6705]	N/A			N/A	

ENSDARG00000103543	gngt2b	2.38	guanine nucleotide binding protein (G protein), gamma transducing activity polypeptide 2b [Source:ZFIN;Acc:ZDB-GENE-091020-4]	N/A			N/A	
ENSDARG00000103580	CABZ01110379.1	1.91		N/A			N/A	
ENSDARG00000103775	thbs1a	1.58	thrombospondin 1a [Source:ZFIN;Acc:ZDB-GENE-120402-2]	N/A			N/A	
ENSDARG00000103816	BX537263.1	0	ID no longer valid	N/A			N/A	
ENSDARG00000103826	gpib	-1.14	glucose-6-phosphate isomerase b [Source:ZFIN;Acc:ZDB-GENE-020513-3]	N/A			N/A	
ENSDARG00000103946	si:dkey-124l13.1	4.38	si:dkey-124l13.1 [Source:ZFIN;Acc:ZDB-GENE-141215-10]	N/A			N/A	
ENSDARG00000104296	zgc:165508	2.25	zgc:165508 [Source:ZFIN;Acc:ZDB-GENE-070719-4]	N/A			N/A	
ENSDARG00000104615	CABZ01087568.1	1.06	ID no longer valid	N/A			N/A	
ENSDARG00000104713	zgc:165653	1.72	zgc:165653 [Source:ZFIN;Acc:ZDB-GENE-070620-24]	N/A			N/A	
ENSDARG00000104790	wu:fi09b08	-5.01	ID no longer valid	N/A			N/A	
ENSDARG00000104919	si:ch211-153b23.3	2.67	si:ch211-153b23.3 [Source:ZFIN;Acc:ZDB-GENE-141216-408]	N/A			N/A	

ENSDARG00000104937	CABZ01084323.1	0.97	protein tyrosine phosphatase, receptor type D [Source:NCBI gene;Acc:100330629]	N/A			N/A	
ENSDARG00000105333	fbn1	3.21	ID no longer valid (fibrillin 1; ZFIN ID: ZDB-GENE-091204-466)	N/A			N/A	
ENSDARG00000105341	si:dkey-9l20.3	-1.03	si:dkey-9l20.3 [Source:ZFIN;Acc:ZDB-GENE-090313-369]	N/A			N/A	

Annexe 8: Review article "Fishing for causes and cures of motor neuron disorders"

Fishing for causes and cures of motor neuron disorders

Patten S. A., Armstrong G. A. B., **Lissouba A**., Kabashi E., Parker J. A., and Drapeau P.

Disease Models & Mechanisms 2014 7: 799-809

10.1242/dmm.015719

© 2014. Published by The Company of Biologists Ltd | Disease Models & Mechanisms (2014) 7, 799-809 doi:10.1242/dmm.015719

REVIEW

Fishing for causes and cures of motor neuron disorders

Shunmoogum A. Patten[1], Gary A. B. Armstrong[1], Alexandra Lissouba[1], Edor Kabashi[2], J. Alex Parker[1] and Pierre Drapeau[1,*]

ABSTRACT

Motor neuron disorders (MNDs) are a clinically heterogeneous group of neurological diseases characterized by progressive degeneration of motor neurons, and share some common pathological pathways. Despite remarkable advances in our understanding of these diseases, no curative treatment for MNDs exists. To better understand the pathogenesis of MNDs and to help develop new treatments, the establishment of animal models that can be studied efficiently and thoroughly is paramount. The zebrafish (*Danio rerio*) is increasingly becoming a valuable model for studying human diseases and in screening for potential therapeutics. In this Review, we highlight recent progress in using zebrafish to study the pathology of the most common MNDs: spinal muscular atrophy (SMA), amyotrophic lateral sclerosis (ALS) and hereditary spastic paraplegia (HSP). These studies indicate the power of zebrafish as a model to study the consequences of disease-related genes, because zebrafish homologues of human genes have conserved functions with respect to the aetiology of MNDs. Zebrafish also complement other animal models for the study of pathological mechanisms of MNDs and are particularly advantageous for the screening of compounds with therapeutic potential. We present an overview of their potential usefulness in MND drug discovery, which is just beginning and holds much promise for future therapeutic development.

KEY WORDS: ALS, HSP, SMA, Zebrafish, Drug discovery, Motor neuron disorders

Introduction

Motor neuron disorders (MNDs) are characterized by progressive loss of motor neurons of the spinal cord (‘lower motor neurons’) or motor neurons of the brain (‘upper motor neurons’), or both, leading to atrophy and/or spasticity of the associated musculature. Spinal muscular atrophy (SMA), amyotrophic lateral sclerosis (ALS) and hereditary spastic paraplegia (HSP) are the most common MNDs, and we summarise their aetiologies and genetics. We then present a critical overview of the methods available to model genetic mutations in zebrafish as well as their limitations. In the main body of the article, we highlight zebrafish models for each of these MNDs and discuss recent advances in developing drug screens, with a special focus on ALS.

SMA is a neurodegenerative disease presented clinically by progressive degeneration of lower motor neurons in the anterior horn of the spinal cord, resulting in hypotonia, muscle atrophy, paralysis and, in severe cases, death (Khaniani et al., 2013). It is a genetically heterogeneous disorder, with most cases displaying a recessive inheritance; however, autosomal dominant and X-linked inheritance have been reported (Greenberg et al., 1988; Jiang et al., 2013). Over 20 studies with zebrafish models of SMA have been published to date and, out of the MNDs, stable genetic models are most advanced for SMA because many of the causative mutations cause loss of function, which, as described below, can be readily studied in zebrafish.

ALS is a late-onset neurodegenerative disorder that affects both upper and lower motor neurons and is the most common MND. Although the majority of ALS cases are sporadic, up to 10% are inherited, with mutations in over two-dozen genes accounting for the majority of familial causes (Robberecht and Philips, 2013). The recent explosion in ALS genetics has attracted many researchers to the field, and zebrafish models have been the first animal models developed for several of these genes, for which some have been advanced to therapeutic screening and drug discovery.

HSP is the collective term for a group of clinically and genetically heterogeneous neurodegenerative disorders characterized by progressive spasticity and weakness in the lower limbs due to loss of upper motor neurons (Harding, 1983). The clinical heterogeneity of HSP is related to a notable genetic heterogeneity; however, insight into the genetic basis of these disorders is expanding rapidly (Dion et al., 2009; Finsterer et al., 2012) and supports a close genetic link between HSP and other neurodegenerative diseases (Novarino et al., 2014). Zebrafish models for the disease have been presented in numerous publications and have been used to provide insights into the pathological mechanisms underlying the disease.

Common pathological pathways between the different MNDs

Although MNDs have quite different aetiologies, they are all typified by progressive paralysis resulting in severe disability. The pathogenesis of MNDs remains to be fully understood and there is a crucial need for the development of novel therapeutic strategies for their treatment. A thorough understanding of disease pathophysiology is necessary to direct rationale design of therapeutic strategies. As mentioned above, MNDs are characterized by the degeneration of upper and/or lower motor neurons and this is due to a dysfunction of several different cellular processes. Despite the apparent heterogeneity in these MNDs (considered below in greater detail for SMA, ALS and HSP in turn, where we describe the major causative genes), several pathogenic pathways are common among at least two of these three diseases (summarized in Fig. 1). For instance, in both SMA and ALS, defects in RNA metabolism are implicated, which mainly lead to splicing anomalies in the nucleus and mRNA transport abnormalities in the cytoplasm. These defects have been implicated by mutations studied in zebrafish models of SMA (Akten et al., 2011; Lotti et al., 2012; Sleeman, 2013), in other models of SMA (Sleeman, 2013) and in various models of mutations in ALS (Ling et al., 2013; Sleeman, 2013). Additionally, ALS-related RNA foci sequester RNA-binding

[1]Department of Neuroscience, FRQS Groupe de Recherche sur le Système Nerveux Central and CRCHUM, University of Montréal, Montréal, QC H3A 2B4, Canada. [2]Institut du Cerveau et de la Moelle Épinière, Centre de Recherche, CHU Pitié-Salpétrière, 75013 Paris, France.

*Author for correspondence (p.drapeau@umontreal.ca)

Disease Models & Mechanisms (2014) doi:10.1242/dmm.015719

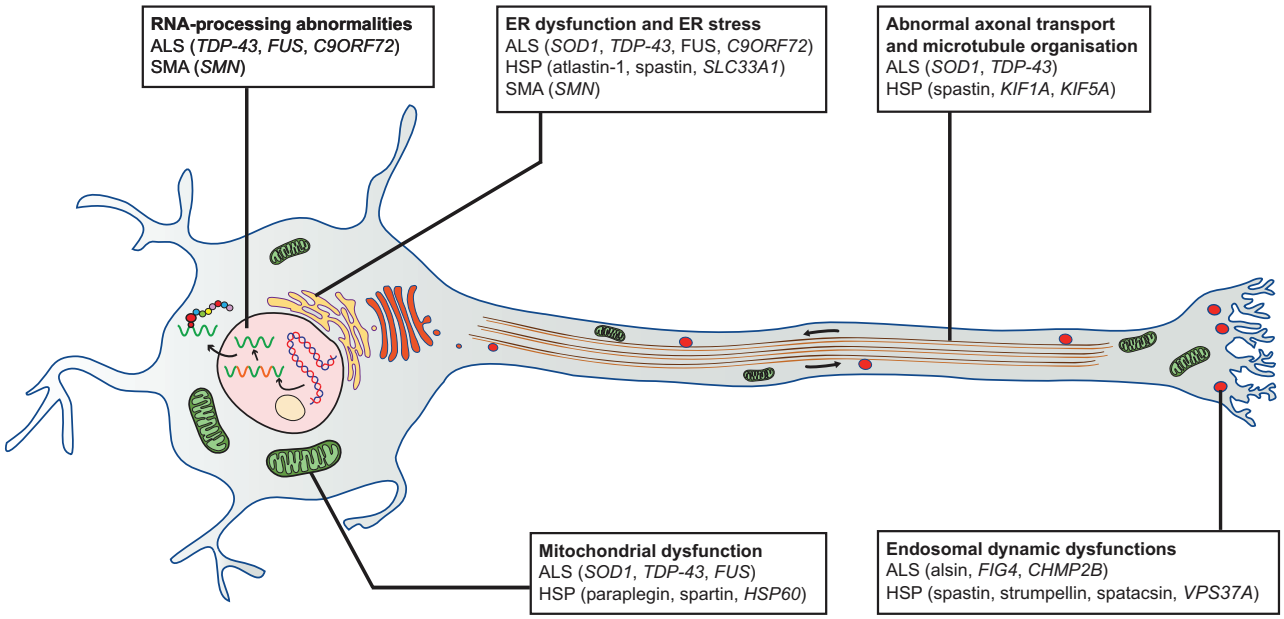

Fig. 1. Common pathological pathways in ALS, SMA and HSP. An illustration of a motor neuron, highlighting common possible mechanisms in the literature linking the MNDs. A non-exhaustive list of genes involved is given for each disease.

proteins and lead to possible RNA processing abnormalities (Gendron et al., 2014). Interestingly, some ALS genes have been shown to interact with genes in SMA and lead to an altered distribution of splicing factors (Achsel et al., 2013). However, no involvement of RNA metabolism has been reported in HSP.

RNA-processing genes implicated in ALS also lead to abnormal axonal transport and microtubule organisation (Godena et al., 2011; Ilieva et al., 2009), and an actin-binding protein was shown to rescue the phenotype in a zebrafish model of SMA (Oprea et al., 2008; Hao et al., 2012; Lyon et al., 2014). This has also been implicated in HSP, where spastin has been shown to be involved in microtubule severing, whereas other less common HSP genes are involved in axonal transport (Blackstone, 2012). Furthermore, many HSP genes are involved in endosomal dynamics (Blackstone, 2012), and dysfunction of endosomal dynamics has been reported for several less-common ALS-associated genes (Chen et al., 2013).

Endoplasmic reticulum (ER) stress as well as mitochondrial dysfunction have been reported as important pathological mechanisms in MNDs. For example, the inclusions found in ALS are thought to be associated with misfolding of mutant proteins and an inability of the unfolded protein response to dispose of them (Matus et al., 2013). Moreover, ER stress has been implicated in zebrafish models of ALS (Vaccaro et al., 2013), and ALS- and SMA-related proteins are important for stress granule formation (Matus et al., 2013). Several HSP genes are also involved in ER morphology and function (Blackstone, 2012). On the other hand, many HSP genes are also involved in mitochondrial dysfunction (Blackstone, 2012), as are ALS genes (Cozzolino and Carrì, 2012).

The zebrafish toolbox: how useful is it for studying MNDs?

In recent years, the zebrafish (*Danio rerio*) has received favourable attention from clinicians owing to its advantages as a model system for the study of disease, because the zebrafish models often closely resemble the relevant human disease (Lieschke and Currie, 2007). Importantly, more than 80% of zebrafish genes share a high level of synteny across vertebrate species, in addition to 50-80% amino acid identity with most human homologues, including homologues for over 80% of disease-causing genes (Howe et al., 2013). The majority of these genes can be manipulated by loss- or gain-of-function approaches in simple transient assays of gene function and by the creation of stable disease models using genome-editing techniques. This unique 'toolbox' makes the zebrafish model system valuable for the study of MNDs, as discussed below.

The genetics underpinning MNDs have undergone a revolution in the last decade. Much of this can be attributed to recent advances in sequencing technologies that have greatly increased the speed and reduced the costs associated with genotyping and identifying variants in individuals afflicted with disease. Nonetheless, validating the pathogenicity of identified variants remains a challenge in human genomics for the identification of causative mutations. Although considerable efforts have been made to generate mammalian models of some of the described disease-causing mutations, zebrafish have offered an inexpensive and rapid alternative to the costly and labour-intensive requirements that accompany the creation of murine models of neurodegenerative disease. This is particularly true for some of the recently identified disease-causing genes associated with MNDs (Table 1). We note that, although no animal model, be it zebrafish or mouse, can reproduce and thus accurately model all of the subtleties of a human disease and thus are not necessarily disease models, these genetic models do reflect important molecular, cellular and even physiological features that are pertinent to disease pathobiology and pharmacological screening.

The easiest approach and therefore usually the first taken to study loss-of-function mutations in zebrafish is the injection of antisense morpholino oligonucleotides. An important caveat of the approach is that knockdown needs to be controlled for off-target toxicity by testing for the lack of effect with mismatched morpholinos and, most importantly for disease models, by demonstrating at least partial (hypomorphic) rescue by the homologous human mRNA. Furthermore, the technique is not appropriate for studying late-onset-disease-related phenotypes such as in many MNDs. Nonetheless, transient knockdowns can be useful for drug testing pertinent phenotypes at earlier embryonic and larval stages, and their

Table 1. Clinical features and the genetics of MNDs

Disease	Motor neuron involvement	Clinical features	Human gene	Zebrafish model
SMA	LMNs	Muscle weakness and atrophy	*SMN1*	Morpholino
				Mutant (Tg: *SMN2*; TILLING: *smn*^{G264D}, *smn*^{Y262X} and *smn*^{L265X})
ALS	UMNs and LMNs	Progressive muscle weakness, atrophy and spasticity	*SOD1*	Morpholino
				Mutant (Tg: *sod1*^{G93R} and *sod1*^{G85R}; TILLING: *sod1*^{T70I})
				Overexpression (*SOD1*^{G93A}, *SOD1*^{A4V}, *SOD1*^{G37R})
			TARDBP	Morpholino
				Mutant (TILLING: *tardbp*^{Y220X}; ZFNs: *tardbp*$^{-/-}$ and *tardbpl*$^{-/-}$)
				Overexpression (*TARDBP*^{G348C},*TARDBP*^{A315T},*TARDBP*^{A382T})
			FUS	Morpholino
				Overexpression (*FUS*^{R521H}, *FUS*^{R521C}, *FUS*^{S57D}, *FUS*^{R495X}, *FUS*^{G515X}, *FUS*^{R521G}, *FUS*^{H517Q}, *FUS*^{P525L})
			C9ORF72	Morpholino (*c13h9orf72*)
HSP	UMNs	Progressive spasticity in the lower limbs	*SPG4* (spastin)	Morpholino
			SPG8 (strumellin)	Morpholino
			SPG11 (spatacsin)	Morpholino
			SPG15 (spastizin)	Morpholino
			SPG3A (atlastin-1)	Morpholino
			SPG46 (*GBA2*)	Morpholino
			SPG42 (*SLC33A1*)	Morpholino
			SPG39 (*PNPLA6*)	Morpholino
			SPG53 (*VPS37A*)	Morpholino
			ALS2	Morpholino
			ARL6IP1	Morpholino
			MARS	Morpholino
			PGAP1	Morpholino
			USP8	Morpholino

ALS, amyotrophic lateral sclerosis; SMA, spinal muscular atrophy; HSP, hereditary spastic paraplegia; UMN, upper motor neuron; LMN, lower motor neuron; Tg, transgenic; TILLING, targeted induced localized lesions in genomes; ZFNs, zinc-finger nucleases. 'Overexpression' refers to zebrafish models whereby the embryos were injected with human mutated mRNA. The references for each zebrafish model are cited in the text.

advantage for high-throughput screening lies in this area (Phillips and Westerfield, 2014). Recently, powerful genome-editing techniques have been developed to generate stable loss-of-function models for neurodegenerative diseases (Schmid and Haass, 2013). These techniques have their own disadvantages because some are complex and expensive [e.g. TILLING (targeting induced local lesions in genomes) and ZFNs (zinc-finger nucleases)], or can carry their own off-target toxicity [e.g. CRISPR (clustered regularly interspaced short palindromic repeats)/Cas], such as transcriptional and post-transcriptional alterations (Varshney and Burgess, 2014). Nonetheless, genome-editing techniques have been used successfully to generate useful zebrafish models of MND, particularly in studies of SMA.

Gain of function is most easily modelled by mRNA injections, either to test for phenotypes induced by mutant alleles (dominant-negative or toxic gain of function, with the former but not the latter rescued by wild-type mRNA), or rescue of gene-knockdown or -knockout phenotypes (to test for loss of function). As with morpholinos, the transient expression of injected mRNA is not useful for late-onset phenotypes but can be quite useful for drug screening in embryos and larvae. Stable transgenesis for the study of gain-of-function mutations is a popular approach in zebrafish using the efficient *Tol2* transposon system (Suster et al., 2009). However, it requires out-crossing over several generations to isolate lines with ideally single insertions and neither too little nor too much transgene expression. Interestingly, a number of promoters are available for neural-specific expression and their inclusion in *Tol2* constructs can be used to create transgenic lines with cell-specific expression patterns (Kabashi et al., 2011b). Several MNDs have been modelled in zebrafish by the introduction of human transgenes, but stable transgenic models also have their limitations, the three major ones being ectopic expression, toxic overexpression and variability due to the genetic background (see Kabashi et al., 2011b). New and possibly simpler strategies have come from recent genome-editing approaches and many MND models using these new approaches are being developed, although no gain-of-function models have been published to date. These are particularly difficult to make because stable transgenic or genomically edited genotypes, even when heterozygous, could prove lethal, so conditional mutations might have to be engineered.

Despite some of these limitations, particularly with regard to recapitulating dominant mutations and missense mutations, the techniques currently available have been used with great success to replicate several aspects of some MNDs, as discussed in detail below. Together with site-specific transgenesis using PhiC31 (Roberts et al., 2014), Cre-*loxP* (Lin et al., 2013), the *Gal4/UAS* system (Halpern et al., 2008) and a range of inducible systems that are amenable for use in the model, these genomic engineering tools will accelerate the development of MND models in the zebrafish.

Zebrafish as a tool for drug screening

Animal models of a disease can be used as tools for therapeutic discovery of compounds that suppress the disease phenotype, regardless of the specific molecular targets. In the last few years, it has become apparent that zebrafish is a powerful model organism amenable to high-throughput drug screening *in vivo* at embryonic and larval stages (North et al., 2007; White et al., 2011; Zon and Peterson, 2005). Thus, this model organism is becoming valuable in the preclinical pipeline to bridge the gap between *in vitro* assays and more costly screens in mammals (Giacomotto and Ségalat, 2010; Lieschke and Currie, 2007). Several studies have explored the potential of zebrafish as a model system for drug screening campaigns for cardiovascular diseases (Chan and Mably, 2011; Chico et al., 2008; Asnani and Peterson, 2014), new cancer

therapies (Liu and Leach, 2011b; Stoletov and Klemke, 2008; Tat et al., 2013) and neural disorders (Baraban et al., 2013; Flinn et al., 2008; Gerlai, 2010; Vaccaro et al., 2013; Vaccaro et al., 2012a). Below we review each of the available models for the three most common MNDs as well as recent progress in developing drug discovery approaches.

Spinal muscular atrophy (SMA)

Background

SMA is a currently incurable neurodegenerative disease characterised by the loss of lower motor neurons, resulting in system-wide muscle atrophy (Hamilton and Gillingwater, 2013). SMA is primarily caused by deletion of the survival motor neuron 1 (*SMN1*) gene (Lefebvre et al., 1995). Clinically, SMA due to SMN1 mutation is classified as type I (severe), II (intermediate), III (mild) or IV (adult-onset) based on disease onset and severity. The *SMN2* gene is an almost identical copy of *SMN1*, and both genes encode the protein SMN (Lefebvre et al., 1995). The severity of the disease also depends on the amount of functional SMN protein produced by *SMN2* and is thus dependent on *SMN2* copy number (Hamilton and Gillingwater, 2013), with none or a single copy in type I SMA and increasing to four or more copies in type IV SMA. Zebrafish studies have primarily focused on *SMN1* because the gene can be readily studied using loss-of-function approaches.

SMN is a ubiquitously expressed nuclear and cytoplasmic protein. It is part of a multiprotein complex localised to the nuclear Gem (for Gemini of coiled bodies) bodies and is necessary for the assembly of small nuclear ribonucleoproteins (snRNPs), a central element of the spliceosome. These Gem bodies are lost in SMA, thus indicating altered splicing as a possible cause for the disease (Sleeman, 2013). Additionally, low levels of SMN seem to disrupt the cellular localisation of some mRNAs and this could be due to a possible role of SMN in the formation and/or function of messenger ribonucleoproteins (mRNP) responsible for transporting mRNAs to distal compartments of the cell (Sleeman, 2013).

Zebrafish models of SMA

In zebrafish larvae, knockdown of *smn* to levels similar to those observed in humans with SMA results in truncated and under-branched ventral root axons and impairments in pathfinding to target musculature (McWhorter et al., 2003). The transient *smn* morphant model can be rescued by wild-type human *SMN* but not disease-causing forms (Carrel et al., 2006). Interestingly, weaker mutations rescued the phenotype at a higher dose, highlighting the sensitivity of the zebrafish system (Workman et al., 2009).

In a subsequent study, three putative *smn* mutations were generated by TILLING (Boon et al., 2009). Two mutations encoded premature stop codons (Y262X, L265X) and resulted in a deletion of the C-terminus, whereas the third encoded a point mutation (G264D) that corresponded to a human mutation associated with a severe form of SMA. Homozygous larvae expressing the Smn protein with the premature stop codon had reduced Smn protein levels by 7 days post-fertilisation (dpf) and died within 9-16 dpf. Homozygous carriers of the point mutation also displayed reduced Smn protein levels but died over a longer timeframe (13-21 dpf). In addition to the early mortality associated with loss of Smn protein expression, neuromuscular junctions (NMJs) from homozygous mutants displayed loss of colocalisation of pre- and post-synaptic markers. Transgenic expression of human SMN in motor neurons slightly increased survival in one of the homozygous mutants expressing the truncated Smn protein and recovered colocalisation of NMJ markers, indicating a cell-autonomous role for SMN in motor neurons (Boon et al., 2009). SMN mutants transgenically expressing human *SMN2* (for which there is no zebrafish homologue) also confirmed that the human *SMN2* gene is spliced in zebrafish and that increasing expression from this transgene can increase survival (Hao et al., 2011). Maternal Smn was removed from *smn* mutants so that early defects in motor neurons could be examined. Maternal:zygotic *smn* mutants were generated and revealed defects in axonal and dendritic branches as well as movement defects, indicating that SMN is crucial for motor neuron development (Hao et al., 2013). By conditionally driving the human *SMN2* gene in these animals by using the heat-shock promoter, it was shown that SMN is needed soon after motor neurons are born to rescue their development (Hao et al., 2013). These experiments show the utility of zebrafish models to test both the temporal and spatial requirement for a particular disease gene. Importantly, these transgenic and mutant approaches recapitulated the morphant phenotypes and thus support the knockdown approach for this gene. Moreover, the zebrafish line generated by Hao et al. represents a useful tool for screening for molecules that affect *SMN2* splicing (Hao et al., 2011).

More recent studies have investigated underlying pathogenic mechanisms in these SMA models. Overexpression of progranulin, whose loss of function (by nonsense-mediated decay) causes fronto-temporal lobar degeneration, rescued the shortened motor neuron phenotype upon *smn* knockdown in zebrafish (Chitramuthu et al., 2010). Plastin 3, an actin-binding and bundling protein identified as a protective modifier of SMA (Oprea et al., 2008), rescued the zebrafish knockdown phenotype, including movement defects, when expressed as either actin-dependent or -independent constructs (Hao et al., 2012; Lyon et al., 2014). As mentioned earlier, defects in RNA metabolism (Ling et al., 2013; Sleeman, 2013) and rescue by the actin-binding protein plastin 3 (Lyon et al., 2014) were observed in zebrafish models of *smn*. Combinations of genomics and morpholino knockdown demonstrated a link between *smn* and the adhesive molecule neurexin 2 (See et al., 2014) and with chondrolectin expressed in motor neurons (Sleigh et al., 2014).

Chemical screens in zebrafish for SMA

In a recent study combining zebrafish, *Drosophila* and mouse models of SMA, dysregulation of ubiquitylation pathways caused β-catenin accumulation, and pharmacological inhibition of β-catenin by quercetin robustly ameliorated neuromuscular pathology (Wishart et al., 2014). Pharmacological or genetic suppression of ubiquitin-like modifier activating enzyme 1 (UBA1) was sufficient to recapitulate an SMA-like neuromuscular pathology in zebrafish, suggesting that UBA1 directly has an important role in disease pathogenesis. Tetrahydroindoles that alter the processing of amyloid precursor protein were tested in these various models and revealed that three of these compounds rescued motor neuron defects in *smn* morpholino knockdown zebrafish (Gassman et al., 2013). More generally, the results suggest that SMA could be an axonopathy (a disease in which the normal function of axons is disrupted), suggesting novel strategies for treating the disease. For example, pharmacological inhibition of pathways that are central to axonopathy have therapeutic potential as a treatment for SMA and many other neurological disorders in which axonal degeneration is a prominent feature.

Amyotrophic lateral sclerosis (ALS)

Background

ALS is a progressive neurodegenerative disorder characterised by the loss of both upper and lower motor neurons, leading to muscle

weakness, paralysis and eventual death by respiratory failure. The age of onset is usually between 50 to 60 years of age and death typically occurs rapidly, 2-5 years after diagnosis (Kiernan et al., 2011). There is currently no cure for ALS and the only US Food and Drug Administration (FDA)-approved drug, riluzole, prolongs survival by only a few months (Miller et al., 2012). Around 90% of ALS cases are sporadic (sALS), with unknown aetiology (although retrospective studies have identified a small number of mutation-associated causes); the remaining 10% of cases are familial (fALS), with more than 20 genes implicated (Chen et al., 2013). Here, we focus on four causative genes, *SOD1*, *TARDBP*, *FUS* and *C9ORF72*, that account for more than half of fALS cases and for which zebrafish models have been developed (Table 1).

Superoxide dismutase 1 (*SOD1*) was the first gene linked to ALS (Rosen et al., 1993) and, to date, more than 170 mutations, affecting essentially every exon, have been reported (http://alsod.iop.kcl.ac.uk). Mutations in *SOD1* are responsible for ~20% of fALS and ~1-7% of sALS (Andersen and Al-Chalabi, 2011). Despite numerous mouse models of *SOD1*, 20 years later it is still unclear how mutations in *SOD1* lead to ALS, although a toxic gain-of-function mechanism has been identified (Boillée et al., 2006). SOD1 is a ubiquitously expressed, mainly cytoplasmic, anti-oxidizing enzyme and the toxicity of mutant SOD1 could be due to many causes (Ilieva et al., 2009).

The TAR-DNA binding protein (*TARDBP*) gene encodes the protein TDP-43, which was first linked to ALS as the major component of the cytoplasmic, ubiquitin-positive inclusions found in the majority of ALS cases, i.e. without mutations (Arai et al., 2006; Neumann et al., 2006). Mutations in *TARDBP* (Kabashi et al., 2008; Sreedharan et al., 2008) are responsible for ~3% of fALS and ~1.5% of sALS cases, and more than 40 mutations have been linked to ALS, the vast majority being located in the C-terminal glycine-rich region, which is responsible for protein-protein interactions that are as-yet unidentified (Lattante et al., 2013). TDP-43 is a mainly nuclear DNA- and RNA-binding protein and is involved in many steps of RNA processing, including transcription, splicing, RNA transport and stress-granule formation (Da Cruz and Cleveland, 2011), but ALS mutations in these functional regions are rare and their functional consequences are not understood.

Shortly after the discovery of *TARDBP* mutations in ALS, mutations in the gene fused in sarcoma (*FUS*; encoding the protein FUS) were identified in individuals with ALS (Kwiatkowski et al., 2009; Vance et al., 2009). More than 50 mutations of *FUS* have now been described in ALS and are responsible for ~5% of fALS and <1% of sALS (Lattante et al., 2013). These mutations are mostly clustered at the C-terminus, at a predicted nuclear-localisation signal (Ling et al., 2013). FUS is a mainly nuclear DNA- and RNA-binding protein. It shares a high functional similarity with TDP-43 and is also involved in several steps of RNA metabolism, including transcription and splicing (Lagier-Tourenne et al., 2012). The identification of *FUS* mutations soon after *TARDBP* highlighted the importance of altered RNA metabolism as a possible cause of ALS.

A huge (1000-fold) GGGGCC hexanucleotide repeat expansion in the non-coding first intron of chromosome 9 open reading frame 72 (*C9ORF72*) was identified in a large percentage of fALS cases (~40%), and was also observed in ~7% of cases of sALS (DeJesus-Hernandez et al., 2011; Renton et al., 2011). The function of the evolutionarily conserved protein is unknown, as is the mechanism of toxicity of the repeat expansions. However, recent evidence implicates the sequestration of RNA-binding proteins in RNA foci formed by sense and antisense repeat-containing *C9ORF72* RNA, as well as repeat-associated non-ATG translation of both sense and antisense transcripts, leading to the expression of six expansion proteins that form cytoplasmic and intranuclear inclusions, although the toxic effect of haploinsufficiency is still debated (Gendron et al., 2014).

Zebrafish models of ALS

Although zebrafish models of *SOD1* toxic gain-of-function mutations appeared much later than mouse and rat models, they have nonetheless contributed recently to our understanding of the cellular and neuronal dysfunction of the disease. In 2007, Lemmens and colleagues demonstrated that overexpression of human mutant $SOD1^{A4V}$, $SOD1^{G93A}$ or $SOD1^{G37R}$ mRNA resulted in aberrant ventral root projections in zebrafish embryos (Lemmens et al., 2007), resembling mouse models of *SOD1* in which an early retraction of presynaptic motor endings, known as ‘dieback’, is observed prior to the death of motor neurons (for review, see Dadon-Nachum et al., 2011; Murray et al., 2010), indicating that early, notable changes occur at the NMJ long before clinical presentation of ALS, which could also be the case for individuals with ALS (Dadon-Nachum et al., 2011). This was the first dominant gain-of-function neurodegenerative disease model to be studied in zebrafish, and validated the use of this animal model for experimental investigation while providing evidence that early changes in neuronal structure could arise *in vivo* following expression of mutant proteins associated with SOD1 pathology. Stable transgenic mutant lines of zebrafish *sod1* (G93R) (Ramesh et al., 2010; Sakowski et al., 2012) have been generated more recently, including useful *sod1* (G93R and G85R) heat-shock reporter lines (McGown et al., 2012). These models display hallmarks of ALS that include an age-related decrease in swim endurance, atrophy of locomotor muscles, paralysis with concomitant loss of NMJ integrity and, in some cases, early death.

Sharp electrode recordings from the motor neuron cell body of postnatal (6- to 10-days old) presymptomatic $SOD1^{G85R}$ mice have revealed hyperexcitability in motor neuron populations in the spinal cord (Bories et al., 2007). An advantage of the larval zebrafish is that it lends easily to electrophysiological investigations not only at the periphery (NMJ) but also centrally, within the spinal cord. A recent report has demonstrated that, in a stable transgenic $SOD1^{G93R}$ zebrafish, spontaneous miniature glycinergic excitatory postsynaptic currents (mEPSCs) onto motor neurons occur at a lower frequency than in motor neurons of wild type and zebrafish expressing human wild-type *SOD1* (McGown et al., 2012). Although the cause of this reduction has not been elucidated, the authors propose that the early reductions in the strength of this synapse onto motor neurons, particularly at early stages in development when synaptic connections are forming, might have lasting consequences whereby even slight increases in excitability during adulthood can promote motor neuron stress (McGown et al., 2012).

In addition to *SOD1*, models for the more recently (since 2008) identified ALS genes *TARDBP*, *FUS* and *C9ORF72* have also been developed in the zebrafish. For these genes, the role of loss of function, toxic gain of function or perhaps their combination is still under evaluation in the field. Consequently, models for both genotypes have been developed, although mostly by transient approaches because knockouts and stable transgenic lines have taken longer to develop. Mutations in the *TARDBP* gene were identified in individuals with both familial and sporadic forms of ALS (Kabashi et al., 2008) and, soon after, a transient zebrafish genetic model was developed (Kabashi et al., 2010b; Sreedharan et al., 2008). In this model, expression of human *TARDBP* mRNA containing one of three missense mutations ($TARDBP^{G348C}$,

TARDBP^{A315T} or *TARDBP*^{A382T}), but importantly not wild-type *TARDBP* at the same level of expression (which is a problem in other models) (see Wegorzewska and Baloh, 2011), resulted in locomotor defects and hyperbranched ventral root projections to trunk musculature, as seen with zebrafish *SOD1* models. Furthermore, it was demonstrated that the knockdown of the zebrafish *tardbp* gene also resulted in locomotor and ventral root defects, which could be rescued by co-injection with wild-type *TARDBP* mRNA but not mutant mRNA (Kabashi et al., 2010b). Given the limitations of the transient approaches used to generate these models, however, the results from these albeit independent studies need to be interpreted with caution. Interestingly, increased NMJ denervation (possibly due to dieback) has also been reported in rat and mouse models of TDP-43 mutations (Swarup et al., 2011; Zhou et al., 2010). In a follow-up study, expression of *TARDBP*^{G348C} mRNA in zebrafish resulted in impaired neuromuscular synaptic transmission, reduced frequency of miniature endplate currents (mEPCs), reduced quantal transmission, orphaned presynaptic and postsynaptic structures at the NMJ, and motor neuron death following exposure to the glutamatergic agonist N-methyl-D-aspartate (NMDA) (Armstrong and Drapeau, 2013a).

These initial studies of *TARDBP* utilized transient genetic models of zebrafish orthologues. Recent efforts to generate *tardbp* knockout lines in zebrafish have highlighted an unexpected subtlety associated with the use of this model organism. Unlike mammals, zebrafish possess a paralogue of *tardbp* [Tar DNA binding protein-like (*tardbpl*)], which lacks the C-terminal glycine-rich region, presumably owing to a chromosome duplication event deep in its ancestral evolution (Postlethwait et al., 2000). Interestingly, a novel splice variant of *tardbpl* has been shown to recover loss of *tardbp* following gene disruption of the latter with ZFNs (Schmid et al., 2013), as well as in another fish line where a premature stop codon (Y220X) in *tardbp* was isolated by TILLING (Hewamadduma et al., 2013). In both studies, inactivation of both *tardbp* and *tardbpl* (the latter either by gene disruption by ZFNs or by knockdown) resulted in a severe phenotype and early lethality, although the phenotype of double heterozygotes has not been reported and might more closely resemble the ALS genotype (if due to haploinsufficiency) and perhaps the (partial) knockdown phenotype. This strong *tardbp/tardbpl* phenotype is highly reminiscent of *Drosophila* knockout models of the related *tbph* gene, which display early lethality in the second instar stage, and *Tardbp* knockout mice, which fail to implant during embryogenesis (Sephton et al., 2010; Voigt et al., 2010; Wu et al., 2010), confirming the important role that TDP-43 plays during developmental processes in disparately related organisms. However, caution is necessary when extrapolating these findings to ALS, because individuals with (heterozygous) mutations in *TARDBP* possess a wild-type copy of *TARDBP* in addition to the allele containing a missense mutation, both of which are expressed throughout the progression of this disease. In addition, it might not be the loss of function owing to haploinsufficiency but rather a toxic gain of function owing to missense mutations that causes the disease. Thus, it would be ideal to generate a heterozygous zebrafish model, with both a mutant and a wild-type allele, but a conditional gain of toxic function might be necessary if this proves lethal.

Although less studied, zebrafish models of other genes associated with ALS have been developed. Injection of human mutant *FUS* mRNA (P525L) resulted in disrupted nuclear import (Dormann et al., 2010) and accumulation in cytosolic stress granules (Bosco et al., 2010), and either mRNA or morpholino injection resulted in locomotor deficits and ventral root projection abnormalities (Kabashi et al., 2011a). Recent work has demonstrated that transient mutant human *FUS*^{R521H} expression resulted in pathological hallmarks of ALS at the zebrafish NMJ, which include reduced fidelity of synaptic transmission, reduced quantal content and abnormal synaptic morphology (Armstrong and Drapeau, 2013b), as for *TARDBP*. FUS and TDP-43 share some structural similarities, and evidence that they might act in a molecular pathway that is separate from SOD1, with TDP upstream from FUS, has been demonstrated by epistasis analyses in zebrafish (Kabashi et al., 2011a) and in *Drosophila* (Wang et al., 2011). However, lines with *fus* knockout or stable *FUS* transgenes are needed to advance studies using these models.

The recently reported hexanucleotide repeat expansion in *C9ORF72* that has been attributed to a large proportion of fALS and sALS cases (DeJesus-Hernandez et al., 2011; Renton et al., 2011) has garnered substantial interest among both ALS and fronto-temporal lobar degeneration researchers. There are no published mammalian models of *C9ORF72*, but a recent knockdown model of the zebrafish orthologue, *c13h9orf72*, demonstrated impaired locomotor activity and abnormal ventral root projections (Ciura et al., 2013). Because there is considerable interest in this gene of unknown function, undoubtedly much attention will be focused on elucidating the molecular and functional role it plays in conferring disease, in particular the possible toxic effects of the expansion in transgenic lines.

Chemical screens in zebrafish for ALS

Studies of a *sod1* mutant in zebrafish opened the possibility of screening small molecules for recovery from the phenotype. A neuronal-stress reporter line (McGown et al., 2013) was used to validate the effectiveness of riluzole in this model, the only drug currently used to treat ALS clinically, and olesoxime and apomorphine-S were found to be effective in an oxidative stress assay (Da Costa et al., 2014). One possible explanation for the anomalies described above occurring at the NMJ in zebrafish expressing mutant TDP-43 is reduced calcium ion entry in the presynaptic terminal during the action potential; these defects were completely prevented in larvae expressing mutant human *TARDBP* treated with L-type calcium channel agonists (Armstrong and Drapeau, 2013a).

As with studies of SMA combining zebrafish with other models, our strategy for drug discovery in ALS was to start with a chemical screen in a *Caenorhabditis elegans* model and then confirm the positive hits in a zebrafish model. Once compounds that reverse or ameliorate the disease phenotype are identified, they can be tested in mammalian systems and/or in clinical trials for FDA-approved compounds (Fig. 2). Worms grown in liquid culture exhibit a thrashing behaviour that is more vigorous than crawling on plates and we have found that this greatly accelerates neuronal dysfunction in transgenic models of ALS mutations (Vaccaro et al., 2012b). As a result, paralysis is manifested in a matter of hours in liquid culture instead of days as on solid agar plates, thus permitting a rapid, large-scale chemical screening assay in *C. elegans*. Starting with an *in vivo* pilot chemical screen using this strategy, we successfully demonstrated that our *C. elegans* and zebrafish ALS mutation models could be used to identify neuroprotective molecules. This, the first *in vivo* chemical genetic screening platform for ALS genes (Vaccaro et al., 2012a), revealed methylene blue (MB) as a potent suppressor of mutant TDP-43 and mutant FUS motor neuron toxicity *in vivo*. In both worms and fish, MB prevented motor deficits and reduced the level of oxidative stress observed upon the expression of mutant proteins. In a subsequent study, we showed

Disease Models & Mechanisms (2014) doi:10.1242/dmm.015719

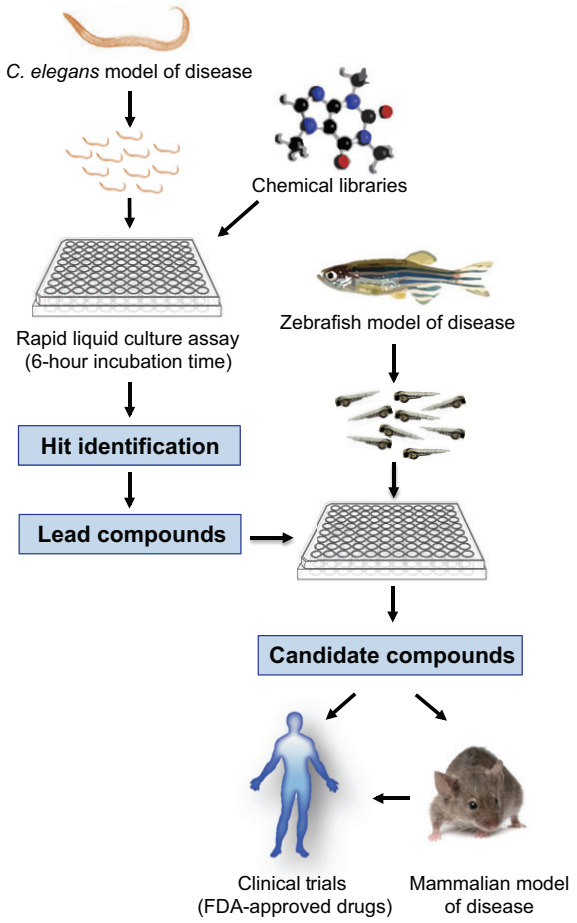

Fig. 2. Motor neuron disorders: from bench to clinic. One proposed strategy for drug discovery for MNDs (and other diseases) is to first start a large and rapid chemical screen in *C. elegans* and confirm the positive hits in a zebrafish. Once positive compounds that reverse or ameliorate the disease phenotype in both models are encountered, they can then be tested in mammal systems and/or go straight to clinical trials, if the compounds are already approved for safety and efficacy by the FDA.

that compounds structurally related to MB, such as salubrinal, guanabenz and the novel compound phenazine, are also potent suppressors of mutant TDP-43 proteotoxicity (Vaccaro et al., 2013). Our experiments demonstrated further that all these neuroprotective compounds function within the unfolded protein response during ER stress and they operate through different branches of this pathway to achieve neuroprotection (Vaccaro et al., 2013).

We have capitalized on the strength of our *in vivo* assays to screen large chemical libraries in the search for potential therapeutic drugs for ALS. We recently isolated a number of chemical suppressors of mutant TDP-43 toxicity (our unpublished data) and in particular we observed that several neuroleptics protect against development of the motor phenotype. The FDA-approved drug that emerged from this screen offers an exciting starting point for further ALS research because one can work back to identify the target(s) of positive hits and investigate their mode of action to better understand the mechanism of disease pathogenesis. In addition to 'repurposing' drugs identified as hits, it is possible to screen novel structural analogues to develop more selective therapeutics. Thus, eventually, it should be possible to identify better drug targets and develop more potent disease modifiers.

Hereditary spastic paraplegia (HSP)

Background

HSP designates a set of inherited heterogeneous disorders characterised by lower extremity weakness and spasticity caused by the progressive degeneration of the upper motor neurons. There is currently no cure, but several drugs are available to alleviate some of the symptoms, e.g. spasticity (Fink, 2013). More than 50 different loci have been discovered, designated SPG (spastic paraplegia) and numbered by order of discovery, with some 60 genes identified to date. Many (~40%) forms of autosomal dominant HSP are due to mutations in *SPG4*, encoding spastin, a ubiquitously expressed, mainly cytosolic protein that has microtubule-severing properties (Blackstone, 2012). Mutations in *SPG3A* (atlastin-1) account for ~10% of autosomal dominant HSP and are the second most common cause of HSP as well as the most common form of early-onset HSP; this form is usually clinically described as uncomplicated (Namekawa et al., 2006). Atlastin is a GTPase important for the formation of tubular ER, where it also interacts with spastin (Blackstone, 2012). *SPG11* (spatacsin) mutations occur for ~21% of autosomal recessive cases of HSP, and all except one of the 100 mutations identified in this gene to date lead to truncation of the protein, indicating a possible loss of function (Stevanin et al., 2008). Mutations in *SPG8* (strumpellin; also known as KIAA0196) have also been reported. They account for ~4% of HSP and are inherited in an autosomal dominant manner (Valdmanis et al., 2007). Strumpellin has been identified as a subunit of the Wiscott-Aldrich syndrome protein and SCAR homolog complex (WASH complex) (Blackstone, 2012). Other less common HSP-associated genes are *Alsin*, *SPG42* (*SLC33A1*), *SPG39* (*PNPLA6*), *SPG53* (*VPS37A*), *SPG46* (*GBA2*) and *SPG43* (*C19ORF12*) (Fink, 2013; Landouré et al., 2013; Martin et al., 2013; Yoon et al., 2013). A recent exome sequencing study identified 18 new putative HSP genes (Novarino et al., 2014). The HSP proteins are involved in many different cellular functions, which underlie the pathogenic mechanisms by which mutations will cause HSP, including disrupted axonal pathfinding and axonal transport, disrupted ER morphology, myelin abnormality, mitochondrial dysfunction, disturbed endosomal dynamics and disturbed lipid metabolism (Blackstone, 2012).

Zebrafish models of HSP

Zebrafish have been widely used to validate the pathogenic nature of genes involved in HSP, with over 40 publications to date (more than for SMA or ALS), although all are studies of transient knockdown because no genetic models of HSP have yet been generated. Most HSP genes cause disease in an autosomal recessive fashion, thus implying loss-of-function and dominant-negative molecular mechanisms, which can be readily modelled at a genetic level in zebrafish. However, because zebrafish lack upper motor neurons, the phenotypes reflect at best a general effect rather than one of a specific nature. A number of reports have convincingly shown that the loss of function of HSP-associated genes lead to major motor neuron defects, usually with impaired locomotion, consistent with the roles of spastin and other less common HSP genes that are involved in axonal transport (Blackstone, 2012). For instance, knockdown of spastin (*SPG4*) caused dramatic defects in spinal motor axon outgrowth, abnormal motility and perturbation of axonal microtubule dynamics (Wood et al., 2006; Butler et al., 2010; Wood et al., 2006). Loss of function of atlastin (*SPG3A*) severely impaired spinal motor axon architecture and fish motility (Fassier et al., 2010). However, because autosomal dominant mutations of *spastin* and *atlastin* are (major) causes of HSP, rather

than loss of function, caution is necessary when interpreting these knockdown models in zebrafish. Motor axons in fish injected with *strumpellin* (*SPG8*) morpholino were also shorter and had abnormal branching and impaired motility, which were rescued upon co-injection of wild-type human *SPG8* mRNA but not mRNA with HSP-related variants, validating the latter as loss-of-function mutations (Valdmanis et al., 2007). Knockdown of either *spatacsin* (*SPG11*) or *spastizin* (*SPG15*) severely compromised branching of spinal cord motor neurons at the NMJ and caused locomotor impairment (Martin et al., 2012). Knockdown of *slc33A1* [encoding Solute carrier family 33 (acetyl-CoA transporter), member 1; *SPG42*) in zebrafish embryos also caused a tail curvature phenotype and abnormal axon outgrowth from the spinal cord (Lin et al., 2008). Knockdown of *gba2* (Glucosidase beta 2; *SPG46*) led to abnormal locomotion and outgrowth of spinal motor axons (Martin et al., 2013). *pnpla6* (*SPG39*) knockdown resulted in developmental abnormalities and motor neuron defects, including axon truncation and branching (Song et al., 2013). A loss of motility was induced in *vps37a* (Vacuolar protein sorting 37A; *SPG53*) knockdown zebrafish larvae (Zivony-Elboum et al., 2012). In a number of cases, these deficits could be rescued using the human orthologous mRNA transcript, but not using the disease-causing mRNA transcript, arguing for loss, rather than toxic gain, of function.

Alsin (*ALS2*) is a gene that is frequently mutated in juvenile HSP and ALS through an autosomal recessive mode of action, which leads, in most cases, to protein truncation. Similarly to *spastin* and *strumpellin* models, knockdown of *alsin* causes shortening of motor axons and a loss of neurons in the spinal cord (Gros-Louis et al., 2008). It is important to note that a number of groups generated *Als2* knockout mice in which the first or the second exon of the mouse *alsin* orthologue is deleted, but none of them observed deficits associated with motor neuron degeneration (Deng et al., 2007; Yamanaka et al., 2006). The motor phenotype in zebrafish caused by knockdown of *als2* by targeting the initial ATG was partially rescued upon overexpression of an alternative transcript whose initiating ATG is located within the fourth exon of *ALS2*. This result suggests that the lack of deficit in the knockout murine models, which relied on the deletion of only the initial exons of this gene, could be attributable to an analogous initiation of translation further downstream (Gros-Louis et al., 2008). This example of incomplete knockout in mice versus comprehensive knockdown in zebrafish illustrates the utility of zebrafish for obtaining a more complete disruption of gene function in some cases.

Finally, a recent exome sequencing study identified 18 new putative HSP genes, four of which (*arl6Ip1*, *mars*, *pgap1* and *usp8*) had morpholino knockdown phenotypes in zebrafish (Novarino et al., 2014). Whereas knockdown of *mars* generated a severe phenotype, the others, including *arl6Ip1* (associated with the ER) and *usp8* (involved in endosomal sorting), yielded knockdown defects in touch-induced and spontaneous motor behaviour as well as motor axon morphology that are relevant to HSP, establishing the power of this combination of human genomics and zebrafish knockdowns for the identification and validation of disease-related variants, respectively. It is worth noting, however, that genetic knockout has not yet been reported for any HSP gene and will be necessary to help advance studies of this disorder using zebrafish models.

So far, no drug test or screens for HSP using zebrafish have been published. Nonetheless, the validation of *strumpellin* mutations (Valdmanis et al., 2007) has allowed the development of a patented diagnostic test for HSP that is licensed to Athena Diagnostics Inc., emphasising the usefulness of variant validation in zebrafish. With the urgent need to develop effective treatments for these diseases, we encourage further drug discovery campaigns for all MNDs using a similar approach to that proposed in Fig. 2 to rapidly identify lead compounds.

Chemical screens in zebrafish models for other neural diseases

Successful efforts in developing therapeutics with other zebrafish neurological disease models bode well as examples for approaches that could be developed for MNDs. In a recent paper, a phenotype-based screen identified clemizole (an FDA-approved compound) as a potential lead compound for Dravet syndrome because it effectively inhibited spontaneous convulsive behaviours and electrographic seizures in zebrafish *scn1Lab* mutants (Baraban et al., 2013). In another successful *in vivo* screen study, using the zebrafish lateral line sensory system as a model system for mammalian auditory hair cells, the collaborative work of the Rubel and Raibel labs identified two small molecules (named PROTO-1 and PROTO-2) (Owens et al., 2008) and an FDA-approved compound (named tacrine) (Ou et al., 2009) that protect hair cells from aminoglycoside-induced death. These compounds also inhibited hair cell death in the mammalian inner ear and subsequently preserved hearing. In a screen of the commercially available Prestwick chemical library, three small molecules were identified that ameliorated muscle pathology and increased survival in a zebrafish model of Duchenne muscular dystrophy (*dystrophin*-null) (Kawahara et al., 2011). Interestingly, one of the chemicals, aminophylline, a nonselective phosphodiesterase (PDE) inhibitor, demonstrated a promising capacity to restore normal muscle structure and upregulate the cAMP-dependent protein kinase A (PKA) pathway in dystrophin-deficient fish (Kawahara et al., 2011). Because similar approaches are underway for SMA and ALS zebrafish models, and could be implemented for HSP, these successful screens in neurological models open the exciting possibility of drug discovery for MNDs, where therapeutic interventions remain severely limited and are in great need of development.

Concluding remarks and perspectives

To date, over a hundred papers have shown that various pathological aspects of MNDs caused by expression of mutated genes can be modelled in the zebrafish. This model is now poised at the beginning of a new age of genome manipulation and the new editing approaches will undoubtedly improve the ability to generate more and better MND models in zebrafish. These models can then be used to study the molecular basis of disease and they will certainly provide novel and useful insights into MNDs. The ability to simultaneously target multiple genes and in different combinations in a single embryo, such as using combinations of morpholinos and mRNAs (Kabashi et al., 2011b; Kabashi et al., 2010a) and by improved genome-editing approaches as reported for the CRISPR/Cas system (Jao et al., 2013) and the *Gal4/UAS* approach (Liu and Leach, 2011a), represents an attractive strategy for the study of epistasis in MNDs, an important aspect for the analysis of complex diseases that is not easily implemented in other models such as mice. Of general interest for MND models, a recent knockdown screen for modifiers of ALS-related genes in zebrafish identified *Epha4* as a gene that, when knocked down, could rescue the phenotype caused by expression of mutant *SOD1* or *TARDBP*. Upon co-knockdown of *SMN1*, *Epha4* also increased survival of mouse and rat models of ALS (Van Hoecke et al., 2012). Furthermore, *EPHA4* expression in individuals with ALS inversely

correlated with disease onset and survival, and loss-of-function mutations were associated with long survival. These results, starting with zebrafish, then validated in mammalian models and ultimately correlated with patient aetiology, nicely indicate the power of the zebrafish model for providing translational insights into MND.

The opportunity to apply discovery-driven approaches *in vivo* in a vertebrate and design high-throughput screens, enabling novel hypotheses to be subsequently tested in mammalian models or in clinical studies, is a major strength of the zebrafish model. Although, to date, there is not a single 'positive hit' published from a zebrafish-based drug screen for neurological disorders that has entered a Phase 1 clinical trial, the protective compounds discovered in the recent studies described above are very promising leads for future investigation. The prospect of using zebrafish for drug discovery opens new avenues for discovering treatments for MNDs.

This article is part of a Special Issue, Spotlight on Zebrafish: Translational Impact. See all the articles in the issue at http://dmm.biologists.org/content/7/7.toc.

Competing interests

The authors declare no competing financial interests.

Funding

This research received no specific grant from any funding agency in the public, commercial or not-for-profit sectors.

References

Achsel, T., Barabino, S., Cozzolino, M. and Carrì, M. T. (2013). The intriguing case of motor neuron disease: ALS and SMA come closer. *Biochem. Soc. Trans.* **41**, 1593-1597.

Akten, B., Kye, M. J., Hao, T., Wertz, M. H., Singh, S., Nie, D., Huang, J., Merianda, T. T., Twiss, J. L., Beattie, C. E. et al. (2011). Interaction of survival of motor neuron (SMN) and HuD proteins with mRNA cpg15 rescues motor neuron axonal deficits. *Proc. Natl. Acad. Sci. USA* **108**, 10337-10342.

Andersen, P. M. and Al-Chalabi, A. (2011). Clinical genetics of amyotrophic lateral sclerosis: what do we really know? *Nat. Rev. Neurol.* **7**, 603-615.

Arai, T., Hasegawa, M., Akiyama, H., Ikeda, K., Nonaka, T., Mori, H., Mann, D., Tsuchiya, K., Yoshida, M., Hashizume, Y. et al. (2006). TDP-43 is a component of ubiquitin-positive tau-negative inclusions in frontotemporal lobar degeneration and amyotrophic lateral sclerosis. *Biochem. Biophys. Res. Commun.* **351**, 602-611.

Armstrong, G. A. B. and Drapeau, P. (2013a). Calcium channel agonists protect against neuromuscular dysfunction in a genetic model of TDP-43 mutation in ALS. *J. Neurosci.* **33**, 1741-1752.

Armstrong, G. A. B. and Drapeau, P. (2013b). Loss and gain of FUS function impair neuromuscular synaptic transmission in a genetic model of ALS. *Hum. Mol. Genet.* **22**, 4282-4292.

Asnani, A. and Peterson, R. T. (2014). The zebrafish as a tool to identify novel therapies for human cardiovascular disease. *Dis. Model. Mech.* **7**, 763-767

Baraban, S. C., Dinday, M. T. and Hortopan, G. A. (2013). Drug screening in Scn1a zebrafish mutant identifies clemizole as a potential Dravet syndrome treatment. *Nat. Commun.* **4**, 2410.

Blackstone, C. (2012). Cellular pathways of hereditary spastic paraplegia. *Annu. Rev. Neurosci.* **35**, 25-47.

Boillée, S., Vande Velde, C. and Cleveland, D. W. (2006). ALS: a disease of motor neurons and their nonneuronal neighbors. *Neuron* **52**, 39-59.

Boon, K.-L., Xiao, S., McWhorter, M. L., Donn, T., Wolf-Saxon, E., Bohnsack, M. T., Moens, C. B. and Beattie, C. E. (2009). Zebrafish survival motor neuron mutants exhibit presynaptic neuromuscular junction defects. *Hum. Mol. Genet.* **18**, 3615-3625.

Bories, C., Amendola, J., Lamotte d'Incamps, B. and Durand, J. (2007). Early electrophysiological abnormalities in lumbar motoneurons in a transgenic mouse model of amyotrophic lateral sclerosis. *Eur. J. Neurosci.* **25**, 451-459.

Bosco, D. A., Lemay, N., Ko, H. K., Zhou, H., Burke, C., Kwiatkowski, T. J., Jr, Sapp, P., McKenna-Yasek, D., Brown, R. H., Jr and Hayward, L. J. (2010). Mutant FUS proteins that cause amyotrophic lateral sclerosis incorporate into stress granules. *Hum. Mol. Genet.* **19**, 4160-4175.

Butler, R., Wood, J. D., Landers, J. A. and Cunliffe, V. T. (2010). Genetic and chemical modulation of spastin-dependent axon outgrowth in zebrafish embryos indicates a role for impaired microtubule dynamics in hereditary spastic paraplegia. *Dis. Model. Mech.* **3**, 743-751.

Carrel, T. L., McWhorter, M. L., Workman, E., Zhang, H., Wolstencroft, E. C., Lorson, C., Bassell, G. J., Burghes, A. H. and Beattie, C. E. (2006). Survival motor neuron function in motor axons is independent of functions required for small nuclear ribonucleoprotein biogenesis. *J. Neurosci.* **26**, 11014-11022.

Chan, J. and Mably, J. D. (2011). Dissection of cardiovascular development and disease pathways in zebrafish. *Prog. Mol. Biol. Transl. Sci.* **100**, 111-153.

Chen, S., Sayana, P., Zhang, X. and Le, W. (2013). Genetics of amyotrophic lateral sclerosis: an update. *Mol. Neurodegener.* **8**, 28.

Chico, T. J., Ingham, P. W. and Crossman, D. C. (2008). Modeling cardiovascular disease in the zebrafish. *Trends Cardiovasc. Med.* **18**, 150-155.

Chitramuthu, B. P., Baranowski, D. C., Kay, D. G., Bateman, A. and Bennett, H. P. (2010). Progranulin modulates zebrafish motoneuron development in vivo and rescues truncation defects associated with knockdown of Survival motor neuron 1. *Mol. Neurodegener.* **5**, 41.

Ciura, S., Lattante, S., Le Ber, I., Latouche, M., Tostivint, H., Brice, A. and Kabashi, E. (2013). Loss of function of C9orf72 causes motor deficits in a zebrafish model of Amyotrophic Lateral Sclerosis. *Annals of Neurology*

Cozzolino, M. and Carrì, M. T. (2012). Mitochondrial dysfunction in ALS. *Prog. Neurobiol.* **97**, 54-66.

Da Costa, M. M., Allen, C. E., Higginbottom, A., Ramesh, T., Shaw, P. J. and McDermott, C. J. (2014). A new zebrafish model produced by TILLING of SOD1-related amyotrophic lateral sclerosis replicates key features of the disease and represents a tool for in vivo therapeutic screening. *Dis. Model. Mech.* **7**, 73-81.

Da Cruz, S. and Cleveland, D. W. (2011). Understanding the role of TDP-43 and FUS/TLS in ALS and beyond. *Curr. Opin. Neurobiol.* **21**, 904-919.

Dadon-Nachum, M., Melamed, E. and Offen, D. (2011). The "dying-back" phenomenon of motor neurons in ALS. *J. Mol. Neurosci.* **43**, 470-477.

DeJesus-Hernandez, M., Mackenzie, I. R., Boeve, B. F., Boxer, A. L., Baker, M., Rutherford, N. J., Nicholson, A. M., Finch, N. A., Flynn, H., Adamson, J. et al. (2011). Expanded GGGGCC hexanucleotide repeat in noncoding region of C9ORF72 causes chromosome 9p-linked FTD and ALS. *Neuron* **72**, 245-256.

Deng, H. X., Zhai, H., Fu, R., Shi, Y., Gorrie, G. H., Yang, Y., Liu, E., Dal Canto, M. C., Mugnaini, E. and Siddique, T. (2007). Distal axonopathy in an alsin-deficient mouse model. *Hum. Mol. Genet.* **16**, 2911-2920.

Dion, P. A., Daoud, H. and Rouleau, G. A. (2009). Genetics of motor neuron disorders: new insights into pathogenic mechanisms. *Nat. Rev. Genet.* **10**, 769-782.

Dormann, D., Rodde, R., Edbauer, D., Bentmann, E., Fischer, I., Hruscha, A., Than, M. E., Mackenzie, I. R., Capell, A., Schmid, B. et al. (2010). ALS-associated fused in sarcoma (FUS) mutations disrupt Transportin-mediated nuclear import. *EMBO J.* **29**, 2841-2857.

Fassier, C., Hutt, J. A., Scholpp, S., Lumsden, A., Giros, B., Nothias, F., Schneider-Maunoury, S., Houart, C. and Hazan, J. (2010). Zebrafish atlastin controls motility and spinal motor axon architecture via inhibition of the BMP pathway. *Nat. Neurosci.* **13**, 1380-1387.

Fink, J. K. (2013). Hereditary spastic paraplegia: clinico-pathologic features and emerging molecular mechanisms. *Acta Neuropathol.* **126**, 307-328.

Finsterer, J., Löscher, W., Quasthoff, S., Wanschitz, J., Auer-Grumbach, M. and Stevanin, G. (2012). Hereditary spastic paraplegias with autosomal dominant, recessive, X-linked, or maternal trait of inheritance. *J. Neurol. Sci.* **318**, 1-18.

Flinn, L., Bretaud, S., Lo, C., Ingham, P. W. and Bandmann, O. (2008). Zebrafish as a new animal model for movement disorders. *J. Neurochem.* **106**, 1991-1997.

Gassman, A., Hao, T., Bhoite, L., Bradford, C. L., Chien, C. B., Beattie, C. E. and Manfredi, J. P. (2013). Small molecule suppressors of Drosophila kinesin deficiency rescue motor axon development in a zebrafish model of spinal muscular atrophy. *PLoS ONE* **8**, e74325.

Gendron, T. F., Belzil, V. V., Zhang, Y. J. and Petrucelli, L. (2014). Mechanisms of toxicity in C9FTLD/ALS. *Acta Neuropathol.* **127**, 359-376.

Gerlai, R. (2010). High-throughput behavioral screens: the first step towards finding genes involved in vertebrate brain function using zebrafish. *Molecules* **15**, 2609-2622.

Giacomotto, J. and Ségalat, L. (2010). High-throughput screening and small animal models, where are we? *Br. J. Pharmacol.* **160**, 204-216.

Godena, V. K., Romano, G., Romano, M., Appocher, C., Klima, R., Buratti, E., Baralle, F. E. and Feiguin, F. (2011). TDP-43 regulates Drosophila neuromuscular junctions growth by modulating Futsch/MAP1B levels and synaptic microtubules organization. *PLoS ONE* **6**, e17808.

Greenberg, F., Fenolio, K. R., Hejtmancik, J. F., Armstrong, D., Willis, J. K., Shapira, E., Huntington, H. W. and Haun, R. L. (1988). X-linked infantile spinal muscular atrophy. *Am. J. Dis. Child.* **142**, 217-219.

Gros-Louis, F., Kriz, J., Kabashi, E., McDearmid, J., Millecamps, S., Urushitani, M., Lin, L., Dion, P., Zhu, Q., Drapeau, P. et al. (2008). Als2 mRNA splicing variants detected in KO mice rescue severe motor dysfunction phenotype in Als2 knock-down zebrafish. *Hum. Mol. Genet.* **17**, 2691-2702.

Halpern, M. E., Rhee, J., Goll, M. G., Akitake, C. M., Parsons, M. and Leach, S. D. (2008). Gal4/UAS transgenic tools and their application to zebrafish. *Zebrafish* **5**, 97-110.

Hamilton, G. and Gillingwater, T. H. (2013). Spinal muscular atrophy: going beyond the motor neuron. *Trends Mol. Med.* **19**, 40-50.

Hao, T., Burghes, A. H. and Beattie, C. E. (2011). Generation and characterization of a genetic zebrafish model of SMA carrying the human SMN2 gene. *Mol. Neurodegener.* **6**, 24.

Hao, T., Wolman, M., Granato, M. and Beattie, C. E. (2012). Survival motor neuron affects plastin 3 protein levels leading to motor defects. *J. Neurosci.* **32**, 5074-5084.

Hao, L. T., Duy, P. Q., Jontes, J. D., Wolman, M., Granato, M. and Beattie, C. E. (2013). Temporal requirement for SMN in motoneuron development. *Hum. Mol. Genet.* **22**, 2612-2625.

Harding, A. E. (1983). Classification of the hereditary ataxias and paraplegias. *Lancet* **321**, 1151-1155.

Hewamadduma, C. A. A., Grierson, A. J., Ma, T. P., Pan, L., Moens, C. B., Ingham, P. W., Ramesh, T. and Shaw, P. J. (2013). Tardbpl splicing rescues motor

neuron and axonal development in a mutant tardbp zebrafish. *Hum. Mol. Genet.* **22**, 2376-2386.
Howe, K., Clark, M. D., Torroja, C. F., Torrance, J., Berthelot, C., Muffato, M., Collins, J. E., Humphray, S., McLaren, K., Matthews, L. et al. (2013). The zebrafish reference genome sequence and its relationship to the human genome. *Nature* **496**, 498-503.
Ilieva, H., Polymenidou, M. and Cleveland, D. W. (2009). Non-cell autonomous toxicity in neurodegenerative disorders: ALS and beyond. *J. Cell Biol.* **187**, 761-772.
Jao, L. E., Wente, S. R. and Chen, W. (2013). Efficient multiplex biallelic zebrafish genome editing using a CRISPR nuclease system. *Proc. Natl. Acad. Sci. USA* **110**, 13904-13909.
Jiang, W., Ji, X., Xu, Y., Qu, X., Sun, W., Yang, Z., Tao, J. and Chen, Y. (2013). Molecular prenatal diagnosis of autosomal recessive spinal muscular atrophies using quantification polymerase chain reaction. *Genet. Test Mol. Biomarkers* **17**, 438-442.
Kabashi, E., Valdmanis, P. N., Dion, P., Spiegelman, D., McConkey, B. J., Vande Velde, C., Bouchard, J. P., Lacomblez, L., Pochigaeva, K., Salachas, F. et al. (2008). TARDBP mutations in individuals with sporadic and familial amyotrophic lateral sclerosis. *Nat. Genet.* **40**, 572-574.
Kabashi, E., Champagne, N., Brustein, E. and Drapeau, P. (2010a). In the swim of things: recent insights to neurogenetic disorders from zebrafish. *Trends Genet.* **26**, 373-381.
Kabashi, E., Lin, L., Tradewell, M. L., Dion, P. A., Bercier, V., Bourgouin, P., Rochefort, D., Bel Hadj, S., Durham, H. D., Vande Velde, C. et al. (2010b). Gain and loss of function of ALS-related mutations of TARDBP (TDP-43) cause motor deficits in vivo. *Hum. Mol. Genet.* **19**, 671-683.
Kabashi, E., Bercier, V., Lissouba, A., Liao, M., Brustein, E., Rouleau, G. A. and Drapeau, P. (2011a). FUS and TARDBP but not SOD1 interact in genetic models of amyotrophic lateral sclerosis. *PLoS Genet.* **7**, e1002214.
Kabashi, E., Brustein, E., Champagne, N. and Drapeau, P. (2011b). Zebrafish models for the functional genomics of neurogenetic disorders. *Biochim. Biophys. Acta* **1812**, 335-345.
Kawahara, G., Karpf, J. A., Myers, J. A., Alexander, M. S., Guyon, J. R. and Kunkel, L. M. (2011). Drug screening in a zebrafish model of Duchenne muscular dystrophy. *Proc. Natl. Acad. Sci. USA* **108**, 5331-5336.
Khaniani, M. S., Derakhshan, S. M. and Abasalizadeh, S. (2013). Prenatal diagnosis of spinal muscular atrophy: clinical experience and molecular genetics of SMN gene analysis in 36 cases. *J. Prenat. Med.* **7**, 32-34.
Kiernan, M. C., Vucic, S., Cheah, B. C., Turner, M. R., Eisen, A., Hardiman, O., Burrell, J. R. and Zoing, M. C. (2011). Amyotrophic lateral sclerosis. *Lancet* **377**, 942-955.
Kwiatkowski, T. J., Jr, Bosco, D. A., Leclerc, A. L., Tamrazian, E., Vanderburg, C. R., Russ, C., Davis, A., Gilchrist, J., Kasarskis, E. J., Munsat, T. et al. (2009). Mutations in the FUS/TLS gene on chromosome 16 cause familial amyotrophic lateral sclerosis. *Science* **323**, 1205-1208.
Lagier-Tourenne, C., Polymenidou, M., Hutt, K. R., Vu, A. Q., Baughn, M., Huelga, S. C., Clutario, K. M., Ling, S. C., Liang, T. Y., Mazur, C. et al. (2012). Divergent roles of ALS-linked proteins FUS/TLS and TDP-43 intersect in processing long pre-mRNAs. *Nat. Neurosci.* **15**, 1488-1497.
Landouré, G., Zhu, P. P., Lourenço, C. M., Johnson, J. O., Toro, C., Bricceno, K. V., Rinaldi, C., Meilleur, K. G., Sangaré, M., Diallo, O. et al.; NIH Intramural Sequencing Center (2013). Hereditary spastic paraplegia type 43 (SPG43) is caused by mutation in C19orf12. *Hum. Mutat.* **34**, 1357-1360.
Lattante, S., Rouleau, G. A. and Kabashi, E. (2013). TARDBP and FUS mutations associated with amyotrophic lateral sclerosis: summary and update. *Hum. Mutat.* **34**, 812-826.
Lefebvre, S., Bürglen, L., Reboullet, S., Clermont, O., Burlet, P., Viollet, L., Benichou, B., Cruaud, C., Millasseau, P., Zeviani, M. et al. (1995). Identification and characterization of a spinal muscular atrophy-determining gene. *Cell* **80**, 155-165.
Lemmens, R., Van Hoecke, A., Hersmus, N., Geelen, V., D'Hollander, I., Thijs, V., Van Den Bosch, L., Carmeliet, P. and Robberecht, W. (2007). Overexpression of mutant superoxide dismutase 1 causes a motor axonopathy in the zebrafish. *Hum. Mol. Genet.* **16**, 2359-2365.
Lieschke, G. J. and Currie, P. D. (2007). Animal models of human disease: zebrafish swim into view. *Nat. Rev. Genet.* **8**, 353-367.
Lin, P., Li, J., Liu, Q., Mao, F., Li, J., Qiu, R., Hu, H., Song, Y., Yang, Y., Gao, G. et al. (2008). A missense mutation in SLC33A1, which encodes the acetyl-CoA transporter, causes autosomal-dominant spastic paraplegia (SPG42). *Am. J. Hum. Genet.* **83**, 752-759.
Lin, H. J., Lee, S. H., Wu, J. L., Duann, Y. F. and Chen, J. Y. (2013). Development of Cre-loxP technology in zebrafish to study the regulation of fish reproduction. *Fish Physiol. Biochem.* **39**, 1525-1539.
Ling, S. C., Polymenidou, M. and Cleveland, D. W. (2013). Converging mechanisms in ALS and FTD: disrupted RNA and protein homeostasis. *Neuron* **79**, 416-438.
Liu, S. and Leach, S. D. (2011a). Screening pancreatic oncogenes in zebrafish using the Gal4/UAS system. *Methods Cell Biol.* **105**, 367-381.
Liu, S. and Leach, S. D. (2011b). Zebrafish models for cancer. *Annu. Rev. Pathol.* **6**, 71-93.
Lotti, F., Imlach, W. L., Saieva, L., Beck, E. S., Hao, T., Li, D. K., Jiao, W., Mentis, G. Z., Beattie, C. E., McCabe, B. D. et al. (2012). An SMN-dependent U12 splicing event essential for motor circuit function. *Cell* **151**, 440-454.
Lyon, A. N., Pineda, R. H., Hao, T., Kudryashova, E., Kudryashov, D. S. and Beattie, C. E. (2014). Calcium binding is essential for plastin 3 function in Smn-deficient motoneurons. *Hum. Mol. Genet.* **23**, 1990-2004.
Martin, E., Yanicostas, C., Rastetter, A., Naini, S. M., Maouedj, A., Kabashi, E., Rivaud-Péchoux, S., Brice, A., Stevanin, G. and Soussi-Yanicostas, N. (2012). Spatacsin and spastizin act in the same pathway required for proper spinal motor neuron axon outgrowth in zebrafish. *Neurobiol. Dis.* **48**, 299-308.
Martin, E., Schüle, R., Smets, K., Rastetter, A., Boukhris, A., Loureiro, J. L., Gonzalez, M. A., Mundwiller, E., Deconinck, T., Wessner, M. et al. (2013). Loss of function of glucocerebrosidase GBA2 is responsible for motor neuron defects in hereditary spastic paraplegia. *Am. J. Hum. Genet.* **92**, 238-244.
Matus, S., Valenzuela, V., Medinas, D. B. and Hetz, C. (2013). ER dysfunction and protein folding stress in ALS. *Int. J. Cell Biol.* **2013**, 674751.
McGown, A., McDearmid, J. R., Panagiotaki, N., Tong, H., Al Mashhadi, S., Redhead, N., Lyon, A. N., Beattie, C. E., Shaw, P. J. and Ramesh, T. M. (2012). Early interneuron dysfunction in ALS: Insights from a mutant sod1 zebrafish model. *Ann. Neurol.* **73**, 246-258.
McGown, A., McDearmid, J. R., Panagiotaki, N., Tong, H., Al Mashhadi, S., Redhead, N., Lyon, A. N., Beattie, C. E., Shaw, P. J. and Ramesh, T. M. (2013). Early interneuron dysfunction in ALS: insights from a mutant sod1 zebrafish model. *Ann. Neurol.* **73**, 246-258.
McWhorter, M. L., Monani, U. R., Burghes, A. H. and Beattie, C. E. (2003). Knockdown of the survival motor neuron (Smn) protein in zebrafish causes defects in motor axon outgrowth and pathfinding. *J. Cell Biol.* **162**, 919-932.
Miller, R. G., Mitchell, J. D. and Moore, D. H. (2012). Riluzole for amyotrophic lateral sclerosis (ALS)/motor neuron disease (MND). *Cochrane Database Syst. Rev.* **3**, CD001447.
Murray, L. M., Talbot, K. and Gillingwater, T. H. (2010). Review: neuromuscular synaptic vulnerability in motor neurone disease: amyotrophic lateral sclerosis and spinal muscular atrophy. *Neuropathol. Appl. Neurobiol.* **36**, 133-156.
Namekawa, M., Ribai, P., Nelson, I., Forlani, S., Fellmann, F., Goizet, C., Depienne, C., Stevanin, G., Ruberg, M., Dürr, A. et al. (2006). SPG3A is the most frequent cause of hereditary spastic paraplegia with onset before age 10 years. *Neurology* **66**, 112-114.
Neumann, M., Sampathu, D. M., Kwong, L. K., Truax, A. C., Micsenyi, M. C., Chou, T. T., Bruce, J., Schuck, T., Grossman, M., Clark, C. M. et al. (2006). Ubiquitinated TDP-43 in frontotemporal lobar degeneration and amyotrophic lateral sclerosis. *Science* **314**, 130-133.
North, T. E., Goessling, W., Walkley, C. R., Lengerke, C., Kopani, K. R., Lord, A. M., Weber, G. J., Bowman, T. V., Jang, I. H., Grosser, T. et al. (2007). Prostaglandin E2 regulates vertebrate haematopoietic stem cell homeostasis. *Nature* **447**, 1007-1011.
Novarino, G., Fenstermaker, A. G., Zaki, M. S., Hofree, M., Silhavy, J. L., Heiberg, A. D., Abdellateef, M., Rosti, B., Scott, E., Mansour, L. et al. (2014). Exome sequencing links corticospinal motor neuron disease to common neurodegenerative disorders. *Science* **343**, 506-511.
Oprea, G. E., Kröber, S., McWhorter, M. L., Rossoll, W., Müller, S., Krawczak, M., Bassell, G. J., Beattie, C. E. and Wirth, B. (2008). Plastin 3 is a protective modifier of autosomal recessive spinal muscular atrophy. *Science* **320**, 524-527.
Ou, H. C., Cunningham, L. L., Francis, S. P., Brandon, C. S., Simon, J. A., Raible, D. W. and Rubel, E. W. (2009). Identification of FDA-approved drugs and bioactives that protect hair cells in the zebrafish (Danio rerio) lateral line and mouse (Mus musculus) utricle. *J. Assoc. Res. Otolaryngol.* **10**, 191-203.
Owens, K. N., Santos, F., Roberts, B., Linbo, T., Coffin, A. B., Knisely, A. J., Simon, J. A., Rubel, E. W. and Raible, D. W. (2008). Identification of genetic and chemical modulators of zebrafish mechanosensory hair cell death. *PLoS Genet.* **4**, e1000020.
Phillips, J. B. and Westerfield, M. (2014). Zebrafish models in translational research: tipping the scales toward advancements in human health. *Dis. Model. Mech.* **7**, 739-743.
Postlethwait, J. H., Woods, I. G., Ngo-Hazelett, P., Yan, Y.-L., Kelly, P. D., Chu, F., Huang, H., Hill-Force, A. and Talbot, W. S. (2000). Zebrafish comparative genomics and the origins of vertebrate chromosomes. *Genome Res.* **10**, 1890-1902.
Ramesh, T., Lyon, A. N., Pineda, R. H., Wang, C., Janssen, P. M. L., Canan, B. D., Burghes, A. H. M. and Beattie, C. E. (2010). A genetic model of amyotrophic lateral sclerosis in zebrafish displays phenotypic hallmarks of motoneuron disease. *Dis. Model. Mech.* **3**, 652-662.
Renton, A. E., Majounie, E., Waite, A., Simón-Sánchez, J., Rollinson, S., Gibbs, J. R., Schymick, J. C., Laaksovirta, H., van Swieten, J. C., Myllykangas, L. et al.; ITALSGEN Consortium (2011). A hexanucleotide repeat expansion in C9ORF72 is the cause of chromosome 9p21-linked ALS-FTD. *Neuron* **72**, 257-268.
Robberecht, W. and Philips, T. (2013). The changing scene of amyotrophic lateral sclerosis. *Nat. Rev. Neurosci.* **14**, 248-264.
Roberts, J. A., Miguel-Escalada, I., Slovik, K. J., Walsh, K. T., Hadzhiev, Y., Sanges, R., Stupka, E., Marsh, E. K., Balciuniene, J., Balciunas, D. et al. (2014). Targeted transgene integration overcomes variability of position effects in zebrafish. *Development* **141**, 715-724.
Rosen, D. R., Siddique, T., Patterson, D., Figlewicz, D. A., Sapp, P., Hentati, A., Donaldson, D., Goto, J., O'Regan, J. P., Deng, H.-X. et al. (1993). Mutations in Cu/Zn superoxide dismutase gene are associated with familial amyotrophic lateral sclerosis. *Nature* **362**, 59-62.
Sakowski, S. A., Lunn, J. S., Busta, A. S., Oh, S. S., Zamora-Berridi, G., Palmer, M., Rosenberg, A. A., Philip, S. G., Dowling, J. J. and Feldman, E. L. (2012). Neuromuscular effects of G93A-SOD1 expression in zebrafish. *Mol. Neurodegener.* **7**, 44.
Schmid, B. and Haass, C. (2013). Genomic editing opens new avenues for zebrafish as a model for neurodegeneration. *J. Neurochem.* **127**, 461-470.
Schmid, B., Hruscha, A., Hogl, S., Banzhaf-Strathmann, J., Strecker, K., van der Zee, J., Teucke, M., Eimer, S., Hegermann, J., Kittelmann, M. et al. (2013).

Loss of ALS-associated TDP-43 in zebrafish causes muscle degeneration, vascular dysfunction, and reduced motor neuron axon outgrowth. *Proc. Natl. Acad. Sci. USA* **110**, 4986-4991.

See, K., Yadav, P., Giegerich, M., Cheong, P. S., Graf, M., Vyas, H., Lee, S. G., Mathavan, S., Fischer, U., Sendtner, M. et al. (2014). SMN deficiency alters Nrxn2 expression and splicing in zebrafish and mouse models of spinal muscular atrophy. *Hum. Mol. Genet.* **23**, 1754-1770.

Sephton, C. F., Good, S. K., Atkin, S., Dewey, C. M., Mayer, P., III, Herz, J. and Yu, G. (2010). TDP-43 is a developmentally regulated protein essential for early embryonic development. *J. Biol. Chem.* **285**, 6826-6834.

Sleeman, J. (2013). Small nuclear RNAs and mRNAs: linking RNA processing and transport to spinal muscular atrophy. *Biochem. Soc. Trans.* **41**, 871-875.

Sleigh, J. N., Barreiro-Iglesias, A., Oliver, P. L., Biba, A., Becker, T., Davies, K. E., Becker, C. G. and Talbot, K. (2014). Chondrolectin affects cell survival and neuronal outgrowth in in vitro and in vivo models of spinal muscular atrophy. *Hum. Mol. Genet.* **23**, 855-869.

Song, Y., Wang, M., Mao, F., Shao, M., Zhao, B., Song, Z., Shao, C. and Gong, Y. (2013). Knockdown of Pnpla6 protein results in motor neuron defects in zebrafish. *Dis. Model. Mech.* **6**, 404-413.

Sreedharan, J., Blair, I. P., Tripathi, V. B., Hu, X., Vance, C., Rogelj, B., Ackerley, S., Durnall, J. C., Williams, K. L., Buratti, E. et al. (2008). TDP-43 mutations in familial and sporadic amyotrophic lateral sclerosis. *Science* **319**, 1668-1672.

Stevanin, G., Azzedine, H., Denora, P., Boukhris, A., Tazir, M., Lossos, A., Rosa, A. L., Lerer, I., Hamri, A., Alegria, P. et al.; SPATAX consortium (2008). Mutations in SPG11 are frequent in autosomal recessive spastic paraplegia with thin corpus callosum, cognitive decline and lower motor neuron degeneration. *Brain* **131**, 772-784.

Stoletov, K. and Klemke, R. (2008). Catch of the day: zebrafish as a human cancer model. *Oncogene* **27**, 4509-4520.

Suster, M. L., Kikuta, H., Urasaki, A., Asakawa, K. and Kawakami, K. (2009). Transgenesis in zebrafish with the tol2 transposon system. *Methods Mol. Biol.* **561**, 41-63.

Swarup, V., Phaneuf, D., Bareil, C., Robertson, J., Rouleau, G. A., Kriz, J. and Julien, J. P. (2011). Pathological hallmarks of amyotrophic lateral sclerosis/frontotemporal lobar degeneration in transgenic mice produced with TDP-43 genomic fragments. *Brain* **134**, 2610-2626.

Tat, J., Liu, M. and Wen, X. Y. (2013). Zebrafish cancer and metastasis models for in vivo drug discovery. *Drug Discov. Today. Technol.* **10**, e83-e89.

Vaccaro, A., Patten, S. A., Ciura, S., Maios, C., Therrien, M., Drapeau, P., Kabashi, E. and Parker, J. A. (2012a). Methylene blue protects against TDP-43 and FUS neuronal toxicity in C. elegans and D. rerio. *PLoS ONE* **7**, e42117.

Vaccaro, A., Tauffenberger, A., Aggad, D., Rouleau, G., Drapeau, P. and Parker, J. A. (2012b). Mutant TDP-43 and FUS cause age-dependent paralysis and neurodegeneration in C. elegans. *PLoS ONE* **7**, e31321.

Vaccaro, A., Patten, S. A., Aggad, D., Julien, C., Maios, C., Kabashi, E., Drapeau, P. and Parker, J. A. (2013). Pharmacological reduction of ER stress protects against TDP-43 neuronal toxicity in vivo. *Neurobiol. Dis.* **55**, 64-75.

Valdmanis, P. N., Meijer, I. A., Reynolds, A., Lei, A., MacLeod, P., Schlesinger, D., Zatz, M., Reid, E., Dion, P. A., Drapeau, P. et al. (2007). Mutations in the KIAA0196 gene at the SPG8 locus cause hereditary spastic paraplegia. *Am. J. Hum. Genet.* **80**, 152-161.

Van Hoecke, A., Schoonaert, L., Lemmens, R., Timmers, M., Staats, K. A., Laird, A. S., Peeters, E., Philips, T., Goris, A., Dubois, B. et al. (2012). EPHA4 is a disease modifier of amyotrophic lateral sclerosis in animal models and in humans. *Nat. Med.* **18**, 1418-1422.

Vance, C., Rogelj, B., Hortobágyi, T., De Vos, K. J., Nishimura, A. L., Sreedharan, J., Hu, X., Smith, B., Ruddy, D., Wright, P. et al. (2009). Mutations in FUS, an RNA processing protein, cause familial amyotrophic lateral sclerosis type 6. *Science* **323**, 1208-1211.

Varshney, G. K. and Burgess, S. M. (2014). Mutagenesis and phenotyping resources in zebrafish for studying development and human disease. *Brief. Funct. Genomics* **13**, 82-94.

Voigt, A., Herholz, D., Fiesel, F. C., Kaur, K., Müller, D., Karsten, P., Weber, S. S., Kahle, P. J., Marquardt, T. and Schulz, J. B. (2010). TDP-43-mediated neuron loss in vivo requires RNA-binding activity. *PLoS ONE* **5**, e12247.

Wang, J.-W., Brent, J. R., Tomlinson, A., Shneider, N. A. and McCabe, B. D. (2011). The ALS-associated proteins FUS and TDP-43 function together to affect Drosophila locomotion and life span. *J. Clin. Invest.* **121**, 4118-4126.

Wegorzewska, I. and Baloh, R. H. (2011). TDP-43-based animal models of neurodegeneration: new insights into ALS pathology and pathophysiology. *Neurodegener. Dis.* **8**, 262-274.

White, R. M., Cech, J., Ratanasirintrawoot, S., Lin, C. Y., Rahl, P. B., Burke, C. J., Langdon, E., Tomlinson, M. L., Mosher, J., Kaufman, C. et al. (2011). DHODH modulates transcriptional elongation in the neural crest and melanoma. *Nature* **471**, 518-522.

Wishart, T. M., Mutsaers, C. A., Riessland, M., Reimer, M. M., Hunter, G., Hannam, M. L., Eaton, S. L., Fuller, H. R., Roche, S. L., Somers, E. et al. (2014). Dysregulation of ubiquitin homeostasis and β-catenin signaling promote spinal muscular atrophy. *J. Clin. Invest.* **124**, 1821-1834.

Wood, J. D., Landers, J. A., Bingley, M., McDermott, C. J., Thomas-McArthur, V., Gleadall, L. J., Shaw, P. J. and Cunliffe, V. T. (2006). The microtubule-severing protein Spastin is essential for axon outgrowth in the zebrafish embryo. *Hum. Mol. Genet.* **15**, 2763-2771.

Workman, E., Saieva, L., Carrel, T. L., Crawford, T. O., Liu, D., Lutz, C., Beattie, C. E., Pellizzoni, L. and Burghes, A. H. (2009). A SMN missense mutation complements SMN2 restoring snRNPs and rescuing SMA mice. *Hum. Mol. Genet.* **18**, 2215-2229.

Wu, L.-S., Cheng, W.-C., Hou, S.-C., Yan, Y.-T., Jiang, S.-T. and Shen, C. K. J. (2010). TDP-43, a neuro-pathosignature factor, is essential for early mouse embryogenesis. *Genesis* **48**, 56-62.

Yamanaka, K., Miller, T. M., McAlonis-Downes, M., Chun, S. J. and Cleveland, D. W. (2006). Progressive spinal axonal degeneration and slowness in ALS2-deficient mice. *Ann. Neurol.* **60**, 95-104.

Yoon, G., Baskin, B., Tarnopolsky, M., Boycott, K. M., Geraghty, M. T., Sell, E., Goobie, S., Meschino, W., Banwell, B. and Ray, P. N. (2013). Autosomal recessive hereditary spastic paraplegia-clinical and genetic characteristics of a well-defined cohort. *Neurogenetics* **14**, 181-188.

Zhou, H., Huang, C., Chen, H., Wang, D., Landel, C. P., Xia, P. Y., Bowser, R., Liu, Y. J. and Xia, X. G. (2010). Transgenic rat model of neurodegeneration caused by mutation in the TDP gene. *PLoS Genet.* **6**, e1000887.

Zivony-Elboum, Y., Westbroek, W., Kfir, N., Savitzki, D., Shoval, Y., Bloom, A., Rod, R., Khayat, M., Gross, B., Samri, W. et al. (2012). A founder mutation in Vps37A causes autosomal recessive complex hereditary spastic paraparesis. *J. Med. Genet.* **49**, 462-472.

Zon, L. I. and Peterson, R. T. (2005). In vivo drug discovery in the zebrafish. *Nat. Rev. Drug Discov.* **4**, 35-44.

Annexe 9: Method article "A simplified method for identifying early CRISPR-induced indels in zebrafish embryos using High Resolution Melting analysis"

A simplified method for identifying early CRISPR-induced indels in zebrafish embryos using High Resolution Melting analysis

Samarut E., **Lissouba A**. and Drapeau P.

BMC Genomics 2016 17:547
doi.org/10.1186/s12864-016-2881-1

Samarut et al. BMC Genomics (2016) 17:547
DOI 10.1186/s12864-016-2881-1

BMC Genomics

METHODOLOGY ARTICLE Open Access

A simplified method for identifying early CRISPR-induced indels in zebrafish embryos using High Resolution Melting analysis

Éric Samarut[1,3*], Alexandra Lissouba[1,2] and Pierre Drapeau [1,3]

Abstract

Background: The CRISPR/Cas9 system has become a regularly used tool for editing the genome of many model organisms at specific sites. However, two limiting steps arise in the process of validating guide RNA target sites in larvae and adults: the time required to identify indels and the cost associated with identifying potential mutant animals.

Results: Here we have combined and optimized the HotSHOT genomic DNA extraction technique with a two-steps Evagreen PCR, followed by a high-resolution melting (HRM) assay, which facilitates rapid identification of CRISPR-induced indels. With this technique, we were able to genotype adult zebrafish using genomic DNA extracted from fin-clips in less than 2 h. We were also able to obtain a reliable and early read-out of the effectiveness of guide RNAs only 4 h after the embryos were injected with the constructs for the CRISPR/Cas9 mutagenic system. Furthermore, through mutagenesis kinetic assay, we identified that the 2-cell stage is the earliest time point at which indels can be observed.

Conclusions: By combining an inexpensive and rapid genomic DNA extraction method with an HRM-based assay, our approach allows for high-throughput genotyping of adult zebrafish and embryos, and is more sensitive than standard PCR approaches, permitting early identification of CRISPR-induced indels and with applications for other model organisms as well.

Keywords: Mutagenesis, CRISPR, Zebrafish, Genotyping, High-Resolution-Melting

Background

With the development of the Clustered regularly interspaced short palindromic repeats (CRISPR) and CRISPR associated endonuclease 9 (Cas9), fast and reliable genotyping has become an inevitable rate-limiting step for in vivo genomic studies. In zebrafish, commonly used genotyping techniques are based on a locus-specific amplification by PCR followed by amplicon digestion of a specific restriction enzyme or sequencing. This requires adequate genomic DNA for the reaction and substantial time to complete the screen. Recently, new techniques have emerged using fluorescent PCR or high-resolution melting curve (HRM) analysis that simplify and shorten genotyping assays [1–3]. Specifically, HRM assays rely on the high-resolution monitoring of the denaturation process of a double-stranded fluorescently-labeled DNA fragment. This technique can identify micro-indels as small as a single nucleotide and even class-4 single nucleotide polymorphisms (SNPs) [4]. While there are numerous commercial methods for extracting genomic DNA, their price and the fact that they usually require multiple manual steps makes them ill-equipped for high-throughput assessment of indels. Moreover, some genomic extraction methods have been developed such as the HotSHOT method [5] but these have been used in standard PCR amplification.

Here we report the combination of the HotSHOT raw genomic extraction method followed by a HRM analysis for genotyping both adult zebrafish and individual embryos. This optimized protocol allows fast (within two hours) and

* Correspondence: eric.samarut@umontreal.ca
[1]Department of Neurosciences, Research Center of the University of Montreal Hospital Center (CRCHUM), Université de Montréal, Montréal, QC, Canada
[3]CRCHUM Tour Viger R09.482, 900 rue saint Denis, Montréal, QC H2X 0A9, Canada
Full list of author information is available at the end of the article

cost-efficient adult genotyping. Indeed, in our hands, HRM genotyping is more than four times cheaper than regular PCR reaction followed by Sanger sequencing. Furthermore, we also took advantage of this method to identify CRISPR-induced mutations in embryos after microinjection of CRISPR-cas9 constructs. Standard methods generally assess the efficacy of CRISPR/Cas9 mutagenesis by extracting DNA from a 24-h embryo and indels are usually detected by T7E1 endonuclease assay, restriction enzyme screening or fluorescent PCR [6–9]. Our optimized protocol allows the reliable detection of CRISPR/cas9-induced indels in four hour old embryos. Furthermore, we show that our HRM-based identification of indels is much more sensitive than standard sequencing of PCR fragment. Lastly, we took advantage of our protocol to identify the earliest time at which we can detect CRISPR/cas9-induced indels in the embryo. Our results show that CRISPR-induced mutations are detectable as early as after the first cell division of the embryo.

Results and discussion

HotSHOT genomic DNA extraction method is suitable for HRM analysis

Our aim was to establish a reliable and cost-effective method for genotyping zebrafish embryos subjected to CRISPR/cas9 mutagenesis that could be used as a precise analysis tool for a broad range of applications. We optimized protocol of raw genomic DNA extraction followed by a 2-steps Evagreen PCR protocol and a HRM analysis. As illustrated in Fig. 1a, our whole genotyping assay could be completed in about two hours. This rapid assessment is particularly important for reducing the time the animal spent in isolated tanks, particularly in laboratories with space limitations. Briefly, genomic DNA is extracted from caudal tail tissue, or from a whole one-day-old embryo by boiling the sample in sodium hydroxide for ten minutes. The high pH of sodium hydroxide is buffered by adding one tenth of the volume of 100 mM Tris HCl pH 8 as described by [10]. Raw genomic DNA is then used as a template in a two-step Evagreen-based PCR reaction in a 96-well plate using a LightCycler 480 device (see material and methods). A final melting step records the fluorescence over an increasing temperature gradient with a high resolution of 0.02 °C per second. We tested this procedure by fin-clipping a heterogeneous population of fish obtained from an incross of two parents carrying a known mutation in *glra4a* gene encoding a glycine receptor subunit, consisting of a deletion of 22 nucleotides (Fig. 1c). Following our procedure, the final melting curve analysis identified three profiles that were confirmed by sequencing to be the expected wild type (*glra4a*$^{+/+}$), heterozygous (*glra4a*$^{+/-}$) and homozygous (*glra4a*$^{-/-}$) genotypes (Fig. 1b, c).

Furthermore, we wanted to see if we could use this method to detect CRISPR-induced mutations directly in the injected embryo. In vitro transcribed RNAs encoding the Cas9 endonuclease and a gene-specific guide RNA (gRNA) are co-microinjected in the one-cell stage zebrafish egg (Fig. 2a). Confirmation of the efficacy of the

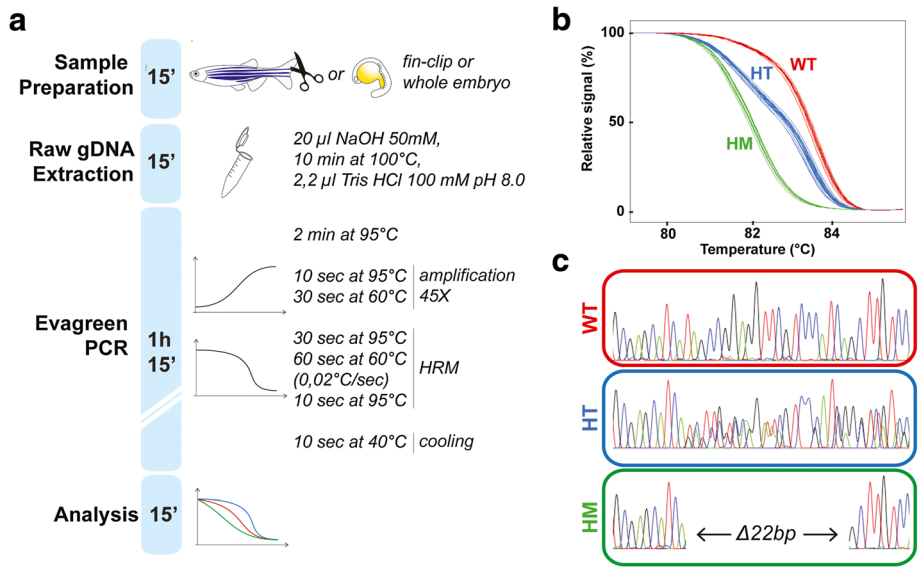

Fig. 1 Genomic DNA is suitable for HRM-based genotyping. **a** Protocol timeline for sample preparation. Genomic DNA extraction, two-steps Evagreen PCR and HRM-based analysis. **b** Genotyping of 21 adult zebrafish obtained by an incross of *glra4a*$^{+/-}$ parents. The HRM curve analysis discriminates wild-type (WT), heterozygous (HT) and homozygous (HM) fish. **c** Sequencing results from each profile identified in (B) confirmed the genotyping and the presence of the 22 base-pair deletion in the heterozygous and homozygous population

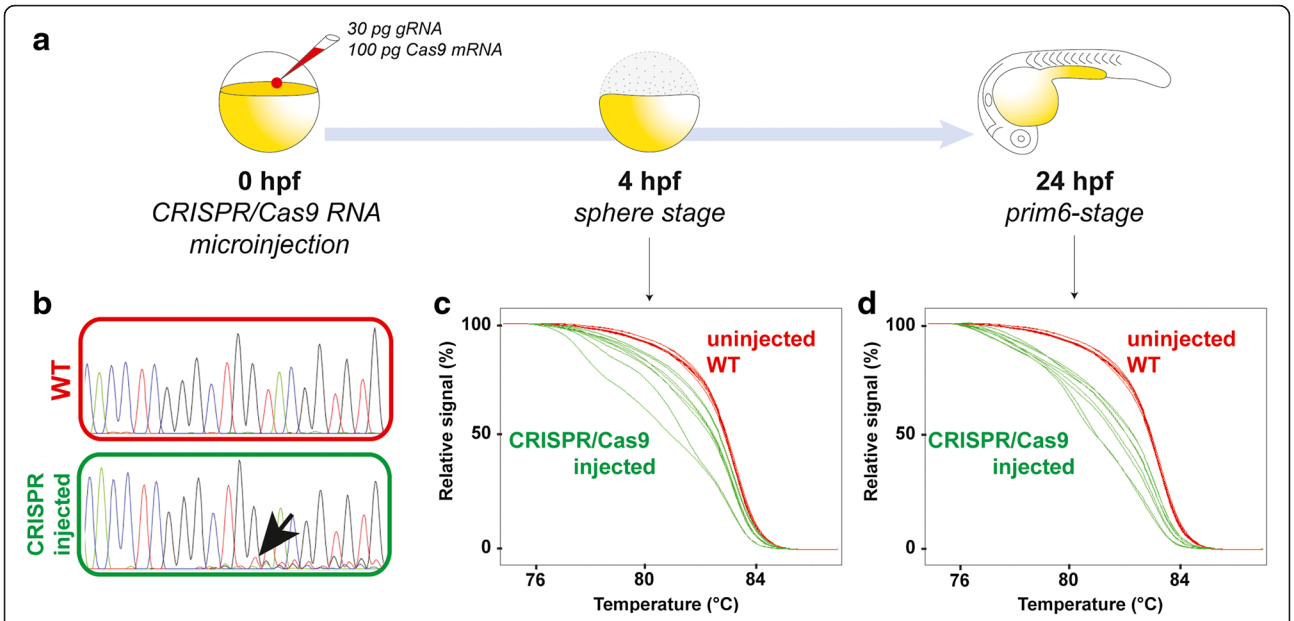

Fig. 2 CRISPR-induced indels can be detected in the late zebrafish blastula. **a** RNAs encoding the Cas9 endonuclease and a guide RNA (gRNA) targeting *gldc* coding sequence are co-microinjected into one-cell stage embryos. The genomic DNA was extracted either at the sphere stage (4 h post-fertilization, hpf) or at the prim-6 stage (24 hpf) using the raw extraction method. **b** Sequencing electropherograms of 8 wild type and 8 CRISPR/Cas9-injected embryos at 24 hpf. The black arrow shows the presence of faint multiple peaks in the CRISPR/cas9-injected embryos, indicating the presence of indels. **c** HRM curve analysis of uninjected wild type (WT, red curves) and CRISPR/Cas9-injected (green curves) embryos at 4 hpf. The green curves are shifted and irregular compared to the red WT curves, indicating the presence of indels at the late blastula stage. **d** Melting curve analysis of uninjected WT (red curves) and CRISPR/Cas9-injected (green curves) embryos at 24 hpf

designed gRNA is crucial for the successful generation of mutant lines. Different techniques are commonly used to detect CRISPR/cas9-induced indels such as PCR sequencing, or restriction enzyme screening but these methods generally assess the efficacy of the mutagenesis one day after microinjection and the results are not always easily interpretable. In fact, detection of indels by PCR sequencing of an injected embryo usually leads to multiple peaks in chromatograms at the indel site and onwards, thus such an analysis might be tricky as it could be easily assimilated as background noise (black arrow, Fig. 2b). To circumvent this problem, new techniques have been developed such as fluorescent PCR or HRM analysis [2, 8, 11].

Thus, we decided to test our HRM-based optimized protocol for the detection of CRISPR/cas9-induced indels within the coding sequence of the glycine decarboxylase *gldc* gene and to confirm that our method allowed the reliable detection of mutations in injected embryos subjected to CRISPR/Cas9-editing (Fig. 2c, d). Indeed, raw genomic DNA extraction followed by HRM analysis (as described in Fig. 1a) from 24 h post-fertilization (hpf) CRISPR-injected embryos led to shifted and irregular melting curves compared to wild type larvae (Fig. 2d). The irregular profiles of these curves are explained by mosaic heteroduplex PCR fragments formed because of the random mutations induced by CRISPR/Cas9 mutagenesis [2]. Moreover, we decided to take advantage of our method to try to detect these indels earlier during development since this would allow a more rapid checkpoint of the mutagenesis efficacy. As shown in Fig. 2c, we successfully identified CRISPR/Cas9-induced mutations in *gldc* by HRM from genomic DNA of a 4 hpf zebrafish blastula. In contrast, at this stage, we were unable to amplify the locus of interest by standard PCR and therefore could not detect the indels by sequencing demonstrating that the HRM-based analysis from a raw genomic extract of a late blastula is more sensitive than standard PCR and allows an early identification of the indels. As a result, this method is very useful to rapidly and accurately assess the efficiency of a CRISPR/cas9 mutagenesis assay in zebrafish.

CRISPR/CAS9 induces indels in the 2-cell stage embryo

Lastly, we decided to go further and try to detect the earliest indels induced by CRISPR/Cas9 system in a third gene: *calpn1a*. To do so, we extracted genomic DNA from early embryos from the very first cell division and onwards until the sphere stage (Fig. 3a). As a result, using our fast HRM assay, we performed mutagenesis kinetics from the very beginning of embryogenesis until the late blastula stage. Interestingly, we were able to detect indels within *calpn1a* coding sequence in embryos as early as the 2-cell stage (just after the first cell

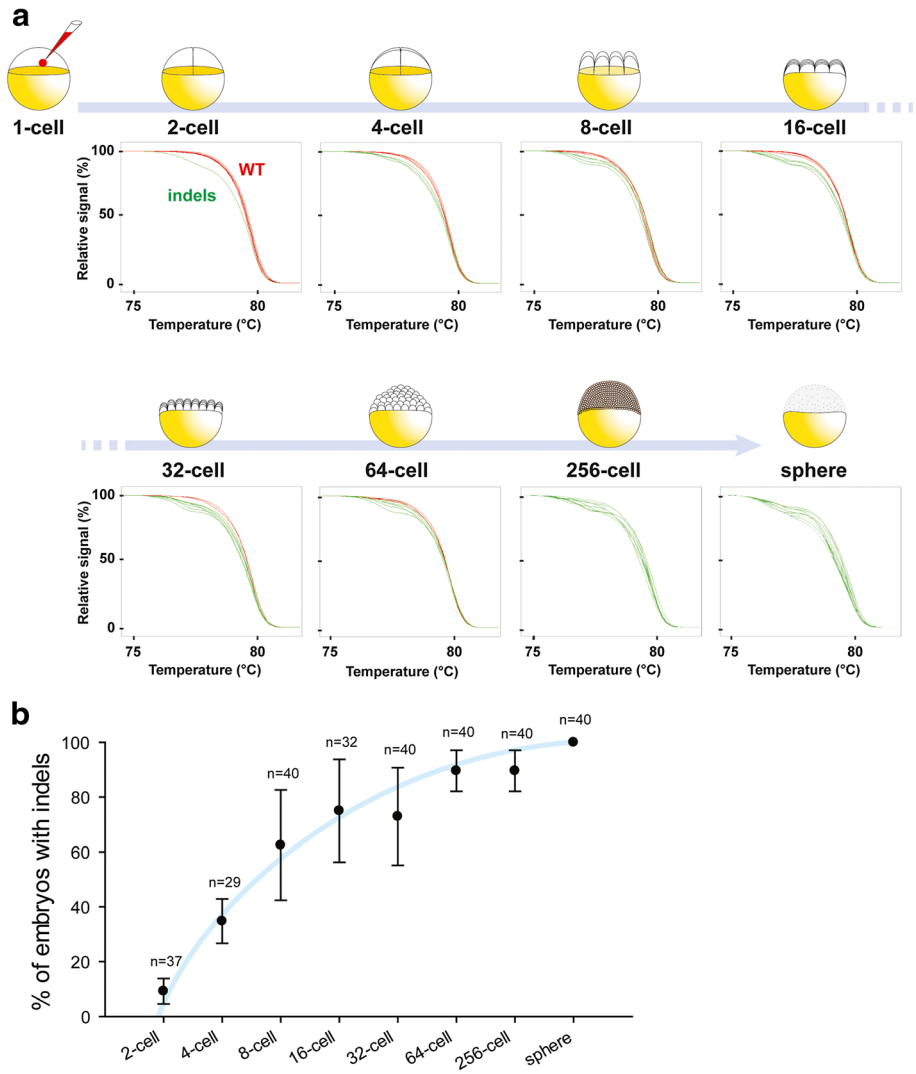

Fig. 3 Mutagenesis kinetics of CRISPR/Cas9-induced injected embryos from 2-cell stage until the sphere stage. **a** Melting curve analysis indicated that indels can be detected as early as 2 cell-stage and the proportion of embryos with indels within *calpn1a* coding sequence increases with time (a sample of 8 HRM curves are shown by timepoint). **b** Quantification of the percentage of embryos with indels within *calpn1a* coding sequence at different stages of development (n indicates the number of individual embryos sequenced per timepoint; at least two independent batches of embryos were used per timepoint). The blue line is an approximation of the trendline

division; $n = 4/37$). To our knowledge, this is the earliest time point at which CRISPR/Cas9 mutagenesis has been identified in zebrafish embryos. The percentage of embryos with indels increases significantly during embryogenesis after each cell division and reached 100 % efficiency at the sphere stage (Fig. 3b). This is illustrated by the increasing number of green non-smooth curves during embryogenesis (Fig. 3a, b). This result demonstrates that the CRISPR/Cas9 system is functional very soon after microinjection but that the DNA repair mechanisms are likely actively reversing the majority of induced mutations. However, error-prone none-homologous end joining allowed mutations to occur at the locus of interest (e.g. *calpn1a*) in about 11 % of embryos after the second cell division and this percentage increases to 70 % in 8-cell embryos (Fig. 3b). Interestingly, our quantification suggests that the majority of CRISPR/Cas9-induced mutations arose between the 8-cell and the 32-cell stages during which we observe the maximum variability in the percentage of embryos bearing mutations. This percentage reached a plateau from the 64-cell stage onwards with only a few non-mutated embryos at this stage ($n = 37/40$) to finally reach 100 % of mutant embryos at the sphere stage ($n = 40/40$).

Conclusions

We propose that the HRM method will expedite genotyping for use with the CRISPR/Cas9 technique.

We demonstrated that this method is able to detect CRISPR/cas9-induced mutations from as early as the 2-cell stage embryo and could therefore be useful to develop new CRISPR/Cas9 procedures to reduce the time required to identify mutant embryos., aiming at shifting the mutagenesis plateau even earlier in development. Ultimately, such optimizations would help reduce the amount of mosaicism usually observed in CRISPR-induced mutants. Of note is that our approach should also be feasible for genotyping other genetic model organisms.

Methods

Fish husbandry

Wild-type Tupfel long fin (TL) zebrafish (*Danio rerio*) were reared at 28.5 °C, kept under a 12-h dark, 12-h light cycle and staged as described previously [12]. They were bred according to standard procedures [13].

sgRNA and Cas9 preparation and microinjection

Gene-specific guide RNAs (gRNA) were designed using the online tool CRISPRscan (http://www.crisprscan.org/). We used the following gRNA sequences (lower case indicate mismatches with the genome sequence and PAM site is indicated in brackets): *calpn1a*, gGAGTTCTGGAGTGCC TTGG(TGG); *gldc*, GGGACACCTCGGGCTGGTA(CGG); *glra4a*, GATGCGAGCATCATAGCCGG(AGG). Synthesis of gRNAs and of Cas9 mRNA was performed as described by [14]. Tubingen long fin (TL) wild-type embryos were collected for microinjection. A 1 nL drop of a mix of 100 ng/μL of Cas9 mRNA and 30 ng/μL of gRNA was injected into one-cell stage embryos using a Picospritzer III pressure ejector. These embryos were then used for genomic DNA extraction at different stages of development.

Fin clipping of adult zebrafish and genomic DNA extraction

Adult fish were anesthetized in tricaine methanesulfonate (MS222) at a final concentration of 160 mg/L and a small piece of the caudal fin was cut with a sharp blade. The fish were immediately put back in fresh water. Genomic DNA extraction was performed in 10 μL (for 2-cell, 4-cell, 8-cell, 16-cell and 32-cell stages) or in 20 μL (all later stages and clipped caudal fin) of 50 mM NaOH from either a clipped caudal fin or from a single whole embryo in its chorion. The samples were boiled for 10 min and 1/10 volume of 100 mM Tris–HCl pH 8 was added to buffer the reaction, as described in [10].

High-resolution melting (HRM)

Primers were designed using the Universal Probe Library Assay Design Center (Roche). glra4a_for: GCAT AAATCCCAAACAAAAGCC; glra4a_rev: CCCCATCG GACTTTCTGG; gldc_for:TTCAGTGAGTATTTGTGT TCTCTACAGG;gldc_rev:TGGTCTGATAGTTGAGTAA GCTCTCC;calpn1a_for:CTTTACCAAAATGTCTATCA GGACG;calpn1a_rev:CGGAGAGCTCATGTTTGTC. All primer sets are available upon request. The PCR reactions were made with 5 μL of the Precision Melt Supermix for HRM analysis (Bio-Rad #172–5112), 0.5 μL of each primer (10 μM) and 2 μL of genomic DNA and water up to 10 μL. The PCR was performed in a LightCycler 480 Instrument II (Roche) using white 96 well plates. Two-step Evagreen PCR reaction protocol was 95 °C for 2 min, then 45 cycles of 95 °C for 10 s and 60 °C for 30 s, followed by 95 °C for 30 s, 60 °C for 60 s, the temperature was increased by 0.02 °C/s until 95 °C for 10 s, then cooling at 40 °C. Curves were analyzed using the Roche LightCycler 480 software version 1.5.1.62.

PCR and sequencing

Primers were designed using the Universal Probe Library Assay Design Center (Roche). glra4a_for: TGGTTGTTAC-CAACATCTGG; glra4a_rev: CTGAAATGATTCAT-GACGC; gldc_for: AATGTATTATTTTTGTGTGAACT GTCCC; gldc_rev: TTCCGTACTTGGCTCTAGTTTGC. All primer sets are available upon request. The PCR reactions were made with 0.5 μL of dNTP (10 μM), 0.5 μL of each primers (10 μM), 2.5 μL of 10x PCR buffer, 0.125 μL of Taq DNA polymerase (GenedireX), 1 μL of genomic DNA and water up to 25 μL. The PCR reaction protocol was 94 °C for 5 min, then 35 cycles of 94 °C for 30 s, 60 °C for 30 s and 72 °C for 45 s and finally 72 °C for 10 min. Samples were sequenced by Genome Quebec/McGill center using Applied Biosystems 3730xl DNA Analyzer.

Abbreviations

Cas9, CRISPR associated endonuclease 9; CRISPR, Clustered regularly interspaced short palindromic repeats; gRNA, guide RNA; hpf, hours post-fertilization; HRM, high-resolution melting; SNP, single nucleotide polymorphisms

Acknowledgements

We thank all lab members and more especially Gary Armstrong for carefully reviewing this manuscript, Meijiang Liao for useful technical assistance and Guy Laliberté and Marina Drits of the CRCHUM zebrafish platform for animal care. We also thank Marc Allard for his efforts at the beginning of this work.

Funding

This project was supported by funding from the FRQS-affiliated GRSNC (Groupe de Recherche sur le Système Nerveux Central), the Québec MEESR (Ministère de l'Éducation, de l'Enseignement Supérieur et de Recherche) and the CRCHUM (ES). AL has a CIHR ALS Canada doctoral award.

Availability of data and material

All the supporting data are present in this manuscript.

Authors' contributions

ES and AL designed, performed and analyzed experiments. ES and AL wrote the manuscript. PD reviewed the manuscript. All authors have read and approved the manuscript.

Competing interests

The authors declare that they have no competing interests.

Consent for publication

N/A

Ethics approval and consent to participate
All experiments were performed in compliance with the guidelines of the Canadian Council for Animal Care and conducted at the Research Center of the University of Montreal Hospital Center (CRCHUM). The vertebrate animal welfare assurance from the Institutional Animal Care and Use Committee (IACUC) for the use of adult zebrafish has been approved on 2015/08/31.

Authors' information
N/A

Author details
[1]Department of Neurosciences, Research Center of the University of Montreal Hospital Center (CRCHUM), Université de Montréal, Montréal, QC, Canada. [2]Department of Pathology and Cell Biology, Université de Montréal, Montréal, QC, Canada. [3]CRCHUM Tour Viger R09.482, 900 rue saint Denis, Montréal, QC H2X 0A9, Canada.

Received: 30 March 2016 Accepted: 30 June 2016
Published online: 04 August 2016

References

1. Wittwer CT. High-resolution DNA melting analysis: advancements and limitations. Hum Mutat. 2009;30(6):857–9.
2. Thomas HR, et al. High-throughput genome editing and phenotyping facilitated by high resolution melting curve analysis. PLoS One. 2014; 9(12):e114632.
3. Vossen RH, et al. High-resolution melting analysis (HRMA): more than just sequence variant screening. Hum Mutat. 2009;30(6):860–6.
4. Liew M, et al. Genotyping of single-nucleotide polymorphisms by high-resolution melting of small amplicons. Clin Chem. 2004;50(7):1156–64.
5. Truett GE, et al. Preparation of PCR-quality mouse genomic DNA with hot sodium hydroxide and tris (HotSHOT). Biotechniques. 2000;29(1):52. 54.
6. Ota S, et al. Multiple genome modifications by the CRISPR/Cas9 system in zebrafish. Genes Cells. 2014;19(7):555–64.
7. Auer TO, et al. CRISPR/Cas9-mediated conversion of eGFP- into Gal4-transgenic lines in zebrafish. Nat Protoc. 2014;9(12):2823–40.
8. Ramlee MK, et al. High-throughput genotyping of CRISPR/Cas9-mediated mutants using fluorescent PCR-capillary gel electrophoresis. Sci Rep. 2015;26(5):15587.
9. Yu C, et al. A PCR based protocol for detecting indel mutations induced by TALENs and CRISPR/Cas9 in zebrafish. PLoS One. 2014;9(6):e98282.
10. Meeker ND, et al. Method for isolation of PCR-ready genomic DNA from zebrafish tissues. Biotechniques. 2007;43(5):610. 612, 614.
11. D'Agostino Y, et al. A Rapid and Cheap Methodology for CRISPR/Cas9 Zebrafish Mutant Screening. Mol Biotechnol. 2016;58(1):73–8.
12. Kimmel CB, et al. Stages of embryonic development of the zebrafish. Dev Dyn. 1995;203(3):253–310.
13. Westerfield, M. The Zebrafish Book: A Guide for the Laboratory Use of Zebrafish (Danio rerio). Eugene, OR: Univ. of Oregon Press, 1995.
14. Moreno-Mateos MA, et al. CRISPRscan: designing highly efficient sgRNAs for CRISPR-Cas9 targeting in vivo. Nat Methods. 2015;12(10):982–8.